FIXED BED COUNTERCURRENT LOW TEMPERATURE GASIFICATION OF DAIRY BIOMASS AND COAL-DAIRY BIOMASS BLENDS USING AIR-STEAM AS OXIDIZER

A Dissertation

by

GERARDO GORDILLO ARIZA

Submitted to the Office of Graduate Studies of
Texas A&M University
in partial fulfillment of the requirements for the degree of

DOCTOR OF PHILOSOPHY

August 2009

Major Subject: Mechanical Engineering

FIXED BED COUNTERCURRENT LOW TEMPERATURE GASIFICATION OF DAIRY BIOMASS AND COAL-DAIRY BIOMASS BLENDS USING AIR-STEAM AS OXIDIZER

A Dissertation

by

GERARDO GORDILLO ARIZA

Submitted to the Office of Graduate Studies of
Texas A&M University
in partial fulfillment of the requirements for the degree of

DORTOR OF PHILOSOPHY

Approved by:

Chair of Committee,	Kalyan Annamalai
Committee Members,	N. K. Anand
	Bing Guo
	Mark Holtzapple
Head of Department,	Dennis L. O'Neal

August 2009

Major Subject: Mechanical Engineering

ABSTRACT

Fixed Bed Counter Current Low Temperature Gasification of Dairy Biomass and Coal-dairy Biomass Blends Using Air-Steam. (August 2009)

Gerardo Gordillo Ariza, B.S.,Universidad Nacional de Colombia;

M.S., Universidad de los Andes

Chair of Advisory Committee: Dr. Kalyan Annamalai

Concentrated animal feeding operations such as cattle feedlots and dairies produce a large amount of manure, cattle biomass (CB), which may lead to land, water, and air pollution if waste handling systems and storage and treatment structures are not properly managed. However, the concentrated production of low quality CB at these feeding operations serves as a good feedstock for *in situ* gasification for syngas (CO and H_2) production and subsequent use in power generation. A small scale (10 kW) countercurrent fixed bed gasifier was rebuilt to perform gasification studies under quasi-steady state conditions using dairy biomass (DB) as feedstock and various air-steam mixtures as oxidizing sources. A DB-ash (from DB) blend and a DB-Wyoming coal blend were also studied for comparison purposes. In addition, chlorinated char was also produced via pure pyrolysis of DB using N_2 and N_2-steam gas mixtures.

The chlorinated char is useful for enhanced capture of Hg in ESP of coal fired boilers. Two main parameters were investigated in the gasification studies with air-steam mixtures. One was the equivalence ratio ER (the ratio of stochiometric air to actual air)

and the second was the steam to fuel ratio (S:F). Prior to the experimental studies, atom conservation with i) limited product species and ii) equilibrium modeling studies with a large number of product species were performed on the gasification of DB to determine suitable range of operating conditions (ER and S:F ratio). Results on bed temperature profile, gas composition (CO, CO_2, H_2, CH_4, C_2H_6, and N_2), gross heating value (HHV), and energy conversion efficiency (ECE) are presented.

Both modeling and experimental results show that gasification under increased ER and S:F ratios tend to produce rich mixtures in H_2 and CO_2 but poor in CO. Increased ER produces gases with higher HHV but decreases the ECE due to higher tar and char production. Gasification of DB under the operating conditions $1.59<ER<6.36$ and $0.35<S:F<0.8$ yielded gas mixtures with compositions as given below: CO (4.77 - 11.73 %), H_2 (13.48 - 25.45%), CO_2 (11-25.2%), CH_4 (0.43-1.73 %), and C_2H_6 (0.2-0.69%). In general, the bed temperature profiles had peaks that ranged between 519 and 1032 °C for DB gasification.

DEDICATION

I want to dedicate this dissertation to my mother, who in spite of her limited education, taught me a love for education. Also, I dedicate this work to my wife and my children for their encouragement throughout my career.

ACKNOWLEDGEMENTS

I would like to express my gratitude to Dr. Kalyan Annamalai for the support and guidance which he has given me during my graduate studies at Texas A&M University. Also, I would like to thank Dr. K.N Anand, Dr. Bing Guo, and Dr. Mark Holtzapple for taking the time to serve on my committee, and for the advice they have given me during this undertaking. I am thankful to Dr. Holtzapple for permitting me to use some equipment in his laboratory and to my wife, Rocio Sierra, for having helped me with that task.

The financial support from the Department of Energy, National Renewable Energy Laboratory (DOE-NREL) Golden, Colorado, under Grant #DE-FG36-05GO85003 is also gratefully acknowledged.

Finally, I want to thank my wife and my children for their support and patience, without which this enterprise would have been impossible.

NOMENCLATURE

Symbol	Definition and units
a	Stoichiometric moles of oxygen
AS	Surface area of gasifier (m^2)
AOF	Oxygen from air to total oxygen from air and steam ratio
b	Stochiometric moles of CO_2
c_i	Oxidizer concentration ($kmol/m^3$)
c	Stochiometric moles of H_2O
CB	Cattle biomass
$CAFO_s$	Concentrated feeding operations
CV_1	Control volume 1
d	Stochiometric moles of SO_2
e	Actual air stochiometric coefficient
D	Inner diameter of gasifier (m)
DAF	Dry ash free
DB	Dairy biomass
DB-ash	Dairy biomass ash blend
d_P	Particle diameter
EES	Engineering equation solver Code
ECE	Energy conversion efficiency
EIA	Energy Information Administration

ER	Equivalence ratio
ER_M	Modified equivalence ratio
$C_{P,A}$	Air specific heat (kJ/kg.K)
e	Actual air coefficient (mol)
f	Actual moles steam supplied as reactant
FB	Feedlot biomass
FC	Fixed carbon
g	Actual moles of CO_2
h	Actual moles CO
$h_{k,p}$	Enthalpy of the products
$h_{k,R}$	Enthalpy of the reactants
HHV	High heating value of gases
HHV_{Gases}	High heating value of gases (kJ/m3)
HHV_i	High heating value of products (kJ/m3)
HHV_{fuel}	High heating value of DB (kJ/kmol)
HRSG	Heat Recovery Steam Generation
i	Actual moles of CH_4
IGCC	Integrated Gasification Combined Cycle
J	Actual moles of H_2S
k	Actual moles of N_2
K_1	Kinetics constant of pyrolysis reaction ($kg/(m^3\ s)$)
K_5	Kinetics constant of the reaction of CO with O_2

K_7	Kinetic constants of shift reaction
K_E	Equilibrium constant of shift reaction
K_j	Kinetic constants of heterogeneous reactions (m/s), j=2, 3, 4, 6, and 8
K_m	Diffusion constant (m/s)
l	Actual moles of H_2 (mol)
LA-PC-Sepsol-DB	Low ash partial compost separated solids dairy biomass
LA-PC-FB	Low ash partial compost feedlot biomass
m_A	Mass of air (kg)
MS	Mass spectrometer
$N_{k,p}$	Moles of the products
$N_{k,R}$	Moles of the reactants
N_{steam}	Moles of steam
Q	Heat
Re	Particle Reynolds number
S:A	Steam to air ratio
SATP	Standard ambient temperature (25°C) and pressure (100 kPa)
S_C	Particle Schmidt number
S:F	Steam to fuel ratio (mole basis)
SCFH	Standard feet cubic per hour
STDEV	Standard deviation
T_p	Adiabatic temperature

T_{peak}	Peak Temperature
Ts	Surface temperature of the particle
TXL	Texas Lignite Coal
$T_{x,t}$	Temperature along gasifier axis (K)
T_{∞}	Ambient temperature (K)
U	Global heat transfer coefficient of the gasifier (kW/ m^2. K)
W_j	Rate of reaction (kmol/m^3. s)
W_5	Reaction rate of $CO+O_2$ reaction
W_7	Reaction rate of shift reaction
X_i	Moles fraction of each fuel product
Y_i	Mass fraction of oxidizer
ΔH_R	Enthalpy of reaction
$\eta_{Gas,E}$	Energy conversion efficiency
ρ	Air density (kg/m^3)
λ	Latent heat of the water (kJ/kg)
ε	Bed porosity or void fraction
$\rho_{biomass}$	Biomass density (kg/m^3)

Subscripts	Definition
2-8	reaction number
fuel	fuel
FC	Fixed carbon

gas	gas
gas max	gas maximun
h	H atoms
i	species and char oxidizer (O_2, CO_2, H_2O, and H_2)
j	Reaction number (2, 3, 4, 6, and 8)
n	N atoms
l	Liquid
O	Oxygen atom
$O_{2,in}$	Oxygen moles entering
s	S atoms

TABLE OF CONTENTS

Page

Page

LIST OF FIGURES

Page

Page

Page

Page

Page

Page

Page

Page

Page

LIST OF TABLES

Page

Page

1. INTRODUCTION

Current energy consumption is 492 quads (4.66 x 10^{11} GJ), but energy consumption is expected to grow to 694 quads by 2030. Combusting fossil fuel produces pollution (NO_x, SO_x) and greenhouse emissions (CO_2). To reduce pollution and increase energy supplies, renewable energy sources must be developed.

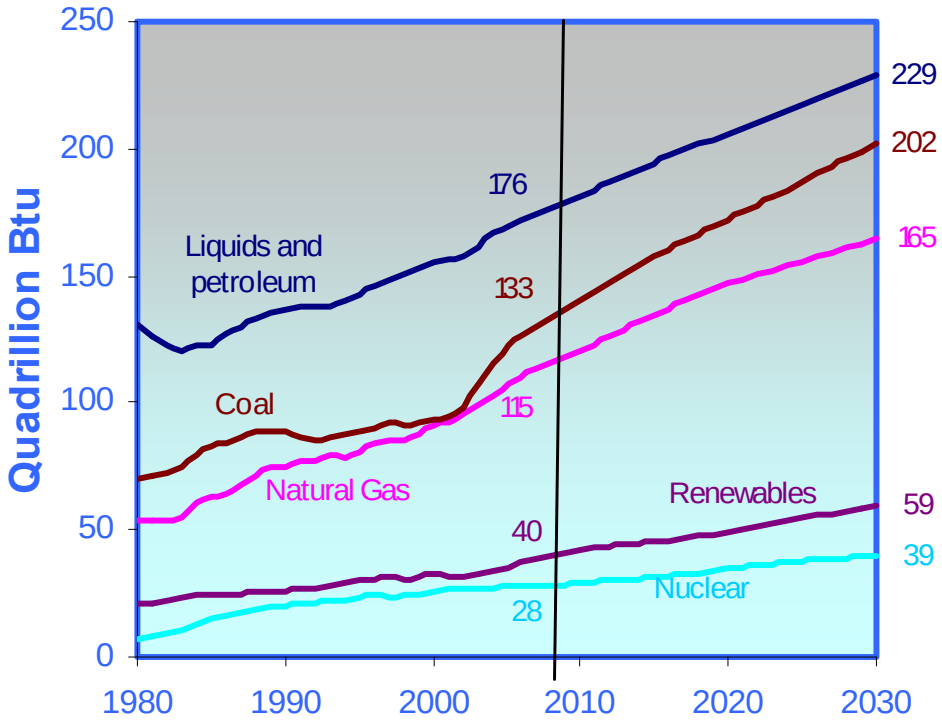

Figure 1. Global projection of annual energy consumption by fuel type, adapted [1]

This dissertation follows the style of *Renewable Energy Journal.*

If global energy consumption continues to grow in according to Figure 1, the energy consumption in 2030 will be about 41 % greater than current consumption. In addition, carbon dioxide emissions would increase about 41% [2] (Figure 2) increasing the concentration of CO_2, because coal and natural gas are projected to be the largest increment in fuel consumption over the projected period. One of the principal causes of global temperature rise is attributed to the greenhouse effect, in which the continued increase in CO_2 concentration in the troposphere traps solar radiation reflected from the earth. In addition to increased pollutants, continuous growth in the energy consumption contributes to increase energy prices. Figure 3 shows the oil price history from 1980 to 2005 and the oil price projection from 2005 to 2030 estimated by [3] for reference and high-price cases. It is apparent from Figure 3 that the oil prices may increase about 85% in the next 22 years if it continues growing according to the high price case. Projections of energy consumption and price are based on the assumption that there is no global recession and economics will continue to grow. However, if there is a global recession, the projections must to be modified. From July 2008 to December 2008, oil prices have fallen by about 300% because of the global recession. The dramatic projections of emissions, energy consumption, and oil prices encourage generation of alternative energy to produce renewable fuels with zero emissions and to decrease the dependency on fossil fuels and its related consequences. If non- conventional fuel were to replace the fossil fuels, the negative impact on the environment and on oil prices could be mitigated.

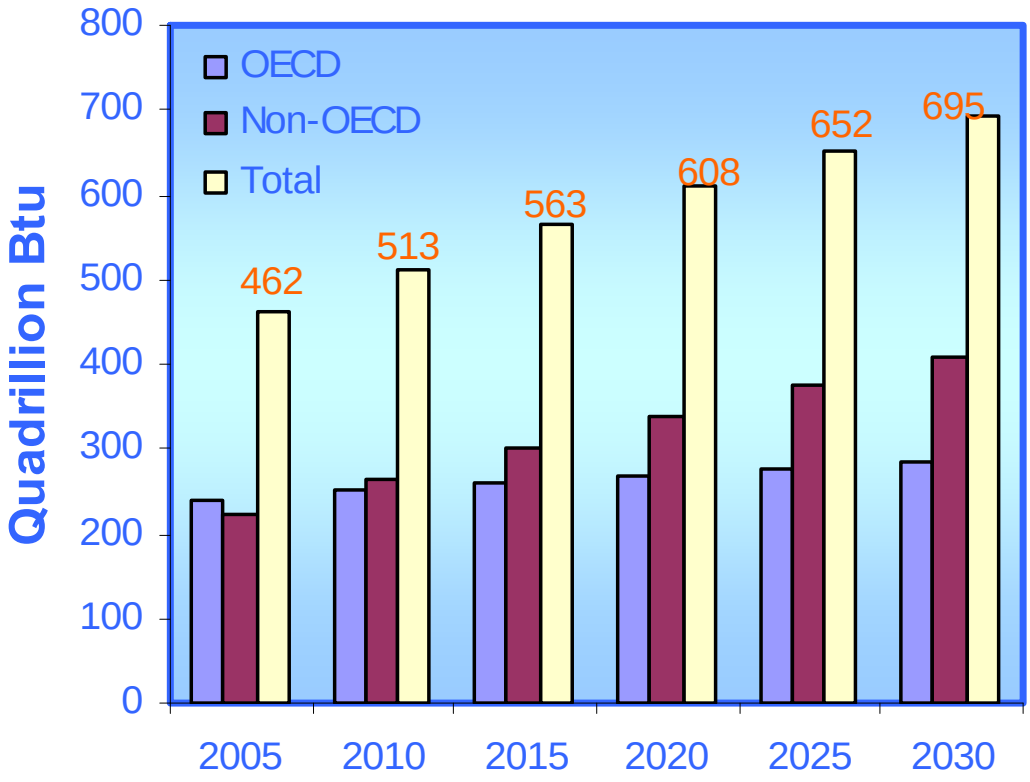

Figure 2. Global projection on annual carbon dioxide emissions, adapted [2]

Biomass fuels (e.g., energy crops, agricultural and forestry residues and municipal, industrial, and animal wastes) can serve as a renewable energy source using biological and thermal gasification and direct combustion processes. The inclusion of biomass as feedstock in thermal conversion processes does not increase the CO_2 concentration in the atmosphere because biomass is a carbon neutral fuel.

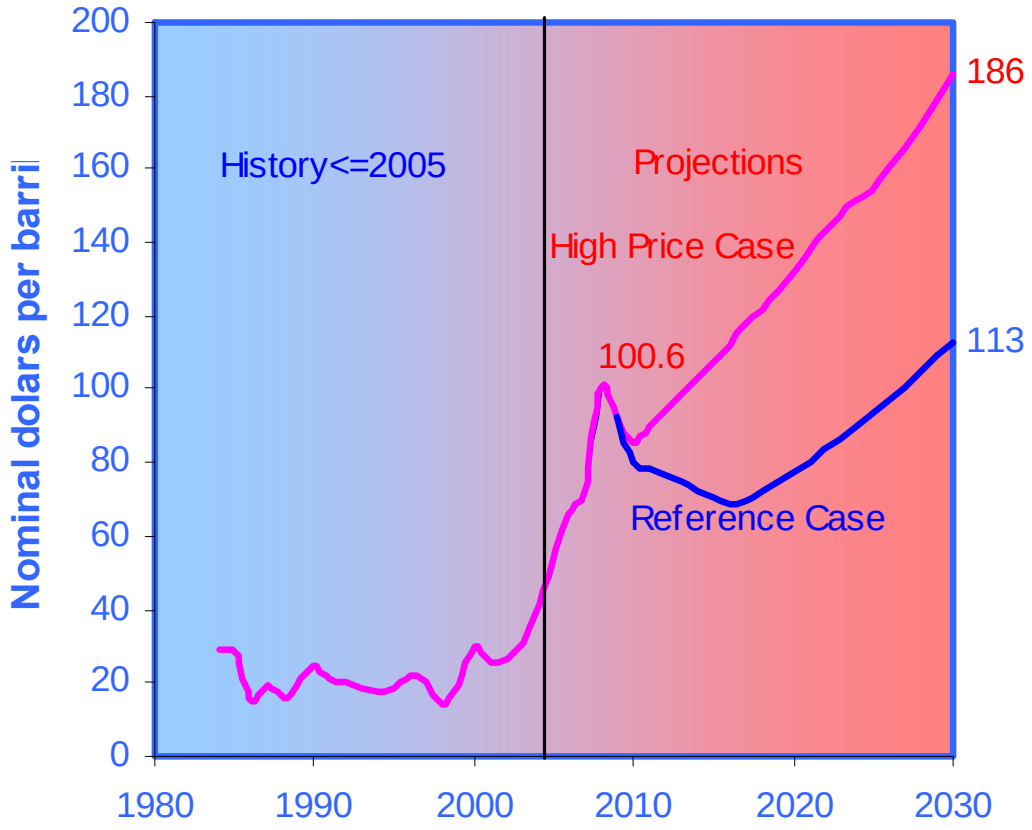

Figure 3. Global projection of oil prices, adapted [3]

Combustion engineers prefer high-grade biomasses (high heat value) because those with low heat value have poor combustion stability. Also, combustion engineers prefer biomasses with low ash content because those with high ash content can cause fouling and slagging problems in the boilers [4]. Direct combustion and partial oxidation of wood and biomass-derived charcoal with air have been amply studied over the last few decades [5][6]. Low NO_x burners, co-firing and reburn processes to reduce NO_x emission produced by combusting of coal in electric power plants [7][8][9]; gasification

of biomass with steam-air [10][11], steam [12] [13], pure oxygen, pure oxygen and steam [14]; and gasification of coal and wastes [15] blends are emerging technologies.

Gasification of biomass with steam (e.g., steam-reforming), is used to produce H_2 enriched mixtures of CO_2; however, this is an endothermic process that requires heat input and lowers gasification efficiency. In contrast, gasification of biomass with air-steam produces a mixture of CO and H_2 (rich mixtures in H_2) and other hydrocarbons that, in theory, can be conducted adiabatically.

The gaseous fuel produced from gasification of biomass could be used for *in situ* power generation and further subjected to a secondary process to convert the CO to H_2 by the water-gas shift reaction, $CO+H_2O = CO_2+H_2$ or submitted to catalysis or bio-catalysis for the production of liquid fuels and chemicals [16](Figure 4).

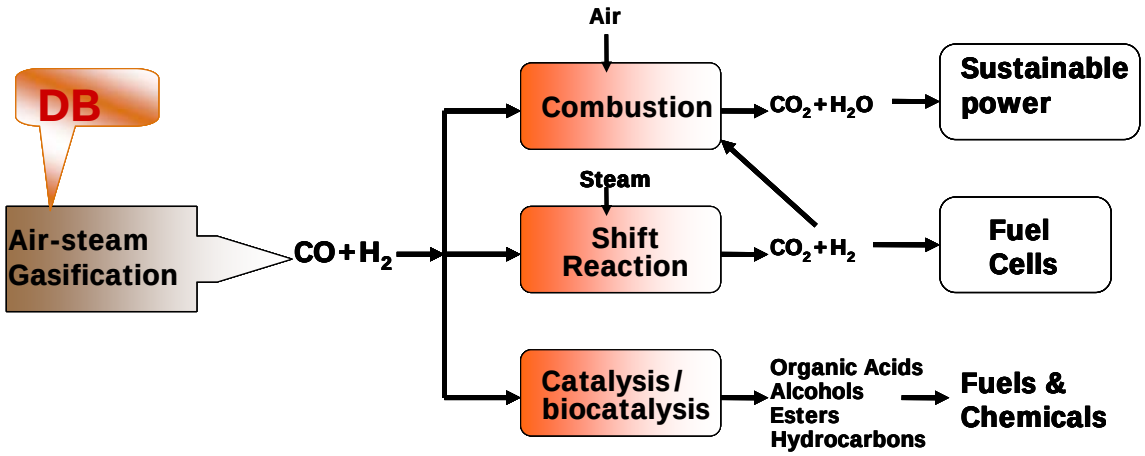

Figure 4. Possible uses of syngas produced via gasification of biomass with steam and air, adapted from [16]

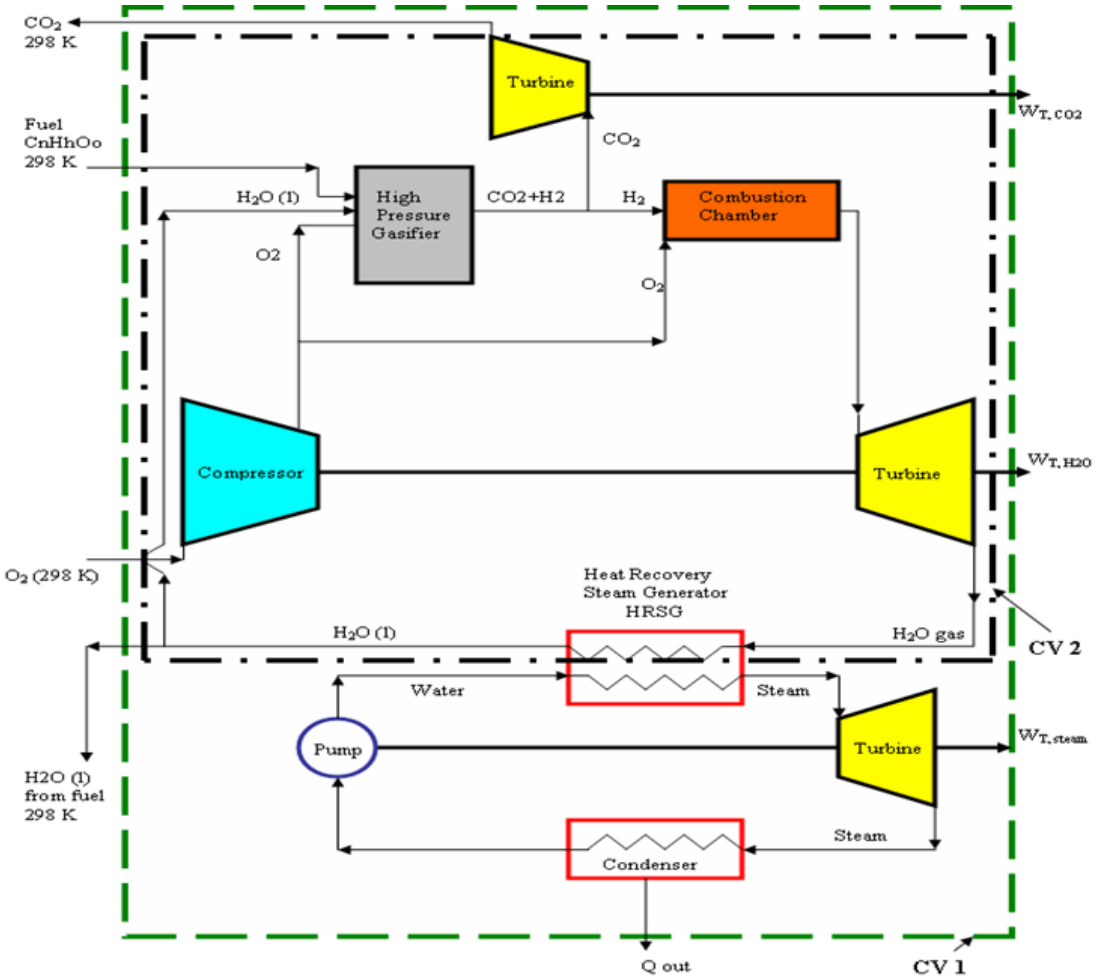

Figure 5. Power generation cycle with hydrogen produced from biomass gasification with steam

The hydrogen produced from the shift reaction (after separation from CO_2) can be used in power plants for energy conversion with zero emission (Future Generation), because hydrogen combustion produces only steam. Figure 5 shows an integrated Gasification Combined Cycle (IGCC) with Heat Recovery Steam Generation or (HRSG) to produce power from oxygen gasification of biomass at high pressure.

In the IGCC shown Figure 5, biomass is used as feedstock in the gasifier to produce CO_2 and H_2 at high pressure and temperature. The H_2 separated from the CO_2 at

high temperature is used in a Brayton cycle to produce primary power whereas the extant heat from the gas turbine is recuperated in the HRSG to produce low-pressure steam which is used for more power generation using Rankine cycle. Also the CO_2 separated from the H_2 is used in a gas turbine to produce more power. The products from the control volumes (CV1) are heat (Q), power (W), water (H_2O), and carbon dioxide (CO_2). The CO_2 produced does not increase the atmospheric CO_2 levels because biomass captures CO_2 and converts it via photosynthesis to organic compounds; in other words, biomass is a CO_2-neutral fuel (Figure 6) which does not increase the C atoms in the atmosphere.

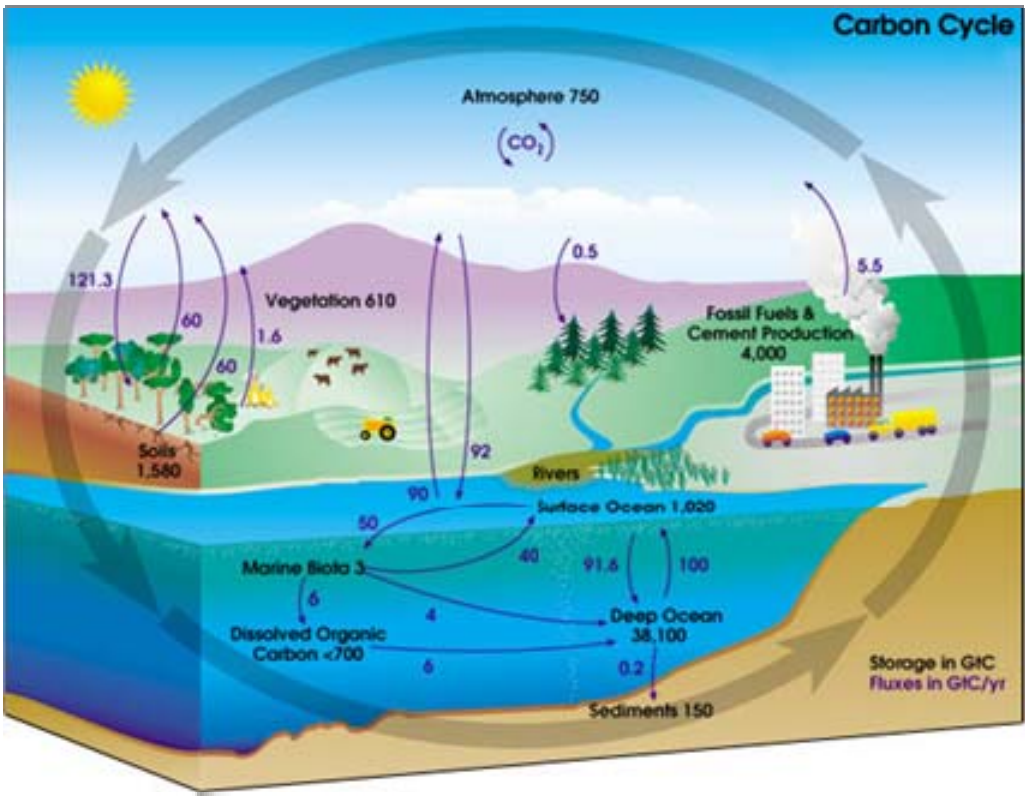

Figure 6. Carbon cycle source, from [17]

The use of wastes as renewable feedstock in thermal conversion processes is important for the following reasons: 1) it uses the energy potential from waste to produce sustainable electrical power and to produce biofuels to mitigate the bioenergy demand, which may increased to several hundred exajouls in the future [18]; 2) it addresses the waste disposal problems in agricultural farms; 3) it may reduces air pollution generated by fossil fuel combustion when the sustainable power from wastes replaces fossil energy.

Large concentrated animal feeding operations (CAFOs) from dairy and feedlot farms in the United States produce a vast amount of animal wastes (or cattle manure called cattle biomass (CB)) [19]. CAFOs have expanded all over the country (including Texas). Since 1978, the average number of animal units and hence animal waste has increased by 56% (cattle) and 176% (poultry litter). Beef cattle are fattened for slaughter in large industrial feeding operations known as feedlots. The feedlots have capacities greater than 20,000 cattle, with several lots as large as 50,000 to 85,000 heads [20]. It is estimated that at any given time, there are over 10,000,000 cattle in feedlots within the United States [21]. There are 70 feed yards in the Texas Panhandle area alone which include Oklahoma and New Mexico. Feedlots in the Texas and Oklahoma panhandle region [22] with capacities ranging from 5,000 to 75,000 heads feed a total of 6-7 million heads (30% of US cattle on feed). The cattle feeding industry in the Texas Panhandle is growing at the rate of approximately 100,000 heads of feedlot per year. Each calf is typically fed over a period of 4–5 months. Each animal can excrete 27 kg (59.5 lb) of FB (including moisture) per day (approximately 5 to 6% of its body weight)

[23]. Therefore, the potential manure production for Texas and for the US is over 70 and 365 million wet tons per year, respectively. Apart from the cattle industry, milk output has steadily risen for the past several years despite the decreasing number of smaller dairy operations in the country [24] and the increasing number of larger dairies with more concentrated production of dairy biomass (DB).

The vast amount of wastes (CB) produced in CAFOs, classified into dairy biomass (DB) and feedlot biomass (FB), may cause land, water, and air pollution if waste handling systems and storage and treatment structures are not properly managed. However, the concentrated production of CB at these feeding operations serves as a good feedstock for thermal conversion processes, such as co-firing and reburn with coal and *in situ* gasification for syngas (CO and H_2) production and subsequent use in power generation. Because of its high ash and moisture content, animal wastes (which include dairy manure or dairy biomass, DB, feedlot manure or feedlot biomass, FB, poultry manure or poultry biomass, PB, swine manure or swine biomass, SB etc.) are considered low grade fuel (low heating value) more suitable for gasification processes than for combustion processes.

Although gasification of wood and charcoal with air as an oxidizing agent is a widely known technology of which extensive literature can be found, animal waste is a new fuel to be tested in gasification. In the past, cofiring experiments have been performed with CB as the cofiring fuel [7] [8]; However cofiring requires fine grinding of CB. Further, gasification experiments were performed on air gasification using batch processes (i. e., without ash removal) by Priyadarsan et al. [25][26].

1.1. Scope of the proposed work

The present research deals with adiabatic fixed bed countercurrent gasification of DB using different combinations of air and steam as the oxidizing source and with a continuous ash disposal system to perform gasification studies near-to-steady state conditions. Countercurrent or updraft fixed bed gasifiers can be operated on a small scale (lower than 10 MW) using biomass with minimum pretreatment; thus, those gasifiers are ideal for sustainable power generation in CAFOs because they produce enough DB to drive small-scale gasifiers. If CAFOs wastes were included as renewable feedstock to replace power generation from coal, gas, and petroleum, the pollutants produced by both wastes disposal and emission from fossil fuels would decrease. Using air-steam as the oxidizing medium in gasification increases the H_2 production because reactions of char and CO with steam are favored. However, it is essential to study the effect of operating conditions like equivalence ratio (ER) and steam-to-fuel ratio (S:F) on gas composition, temperature profile, gross heating value of species, and energy recovery in a small gasifier (10 kW) so that the results obtained can be useful in the operation of on-site small-scale gasification facilities.

2. LITERATURE REVIEW

This section presents a background on biomass gasification and earlier studies on gasification of cattle biomass.

2.1. Background on gasification

In wet biomass gasification, the fuel material undergoes four basic processes: drying, pyrolysis, partial oxidation, and reforming. Figure 7 shows a schematic of a fixed- bed counter-flow gasifier.

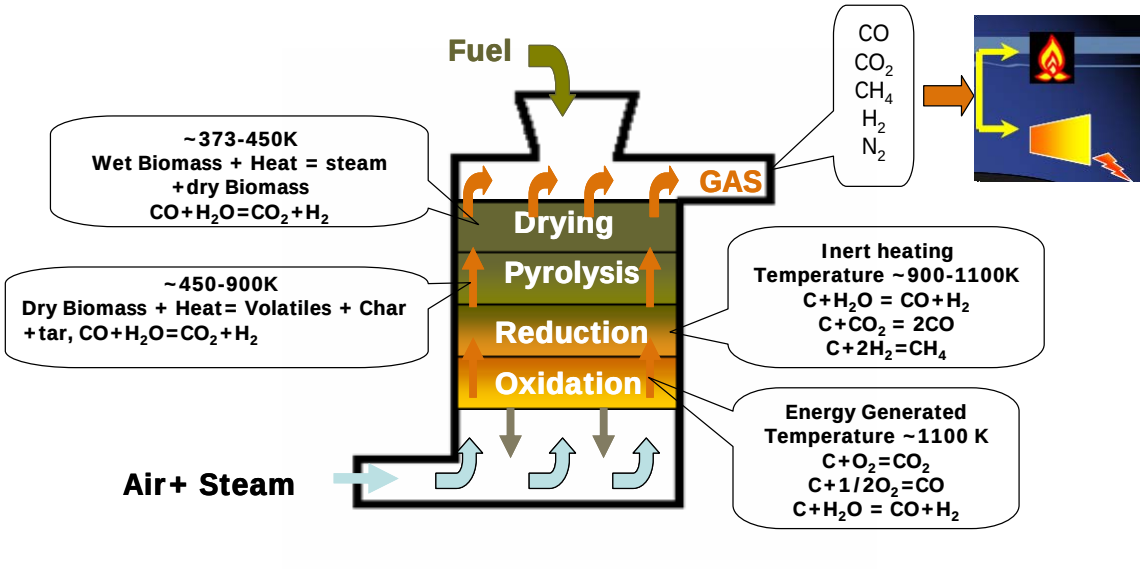

Figure 7. Schematic of a fixed bed gasifier, adapted from [26]

Fuel is fed from the top of the gasifier while air or air-steam is supplied at the bottom. During drying, the moisture is removed at about 300 K. After drying the biomass heats up to about 600 K. Then, under pyrolysis, biomass releases volatile matter (VM) and char at about 600 K [27]. At a higher temperature (~1000 K), the tar contained in VM cracks to produce other compounds, such as hydrocarbons, carbon dioxide, carbon monoxide, hydrogen, and steam. Additionally, the char produced in pyrolysis react with oxygen and steam, or CO_2 to produce partially oxidized compounds. Reforming is the reaction of char and steam to produce $CO+H_2$ and the posterior reaction of CO with steam to produce CO_2 and H_2.

Many types of reactors have been developed around the world; however, the most relevant are fixed-bed, fluidized-bed, and entrained-flow [28] [29]. The main difference of those reactors concern how the biomass and oxidizer are moved in the reactor. The form in which the biomass and the oxidizer move along the axis of the reactor affects the gases and fuel profile temperature. Figure 8 shows the principal reactor types and the profile temperature for gasification of coal with air. In an updraft fixed-bed gasifier, the biomass moves down and the gases move up (Figure 7). In contrast, with downdraft gasifier, both the biomass and the gases move down; as a result, the temperature of gases leaving an updraft gasifier is lower than those leaving a downdraft gasifier. The temperature profile in both the fluidized-bed and entrained gasifier is almost constant and the gas temperature leaving the gasifier is higher than that of the gases leaving an updraft gasifier.

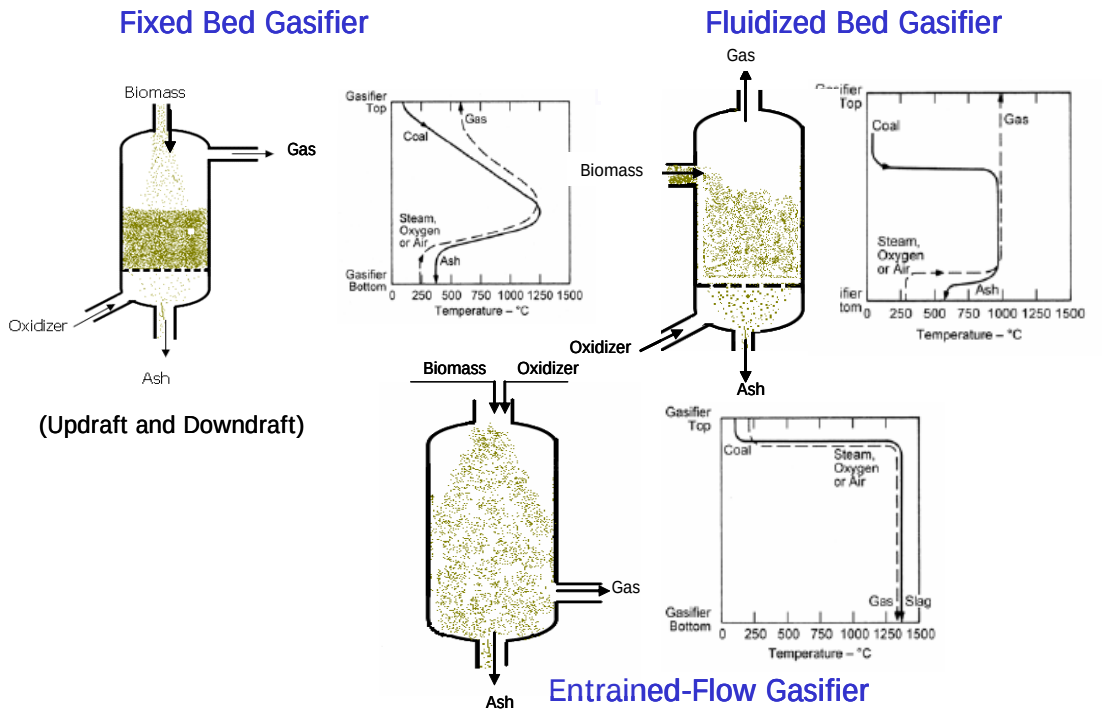

Figure 8. Types of gasifiers and their temperature profile, adapted from [28]

Because fluidized-bed and entrained bed gasification require much higher air velocity compared to fixed-bed gasification, the fluidized-bed and entrained-bed gasifiers are suitable for large-scale applications. For small-scale applications (power<10 MW) fixed-bed gasifiers are well suited. Updraft (countercurrent) fixed-bed reactors are the oldest and historically most common method used to generate heat and power, but in the last two decades, large–scale fixed-bed reactors have lost part of their industrial market [30]. Small-scale updraft fixed-bed gasifiers have high thermal efficiency and require minimal pretreatment of the supplied biomass, so they have maintained commercial interest, especially for *in situ* power generation [28].

Table 1 summarizes the performance of the most common biomass gasifiers that use air. In a downdraft gasifier, gases are produced in the pyrolyis zone past the high-temperature region where the tar and hydrocarbons crack to produce more H_2 and less tar [29]; however, the high ogase temperature leaving the gasifier leads to low energy conversion efficiency because sensible losses are high. The updraft gasifier produces more CO and tar and the fluidized bed gasifier produces more CH_4 and less hydrogen.

Table 1.Typical specie production from the most common gasifiers, adapted from [16][29]

	Gaseous products						Gas quality	
Gasifier type	H_2	CO	CO_2	CH_4	N_2	HHV (MJ/m^3)	Tars (g/m^3)	Dusts
Air-blown updraft	11	24	9	3	53	5.5	~50	Low
Air-blown downdraft	17	21	13	1	48	5.7	~1	Medium
Fluidized bed	9	14	20	7	50	5.4	~10	High

Figure 7 shows the four basic biomass gasification processes occurring in a countercurrent fixed-bed gasifier [26]. In the drying zone, the biomass slowly heats and releases H_2O; then, the dry biomass descends to the pyrolysis zone where the solids pyrolyze to produce light gases, tar, and char. In the reduction zone some char produced in the pyrolysis zone reacts with CO_2 and H_2 produced in the combustion zone to produce more CO and CH_4. Finally, in the oxidation zone, the oxygen and the steam content in the oxidizing source react with fixed carbon (char) that descends from the reduction zone to produce CO_2, CO, H_2, and heat. By convection and diffusion, the thermal energy produced there is carried by to the higher zones to supply energy required in pyrolysis and drying.

2.1.1.Reactions in gasifiers

Biomass gasification is a complex process because the large number of reactions that occur, and the considerable number of biomass components. However, biomass gasification with air-steam can be globally modeled with reactions 1 to 8 [5] [10].

$$\text{Solid biomass + heat} \rightarrow \text{VM + char} \quad (1)$$

$$C + O_2 \rightarrow CO_2,\ \Delta H_R = -32765 \text{ kJ/kg of C} \quad (2)$$

$$C + 1/2\ O_2 \rightarrow CO,\ \Delta H_R = -9205 \text{ kJ/kg of C} \quad (3)$$

$$C + CO_2 \rightarrow 2CO,\ \Delta H_R = 14360 \text{ kJ/kg of C} \quad (4)$$

$$CO + 1/2 O_2 \rightarrow CO_2,\ \Delta H_R = -10105 \text{ kJ/kg of CO} \quad (5)$$

$$C + H_2O \rightarrow CO + H_2,\ \Delta H_R = 10390 \text{ kJ/kg of C} \quad (6)$$

$$CO + H_2O \rightarrow CO_2 + H_2,\ \Delta H_R = -1470 \text{ kJ/kg of CO} \quad (7)$$

$$C + 2H_2 \rightarrow CH_4,\ \Delta H_R = -6230 \text{ kJ/kg of C} \quad (8)$$

where enthalpy of reaction $\Delta H_R < 0$ indicates exothermic reaction and $\Delta H_R > 0$ indicates endothermic reaction. Heterogeneous Reactions (2), (3), and (6) occur in the combustion zone whereas the reaction of char with species produced in the combustion zone (Reactions 4 and 8) occurs in the reduction zone. The CO produced in the combustion zone and reduction zone reacts with H_2O (Reaction 7) in the downstream zones. The net enthalpy of the global air-steam gasification process can be kept at zero (adiabatic gasification) by feeding the gasifier with the appropriate air/steam ratio. The rate of the above reactions depends principally on temperature, pressure, species concentration, and

particle size, and it can be estimated using the Arrehenius law. The time scales for heterogeneous reactions are much longer compared to those of the homogeneous reactions. Assuming the single-particle model and accounting the simultaneous effects of diffusion and intrinsic chemical kinetics, the rate of reaction of the heterogeneous reactions of char with O_2, H_2O, CO_2, and H_2 can be estimated with Equation (9) [30][31].

$$\overset{\circ}{W}_j = \frac{[C_i]}{\frac{1}{K_m} + \frac{1}{K_j}} A_p \nu_p \tag{9}$$

$$K_j = A_j \exp(-\frac{E_j}{R_u T_s}) \tag{10}$$

$$A_p \nu_p = \frac{6\,(1-\varepsilon)}{d_p} \tag{11}$$

$$K_m = \frac{2.06 U_G}{\varepsilon} R_E^{-0.575} S_C^{-2/3} \tag{12}$$

where $\overset{\circ}{W}_j$ is the reaction rate (kmol m^{-3} s^{-1}) per unit char mole consumed, j is the reaction number (2, 3, 4, 6, and 8), i is the oxidizer (O_2, CO_2, H_2O, and H_2), d_p the diameter of the particle (m), C_i the oxidizer concentration (kmol m^{-3}), K_j the kinetics constant (m s^{-1}), K_m the diffusion constant (m s^{-1}), □ the bed porosity (fraction) or void fraction, Re the particle Reynolds number, and S_C the particle Schmidt number.

The reaction rate of the homogenous equation of CO with O_2 and H_2O can be estimated with Equations (13) and (14) respectively [31].

$$\overset{\circ}{W}_5 = \varepsilon K_5 [CO][O_2][H_2O]^{-0.5} \quad (13)$$

$$\overset{\circ}{W}_7 = \varepsilon K_7 \{[CO][H_2O] - \frac{[CO_2][H_2]}{K_E}\} \quad (14)$$

In Equation (14), K_5 is the kinetic constant of the reaction of CO with O_2 whereas K_7 and K_E correspond to kinetics and equilibrium constants of the water shift reaction, respectively. Di Blasi et al. [31] present the following equation to estimate the pyrolysis reaction rate (kg m^{-3} s^{-1}), where $\varphi_{biomass}$ is the biomass density (kg m^{-3}).

$$\overset{\circ}{W}_1 = K_1 \varphi_{biomass} \quad (15)$$

The kinetic constants used to estimate the reaction rates of global Reactions (2-10) which occur in gasification processes are summarized in Table 2. The kinetic constant of the pyrolysis reaction (K_1) corresponds to wood.

The primary products in combustion and gasification of char with O_2 are CO and CO_2. According to Walker et al. [32], the CO/CO_2 reaction rate ratio increases with temperature. Annamalai et al. [33] states that the reaction rate of the C with O_2 to produce CO_2 is significant at lower temperatures ($T < 800$ K) and that the Reaction 3 is important under typical combustion conditions.

Table 2. Kinetics constants

Kinetics Constant	Value	Source
K_1	$1.516 \times 10^3 \exp(-75549/T_s)$ (s^{-1})	Di Blasi et al. [31]
K_E	$0.0265 \times \exp(-3966/T_G)$ ($s\ m^{-3}mol^{-1)}$	Di Blasi et al. [31]
K_2	$1.6 \times 10^5 \exp(-20000/T_s)$ ($m\ s^{-1}$)	Annamalai et al. [34]
K_3	$2.3 \exp(-11100/T_s)$ ($m\ s^{-1}$)	Hobbs et al. [30]
K_4	$589 \exp(-26800/T_s)$ ($m\ s^{-1}$)	Hobbs et al. [30]
K_5	$1.3 \times 10^{11} \exp(-15105/T_s)$ ($m\ s^{-1}$)	Di Blasi et al. [31]
K_6	$589 \exp(-26800/T_s)$ ($m\ s^{-1}$)	Hobbs et al. [30]
K_7	$2.78 \times \exp(-1513/T_G)$ ($m^3\ mol\ s^{-1}$)	Di Blasi et al. [31]
K_8	$589 \times 10^{-3} \exp(-26800/T_s)$ ($m\ s^{-1}$)	Hobbs et al. [30]

However, under gasification conditions, the concentration of oxygen reduces immensely and the concentrations of CO_2 and H_2O become significant. Under these conditions, Reactions 4 and 6 are significant, especially at high temperatures. Following [33], the reaction rate ($kg/kmol.m^2$) can be estimated with Equation 16 for temperatures ranging between 730 and 1170 K.

$$\frac{\dot{m}_{CO}}{\dot{m}_{CO_2}} = 2500 \exp(-6240/T_s) \tag{16}$$

where T_s is the char particle surface temperature, which can be estimated with Equation 17 for a char particle burning under diffusion controlled conditions and without including radiactive losses [33].

$$\frac{c_P(T_S - T_\infty)}{h_C} = B \tag{17}$$

$$B = \frac{Y_{O2_\infty}}{\nu_{O2,3}} \tag{18}$$

where T_s is the surface temperature of the particle (K), c_p the specific heat of the oxidizer (kJ/kg.K), Y_{O2_∞} mass fraction of the oxidizer, $\nu_{O2,3}$=1.33, and h_c reaction enthalpy (kJ/ kg of C burned to produce CO) of Reaction (3). According to [34] and [35], the oxidation of char with oxygen under gasification conditions (low concentrations of O_2) with particle size greater than 1/4" is diffusion controlled.

2.2. Previous studies on gasification of cattle biomass

In this section some relevant previous studies on gasification of cattle biomass are presented (CB).

As early as 1948, a modeling study was developed by Parents et al. [36] to estimate the equilibrium enthalpy changes and equilibrium species (CO, H_2, H_2O, CO_2, and CH_4) of char-steam-oxygen reactions as a function of the temperature and pressure. The information is also available in Klass [5].

$$C_{(s)} + aO_2 + bH_2O \rightarrow cH_2O + dCO + eCO_2 + fH_2 + gCH_4 \tag{19}$$

The oxygen-to-steam ratio required to maintain the enthalpy change for the assumed products species (Equation 19) at zero is represented in Table 3 for various pressures and equilibrium temperatures. The results show that at constant pressure, increased temperatures require increased oxygen/steam ratios to maintain a net enthalpy change of zero in the reaction, because more H_2O reacts with C to produce H_2 and CO. On the other hand, at constant temperature, increased pressures require decreased oxygen/steam ratios, because more CO_2 is produced at high pressure.

Table 3 Oxygen-to-steam ratio required for the adiabatic equilibrium reaction C-oxygen-steam, adapted from [5]

	Oxygen-to-steam ratio (SATP m3/kg) at indicated pressure				
Temperature (K)	0.1013 MPa	1.0133 MPa	2.0265 MPa	3.0398 MPa	4.0530 MPa
900	3.10	1.10	1.00	0.80	0.70
1000	6.80	2.60	2.00	1.60	1.40
1100	10.90	5.40	4.00	3.20	2.90
1200	11.70	8.80	6.70	6.00	5.30
1300		11.10	9.70	8.70	8.10
1400	12.80	11.90	11.20	10.60	10.30
1500	13.00	12.10	11.90	11.70	11.40

In 1980, Raman et al. [37] studied the effect of the temperature on yield, gas composition, and energy recovery. The study was performed on fluidized gasification of feedlot biomass (FB) using, as oxidizer, a mixture of gases (H_2O, O_2, and CO_2) produced by combusting propane with air. A small-scale fluidized gasifier, designed initially for coal gasification, was used for the investigation and operated under the following conditions: reactor temperature ranging from 900 to 994 K and flow rate of FB varying from 10 to 20 kg/h. To maintain the desired temperature and reduced oxygen concentration in the reactor, propane was burned in the plenum under starved air

conditions, i.e., propane was burned with oxygen deficit to avoid O_2 in the products. They concluded that increasing the gasifier temperature improves the yield and energy recovery.

Table 4. Results on yield and gas composition reported for an experimental bed reactor temperature at 980 K, adapted from [37]

	Dry off Gas[a]	Dry burned Gas[b]	*Dry produced Gas*[c]
H_2, (%)	14.03	4.25	38.69
N_2, (%)	56.48	78.89	0.0
CH_4, (%)	4.31	0.20	14.67
CO, (%)	11.07	5.10	26.12
CO_2, (%)	11.42	11.57	11.06
C_2H_4, (%)	1.75		1.76
C_2H_6, (%)	0.44		6.16
C_3H_6, (%)	0.50		1.54
Volumetric rate, Nm^3/h	17.38	12.44	4.94

[a] Gases measured at the top of the gasifier (leaving the gasifier)
[b] Gases produced by combustion of propane with air (measured at the plenum)
[c] Gases estimated as dry off gas - dry burned gas

Table 4 shows the gas composition produced by the combustion of propane (dry burned gas), the gas composition leaving the gasifier (dry off gas), and the gas produced by gasification (dry produced gas). The gas produced by FB (calculated as the difference between dry off gas and dry burned gas) shows a high concentration of CO and H_2, because the composition is estimated without the presence of N_2. However; the dry off gas (gases leaving the gasifier) shows a lower amount of CO and H_2.

Figure 9 shows the effect of the reactor temperature on the percentage of energy recovery (energy in gases/energy in fuel). Increasing reactor temperature from ~900 to ~980 K increases the percentage of energy recovery from 20 to 60%.

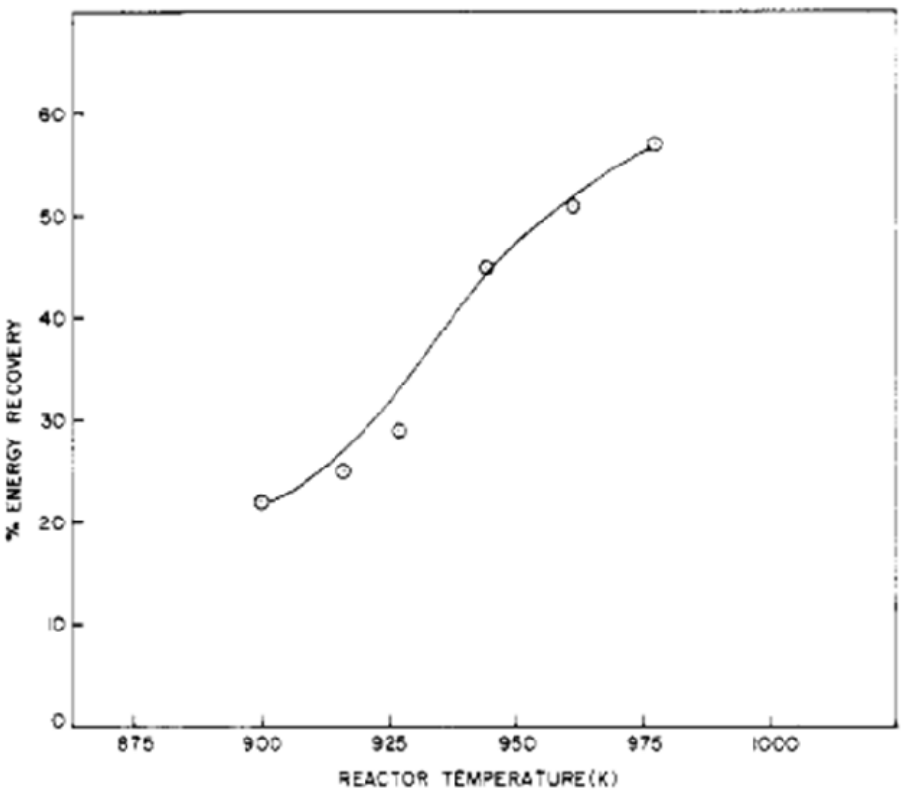

Figure 9. Energy recovery as a function of reactor temperature, from [37]

In 1987, gasification of Texas lignite coal was studied by L. R. Russell et al. [38] in a pilot-scale fluidized bed reactor at 810 kPa using, as an oxidizer, a mixture of pure oxygen and steam, preheated to 800 K. The experiments were performed at gasifier temperatures ranging between 1030 and 1200ºC and at molar steam-coal ratio ranging between 1 and 2.5. The reported results showed that the operating temperature had the maximum effect on gas composition. A typical gas mixture 5 cm above the bed of the gasifier, where the temperature was 1118 K and molar steam/coal ratio was at 2.27, was found to be 45% H_2, 13.8% CO, 33% CO_2, 5.3% CH_4 and 1.8% N_2. The H_2/CO ratios in the products ranged between 1.5 and 4.5 under the operating conditions.

A modeling study to estimate the feasibility of producing energy from non-adiabatic gasification of DB, using a system previously developed for gasification of coal (Figure 10), was developed by Young et al. [39] in 2003.

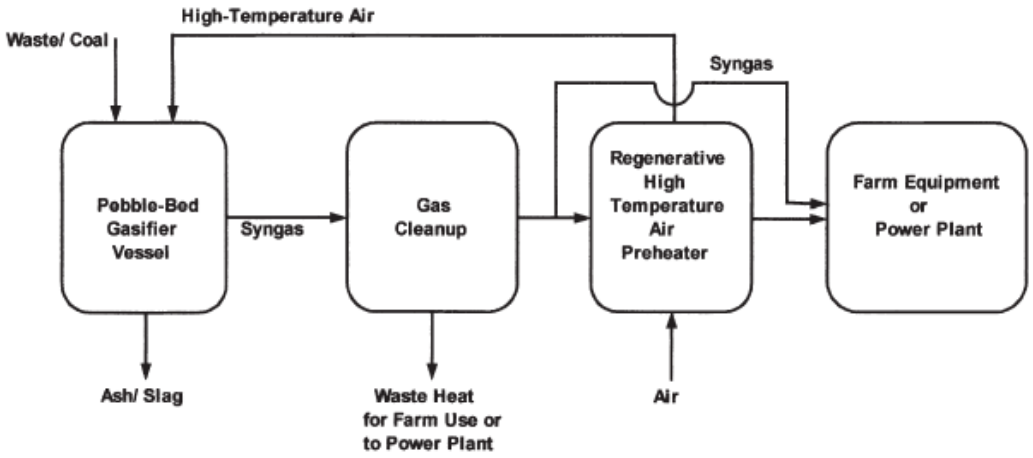

Figure 10. Gasification system used to study the feasibility of production of energy from dairy biomass, from [39]

They estimated the performance of the coal gasification facility represented in Figure 6 when it is operated with DB under the following operating conditions: air preheated at 1500 K, pressure at 100 kPa, and variable air/fuel ratio with the purpose of changing reaction temperature.

The results of performance calculations indicated energy conversion efficiency ranging from 65 to 85%, depending on the operating conditions. The gas composition, which was estimated with an equilibrium model at a reaction temperature of 1676 K, was reported to be 26.9% CO, 6.1% CO_2, 17.1% H_2, and 49.9% N_2. The estimated heating value of this gas mixture was 5090 kJ/kg.

In 2005, Priyadarsan et al. [25] conducted gasification experiments at ambient pressures using two flows of pure air (1.27 standard m^3 h^{-1} and 1.7 standard m^3 h^{-1}) for partial oxidation in a small scale (10 kW, or 30000 Btu/h) fixed-bed gasifier but without an ash disposal system. As such, steady state could not be maintained during the experiments. The fuels tested included FB, Wyoming sub-bituminous coal (WYC), and WYC-FB blends of two different particle sizes. They concluded that particle size did not affect the species composition and the bed profile temperature. They collected the gas samples and used an HP 6890 gas chromatograph to measure the concentrations of CO, CO_2, CH_4, and H_2. The gas composition measured at the top of the gasifier during the investigation was almost constant at (7-10% of H_2), (27-30% of CO), (1-3% of CH_4), and (2-6% of CO_2). Additionally, this study showed that the bed temperature profile peaked where the combustion (char oxidation) occurs.

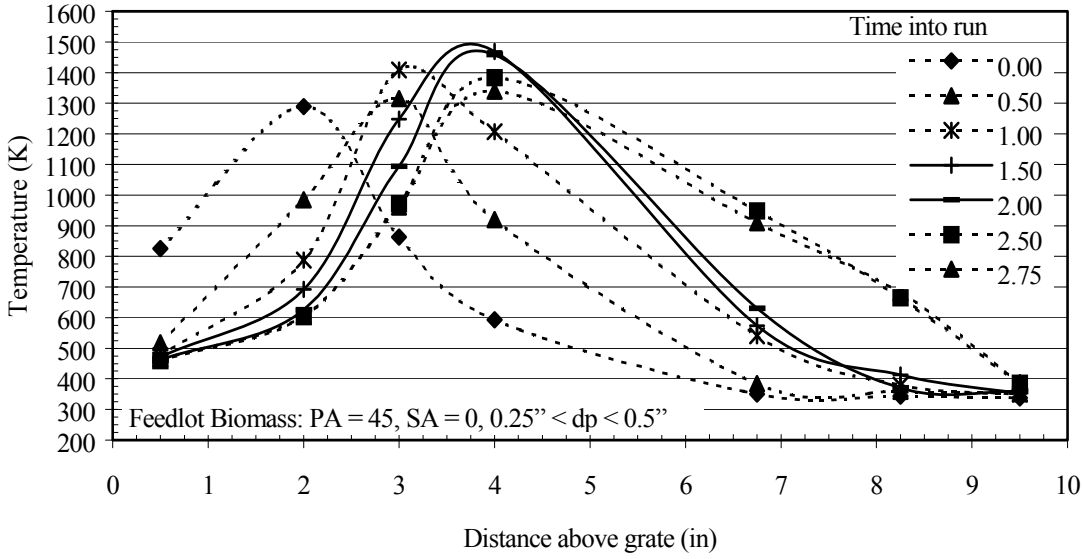

Figure 11. Temperature profile for FB (0.25" – 0.5") at air flow rate of 45 SCFH (experiment run for 2.75 hours), from [42]

As mentioned earlier, the peak started moving toward the bed surface because ash was not removed; it accumulated at the bottom creating a dead zone at the bottom of the bed, using a simple model they predicted the movement of peak temperature location with time, Figure 11.

Figure 12 shows the results of temperature and species profile obtained for FB gasification with an air flow of 45 SCFH at t = 15 min. For this particular case, the peak temperature occurred at ~2.25 in above of the grate; beyond which it started to decrease to 700 K. The CO measured through the bed shows some small changes near the grate but achieved steady state at ~ 27%; On the other hand, the production of other gases (H_2, CO_2, and CH_4) increases with distance above the grate surface.

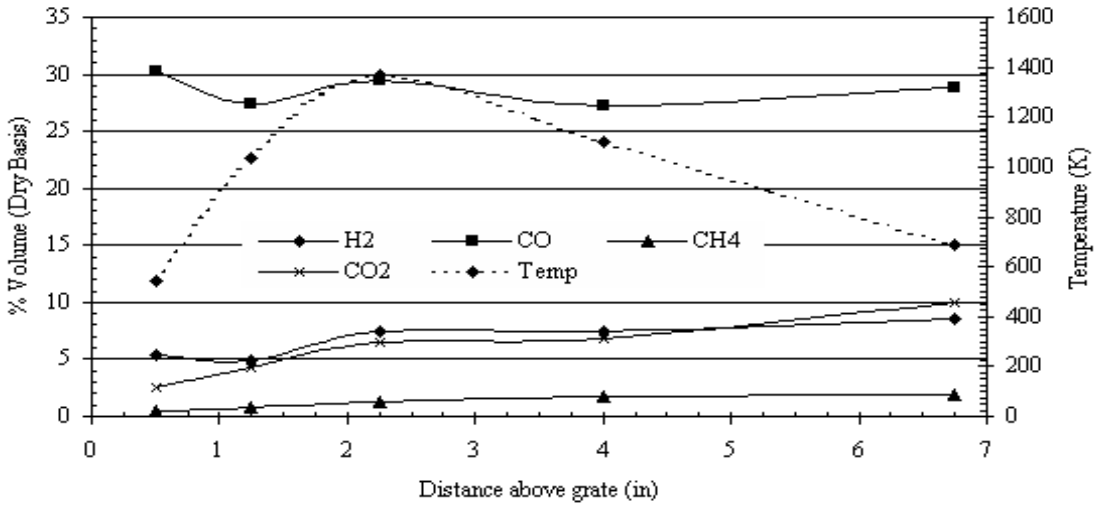

Figure 12. Gas specie and temperature profile measured along of the bed for FB gasification at flow rate of 45 SCFH and particulate size (0.157”- 0.25”), from [42]

From the results shown in Table 5 compared to adiabatic gasification of FB with air, it is apparent that non-adiabatic gasification of FB with gases produced from combusting propane (at 980 K) in a fluidized bed produces more H_2 (14.03%) and hydrocarbons (CH_4, C_2H_4, C_2H_6, and C_3H_6) and less CO. Raman et al. [37] used as oxidizing source gases with 4.25% H_2 content whereas Priyadarsan et al. [25] used pure air. If the H_2 (4.25%) in the oxidizer were discounted from the gases produced by Raman et al. [37], the hydrogen content in gases produced by the fluidized and fixed beds would be the same (Table 5). The HHV of gas produced by fluidized-bed gasification is higher than the HHV of gas produced by fixed bed gasification because of the high energy density of the hydrocarbons (HHV of HC=38000 kJ/m^3) compared to the energy density of CO and H_2 (~11,000 kJ/m^3).

Table 5. Gas composition and HHV of gases reported by Pattabhi, R, 1980 [37] and Priyadarsan, 2000 [25] for gasification of FB in a fluidized bed reactor at 980 K and an adiabatic fixed reactor respectively

	Fluidized -bed gasification with gas produced from methane combustion at 980 K [37]	Adiabatic fixed-bed gasification with air [25]
H_2, %	14.03	8.50
N_2, %	56.48	57.5
CH_4, %	4.31	1.5
CO, %	11.07	28.5
CO_2, %	11.42	4
C_2H_4,%	1.75	
C_2,H_6,%	0.44	
C_3H_6, %	0.50	
HHV	5763 kJ/Nm^3	4825 kJ/Nm^3

Table 6. Summary of review on gasification

Subject	Fuel	Operating Conditions	Products	HHV	ECE
Fluidized Bed [38]	TXL Coal	P = 810 kPa $T_{reactor}$ = 1118 °C Oxidizer = steam+O_2, $T_{Oxidizer}$ = 800 K S:F = 2.27	H_2=45.7% CO=13.8% CO_2=33% CH_4=5.3% N_2=1.8%	10494 kJ/kg	
Fluidized bed [40]	Subbituminous Powder River Coal	P = 3.03 MPa Oxidizer = Steam +Air, Coal = 31.8 kg/h Air = 27.5 kg/h Steam = 7.2 kg/h	H_2=19% CO=12% CO_2=12%	3533 kJ/kg	
Counter-Flow Fixed gasifier [41]	Rice husk	Feedstock = 10 kg/h SR = 0.12 $T_{reactor}$ = 600 °C measured at bed center	H_2 =7 .4% CO = 25% CO_2 = 16.9% CH_4 = 2.5% N_2 = 56%	4005 kJ/kg	
Counter Flow Fixed gasifier [6]	Nutshells	Oxidizer= Air Air/fuel=1.159	H_2 = 6-7.3% CO = 28.4-30% CO_2 = 6.7-7% CH_4 = 1.7-1.9% N_2 = 56%	5.3 to 5.6 MJ/kg	
Counter Flow Fixed gasifier [6]	Olive Husk	Oxidizer= Air Air/fuel=1.38	H_2 = 6.4-8% CO = 26.2-28.5% CO_2 = 7.5-6.2% CH_4 = 1.4-1.6% N_2 = 56%	4.8 to 8.5 MJ/kg	
Fluidized bed [37]	Feedlot Biomass	Oxidizer= Gases from combustion of propane T=900-994 °C Fuel=10-20 kg/h	H_2 = 14.3% CO = 11.7% CO_2 = 11.42% CH_4 = 4.31% C_2H_4 = 1.75 N_2 = 56.48%	5763 kJ/kg	20 to 60%
Counter Flow Fixed gasifier [25]	Feedlot Biomass	Oxidizer=air Air Flow=1.7-1.7 STAP m^3/h	H_2 = 7-10% CO = 27-30% CO_2 = 2-6% CH_4 = 1-3%	4825 kJ/kg	
Fluidized bed modeling [39]	Dairy Biomass	Oxidizer = Air at 1227 °C P = 100kPa $T_{gasifier}$ = 1400 °C	H_2 = 17.1% CO = 26.9% CO_2 = 6.1% N_2 = 49.9%	5090 kJ/kg	65 to 85%

From the literature review, it is apparent that there no published studies use air and steam in fixed-bed gasifiers with DB as fuel and operate under steady state conditions. Moreover, in fluidized-bed gasification, the oxygen concentration is nearly uniformly

throughout the bed, which oxidizes some H_2 produced by steam reforming reactions; therefore, H_2 production is typically less. Because the present study uses a fixed-bed reactor with a temperature peak within the bed and oxygen is available only near the bottom of bed, H_2 production should be enhanced with air-steam mixtures. A summary of review on gasification is presented in Table 6.

3. OBJECTIVE AND TASKS

The overall objective of the current research is to conduct an *in situ* gasification of dairy biomass (DB) using a fixed bed gasifier. To achieve the overall objective, the following tasks must be performed.

1. Modify the gasifier facility (10 kW or 30,000 Btu/h).
2. Build a steam generator to feed steam into the gasifier plenum.
    a. Construct an ash disposal system to run experiments under steady-state conditions.
    b. Acquire a mass spectrometer (MS) and the gas mixtures necessary to calibrate the MS.
    c. Perform calibration and analysis set-up on the MS.
    d. Mount a temperature data acquisition system.
    e. Develop a sampling system to prepare the gas samples to be analyzed by a mass spectrometer (MS).
    f. Install a heater system to heat the gasifier.
    g. Set up a control panel to control the gasifier operating conditions.
    h. Assemble the gasification facility.
3. Characterize the feedstocks.
4. Perform global modeling studies on gasification to determine operating conditions.
5. Conduct experiments on gasification with air, air-steam, and obtain data on bed temperature profile and gas composition under various operating conditions and verify that the system operate near adiabatic conditions.

6. Produce chlorinated char via pure pyrolysis of DB using N_2 and N_2-steam gas mixtures.

4. EXPERIMENTAL SET UP AND PROCEDURE

This section presents a description of the experimental facility and the procedure developed for each task.

4.1. Modifications

A 10-kW gasifier located in the Mechanical Engineering Biomass Laboratory at Texas A&M University previously constructed by [42] was modified; they did not have ash disposal system and there was no gas conditioning system (Figure 13).

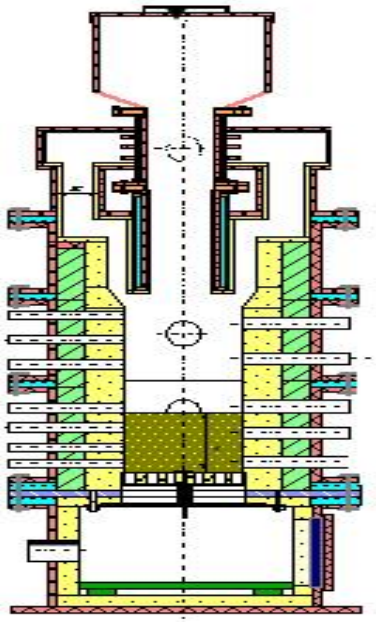

Figure 13. 10-kW fixed bed gasifier, from [42]

The gasifier represented in Figure 13 is a 10-kW batch-type, countercurrent, fixed-bed reactor. It was constructed of castable alumina refractory tube with an inner and outer diameter of 13.9 cm (6 in) and 24.5 cm (10 in) respectively. The refractory tube is surrounded by 4.45 cm (1.75 in) of insulating blanket to minimize heat losses. The blanket is enclosed within a steel outer tube with an inner diameter of 34.3 cm (13.5 in). The total height of the gasifier is 72 cm and is divided into four sections of 24 cm, 19 cm, 14 cm, and 15 cm. The sections are joined using ring type flanges of 1.27 x 35.6 x 50 cm. The following modifications were performed:

a) A steam generator was built to generate the vapor required for the gasifier. The generator supplies vapor at ~393 K and at ~1 bar. The steam generator was provided with a release valve and a water level visor to prevent overpressure and to control the water level. The steam generator was calibrated to determine the rate of evaporation as a function of power supplied to the heater elements.

b) A conical gyratory cast iron grate with 0.25-in-diameter holes was constructed. The number of holes was selected to provide 30% free area to drain the ash and to allow the oxidizer flow. To evacuate continuously ash from the gasification chamber to the plenum, the grate was constantly vibrated by a pneumatic vibrator of variable frequency. The ash evacuation rate from the chamber was controlled by changing the vibration frequency of the vibrator. The gasifier plenum was modified to assemble the conical vibratory grate. The refractory of the plenum was constructed and the plenum base was drilled to assemble the shaft that supports the conical grate. The

shaft was fixed to the base of the plenum by a mechanical seal to avoid pressure looses. A pneumatic mechanical vibrator was coupled to the shaft to vibrate the grate.

c) A mass spectrometer was acquired to continuously measure the concentrations of CO_2, CO, CH_4, C_2H_6, H_2 and N_2 in real time. Also, gas mixtures required to calibrate the MS for each gas analyzed were acquired. The list of calibration mixtures is presented in Appendix F.

d) Eight temperature ports were placed along of the gasifier axis in order to measure the temperatures with Type K thermocouples.

e) A temperature recorder was acquired to monitor temperatures continuously. The data were stored in a flash card for later analysis.

f) Several sampling ports were provided along of the reactor.

g) A sampling system was constructed to prepare the samples before they were analyzed by the MS in real time and continuously because the MS cannot allow particles or tar to enter the system.

h) Although most of the experiments were performed adiabatically, the experiment facility also has a heater system, which consists of two super-heater elements regulated by a power controller to maintain a desired temperature in the gasifier if non-adiabatic gasification is required or to supply heat for pyrolysis of fuel when char production is desired in absence of oxidant. A new combustion chamber was constructed to install the heater elements.

i) A control panel was built to control the flows of air and steam into the gasifier, the flows of heat to the heater elements of the reactor and the steam generator, and the

gas sample flow through the sampling unit. Additionally, the devise for monitoring and recording the temperature also was mounted to the control panel.

Pictures of the modification performed in the gasifier are presented in the Appendix A.

4.2. Gasification facility

Figure 14 shows a schematic of the 10-kW gasification facility with all modifications. The facility consist of i) a steam generator to produce the steam for the gasifier, ii) an ash evacuation system so that experiments can be run continuously with periodic ash disposal, iii) a sampling system to condition the gas samples for real time and continuous analysis of gases, iv) a data acquisition system to monitor the evolution of the temperature profiles within the gasifier bed, and v) a control panel to control the flows of steam and air, and heat to the heater elements placed in the steam generator and the gasifier. Periodically fuel is fed at the top of the facility, while the mixture of air and steam is supplied at the bottom (plenum).The air and steam (water) flow rate are controlled by using rotameters. i) Steam Generator: The steam generator has a cylindrical 10-cm-internal-diameter vessel heated by a variable-power (0.1-1.2 kW) tape-type heating element rolled around the vessel. The rate of steam generated (0.1-1.5 kg h^{-1}) can be controlled by changing the power supplied to the heating element. The steam generator was calibrated to measure the rate of vapor produced as a function of the power input. ii) Ash Evacuation System: The facility has an ash evacuation system

compose of a conical grate which was continuously vibrated by a pneumatic vibrator of variable frequency. The ash evacuation rate from the chamber can be controlled by changing the vibration frequency. The grate can also be rotated manually to remove the residual ash from the chamber after each experiment. iii) Sampling System: The facility has provisions to withdraw samples from different ports placed along of the gasifier. The sampling system is composed of two condensers each of which was cooled with ice-cold water to condense water and tar and three filters to capture the particulate material. After the samples are conditioned, they are continuously analyzed in real time by the MS. The composition of the gases is stored in a computer for posterior analysis. iv) Data Acquisition System: The temperature of the bed is measured every 60 seconds using Type-k thermocouples placed at eight locations along the gasifier axis. The temperature data is recorded into a flash card. v) Control Panel: The air, steam, and samples flow rates are regulated from a panel control. Also, the power supplied to the heater elements is controlled from the control panel. The temperature recorder is assembled in the control panel to monitor temperatures.

The adiabaticity of the reactor was checked by determining the overall heat transfer coefficient (U) and then estimating the heat loss; the U was measured by letting the reactor to cool down after the experiment and storing the change of temperature.

Appendix A presents figures of the modifications performed on the gasifier at Texas A&M University along with pictures of the reformed gasified facility.

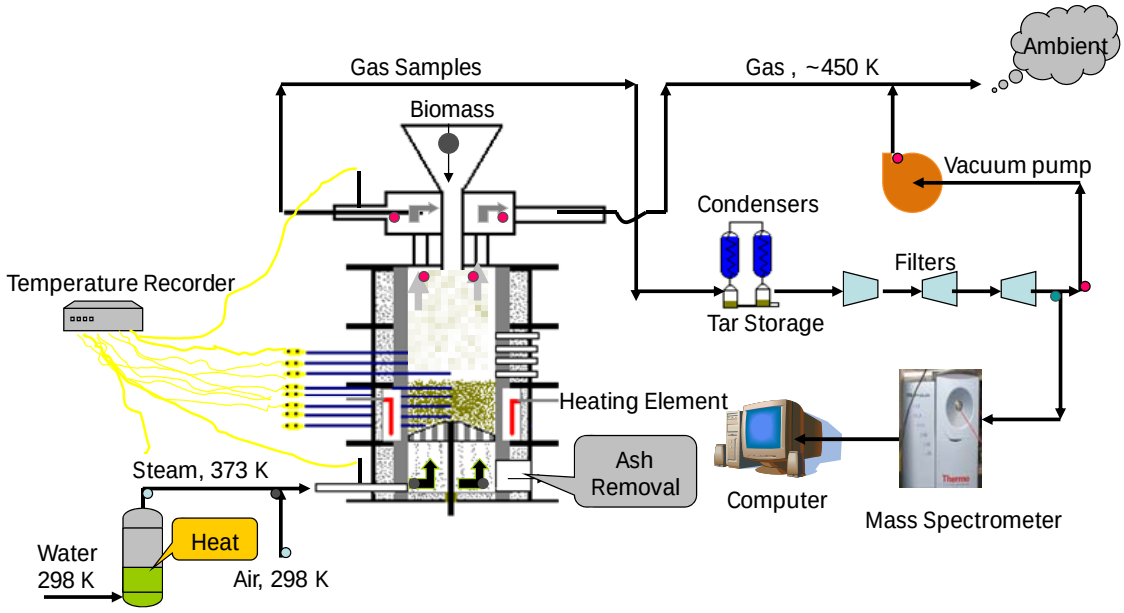

Figure 14. Gasification facility

4.3. Experimentation

Experiments on fixed-bed gasification of DB were performed to study the effect of the ER and S:F ratio on gas composition and bed-temperature profile. The gasification experiments were performed for the following cases:

a) Base case

- Bed height at 17 cm (~6.75 in)
- Fuel: Low-Ash separed solids dairy biomass (LA-PC-sepsol-DB).
- Particulate size, d_p = ~6.25 cm (o.25 in) for DB and ~3 mm (~0.125 in) for coal
- Fuel flow rate 1 kg h^{-1} (2.2 lb_m h^{-1})
- Air flow ~1.13 normal m^3h^{-1} (40 SCFH) at 298 K (536 R)

- Steam flow rate at 0.3 kg/h (~0.66 $lb_m\ h^{-1}$)
- Equivalence ratio (ER) at 3.18
- Steam-to-fuel ratio (S:F) at 0.68

b) Parametric cases

- Fuel: LA-PC-Sepsol-DB, Coal-LA-PC-Sepsol-DB blend (90% LA-PC-Spsol-DB, 10% Coal), and Ash - LA-PC-Sepsol-DB blend (90% LA-PC-Sepsol-DB, 10% ash)
- Air flow between 0.57 and 2.26 normal $m^3\ h^{-1}$ (20 and 80 SCFH) at 298 K (536.4 R)
- Steam flow rate between 0.18 and 0.5 kg h^{-1}(0.4 and 1.1 $lb_m\ h^{-1}$) at 373 K (671.4 °R)
- Equivalence ratio (ER) between 1.59 and 6.36
- Steam-to-fuel ratio (S:F) between 0.35 and 0.8

Experiments with i) DB-coal blends (90% DB-10% coal) ii) DB-ash blends (90% DB-10% ash) were used to determine catalytic effect if there was a on gasification.

4.3.1.Experimental procedure

A typical experiment started with preheating the gasifier with a propane torch placed under the grate to heat the grate and combustion chamber. When the temperature at a location 2 cm above the grate reached 1073 K (1931.4 °R) (~after 2 h) the torch was turned off and biomass was added to the gasifier; addition continued until the bed height

attained 17 cm (~6.75 in). Subsequently, the fuel port was closed and the flows of steam and air were adjusted to the desired experimental conditions. As the biomass was pyrolyzed and the char was burned, the bed height decreased and ash accumulated; thus, biomass was added every 10 min and in batches as required. The bed temperatures were also measured. In the earlier batch experiments by Priyadarsan et al. [25] , there was no ash disposal system; therefore, the temperature peak shifted towards the bed surface because ash accumulated at the gasifier bottom. In the experiments discussed here, the ash was removed periodically using a vibrator at the bottom of the grate to maintain the peak temperature at the same location. When the temperatures achieved pseudo-steady state (~1 h) the gas sampling unit was turned on and the gas analysis was performed continuously by the mass spectrometer (MS) for ~20 min. The samples were taken from the gasifier top and passed through the sampling system to condense tar and steam, and to filter out the particles in the gases to protect the MS from possible damage. The temperatures were measured at 60-s intervals and at eight locations along the gasifier axis. The collected tar was characterized using ultimate and proximate analysis. Samples of ash were collected to determine if char was present. The experimental data were analyzed and the resulting temperature profiles, peak temperatures, gas composition, HHV, and energy conversion efficiency are presented as a function of ER and S: F ratio. Additionally, the experimental data were compared with the data estimated from modeling.

The MS was calibrated every 72 h under a program that considers the effects of linearity, sensibility and overlapping of all the possible gas peaks analyzed. After

calibration, mixtures of well-known composition were analyzed using the MS to verify the calibration accuracy Additionally, a program for analyzing CO_2, CO, CH_4, C_2H_6, H_2 and N_2 was performed on the MS to control the peaks measured. The peaks were determined by the molecular weight of each gas and the ion charge. The ions can have a charge of 1e, 2e, and occasionally 3e depending if they have one, two, or three electrons removed during the ionization process. The peaks are defined as: M/charge, e.g., for N_2, 28/1, 28/2, 28/3, etc.

4.3.2.Pyrolysis procedure

The same gasification facility used for gasification experiments was used to perform the pyrolysis experiments. DB was subjected to a pyrolysis process to volatilize a fraction of the VM content and to produce chlorinated carbon. Two types of char were produced using i) 0.142 SATP m^3/h (5 SCFH) of pure N_2 and ii) a mixture made of 0.142 SATP m^3/h of N_2 and 1.53 m^3/h of steam as carrier gases.

A typical experiment started by preheating the empty gasifier with a propane torch placed under the grate to heat the grate and the combustion chamber. When the temperature at a location 2 cm above the grate reached ~1073 K (~after 2 h) the torch was turned off and biomass was added to the gasifier; subsequently, the fuel port was closed and the flow of carrier gas was adjusted to the desired experimental conditions. Then, the gasifier pressure was set at 5 mm of vacuum and the gasifier was cooled down. When the maximum temperature in the gasifier achieved ~423 K, the flow of carried gas

was turned off and the gasifier was closed completely to cool to ambient temperature. The temperatures were measured using Type-K thermocouple at 60-s intervals and at eight locations along the gasifier axis during the heating and cooling period. Gas samples were not analyzed. When the gasifier temperature reached approximately ambient temperature, char samples were collected and weighed to determine the amount of mass pyrolyzed. They were analyzed using ultimate and proximate analysis. The experimental data were analyzed and the resulting temperature profiles are presented in the results section.

4.3.3.Calibration of the steam generator

The steam generator was calibrated to insure the flow of steam supplied to the gasifier. The calibration curves are presented in this section.

Figure 15 shows the rate of water evaporated by the steam generator vs the percentage of power supplied to the heater element surrounding the steam generator pipe. Although the calibration curve assures a reliable flow of steam leaving the steam generator, a glass pipe visor was installed to monitor the level of water in the steam generator. During the experiments the water level was maintained constant to insure that the rate of steam leaving the steam generator corresponded to the rate of water entering. The rate of water entering to the steam generator was controlled by a liquid flow controller while the power supplied to the heater element was controlled using a power

controller. The steady-state operation of the steam generator was verified before each experiment with the purpose of insuring a constant flow of steam entered the gasifier.

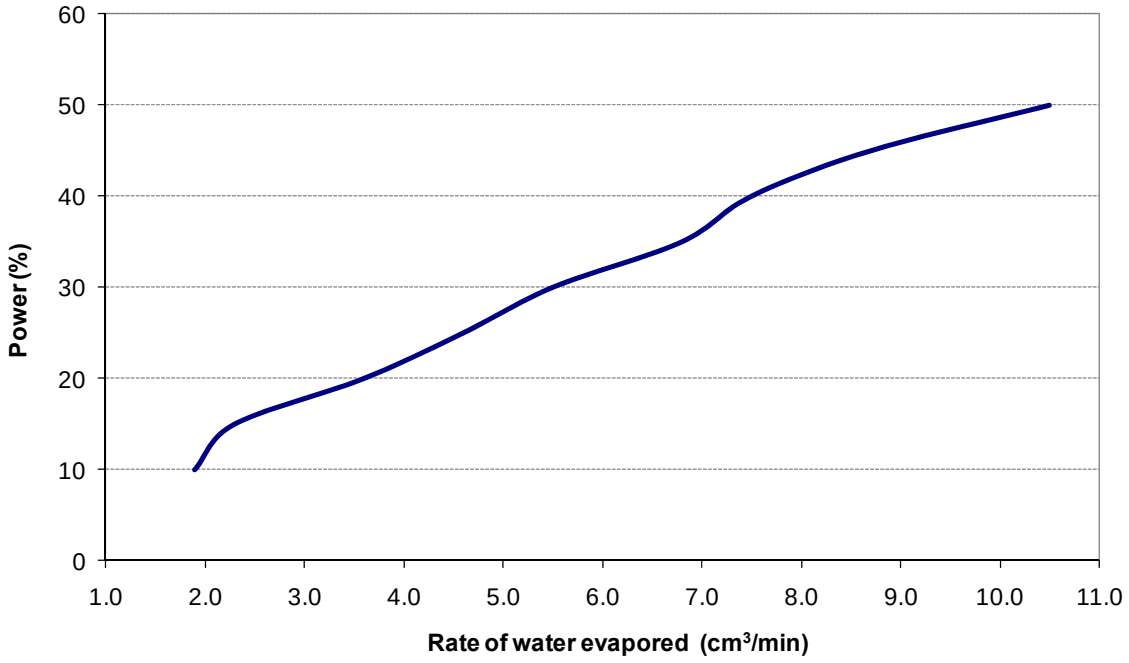

Figure 15. Rate of vapor produced by the steam generator as a function of the power supplied

4.3.4. Verification of adiabaticity of the gasifier

The global heat transfer coefficient of the gasifier was estimated using the lumped capacitance method [43]. Taking as control volume the air and the refractory tube in the gasifier, neglecting the temperature gradients within the control volume, and assuming the refractory tube temperature as the air temperature the maximum global heat transfer coefficient of the gasifier can be estimated by solving Equation 20. The

heat stored in the insulation layer and the external steel pipe was neglected because the insulation thermal-capacitance is negligible and the steel tube temperature is very low compared to that of the refractory tube.

$$mC_p \frac{dT_{(X,t)}}{dt} = UA_S(T_{(X,t)} - T_\infty) \tag{20}$$

where $T_{x,t}$ denotes air temperature along of the gasifier axis, T_∞ ambient temperature, m^*C_P thermal capacitance of the refractory-tube, U global heat transfer coefficient from the refractory tube to the ambient, and A_s external refractory tube surface area. The air thermal capacitance per meter of gasifier (0.023 kJ/(m.K)) was neglected because it is very low compared to that of the refractory (~57 kJ/(m.K)). Separating variables and considering C_P constant, the differential Equation 20 can be integrated to yield the ordinary linear Equation 21.

$$\mathrm{Ln}(T_{(X,t)} - T_\infty) = \mathrm{Ln}(T_{(X,0)} - T_\infty) - \frac{4UD}{(D^2 - d^2)C_p\varphi}t \tag{21}$$

In Equation 21 D and d are the refractory tube external and internal diameter, respectively and ρ the refractory density. U can be determined using experimental data to find the slope ($4UD/((D^2\text{-}d^2)C_P\,\rho)$) of Equation 21.

The cooling temperatures measured at various locations along the gasifier axis are plotted in Figure 16. The slope of the linear curves does not change much with

gasifier height, which indicates that the global heat transfer coefficient is almost constant along of the gasifier axis. The slope of the plots yield $(4UD/((D^2-d^2)C_P \rho)) = 0.0001$ or U=0.007 kW/ m^2 K. The curves of cooling temperatures do not match exactly with the lineal regressions because the global heat transfer coefficient depends on temperature.

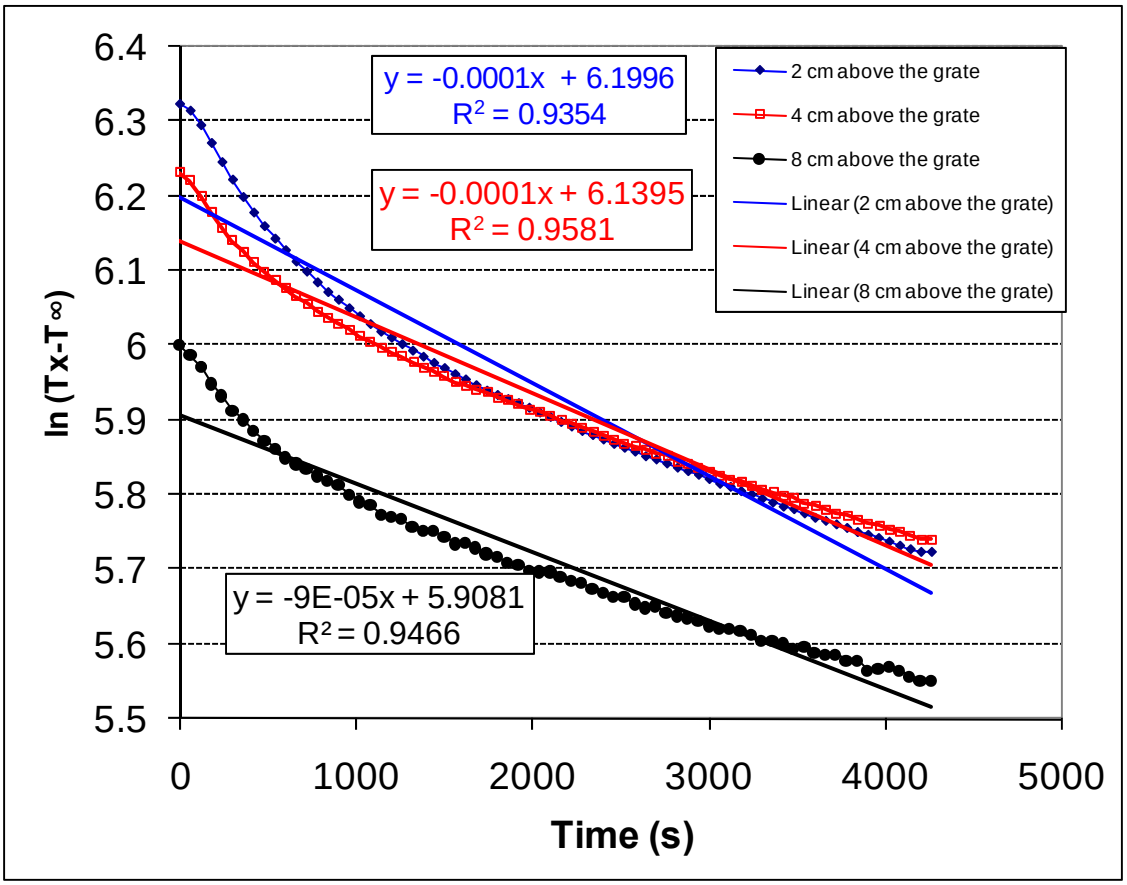

Figure 16. Dynamic log temperature measured at different locations in the gasifier

Figure 17 shows that the global transfer coefficient of the gasifier is directly proportional to temperature. In other words, increased temperatures lead to higher global heat transfer coefficients. Although the global coefficient was derived for temperatures

ranging from 350 to 500 °C, the information can be used to estimate the global heat transference coefficient at other temperatures. The results indicate that the global heat transfer coefficient of the gasifier is low *(U*=0.0001*T-0.0653 (kW/m^2.K)). The *U* estimated is higher than the real because it was derived using the maximum thermal capacitance (refractory tube) and temperature (air temperature). If real refractory tube temperature (lower than the air) were considered in the calculations the *U* value would be closer to real value.

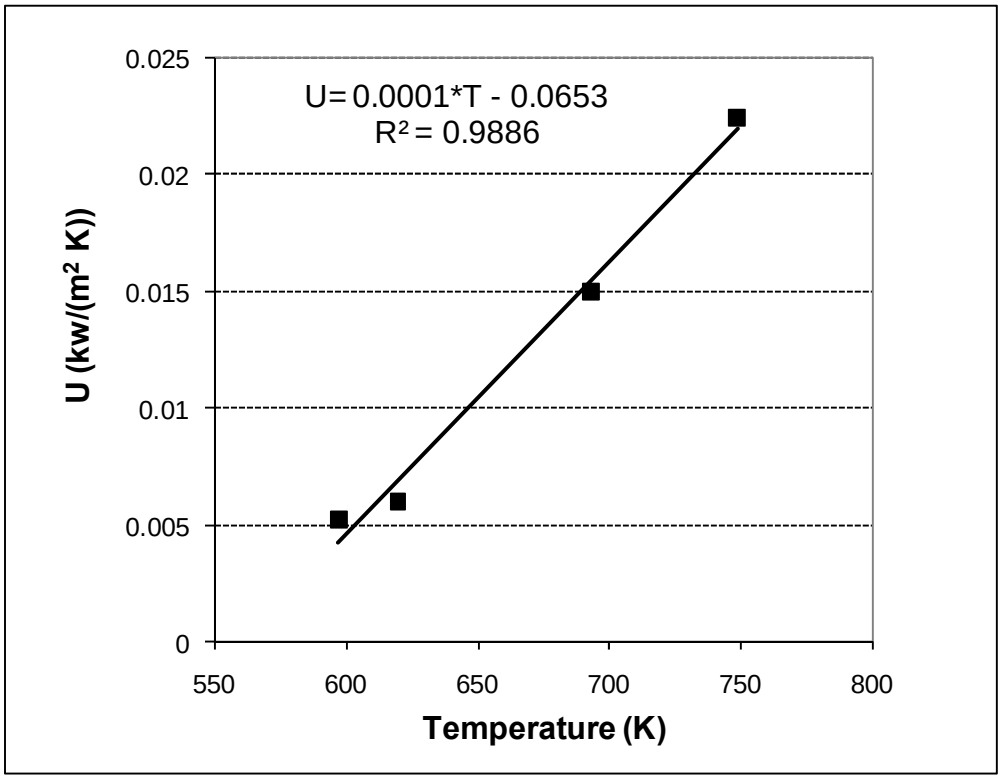

Figure 17. Global heat transfer coefficient as function of the gasifier temperature

5. MODELING

In this section, model is presented to study the effect of adiabatic temperature (T_p), ER_M, AOF, ER, and S:F on gas composition produced by gasifier when fired with DB, FB, WYC, and TXL. Two types of models are presented: 1) atom conservation with specified products gases and 2) Equilibrium model.

5.1. Atom conservation

To determine the operating conditions of the gasfier, the following analysis is conduced.

5.1.1.Maximum ER with air and air-steam

The maximum ER at which all the fixed carbon (FC) content in a fuel reacts with O_2 to produce CO or with air and steam to produce CO, H_2, and N_2 can be calculated using data from proximate analysis of the fuel.

$$CH_hO_oN_nS_s \rightarrow b'VM + c'C(s), \text{ (pyrolysis)} \quad (22)$$

$$C_{(s)} + 1/2O_2 \rightarrow CO \text{ (partial oxidation of char)} \quad (23)$$

$$HV_{Fuel,DAF} = HV_{VM}*(1-FC_{DAF}) + FC_{DAF}*HV_{FC} \quad (24)$$

where $HV_{FC} = HV_{CO}*28/12$. Using (24) one can solve for HV_{VM}.

$$HV_{VM} = \frac{HV_{Fuel,DAF} - FC_{DAF} * HV_{FC}}{1 - FC_{DAF}} \quad (25)$$

$$HV_{gas} = HV_{DAF} - \frac{FC_{DAF}\left[HV_{FC} - \left(\frac{28}{12}\right)HV_{CO}\right]}{1 + \left(\frac{16}{12}\right)\left(\frac{1}{Y_{O_2,in}}\right)FC_{DAF}} \quad (26)$$

The maximum allowable ER for oxidizing all the FC_{DAF} to CO is given as:

$$ER_{Max\ FC\rightarrow CO} = \frac{1 + h/4 + s - o/2}{c'/2} \quad (27)$$

If heat is released in partial oxidation of C to CO and is used to strip H_2 from H_2O, then more H_2 can be produced. However, additional oxygen is also available from H_2O. Then:

$$C + a'O_2 + (1-2a')H_2O_I + a'\left(\frac{N_2}{O_2}\right) \rightarrow CO + (1-2a')H_2 + a'\left(\frac{N_2}{O_2}\right),\ 2a'<1 \quad (28)$$

Letting $\Delta H_R = 0$ for Reaction 28, it can be shown that $a' = [1-(\bar{h}_{fCO} / \bar{h}_{fH2O(l)})]/2$ = 0.307 moles of O_2 for each atom mole of carbon (or 0.818 kg of oxygen per kg C); with a'=0.307mol of O_2/mol of C atom and $a''=a'$*C' mol of O_2/mol of DAF fuel. The AOF is given as $2a'$=2*0.307 and S:F=(1-2a")=(1-2*0.307c').

$$\mathrm{ER} = \frac{1 + h/4 - o/2 + s}{a'^{*}C'} \tag{29}$$

$$\mathrm{ER}_{\mathrm{M}} = \mathrm{ER} * 2a' = \frac{(1 + h/4 - o/2 + s)2}{c'} \tag{30}$$

The product mass per kg of carbon can be computed as 2.397 + 0.818*{(1-Y_{O2in})/Y_{O2in}}. Then, the maximum heat value for each kg of dry, ash-free (DAF) biomass supplied at an *adiabatic gasifier* must be the same energy leaving the products which now consists of combustible gases and nitrogen.

$$\mathrm{HV}_{\mathrm{gas,max}} = \frac{\mathrm{HV}_{\mathrm{fuel}}}{\mathrm{VM} + \mathrm{FC}\left(1.579 + \dfrac{0.818}{\mathrm{Y}_{\mathrm{O_2,in}}}\right)} \tag{31}$$

where the denominator represents the sum of the fuel mass and $N_2 + O_2$ gas mixture supplied such that all the oxygen is used in partial oxidation of C.

5.1.2.Any ER and S:F ratio

Complete combustion (theoretical or stochiometric combustion) of any fuel containing C, H, N, O, and S, with air, means that all the combustible components in the fuel are burned completely with oxygen to yield energy. Here, the heating value of the fuel is completely converted into sensible energy of products leaving the combustor.

$$\mathrm{CH}h\mathrm{O}o\mathrm{N}n\mathrm{S}s + a\mathrm{O}_2 \rightarrow= b\mathrm{CO}_2 + c\mathrm{H}_2\mathrm{O} + d\mathrm{SO}_2 \quad (32)$$

On the other hand, the gasifer requires partial oxidation of the fuel so that combustible gaseous mixture is produced. In addition to air steam is also used to promote the steam-reforming reaction in order to produces H_2-rich gas mixtures. The overall reaction of any biomass with air and steam is represented in equation 33. However, besides the species indicated as products, other reactions might occur in the gasification processes, which can produce other species in trace amount.

$$\mathrm{CH}h\mathrm{O}o\mathrm{N}n\mathrm{S}s + e(\mathrm{O}_2 + 3.76\mathrm{N2}) + f\mathrm{H2O} \rightarrow g\mathrm{CO}_2 + h\mathrm{CO} + i\mathrm{CH4} + j\mathrm{H2S} + k\mathrm{N2} + l\mathrm{H2} \quad (33)$$

where the six product species are CH_4, CO, CO_2, H_2, H_2S, and N_2, *e* corresponds to the moles supplied by air and *f* refers to the moles supplied by external steam and inherent moisture in the biomass.

Equivalence ratio (ER), which is the ratio of the actual fuel-air ratio to the theoretical fuel-air ratio, defines the rich and lean regions of the reaction. In processes where the oxidizer used in gasification is a mixture of air and steam, the equivalence ratio (ER) definition can be modified as stochiometric oxygen to actual oxygen supplied by both air and steam. Equations (34) and (35) define the equivalence ratio in two forms:

Conventional equivalence ratio (ER)

$$\mathrm{ER} = \frac{\text{stochiometric air moles}}{\text{actual air moles}} = \frac{a}{e} \tag{34}$$

Modified Equivalence Ratio (ER_M)

$$\mathrm{ER_M} = \frac{\text{Stochiometric oxygen}}{\text{Actual oxygen through air and steam}} = \frac{2a}{2e+f} \tag{35}$$

The oxygen split between the air-steam mixtures in the gasification processes depends on the ratio between the oxygen supplied by the air to the total oxygen supplied by both air and steam, this mole ratio is called the Air Oxygen Fraction mole ratio (AOF).

$$\mathrm{AOF} = \frac{\text{Oxygen through air}}{\text{Oxygen throug air and steam}} = \frac{2e}{2e+f} = \mathrm{ER_M}\left(\frac{e}{a}\right) \tag{36}$$

Note that AOF ratio does not represent the mole value of air to steam. The definition provided by Equation (36) yields a finite range of AOF from 0 (gasification only with steam, $e = 0$) to 1 (gasification of DAF biomass only with air, $f = 0$). Using Equation (34) and (36) in Equation (35).

$$\mathrm{ER_M} = \mathrm{AOF}\left(\frac{a}{e}\right) = \mathrm{ER} * \mathrm{AOF} \tag{37}$$

$$\mathrm{S:F} = \frac{\text{mols of steam}}{\text{kmol of DAF biomass}} = f \tag{38}$$

Under adiabatic gasification, the energy conservation can be represented by Equation (39).

$$\sum_k N_{k,p} h_{k,p}(T_p) = \sum_k N_{k,R} h_{k,R}(T_R) \tag{39}$$

where $N_{k,\,\mathrm{p}}$ and $h_{\,k,p}$ are the moles and enthalpies of the products at temperature T_P and $N_{k,R}$ and $h_{\,k,R}$ the moles and enthalpies of the reactants at temperature T_R. Equation 39 states that the total energy in the reactants equals the total energy in the products. Nevertheless, in gasification processes where the principal objective is to produce fuel gases, the recovered energy in the fuel gases per each fuel unit is lower than that supplied with the reactants. In other words, the energy conversion efficiency in

gasification processes is always lower than 100%. The gross heating value of the gases produced in gasification processes (HHV) can be estimated from: a) basic biomass analysis [44] and b) gas composition.

5.2. Equilibrium modeling

Equilibrium modeling has also been used to estimate the adiabatic dry gas composition for about 150 species in the product gas. The NASA equilibrium code PC version was used to solve for species including char and adiabatic temperature.

5.3. Modeling procedure

As discussed earlier, gasification of biomass with air and steam under ideal conditions yields a mixture of gases primarily composed of CO_2, CO, CH_4, H_2, and N_2 (Equation 33). Other compounds are produced in trace amounts. The molar composition of the above products under ideal kinetic gasification conditions can be predicted using a) mass and energy conservation equations and atom balance and b) chemical equilibrium with a larger number of species including char.

The effect of modified equivalence ratio ER_M and AOF on gasification of feedlot biomass (FB), dairy biomass (DB), Wyoming coal (WYC), Texas lignite coal (TXL) were estimated for comparison purposes. Composition of products such as CO, CO_2,

CH_4, N_2, and H_2, were predicted with atom balance whereas NASA equilibrium code PC version was used to predict composition of almost 150 species including char.

a) Atom balance model: A system of eight equations and eight unknowns can be solved using five equations formed from five atom balance of the components present in the biomass (C, H, O, N, and S) and three more equations: (35), (36), and (39) or Equations (34), (38), and (39). This system can be solved to obtain the moles of CO_2, CH_4, H_2, CO, N_2, and H_2S as a function of the adiabatic temperature, T_P in Equation (39), ER, and S:F or T_P, ER_M, and AOF. Annamalai et al. [45] have used this method for three reactants (fuel, O_2, and steam) and four products (CO_2, H_2, N_2, and SO_2).

Once solved for the product's species, the HHV of the gases and the energy conversion efficiency (energy recovery) of the gasifier were calculated with Equations (32) and (33).

b) Equilibrium model**:** As discussed earlier, the NASA equilibrium code PC version was used to solve for species including char and adiabatic temperature. The presence of $H_2O(g)$ in the products was not considerated in the modeling studies conducted to study the effect ER_M and AOF to compare the results to that obtained by atom model in which H_2O was not considered in the products. The NASA program was run for adiabatic conditions. The input data included the enthalpy of the reactants, reactant moles (DAF fuel, air, and total steam from both external and moisture), reactants temperature (298 K for air and 373 K for steam), and pressure. The output data were equilibrium gas composition of 150 species including solid carbon.

Atom and equilibrium modeling were developed under the operating conditions shown in Table 7. The DB is represented by the empirical formula ($CH_hN_nO_oS_s$) derived from ultimate and proximate analysis.

Table 7. Conditions used in modeling studies

Parameter	Value
Pressure (kPa)	100
Equivalence ratio (ER)	1.5-7.0
Modified equivalence ratio (ER_M)	2-8
Steam to fuel ratio (S:F)	0.35-0.80
Oxygen from air to total oxygen (AOF)	0.2-0.8
Steam temperature (K)	373
Inlet air and fuel temperature (K)	298
Temperature of products[a] (K)	873-1473

[a] only for atom mode

6. MODELING RESULTS

In this section results of modeling studies are presented. Tables on gas composition as a function of the AOF, ER_M, and T_P are presented in Appendix C for WYC, TXL, DB, and FB. this appendix also presents tables of DB as a function of ER and S:F ratio. Prior to the experimental gasification with air-steam of dairy biomass (DB), adiabatic atom balance and equilibrium model were performed to predict the effect of operating conditions, such as equivalence ratio (ER) and (S: F) on gas composition, HHV of the gases, and energy conversion efficiency for DB gasification. The effect of modified equivalence ratio ERM and AOF on gasification of feedlot biomass (FB), dairy biomass (DB), Wyoming coal (WYC), Texas lignite coal (TXL) were estimated for comparison purposes. Composition of products such as CO, CO_2, CH_4, N_2, and H_2, were predicted with atom balance whereas NASA equilibrium code PC version was used to predict composition of almost 150 species including char.

6.1. Atom conservation

This section presents the effects of the adiabatic temperature (T_p), ER, ER_M, AOF, and S:F ratio estimated by atom conservation.

6.1.1. Effect of the reactor temperature

Figure 18 shows the effect of the adiabatic gasifier temperature on the production of CO, CO_2, H_2 and CH_4 for gasification of DB, FB, TL, and WC. The ER_M was set to 2 and AOF to 0.25. Increasing gasifier temperature (T_P) in Equation (26) and maintaining constant both ER and AOF implies more thermal energy in the product gases leaving the peak temperature zone; thus, there must be more oxidation of combustibles to CO_2 to produce the sensible heat required and hence less oxygen available to produce CO.

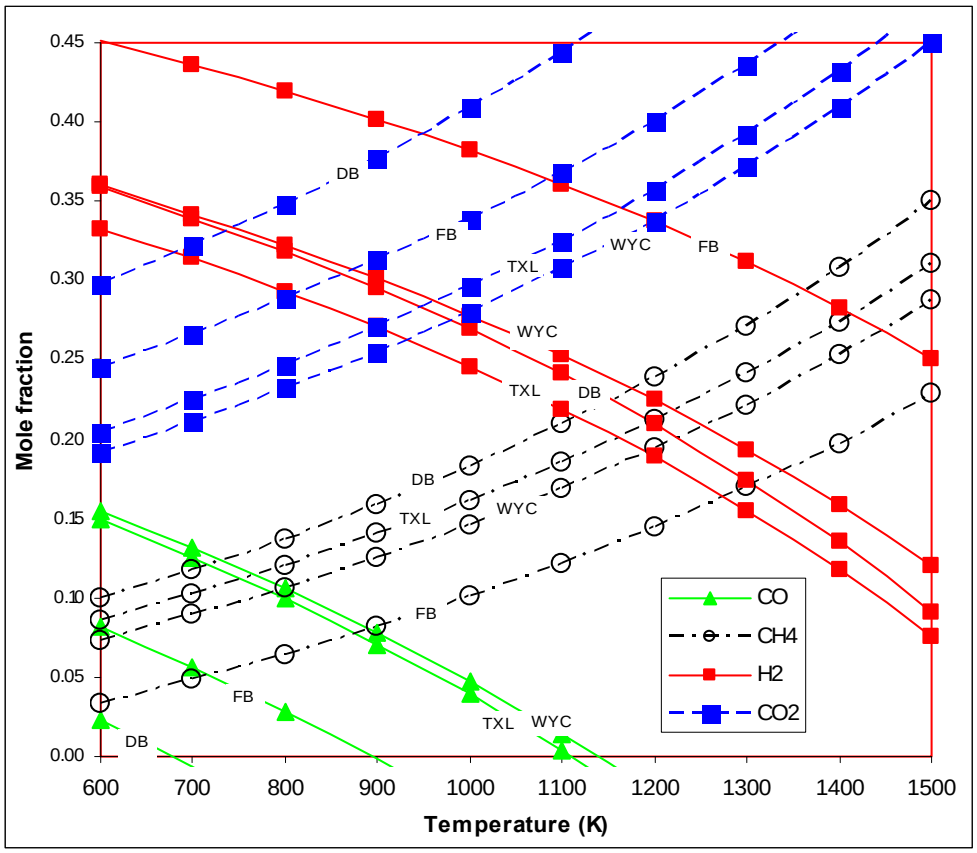

Figure 18. Effect of adiabatic gasifier temperature on CO, CH_4, H_2, and CO_2 production for FB, DB, TXL, and WYC with ER_M and AOF at 2 and 0.25, respectively, estimated with atom balance

From Figure 18, it is apparent that higher adiabatic temperatures of gases leaving the reactor, inrease the CO_2 concentration and lower the CO concentration, which is required by energy conservation.

Additionally, the results show that for the same operating temperatures, coals produce less CO_2 and more CO compared to FB and DB because the FC is higher for coal compared to FB and DB and hence more heat is available for oxidation of FC to produce CO. Because coal does not require a long amount of oxidation of FC to CO_2. On the other hand, higher temperatures favor the production of CH_4 but have a negative effect on the production of H_2, as shown in Figure 18.

As discussed before, increasing the reactor temperature requires more oxidation of C to CO_2, and hence more O atoms leave via CO_2 and thus there is less CO. As a result, lesser C atoms leave via CO_2 and CO (i.e., for fixed oxygen input) and hence the remaining carbon must leave with hydrogen in the form of CH_4. In other words, less oxidation of C to CO_2 implies more C leaves via CO and thus less C leaving via CH_4. For example, decreasing 0.1 moles of CO_2 in the products implies increasing 0.2 moles of CO for the same oxygen atom consumption and decreasing 0.1 C atoms available to produce CH_4; hence, more H atoms are available for conversion to H_2. DB and FB have higher H contents, but FB has more oxygen (30% more) content and a lesser HHV (3% less) and thus requires less external air for partial oxidation.

6.1.2. Effect of ER_M

Figure 19 shows the effect of the ER_M on species production for AOF of 0.25 and adiabatic temperature of 800 K.

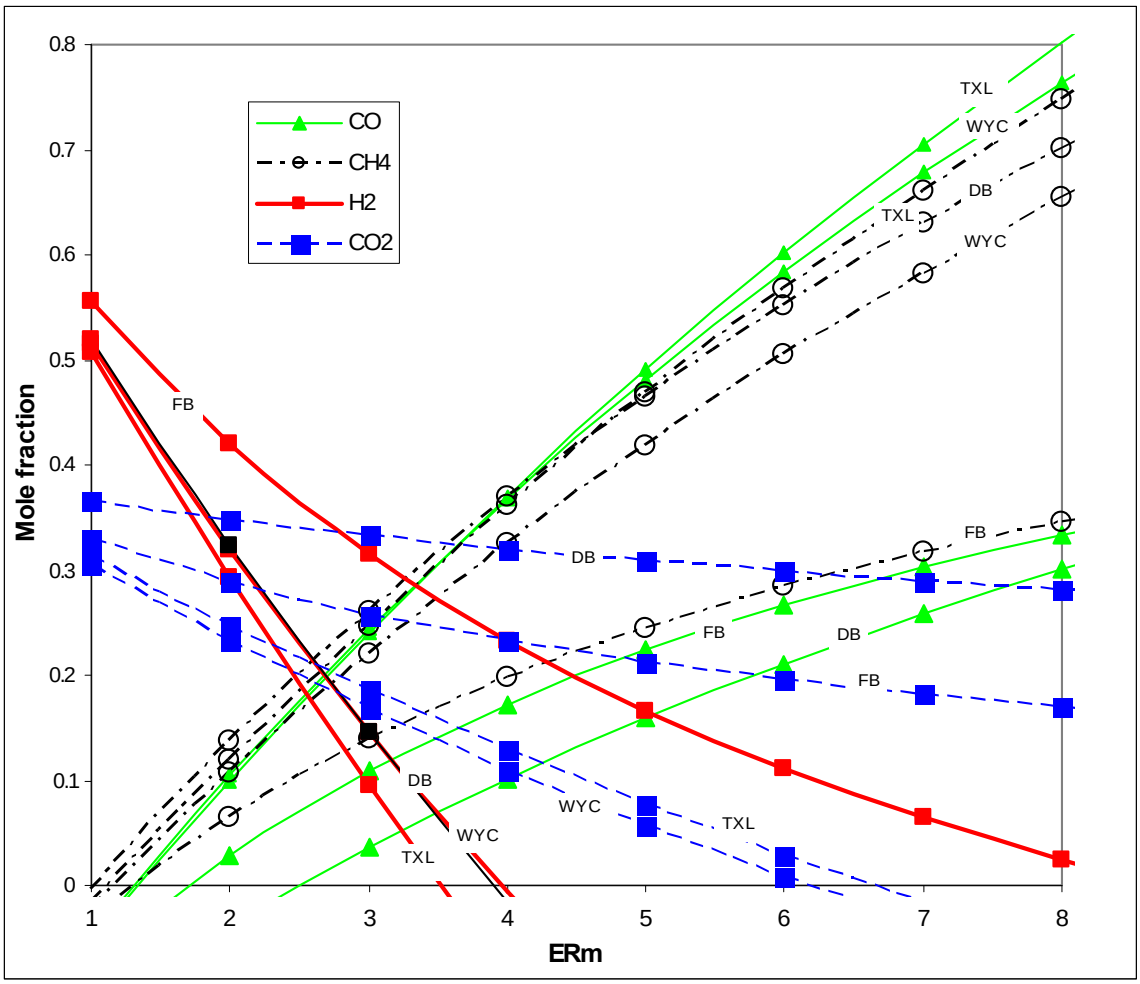

Figure 19. Effect of the ER_M on CO, CO_2, CH_4 and H_2 production for FB, DB, TXL, and WYC with AOF at 0.25 and temperature at 800 K, estimated with atom balance

Increasing ER_M at constant temperature and at constant AOF implies increasing ER or decreasing oxygen (less air) supplied to the gasifier; hence, the oxidation of char occur in a t O_2-H_2O deficient environment, which produces CO-rich mixtures. Also, because less C leaves with CO and CO_2 under increased ER_M, more C must leave with CH_4 and hence more H atoms must leave with CH_4 and fewer H atoms are available for conversion to H_2. To produce H_2 at 800 K.

Figure 19 shows that the ER_M must be kept below ~ 4 for DB and WYC, 3.5 for TXL, and 8.5 for FB during the experiments with AOF at 0.25.

6.1.3. Effect of AOF

Figure 20 shows the results from the atom balance model on production of CO, CH_4, and H_2 as a function of AOF at fixed ER of 2 and reactor temperature of 800 K. The decreasing of AOF at fixed ER_M implies increased ER (ER_M = ER*AOF) and hence less oxygen supplied with air. As before, this increases CH_4 and H_2 and lowes contents of CO and CO_2. The curves of Figure 20 suggest that at constant ER_M and constant temperature, H_2 can be produced within $0 < AOF < 1$. In other words, it is possible to produce H_2 by gasification of biomass with air, steam or steam-air mixtures.

In general, the atom model shows that the effect of changes in ER_M and temperature on H_2 is more significant than changes in AOF. The productions of CO and CH_4 are possible only under certain restricted conditions. For instance, to produce CO with DB at $ER_M = 2$ and $T_{Reactor} = 800$ K, AOF must be maintained higher than 0.3,

whereas the production of CH_4 with FB is possible only for AOF lower than 0.35. Alternatively, the atom model shows that production of CH_4 and CO is very sensitive to changes of all parameters (ER, AOF, and T_P).

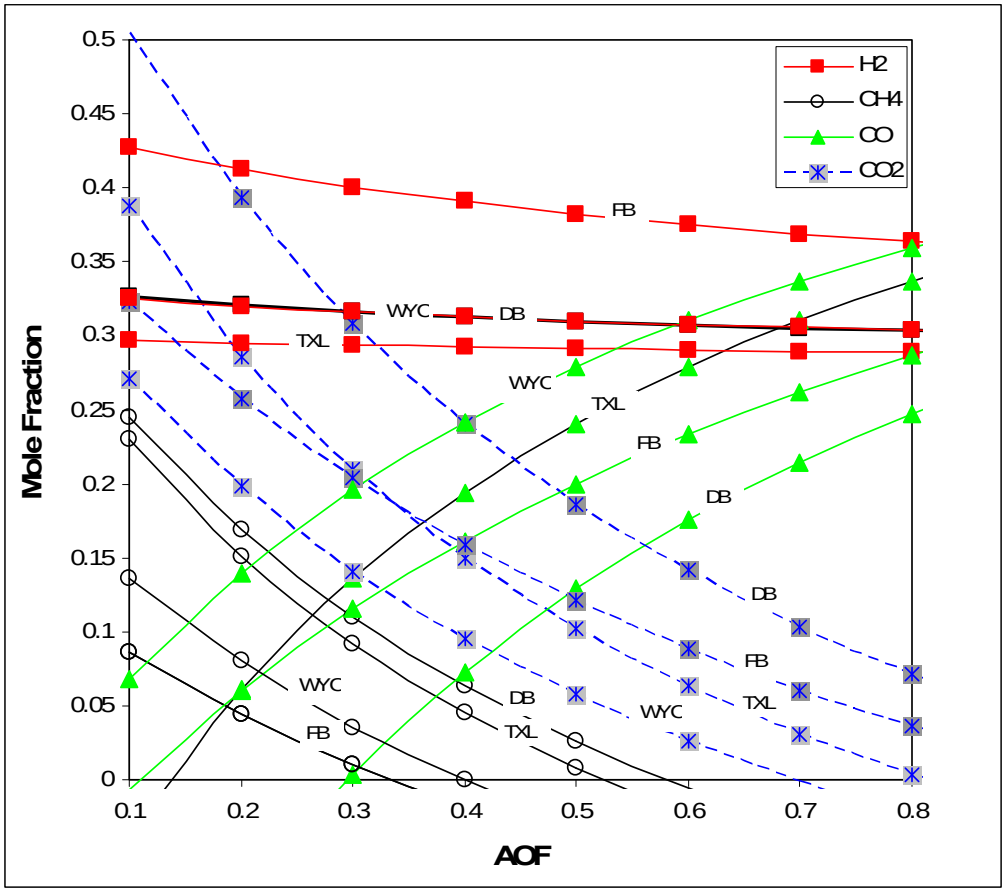

Figure 20. Effect of the AOF on CO, CH_4, CO_2 and H_2 production for FB, DB, TXL, and WYC with ER_M at 2 and temperature at 800 K, estimated with atom balance

Additionally, the curves in Figures 18, 19, and 20 illustrate that under the same gasifier conditions (T_P, ER_M, and AOF), FB is better than other biomasses to produce

H_2, but it is not as good as the coals and DB to produce CH_4. This is because there is more hydrogen content in FB compared with TXL, WYC, and DB.

6.1.4. Effect of the ER and S:F ratio

In this section, results are presented for the effect of ER and S:F on gas composition estimated with atom modeling at 1000 K. The effect of ER and S:F ratio on CH_4 production is shown in Figure 21.

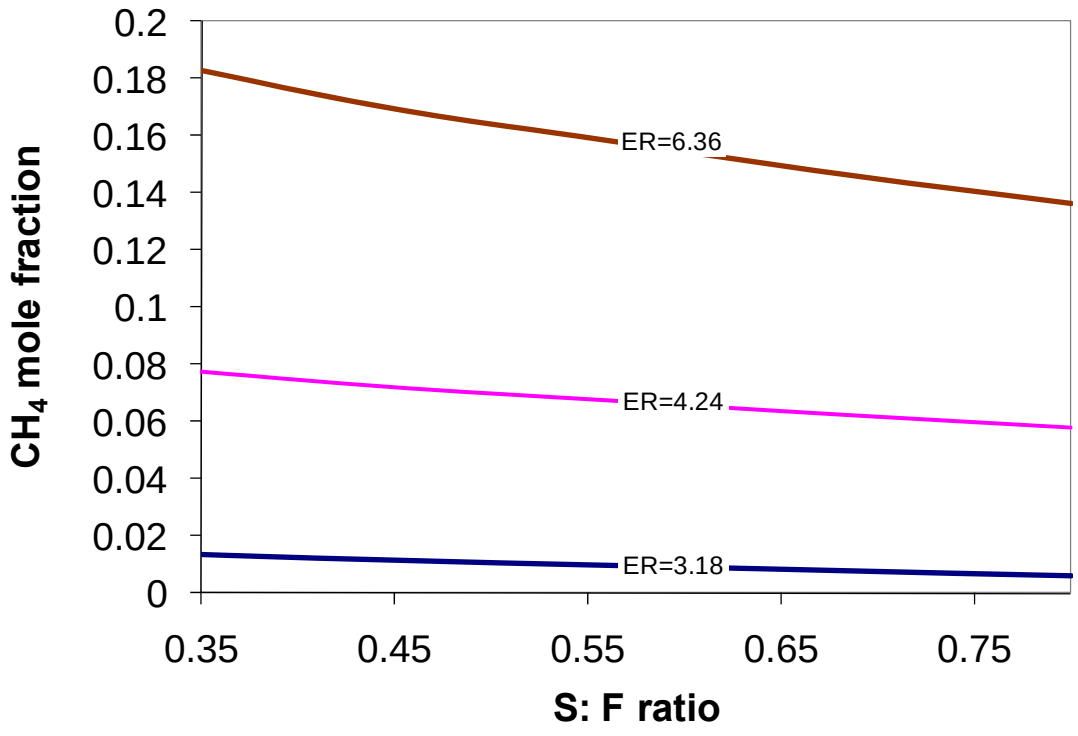

Figure 21. Effect of the S:F ratio on adiabatic concentration of CH_4 for various ERs, estimated with atom balance model at 1000 K

It can be seen that at constant ER, increased S:F ratios produces mixtures lower in CH_4, but at constant S:F, increased ER produces mixtures rich in CH_4. It is evident that at higher ER changes on S:F affect the CH_4 concentration more than at lower ERs. For instance, at ER=6.36, increasing S:F from 0.35 to 0.8 decreases the CH_4 concentration by ~5% whereas at ER=3.18, the same increase on S:F decreases the concentration of CH_4 by only ~1%.

Figures 21 and 22 show that S:F ratio affects the CO and CH_4 concentrations similarly; however, the CO concentration decrease steeply with increase in S:F compared to the concentration of CH_4. Conversely, the effect of ER on CO and CH_4 concentrations is different. At constant S:F, the increase in ER tends to produce mixtures poor in CO but rich in CH_4.

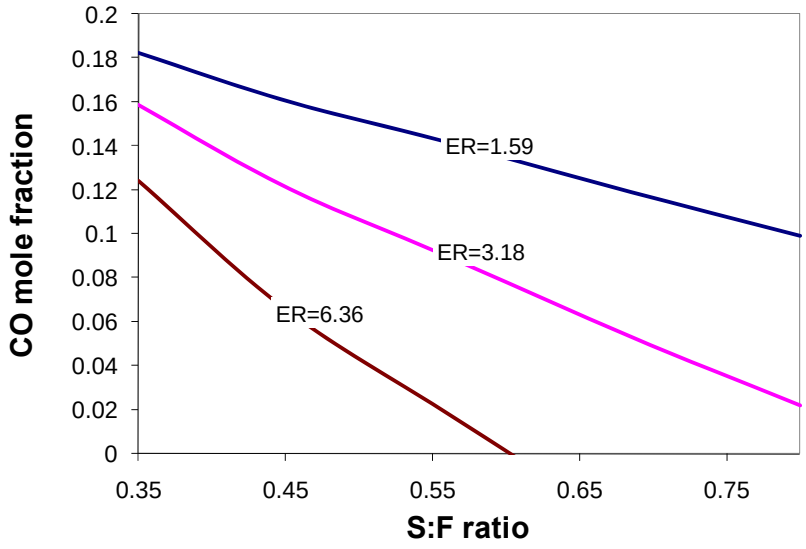

Figure 22. Effect of S:F ratio on adiabatic CO concentration for various ERs, estimated with atom balance model at 1000 K

At constant ER, increasing the S:F increases steam supplied with the oxidizing source; thus, as discussed before, the reaction occur in an H_2O-rich ambient which favors the steam reforming reaction (Equation 6) and shift reaction (equation 7) producing mixtures rich in H_2 and CO_2 but poor in CO (Figures 22, 23, and 24).

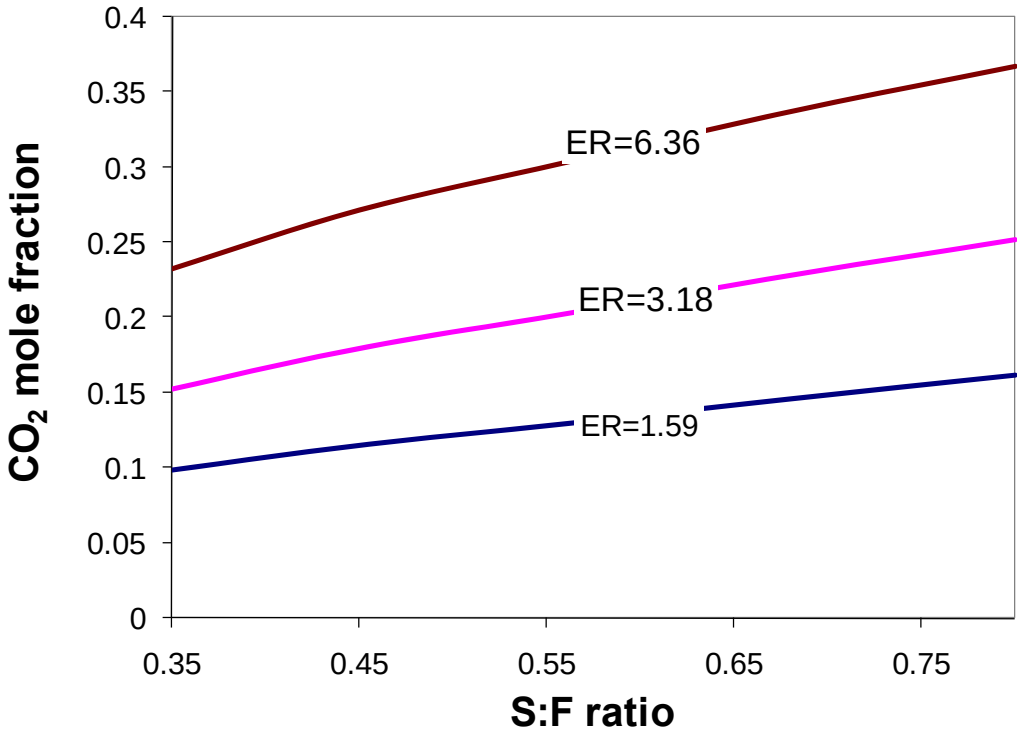

Figure 23. Effect of S:F ratio on adiabatic CO_2 concentration for various ERs, estimated with atom balance model at 1000 K

It is apparent from Figures 20 to 24 that the effects of AOF and S:F are different on concentrations of CO, CO_2, and H_2 but similar on concentration of CH_4. At constant ERM, increasing AOF implies decreasing ER, increased oxygen through air, increased steam concentration and air moles supplied in the oxidizer respectively whereas at

constant ER increased S:F ratios increase the steam moles supplied but maintain constant the air moles in the oxidizer. In other words, higher S:F ratios and lower AOFs indicate a oxidizing source rich in H_2O which favors the char steam and shift reactions to produce more H_2 and CO_2 and less CO.

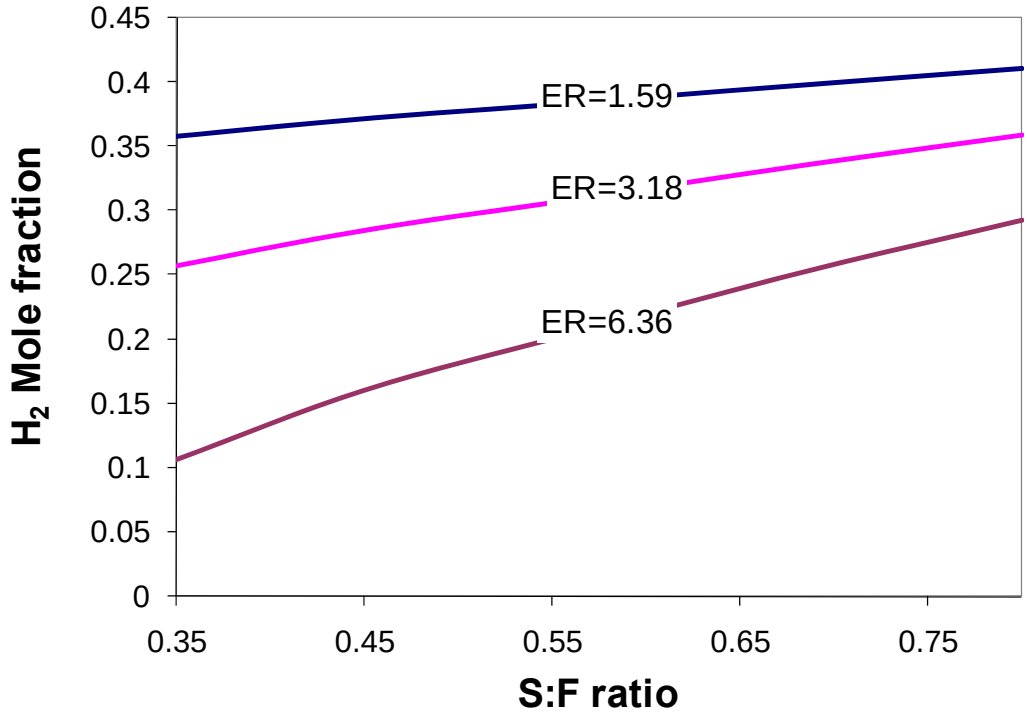

Figure 24. Effect of S:F ratio on adiabatic H_2 concentration for various ERs, estimated with atom balance model at 1000 K

6.2. Equilibrium modeling

The atom-computed equilibrium equation allows only limited number of species (CO, CO_2, CH_4, H_2, N_2, and H_2S). With CEA NASA equilibrium program more species can be estimated. The effect of ER, ER_M, AOF, and S:F ratio on gas composition, HHV,

and energy recovery estimated by the CEA NASA equilibrium program are presented in this section. As discussed before, the ER_M and AOF were studied for gasification of TXL, WYC, DB, and FB using the NASA equilibrium code PC version to solve for ~ 150 species (including char) without the presence of $H_2O_{(g)}$ and adiabatic temperature. The parameters ER and S:F were investigated for gasification of DB only and with the presence of $H_2O_{(g)}$ in the products and adiabatic temperature. As discussed earlier, the input data included the moles of DAF fuel, air, and total steam (external and moisture) and the enthalpy of the reactants mixture. Appendix D presents tables on gas composition HHV and energy recovery.

6.2.1. Effect of ER_M and AOF

The equilibrium model provides information on adiabatic temperature, gas composition, HHV of gases, and energy conversion efficiency as functions of the ER_M and AOF. Although, the study was performed for about 150 species, only significant species are reported here. For constant ER_M and constant AOF, the atom conservation model gives a range of the probable adiabatic temperatures of the products (Equation 26), while the equilibrium model provides information on the unique possible final adiabatic equilibrium temperature of the products for any specified group of species. The estimated adiabatic equilibrium temperatures for gasification of DB, FB, and TXL are illustrated at several AOFs and two ER_M (2 and 8) in Figure 25. For AOF > 0.25, the three biomasses show a monatomic reduction of equilibrium temperature with increased

ER_M. This is due to lower CO_2 production caused by deficient oxygen in the adiabatic gasifier. On the other hand, increasing AOF (i.e., reducing the steam supplied) at constant ER_M raises the equilibrium temperature because of the reduction in the endothermic reaction of steam with carbon. From Figure 25, it is evident that at lower ER_M, the temperature is more sensitive to changes in AOF than at higher ER_M. Also, at AOF > 0.4, the temperature is more affected by variations of ER_M (e.g. for gasification of DB with $ER_M = 2$ and $ER_M = 8$, increasing the AOF from 0.2 to 0.8, increases the temperature by 111% and 23% respectively).

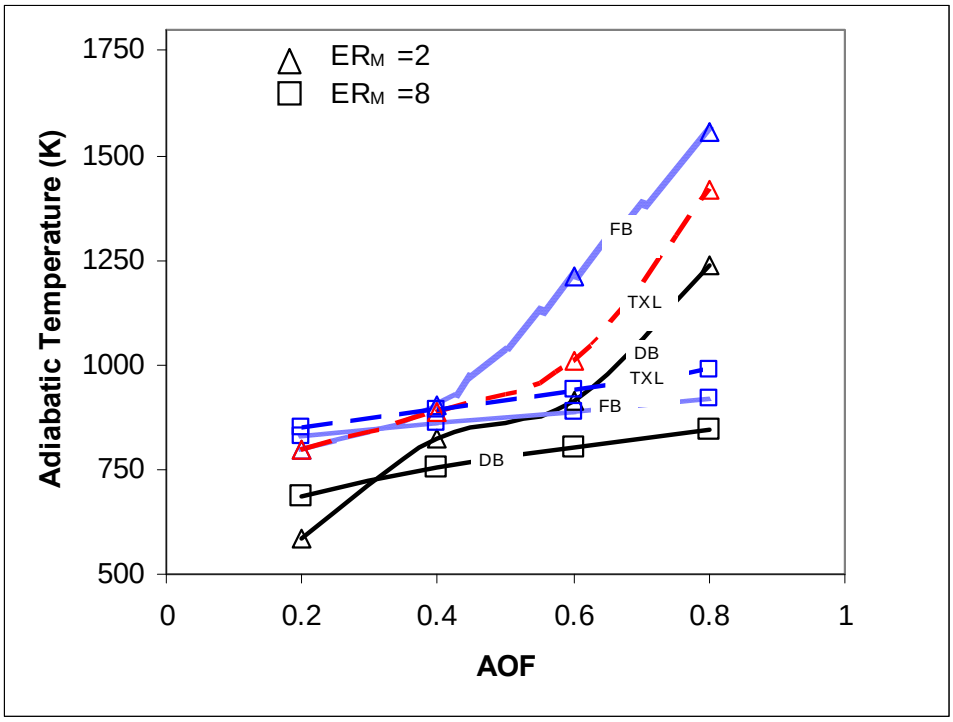

Figure 25. Effect of the AOF and ER_M on adiabatic equilibrium temperature for DB, FB, and TXL

As discussed before, decreasing AOF at constant ER_M decreases the air-to-steam ratio supplied to the gasifier and there are more H atoms available, which favor

Reactions (6), (7), and (8). As a consequence, the production of CH_4 and H_2 is increased, but the CO production is diminished (Figure 26). However, at $ER_M = 2$, the concentration of CO is not affected by AOFs > 0.6.

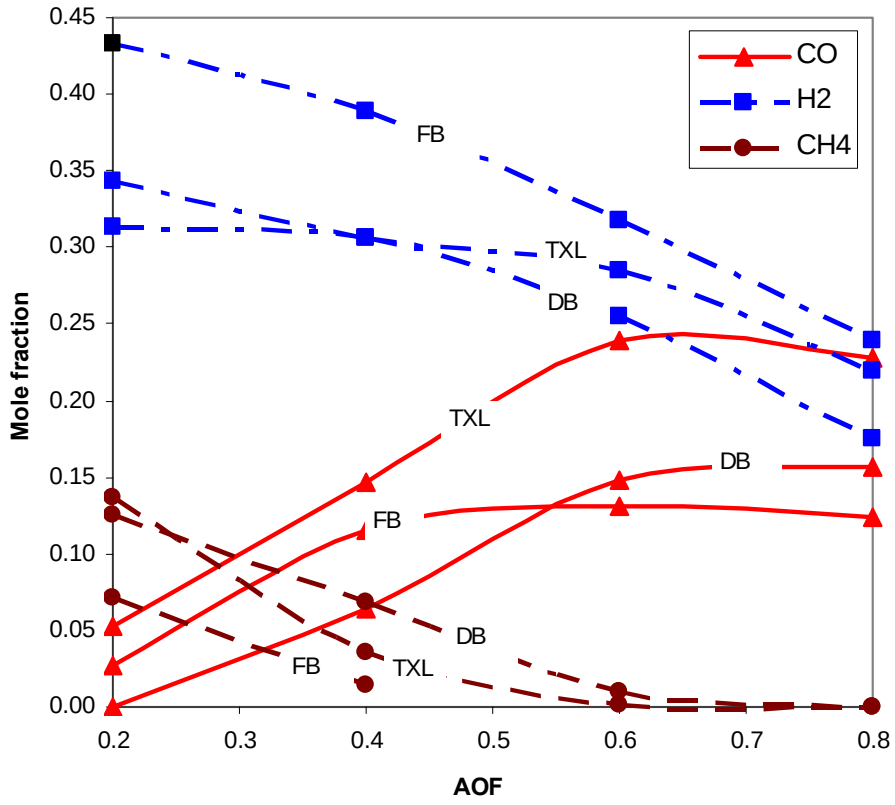

Figure 26. Effect of the AOF on production of H_2, CO, and CH_4 for FB, DB, and TL with ER_M at 2, estimated with equilibrium model

Increasing ER_M at constant AOF implies decreasing the oxygen supplied with the air. Thus, there is less oxygen to produce CO from the reaction of carbon and oxygen that is exothermic resulting in lower temperatures (Figure 25) not high enough for H_2 to

be stripped from H_2O in the steam reforming reaction. Figure 27 shows the effect of ER_M on concentrations of CO and H_2 for DB and FB at various AOFs.

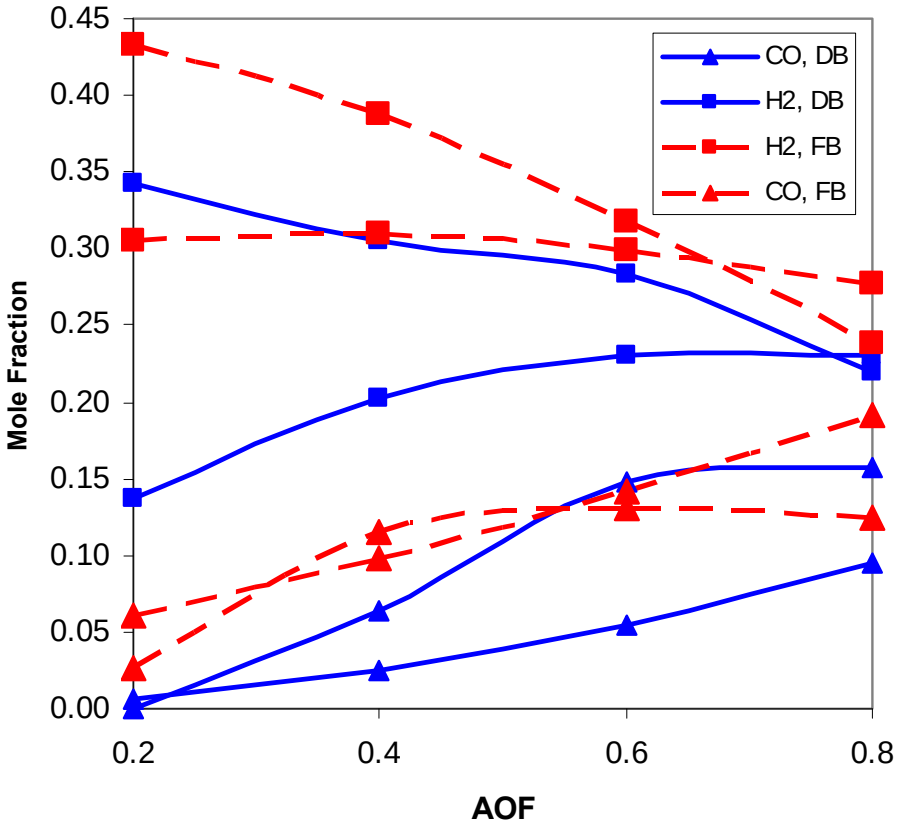

Figure 27. Effect of the ER and AOF on production of H_2 and CO for DB and FB, estimated with equilibrium model

FB biomass has more oxygen and hydrogen in the fuel compared to DB; the availability of O in the fuel results in more CO production which promotes the shift reaction of CO with steam to produce H_2 and CO_2. Additionally, more H in the fuel raises the production of H_2. Figure 27 shows that the production of H_2 with DB and FB is

possible at 0.2 < AOF < 0.8 and 2 < ER_M < 6, whereas the production of CO with DB is only possible for ER_M > ~0.20. Due to the higher hydrogen content in FB, the production of CO is even possible at lower ER_M as compared to that of DB.

Both atom and equilibrium models show that FB is more prone to produc H_2 rich mixtures than DB because of its higher H content.

Extrapolation of the H_2 curves in Figure 27 suggests that the maximum equilibrium concentration of H_2 (~48%) can be obtained for FB with ER_M at 2 and AOF at 0. However, at those operating conditions, the adiabatic temperature is very low (~600 K), where reaction rates are extremely low.

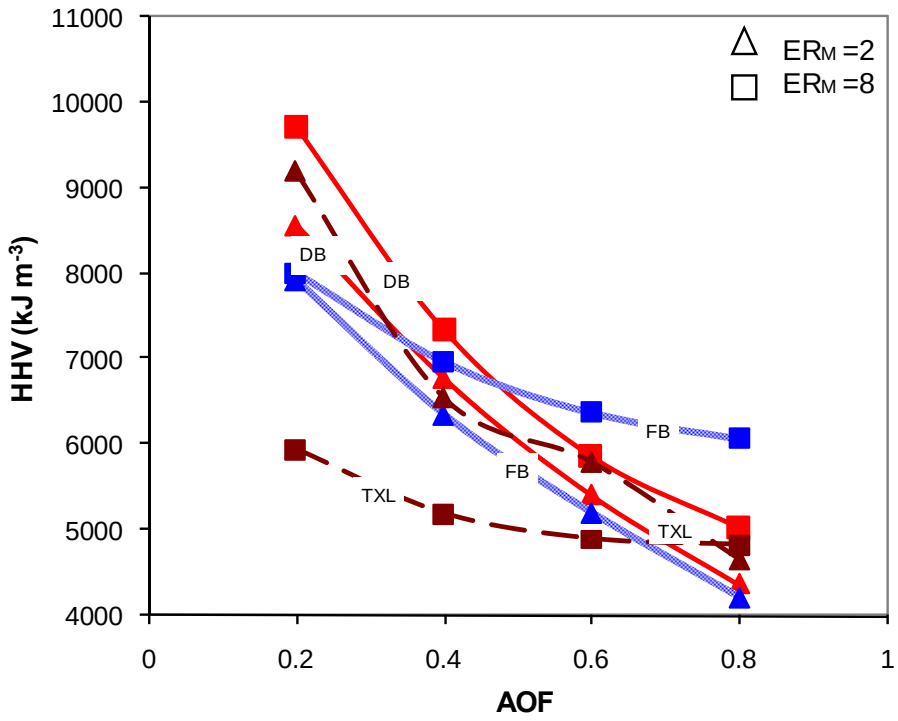

Figure 28. Effect of the AOF and ER_M on HHV for DB, FB and TXL

Figure 28 shows the HHV of the products estimated by equilibrium for TXL, DB, and FB at many AOFs and ER_M = 2 and 8. As stated before, at constant ER_M, decreased AOF produces mixtures richer in CH_4 and H_2, which have higher HHVs. Although the HHV with steam and air gasification provides a measure of energy density, it does not provide a measure of actual degree of energy conversion (energy recovery) in gasification processes.

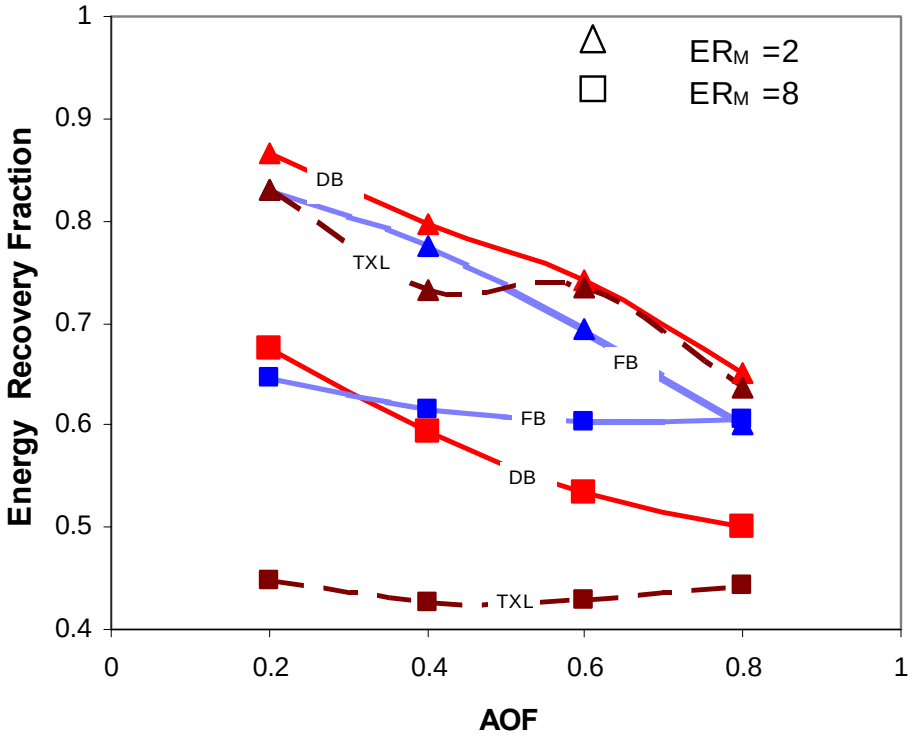

Figure 29. Effect of the AOF and ER_M on energy recovery for DB, FB and TXL

Increasing AOF decreases energy recovery (Figure 29), but at higher ER_M, the decrease is not much. At constant AOF, higher ER_M implies lesser mass flow of air to

react with char and the process is almost pure pyrolysis (char production), which produces less mass of gases per kg of fuel resulting in lower energy recovery. Generally, methane-and hydrogen-rich mixtures have greater HHV and provide better energy conversion efficiency, because the methane has higher energy density (36,250 kJ/m^3) compared to CO (11,543 kJ/m^3). Higher temperatures increase the sensible heat of the gases, but produce gases with lower energy density and lower energy recovery.

6.2.2. Effect of ER and S:F ratio

The effect of ER and S:F on equilibrium gas composition, HHV, and ECE was estimated only for gasification of the base fuel (DB). Tables of results are included in Appendix D.

Figures on gas composition, adiabatic temperature, HHV, and ECE are presented in this section as a function of ER and S:F ratios. Figure 30 shows the effect of S:F ratio on equilibrium gas composition for gasification of DB at ER=3.18.

Increasing S:F ratio implies more steam available in the gasifier for the heterogeneous reaction $C+H_2O \rightarrow CO+H_2$ and the homogeneous reaction $CO+H_2O \rightarrow CO_2+H_2$. Thus, gasification of DB under increased S:F ratios produces equilibrium mixtures rich in H_2 and CO_2 but poor in CO. Additionally, there are more H atoms in the gasifier to react with the C atoms to improve CH_4 production.

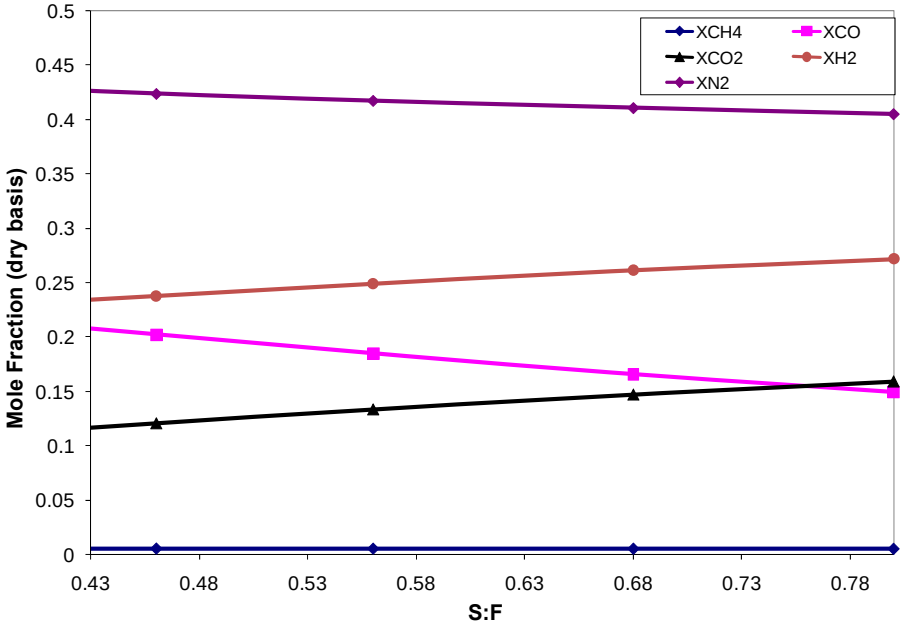

Figure 30. Effect of the S:F ratio on gas composition estimated with equilibrium model for DB at ER=3.18

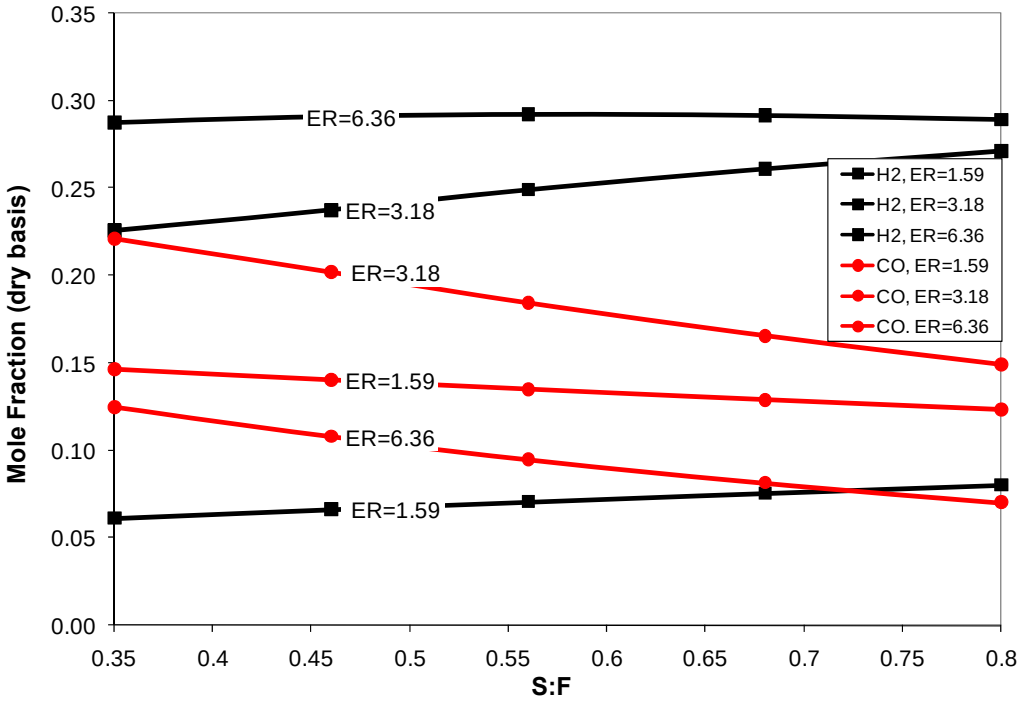

Figure 31. Effect of the S:F ratio on gas composition estimated with equilibrium model for DB at various ERs

Figure 31 shows the effect of the S:F ratio on H_2 and CO content in the products for diverse ERs. At constant S:F, higher ERs imply less oxygen entering the gasifier for the reaction $C+1/2\ O_2 \rightarrow CO$; hence, there are more C atoms available to react with the steam to produce CO and H_2. The remaining steam reacts with CO to produce more H_2 and CO_2. More C atoms consumed by the shift reaction means less C atoms leaving as CO.

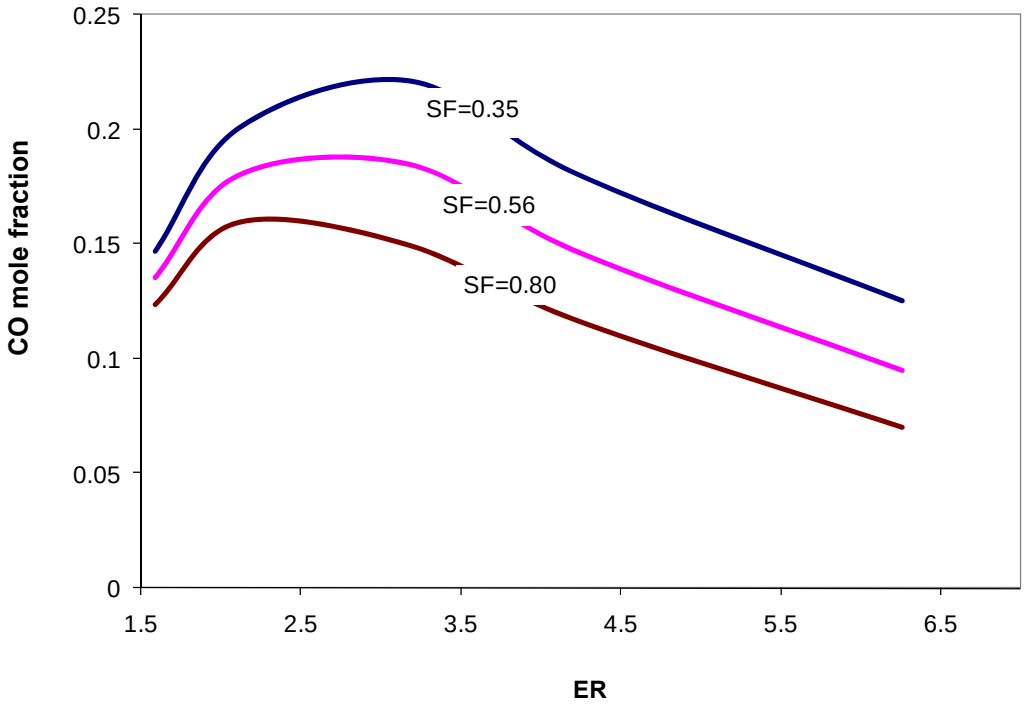

Figure 32. Effect of the ER ratio on CO composition estimated with equilibrium model for DB at various S:F ratios

However, the CO and H_2 curves show a peak with the ER which is better illustrated in Figures 32 and 33. The CO mole fraction increases with increased ER until

ER=3.18 beyond which starts to decrease. The lowest value of CO is reached at ER = 6.36 and S:F = 0.80 (Figure 32). The concentration of H_2 also shows an inflection point at ER=3.18. At ER<3.18, increased ER increases the concentration of H_2 very strongly but at ER>3.18, the effect of the ER on the fraction of H_2 is rather weak (Figure 33).

The results suggest that the steam to-air ratio entering the gasifier affects the H_2/CO ratio leaving the gasifier. At constant S:F, increasing the ER (decreased oxygen supplied through air) increases steam-to-air ratios. It is evident from the results, that higher steam to air ratios increases the H_2/CO ratio.

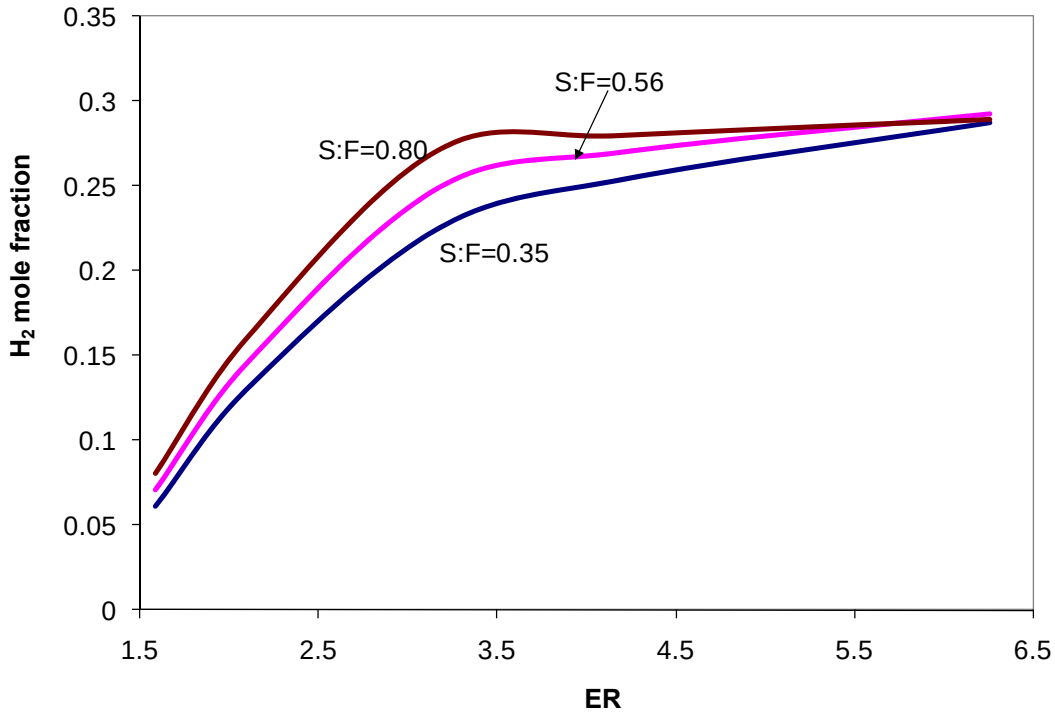

Figure 33. Effect of the ER ratio on H_2 composition estimated with equilibrium model for DB at various S:F ratios

Figure 34 shows the effect of ER on CO_2 for different S:F ratios. At ER > 2.12, increasing both ER and S:F produces CO_2 rich mixtures, whereas at ER < 2.12, the CO_2 decreases with increased ER and S:F ratios. As discussed before, it is because of the higher steam concentration in the bed, which favors the reaction of CO with steam (shift reaction) to produce more H_2 and CO_2. As shown in Figure 35, more available H atoms in the gasifier lead to CH_4-rich concentrations. However, the results show that at ER < 3.18, the effect of the S:F ratio on CH_4 concentration is negligible. The production of CH_4 is only possible at ER > 2.12, but within 0.35 < S:F < 0.80. In general, equilibrium modeling shows that the effect of the ER on CO is different than that of CO_2. Increasing CO implies decreasing CO_2.

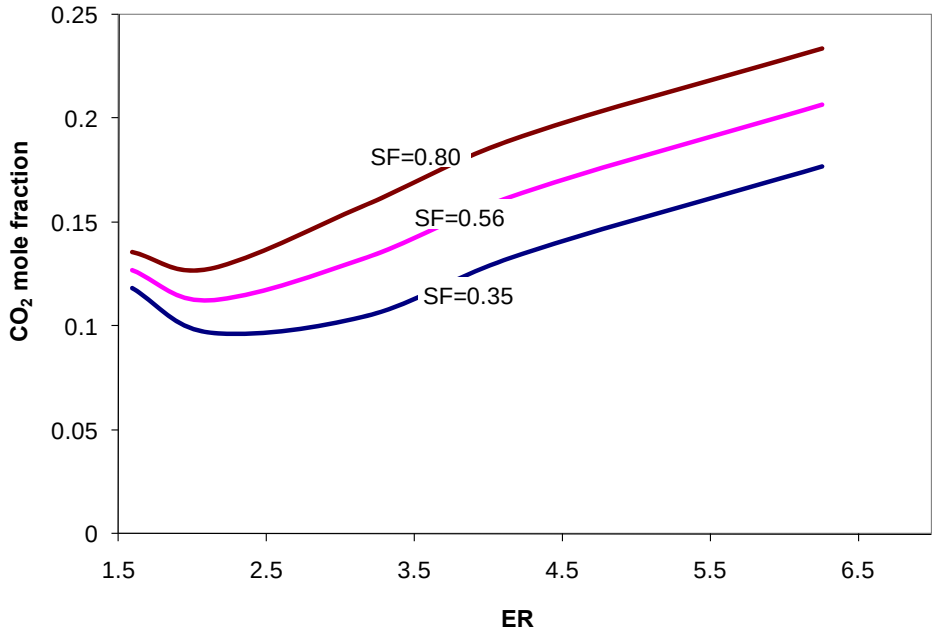

Figure 34. Effect of the ER ratio on CO_2 composition estimated with equilibrium model for DB at various S:F ratios

Even though increased ER and S:F improve the CO_2 concentration, the adiabatic temperature decreases with the rise of both ER and S:F (Figure 36). This suggests that most of the CO_2 produced is from the reaction of CO with steam (slightly exothermic) instead of the char-oxygen reaction, which is strongly exothermic. However, the effect of S:F on adiabatic temperature is rather weak.

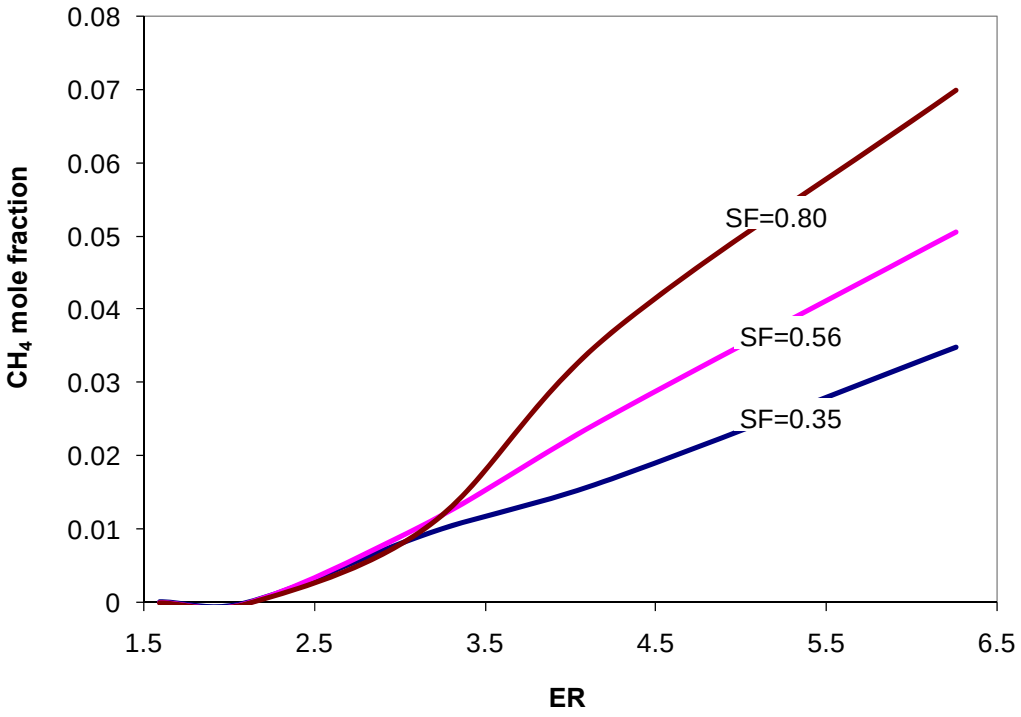

Figure 35. Effect of the ER ratio on CH_4 composition estimated with equilibrium model for DB at various S:F ratios

In general, at ER < 2.12 (increased oxygen through air), the concentrations of CO and H_2 increase and the concentration of CO_2 and adiabatic temperature decrease with increased ER (Figures 32 through 36) indicating that the heterogeneous C-H_2O reaction

(which is endothermic, ΔH_R=10,390 kJ kg^{-1} of C) is more important than the homogeneous CO-H_2O reaction, which is a slightly exothermic (ΔH_R=-1470 kJ kg^{-1} of CO). At 2.12 <ER <3.18 (less O_2 supply), the shift reaction begins to be important because the H_2O concentration is much higher. Hence, CO production stars to decrease whereas the production of H_2 increases. The CO with H_2O reaction is slightly exothermic.

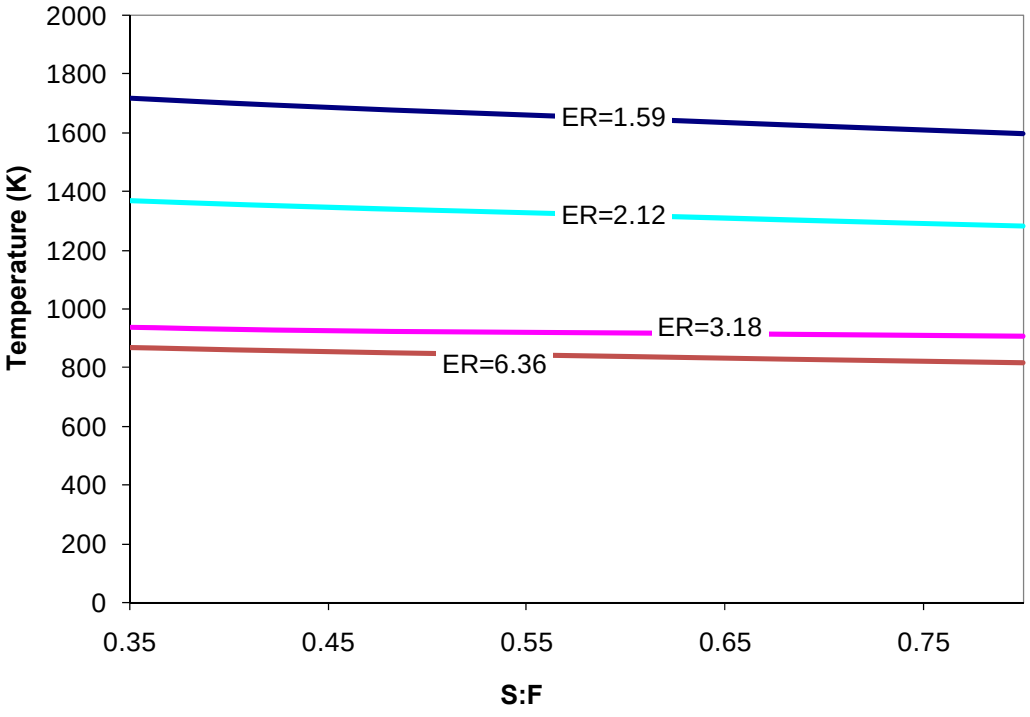

Figure 36. Effect of S:F ratio on adiabatic temperature estimated with equilibrium model for DB at various ER

On the other hand, at ER > 3.18 the shift reaction seems to be more important than the char reaction with steam; hence, the CO_2 and H_2 concentrations increase

whereas the concentration of CO decreases. At ER < 3.18, the adiabatic temperature increases strongly with decreased ER because of the endothermic effect of the C-steam reaction.

At ER > 3.18, increase in ER increases the concentration of CO_2 more steeply compared to H_2 (Figures 33 and 34), which indicates that a fraction of the H atoms input is used to produce CH_4 (Figure 35).

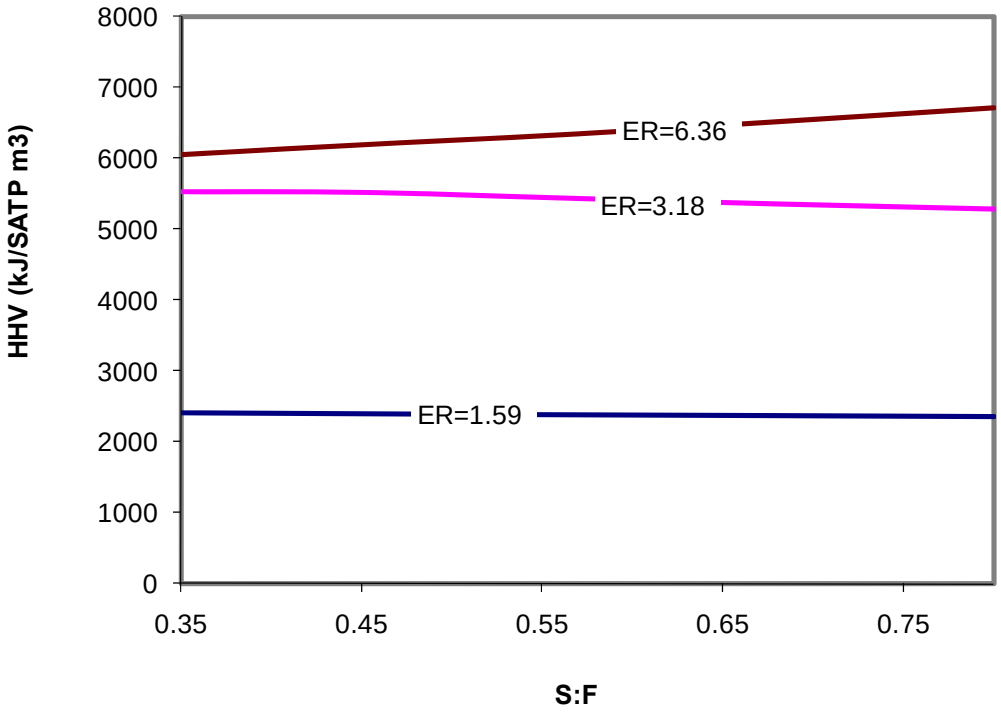

Figure 37. HHV of the species vs S:F estimated with equilibrium model for DB at various ERs

Figure 37 illustrates the energy density (HHV) of the products estimated by CEA NASA equilibrium program for DB gasification for several ERs and as a function of the S:F ratio. Gasification at high ER produces CH_4-and H_2-rich mixtures, which have a

high HHV because of the high HHV of CH_4 and H_2. At ER < 3.18, the effect of S:F ratio on HHV is not important because at ER < 3.18, the effect of S:F on the CH_4 concentration is insignificant. On the other hand, at ER > 3.18 increased S:F ratios lead to CH_4-rich mixtures that, as stated before, have a high gross heating value.

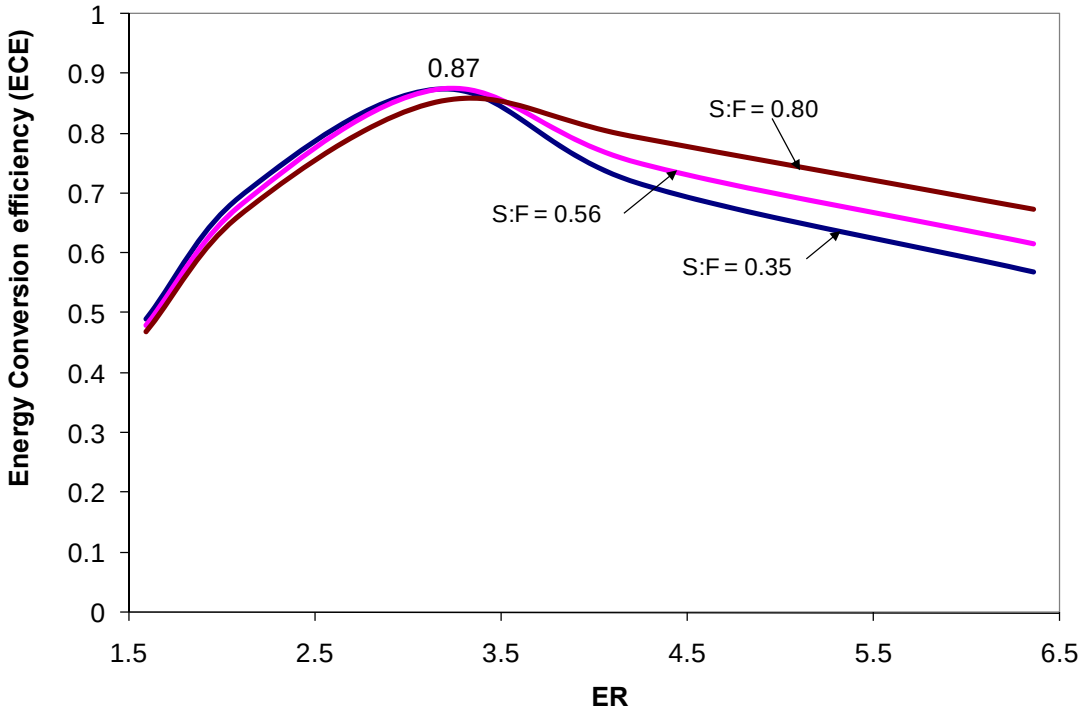

Figure 38. Energy recovery estimated by equilibrium model for DB as function of the ER at different S:F ratios

The energy conversion efficiency ECE defined as the ratio of HHV in the gases to the HHV input in the fuel gives information on the gasifier performance. The ECE estimated by the equilibrium model is illustrated in Figure 38 as function of ER for various S:F ratios.

The curves of energy recovery show a peak at ER = 3.18. At ER < 3.18, increasing ER (decreasing O_2 supply through air) increases the energy recovery until 0.87 beyond which it starts to decrease. Even though, at ER > 3.18, the HHV of the gases increases with higher ER (Figure 37), the energy recovery decreases indicating that gasification under ER > 3.18 produces char. As discussed before, high ER can lead to the lack of enough oxygen to burn completely all char. Then, the process tends to be pure pyrolysis, which produces mixtures with higher concentrations of fuel gases, but lower energy recovery because of char production. The char yields obtained by equilibrium model are presented in Appendix D.

7. EXPERIMENTAL RESULTS ON GASIFICATION

This section presents results on experiments performed on gasification of DB, DB-coal blend, and DB-ash blend using mixtures of steam and air as oxidants. Some experiments were performed with DB using air only to compare the results with [25] on fixed bed gasification of FB without ash disposal.

7.1. Fuel and ash characterization

Prior to presenting modeling and experimental results, the properties of fuels and ash used in the present study are presented. All fuels were supplied by the Texas A&M Agricultural Research & Extension Center, Amarillo, Texas. The DB samples were taken from dairy biomass separated solids prior to composting and were provided as coarse grain with ~1/4" particle size. DB is termed as DB-Sepsolids-PC-2006.

7.1.1. Fuel characterization

The properties of the selected fuels were characterized by ultimate and proximate analyses of pure DB, pure FB, pure WYC, and pure TXL, including heating values (HHV).The properties of DB-WYC blends were determined using the mass of the DB and WYC in the blend.

Table 8 Ultimate and proximate analysis on an as-received basis

Fuel Name	Texas Lignite (TXL)	Wyoming coal (WYC)	Dairy Biomass (DB)	Feedlot biomass (FB)
Dry loss (%)	38.34	22.81	25.26	22.32
Ash (%)	11.46	5.45	14.95	16.42
VM (%)	24.79	34.5	46.84	50.08
FC (%)	25.41	37.25	12.95	11.18
VM_{DAF} (%)	49.00	48.00	78.00	82.00
FC_{DAF} (%)	51.00	52.00	22.00	18.00
C (%)	37.18	54.07	35.27	32.7
H (%)	2.12	3.44	3.1	3.34
N (%)	0.68	0.81	1.9	1.89
O (%)	9.61	13.08	19.1	22.81
S (%)	0.61	0.39	0.42	0.52
HHV (kJ/kg)	14290	21385	12844	12788
DAF HHV(kJ/kg)	28466	29809	21482	20875
Dry HHV (kJ/kg)	23175	27704	17185	16462
Emprical Formulae	$CH_{0.68}N_{0.0157}O_{0.19}S_{0.006}$	$CH_{0.76}N_{0.013}O_{0.18}S_{0.003}$	$CH_{1.06}N_{0.047}O_{0.405}S_{0.0045}$	$CH_{1.23}N_{0.05}O_{0.523}S_{0.006}$
$ER_{MAX\ FC \rightarrow CO}$	3.16	3.2	5.8	6.14
Stoch. air:fuel ratio, mol basis	5.147	5.249	5.077	5.008
$ER_{FC \rightarrow CO+H2+N2}$	5.15	5.21	10.01	9.45
$AOF_{FC \rightarrow CO+H2+N2}$	0.614	0.614	0.614	0.614
$HHH_{FC \rightarrow CO}$ (kJ/kg gas)	6113	6307	8706	9393
$HHV_{FC \rightarrow CO+H2}$ (kJ/kg gas)	9320	9594	11459	12020

Using ultimate and proximate analysis and atom conservation, the empirical formulas were calculated [33] (Table 8). Coal has more fixed carbon than DB and FB, but less volatile matter (VM). The ash content of DB and FB is higher than those of coals. The Following were calculated: i) maximum ER at which all the FC content in the fuel react with O_2 to produce CO, ii) the ER and AOF at with all FC react with air and steam to produce CO, H_2, and N_2, and iii) the HHV of gasification producing VM and CO (Equation 29) and VM, CO and H_2 (maximum HHV, Equation 31). The results are shown in Table 8.

Figure 39 presents comparative proximate analysis of TXL, WYC, FB, and DB on an as-received basis.

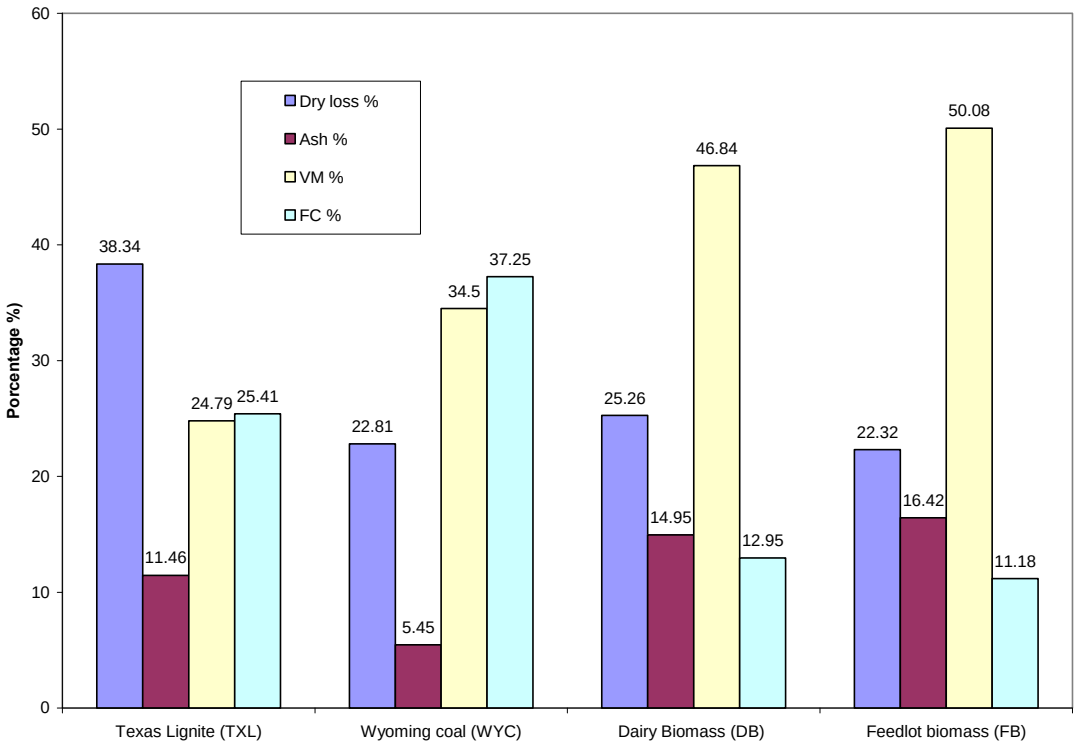

Figure 39. Comparative proximate analysis of the fuels

For the studied fuels Figure 39 shows that the fixed carbon (on as received basis) content in coal is the highest and the ash content the lowest. On the other hand, the volatile matter (VM) content in coals is lower compared to that of DB and FB; therefore, cattle biomass (DB and FB) releases more gaseous pyrolysis products per unit mass of DAF fuel than coal. TXL coal has the highest moisture content (~38%) whereas WYC (22.8%) is the fuel with lowest moisture content. Both FB and DB have higher ash contents; thus, the ash disposal must handle high rate.

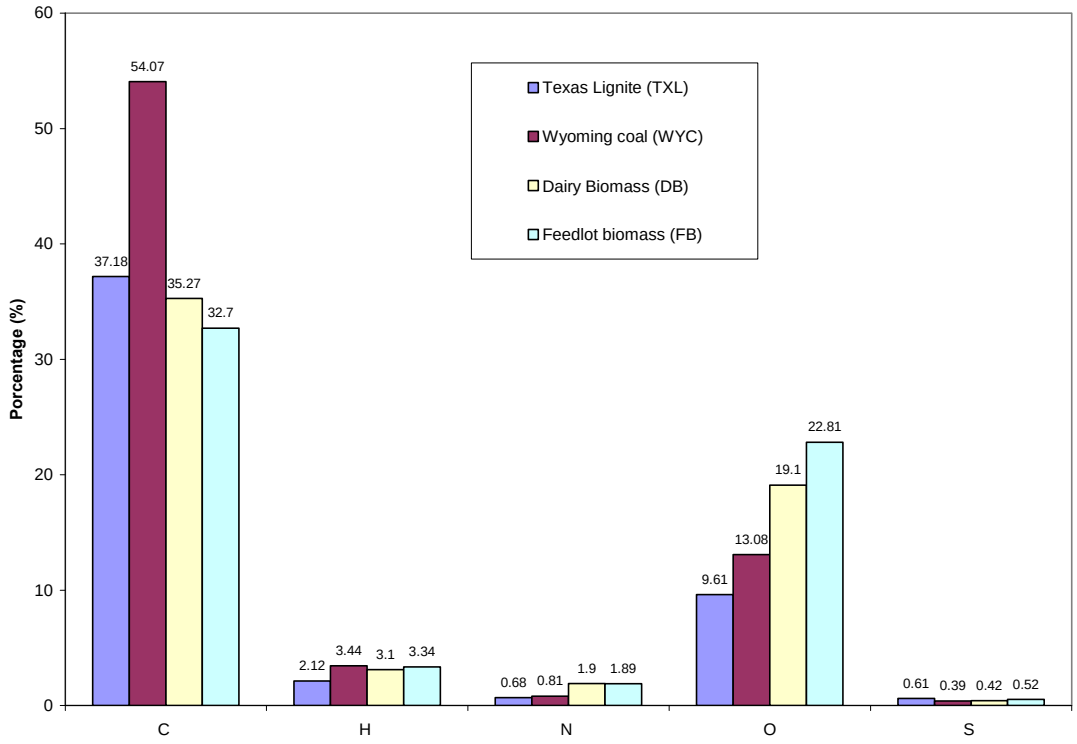

Figure 40. Comparative ultimate analysis of the fuels

Figure 40 shows the ultimate analysis of the fuels. Note that the H and O indicate organically bound hydrogen and oxygen (i.e., they have been separated from the hydrogen and oxygen contained in the form of moisture in the fuel). WYC has higher organic carbon content (~54%) compared to other fuels. The H and S content in the fuels is comparable whereas the O content in cattle biomass (DB and FB) is higher than coals. Although the H weigh fraction reported on an as-received basis for all the feedstocks is comparable, on a DAF basis, the H atoms content in DB and FB is higher compared to those of coals. As shown in the empirical formula reported in Table 7, the H atoms content in DB and FB are 56% and 81%, respectively, higher than the H atom content in

TXL. FB is the feed-stock that has the maximum H content on a DAF basis, whereas TXL has the lowest H content. FB has 16% more H than DB.

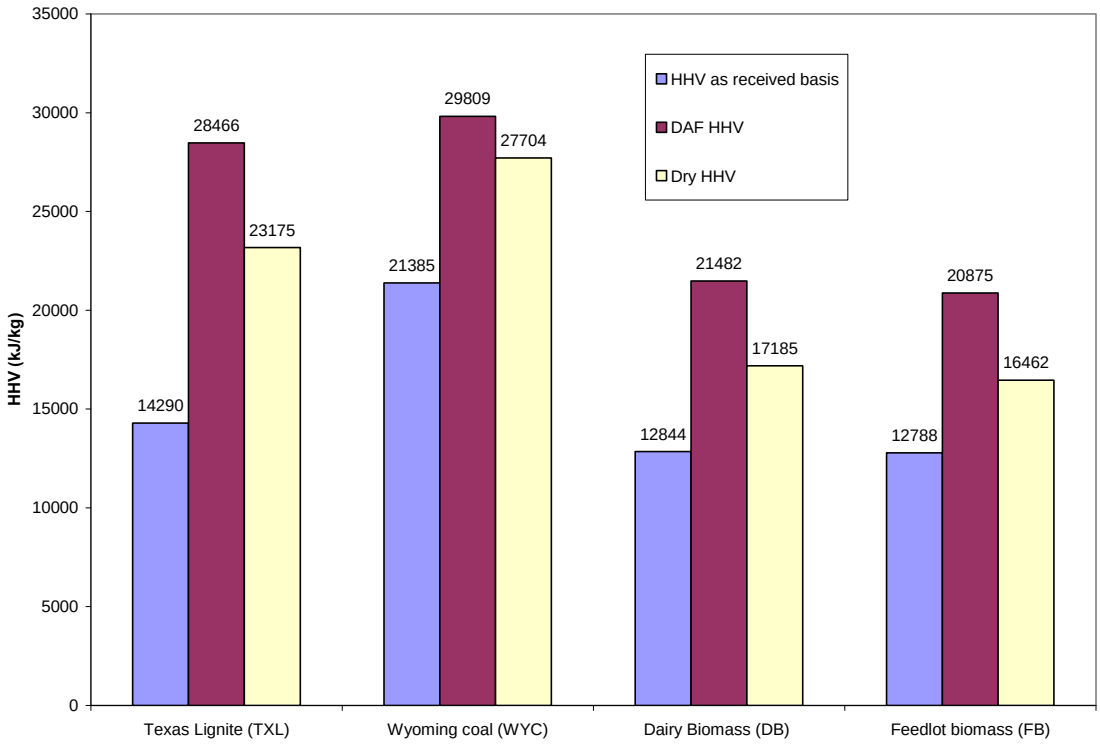

Figure. 41. Comparative HHV of the fuels

Figure. 41 presents the HHV of the fuels. Coals, which have high FC, low ash, and low oxygen content compared to cattle biomass have the higher gross heating value. Increased C/O ratio in fuels tend to increase the HHV because of the high heating value of C. On the other hand, fuels with high ash content tend to have low HHV. Fuels with low HHV, considered as “low-Btu” fuels, are more appropriate for gasification than for direct combustion where the combustion temperatures would be too low.

90% DB:10%WYC fuel characterization

Table 9 presents the characteristics of DB:WYC blend fuel. As discussed before the properties were determined using the mass of DB anWYC.

Table 9. Characterization of 90% DB: 10% WYC

Fuel Name	**90% DB: 10% WYC**
Dry loss (%)	25.015
Ash (%)	14
VM (%)	45.606
FC (%)	15.38
VM_{DAF} (%)	0.75
FC_{DAF}(%)	0.25
C (%)	37.15
H (%)	3.13
N (%)	1.791
O (%)	18.498
S (%)	0.417
HHV (kJ/kg)	13698.1
DAF HHV(kJ/kg)	22315
Dry HHV (kJ/kg)	18237
Emprical formula	$CH_{1.03}N_{0.043}O_{0.39}S_{0.001}$
$ER_{MAX\ FC \rightarrow CO}$	5.14
Stochiometric air:fuel ratio, mol basis	5.06
$ER_{FC \rightarrow CO+H2+N2}$	8.37
$AOF_{FC \rightarrow CO+H2+N2}$	0.61
$HHH_{FC \rightarrow CO}$ (kJ/kg gas)	8192.00
$HHV_{FC \rightarrow CO+H2}$ (kJ/kg gas)	11730.00

7.1.2. Ash characterization

Table 10 shows the ash analysis used in the experiments. The significant components are silicon and calcium (42.73%); other compounds such as aluminum and

magnesium oxides are present in a lower amount (~12.15%).Aluminum and magnesium oxides have been used as catalysts in previous gasification studies of biomass [15], [44].

Table 10. Ash from DB analysis

Compound	DB ash
Silicon, SiO_2	35.13
Aluminum, Al_2O_3	6.02
Titanium, TiO_2	0.21
Iron, Fe_2O_3	2.67
Calcium, CaO	17.60
Magnesium, MgO	6.12
Sodium, Na_2O	1.96
Potassium, K_2O	6.85
Phosphorus, P_2O_5	7.21
Sulfur, SO_3	2.55
Chlorine, Cl	0.32
Carbon dioxide, CO_2	2.15
Total ash analysis	88.79

7.2. Operating conditions

Table 11 and Table 12 summarize the experimental conditions. The flows of water and steam were varied to set the ER and S:F at the desired operating conditions. The maximum ER at which all the FC content in the fuel react with O_2 to produce CO, the ER and AOF at with all FC react with air and steam to produce CO, H_2, and N_2, and the HHV of gasification producing VM and CO (Equation 29) and VM, CO and H_2 (maximum HHV, Equation 31) were presented earlier in Table 8 for all fuels.

Table 11. Experimental conditions for parametric fuels (DB-ash and DB WYC)

Air flow (SATP m^3/h) (SFCH)	Steam flow (kg h^{-1})	ER	S:F
0.57 (20)	0.19	6.36	0.35
	0.43		0.80
0.85 (30)	0.19	4.24	0.35
	0.43		0.80
1.13 (40)	0.19	3.18	0.35
	0.43		0.80
1.70 (60)	0.19	2.12	0.35
	0.43		0.80
2.3 (80)	0.19	1.59	0.35
	0.43		0.80

Table 12. Experimental conditions for DB (base fuel)

Air flow (SATP m^3/h) (SFCH)	Steam flow (kg h^{-1})	ER	S:F
0.56 (20)	0.19	6.26	0.35
	0.30		0.56
	0.36		0.68
	0.43		0.80
0.85 (30)	0.19	4.24	0.35
	0.30		0.56
	0.36		0.68
	0.43		0.80
1.13 (40)	0.00	3.18	0
	0.19		0.35
	0.30		0.56
	0.36		0.68[a]
	0.43		0.80
1.70 (60)	0.00	2.12	0.00
	0.19		0.35
	0.30		0.56
	0.36		0.68
	0.43		0.80
2.30 (80)	0.19	1.59	0.35
	0.30		0.56
	0.36		0.68
	0.43		0.80

[a] base case

To match previous studies by [25] in gasification of FB but without ash disposal, two flows of air (40 and 60 SFCH) were studied in air-gasification of DB. The flows of steam and air were chosen to set the scale of the flowmeters, and the ranges of the ER and S:F were based on the results obtained in modeling studies.

7.2.1. Base case

- Fuel DB
- Air Flow rate 1.13 m^3/h
- Steam Flow rate 0.36 m^3/h
- ER 3.18
- S:F 0.68

ER > 6.36 was not studied because the peak temperatures within the bed were lower than that required for burning char (Figure 36). When the temperature in the combustion zone is lower than the char ignition temperature, heat is not released and gasification is not self sustainable.

Temperatures were measured using thermocouples Type K and stored in a flash card for posterior analysis. The flows rates of air were controlled using flow controllers. The flow rate of steam was controlled by controlling of the flow of water and power input to the steam generator, and by maintaining the level of water constant during the experiments. The evaporation rate in the steam generator was adjusted to the rate of

water entering to the steam generator by controlling the power input in the heater element. As shown before, the steam generator was previous calibrated to decrease the uncertainty in the results.

7.3. Uncertainty analysis

As discussed before, the gases were analyzed in a real time and continuously using a MS. The MS was calibrated every 72 hours for overlapping, linearity, and sensitivity. The calibration was checked out by measuring known compositions of mixtures. Appendix F presents details on the MS calibration. To estimate the uncertainty in the gas composition, standard deviation was determined for the data. The uncertainty for each gas is calculated as the ratio between the standard deviation and the average value measure. Additionally, the uncertainty of the temperatures is estimated as the ratio between the uncertainty of the device (±1.5 °C) and the measured value.

Table 13 presents the maximum, minimum, and average of the uncertainty estimated for gasification of DB, DB-ash, and DB-WYC.

Table 13 Gases data uncertainty (%) for gasification of DB, DB-ash, and DB-WYC

Gases	DB uncertainty (%)			DB-ash uncertainty (%)			DB-WYC uncertainty (%)		
	Max	Min	Average	Max	Min	Average	Max	Min	Average
CO_2	11.94	4.18	8.06	16.55	4.63	10.59	13.80	3.54	8.67
CO	31.54	10.54	21.04	26.27	12.64	19.46	17.89	12.63	15.26
N_2	6.48	3.10	4.79	7.16	4.15	5.66	5.64	4.32	4.98
H_2	21.65	15.98	18.81	23.52	17.30	20.41	29.87	12.06	20.96
CH_4	31.43	9.66	20.55	35.02	9.26	22.14	42.83	3.73	23.28
C_2H_6	23.89	6.95	15.42	32.60	7.38	19.99	32.47	4.52	18.50

Although the standard deviations of the CH_4, C_2H_6, and CO are low, the uncertainties of those gases are high because of the low average values measured. The data on gas composition of samples taken at the top of the gasifier showed a cyclic dynamic behavior in the vicinity of an average value. In general, the value fluctuated within ~15% of the average value.

As shown in Table 14, the uncertainty in the temperatures data is lower than that of the gas data. Higher uncertainties in temperature occur at the gases stream because of the value of the temperature decrease with increased distances above of the grate. The total uncertainty was estimated to be ~0.55% which is practically negligible.

The repeatability of the gas data lies between about ± 10 % of the values presented in this dissertation for gasification of pure DB, and +8 and -11% for gasification of DB-ash.

Table 14 Temperature data uncertainty (%) for gasification of DB, DB-ash, and DB-WYC

Temperatures along	DB uncertainty (%)			DB-ash uncertainty (%)			DB-WYC uncertainty (%)		
Gasifier axis	Max	Min	Average	Max	Min	Average	Max	Min	Average
2 cm above of grate	0.31	0.20	0.26	1.38	0.24	0.81	0.27	0.21	0.24
4 cm above of the grate	0.28	0.15	0.22	0.27	0.16	0.21	0.23	0.15	0.19
7 cm above of the grate	0.36	0.15	0.25	0.26	0.15	0.20	0.27	0.15	0.21
10 cm above of the grate	0.40	0.18	0.29	0.34	0.17	0.25	0.35	0.19	0.27
13 cm above of the grate	0.54	0.21	0.38	0.39	0.18	0.28	0.46	0.23	0.35
20 cm above of the grate	1.52	0.38	0.95	1.50	0.19	0.84	1.53	0.41	0.97
24 cm above of the grate	1.32	0.46	0.89	1.66	0.41	1.04	1.50	0.43	0.97
28 cm above of the grate	1.66	0.47	1.07	1.70	0.63	1.16	1.13	0.44	0.79

7.4. Temperature

This section presents experimental results on temperature profile. Figure 42 shows the evolution of axial temperatures during a typical experiment after the peak

temperature achieved nearly steady state (approximately 2 h). The time taken to preheat the bed with propane gas until the peak temperature of the bed achieved almost steady state was about 2 h. Once the steady-state condition was achieved, to establish T_{peak} at some location, the gas analysis and temperature data were stored started for 20 minutes (Figure 42).

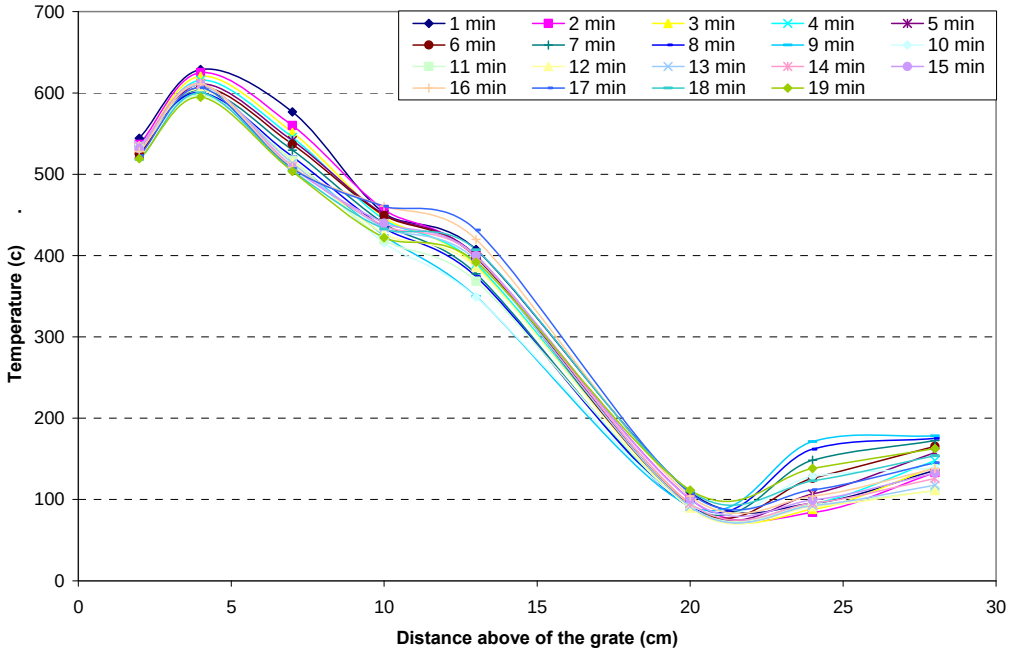

Figure 42. Dynamic temperature profile for a typical gas analysis at ER=3.18 and SF=0.8

Temperature was measured at eight locations along the gasifier. When plotted data, the points were connected to show trends; however, the connecting line may not accurately show the correct temperature profile, because there may be a peak between two consecutive points that could be different from that shown in the Figure 42. Under such conditions, a note shall be made about the actual temperature profile.

Figure 42 shows that the peak temperature was about the same distance (~4 cm) above the grate, indicating quasi-steady behavior of the bed. Also, the temperature profile curves show that temperature reached a near steady-state (SS) condition; therefore, it was appropriate to assume steady-state conditions during the last 10 min of each experiment. Although the trend of the temperature curves is the same, a complete steady-state temperature condition was difficult to achieve because of the batch feeding conditions.

As discussed before, heterogeneous oxidation occurs near the bottom of the bed where mostly char reacts with oxygen to produce heat required to drive the gasification process. Under gasification conditions, char oxidation is essentially diffusion controlled; therefore, char oxidation rate depends upon O_2 availability in the free stream. Thus, if the free-stream gas is severely depleted in O_2, the char oxidation rate with O_2 is reduced and the endothermic reactions of char with steam and CO_2 could become significant. Therefore, the temperature in the combustion zone (maximum temperature) depends on of the concentration of O_2, H_2O, and CO_2 in the combustion zone. Above the combustion zone are reduction, pyrolysis, and dry zones where the temperature decreases because most of the reactions occurring there are endothermic. Below the peak temperature, the bed is dominated by the presence of ash and hence the temperature starts to decrease. At the same time, if the rate of decrease in oxygen mass with distance is very high, the oxidation zone in the gasifier is rather thin. Then there is an overlap in the exothermic oxidation and endothermic gasification zones.

7.4.1. Base case

For the base case in which ER = 3.18 and SF = 0.68, Figure 43 shows the average temperature profile obtained during the last 10 min of the gas analysis.

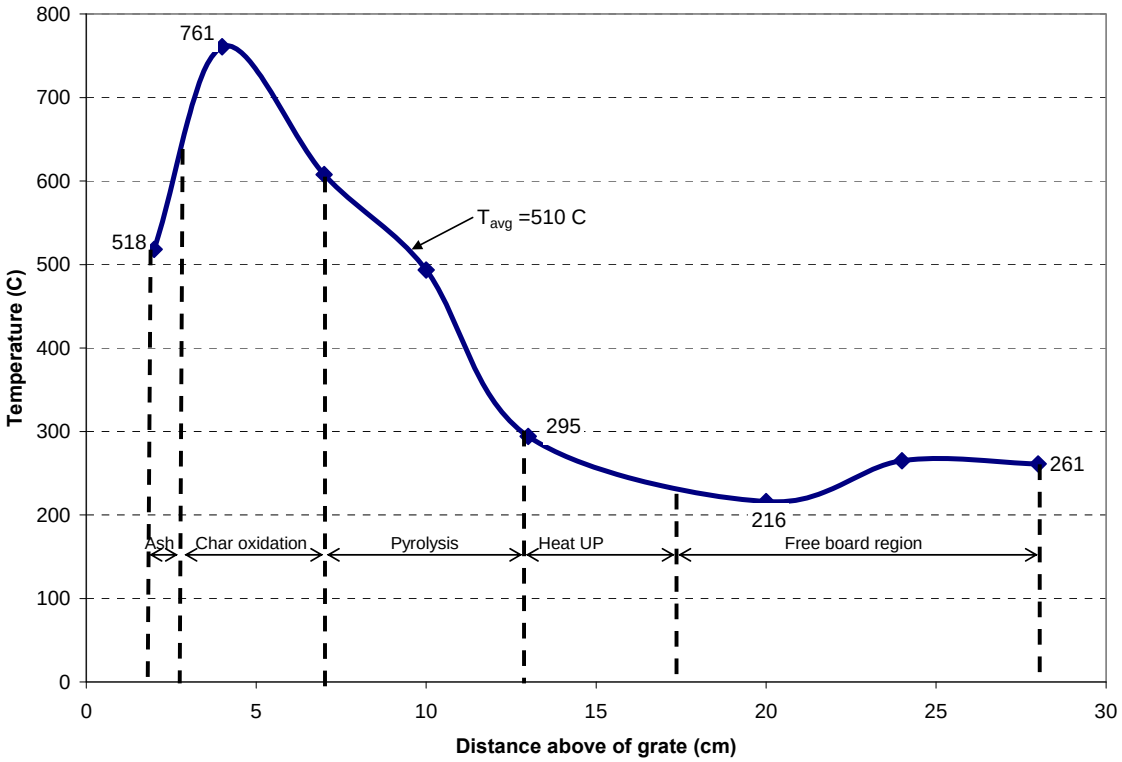

Figure 43. Temperature profile along the gasifier axis for base case ER = 3.18 and SF = 0.68

During the experiment, the bed height was kept at ~17 cm by feeding cold DB and discharging ash through the grate. From the temperature profile, the different regions in the bed can be qualitatively identified. As described earlier, the peak temperature occurs in the combustion zone whereas the other regions of the bed are

characterized by a rapid temperature fall from drying and devolatilization of the biomass. In the drying and devolatilization zones, the biomass loses mass that carries sensible heat away from the biomass particles, which reduces the temperature. Down-stream of the top bed surface, the temperature tends to be constant or to increase a little because of the released heat by the shift reaction of CO with H_2O. The temperature in the ash region below the combustion region (2 cm above the grate) is usually lower that the peak temperature. This is caused by ash accumulation at the base of the bed; in other words, the concentration of char at the bottom of the bed decreases which reduces the temperature.

AS DB gradually moves down, the particles heat up, and release water vapor first and then pyrolyzes at higher temperatures. The TGA curve of DB shown in [27] indicates that pyrolysis starts occurring at 570 - 600 K. The average temperature (510 °C) shown in Figure 43 is the integrated average temperature of the bed. Because O_2 and H_2O are available at the bottom of bed, most of the oxidation occurs near the bottom of the bed resulting in temperatures of about 761 °C (peak temperature), which correspond to particle temperature of char producing CO and H_2 by reacting of char with steam and oxygen (Reaction 3 and 6). As discussed in Section 2.1, for negligible steam carbon reaction and considering only Reaction 3, the particle temperature under negligible reduction losses can be derived using Equation 17. For instance, for S:F = 0.38 (cp of air = 1.15 kJ/(kg.K), *cp* of the steam = 2.3 kJ/(kg.K), *cp* of mixture = 1.4 kJ/ (kg.K), YO_2 = 0.182, and $hc,_I$ = 9204 kJ kg^{-1}). The T_p is estimated as 1275 K, which corresponds to a higher value than the measured value (1034 K or 761 °C) at the bottom bed (Figure 43).

The lower experimental temperature (1034 K) compared to that evaluated with Equation 17 (1275 K), indicates that char may react with both O_2 and steam at the bottom of the bed to produce CO and H_2. When the steam carbon reaction is included in the model and if diffusion control in heterogeneous reactions is assumed, the estimated T_p is much lower than that of the experimental data. Under similar operating conditions (ER = 3.68 and S:F = 0.68) the temperature computed from the current equilibrium model is about 900 K (Figure 36), which is higher than the average measured value (783 K or 510 °C).

If the pyrolysis temperature starts occurring at 570-600 K [27] and the char ignition temperature is ~870 K, then from Figure 43, it is apparent that the combustion and pyrolysis regions occurs between ~3 and ~7cm and between ~7 and ~13 cm, respectively. The dry region moves from ~13 to ~18 cm. The small change in temperature (after 18 cm indicates) indicates that the gas stream region start to occur at 18 cm above the grate.

The slight temperature increase observed above of the bed surface, in the free-bound region, indicates that the homogenous exothermic reactions of combustible gases with the steam liberated by the biomass possibly produce CO_2, H_2, and heat.

7.4.2. Temperature profiles with air and steam for base fuel

Figures 44 to 47 show experimental results on temperature profiles as a function of the ER and for different SF ratios.

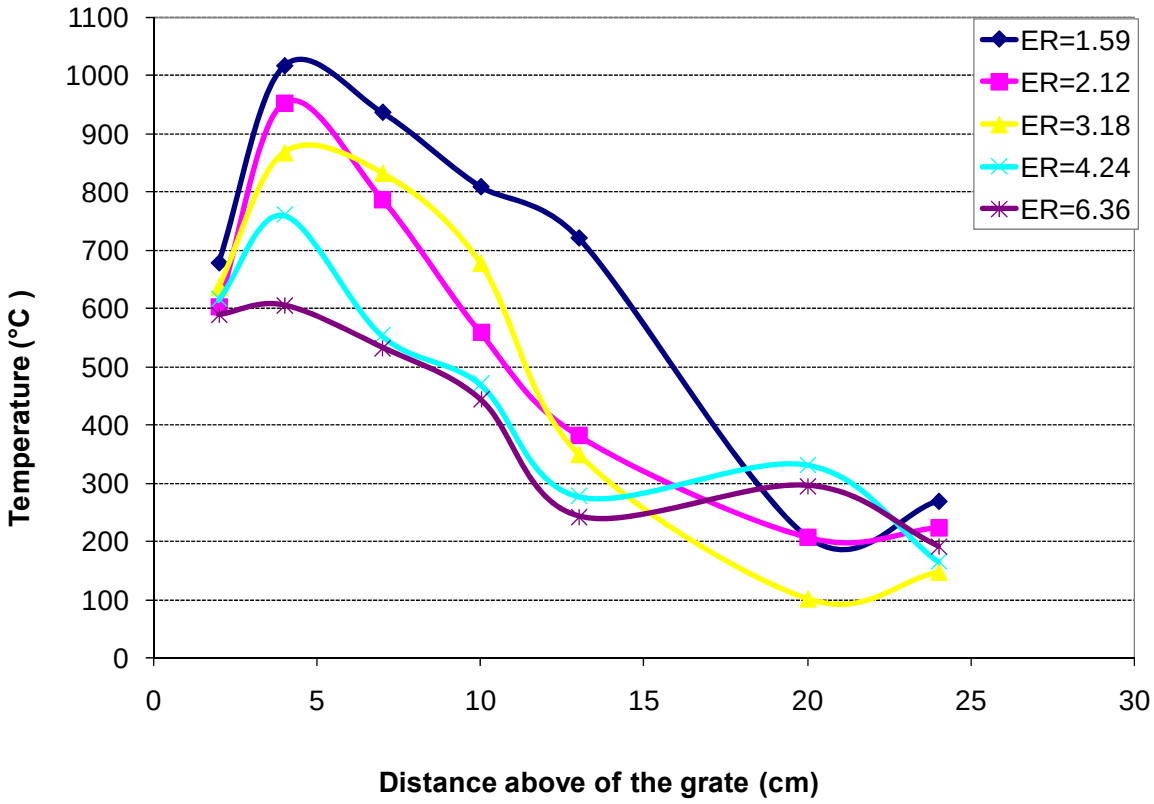

Figure 44. Temperature profile along the gasifier axis for SF=0.35 and various ERs

The general trend of the temperature profiles for 0.35 < S:F < 0.8 and 1.59 < ER < 6.36 show that the peak temperature in the combustion zone decreases with increased ER and the peak temperature is located somewhere between ~4 and ~5 cm above the grate. This results from continuous ash disposal from the combustion chamber to the gasifier plenum. In the earlier co-gasification studies developed by [25], the peak temperature shifts continuously toward the free surface because of ash accumulation in the bed bottom that had no ash-disposal system.

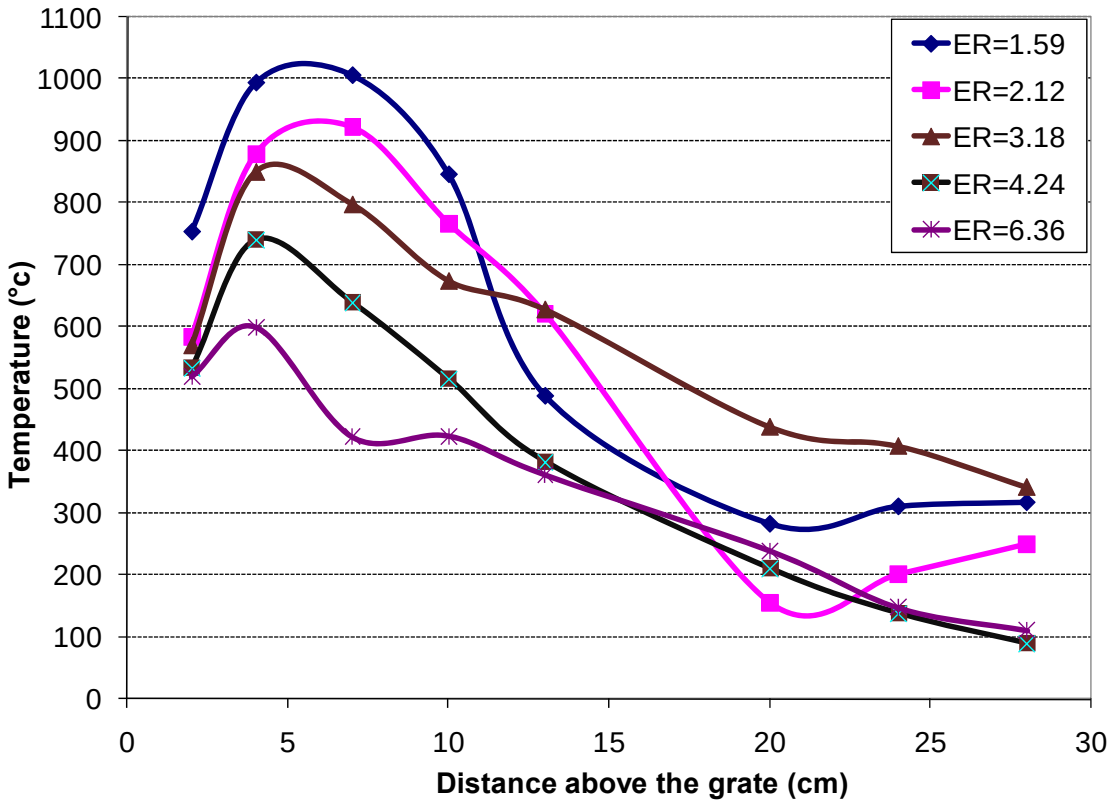

Figure 45. Temperature profile along the gasifier axis for SF = 0.56 and various ERs

Increased ERs means less oxygen supply; hence, the reaction of char and oxygen 0ccurs in a poor O_2 and rich H_2O environment that promotes the endothermic reaction of char with steam. Additionally, the reaction of C atoms and O_2 that is diffusion controlled produces more CO than CO_2 because of the low oxygen concentration [33] in the combustion region.

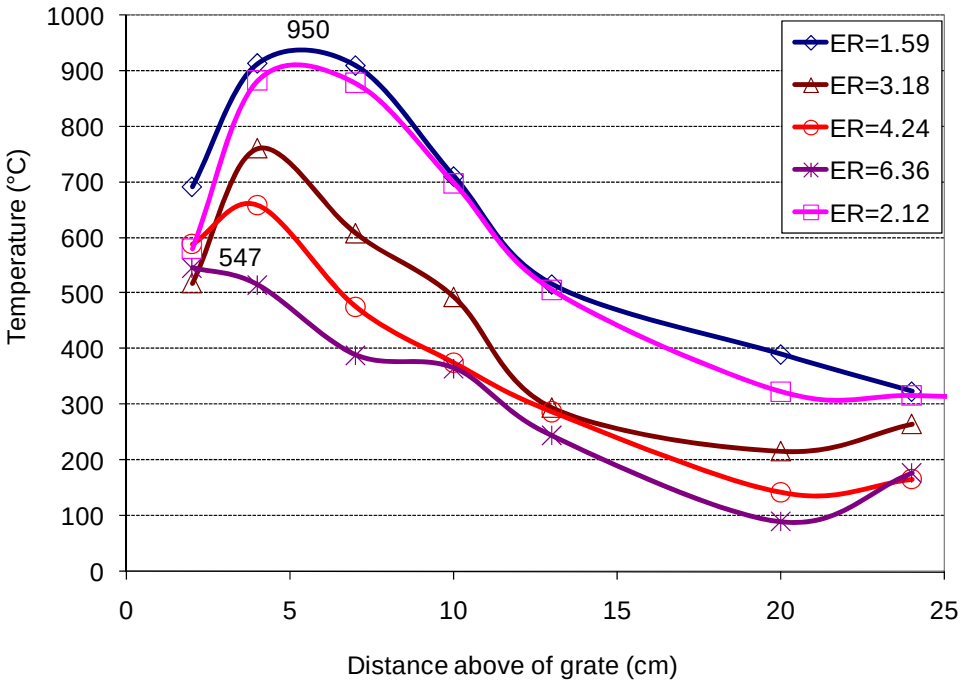

Figure 46. Temperature profile along the gasifier axis for SF = 0.68 and various ERs

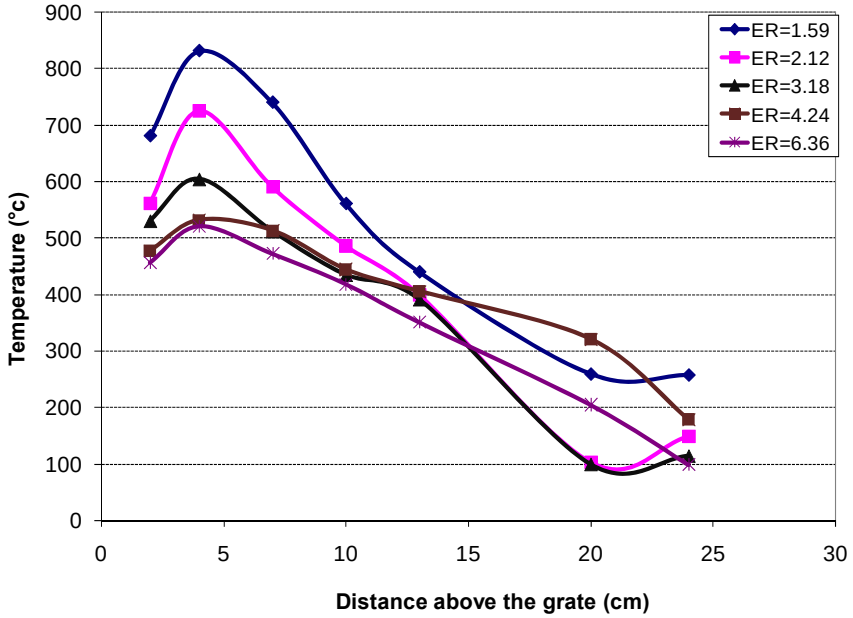

Figure 47. Temperature profile along the gasifier axis for SF = 0.80 and various ERs

The temperatures 2 cm above of the grate are lower than in the peak zone, indicating that much of the material available in the bottom of the bed is ash. It is also apparent that below the peak zone at 2 cm above the grate, the temperature is not monotonically decreasing with increasing ER.

The temperature in the reduction, pyrolysis, dry, and gases zones tends to decrease with increased ER (Figures 43 and 47). However, at some locations, the temperature increases with increased ER because the biomass is fed to the gasifier in batch form and it is very difficult to achieve steady state, particularly near the top surface. When biomass is added to the gasifier, the bed materials placed above the combustion zone move downward and the gas stream is destabilized producing temperature changes. Furthermore, the biomass added in each experiment is not distributed uniformly in the gasifier causing a different temperature profile.

7.4.3.Temperature profile with air for base fuel (DB)

Figure 48 shows results on temperature profile of DB gasification using pure air as oxidizer for ER = 2.12 and ER = 3.18.

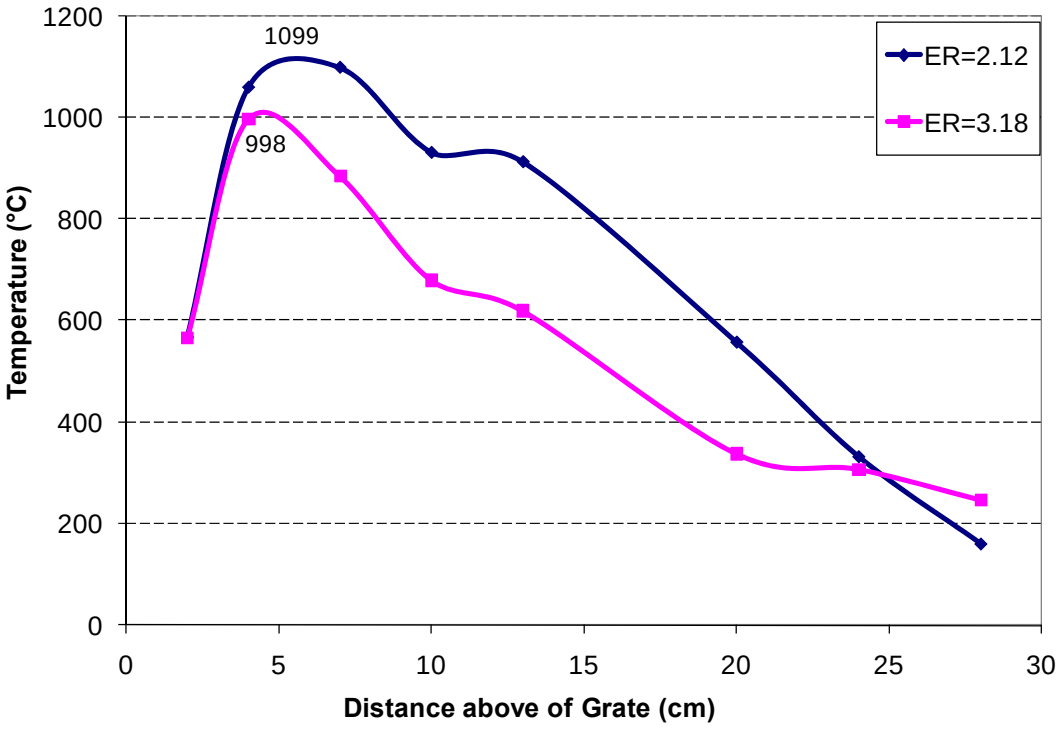

Figure 48. Temperature profile along the gasifier axis for gasification with air only at ER = 2.12 and ER = 3.18

Performing similar calculations as mentioned in a previous section, the particle temperature for gasification with air producing CO is estimated to be about 1754 K at ER = 2.12 (estimated with Equation 17), whereas the experimental peak temperature is about 1373 K (1100 °C) (Figure 48). The higher theoretical value results principally because of i) lower C_p, ii) CO_2 production due to increased O_2 concentration in the bottom of the bed, iii) neglect of the radiative losses, and iv) the finite kinetics controlled chemicals reaction.

The air flow rate is an important variable influencing the temperature profile in the bed. Increasing the air flow rate increases the availability of more O_2 to the fuel and

hence, CO can oxidize to CO_2, which results in an increase of the peak temperature in the bed.

From Figures 44 through 48, the peak temperature, which coincides with the char oxidation zone of the bed, is higher for gasification with air (~1100 °C) than that for gasification with air-steam mixtures (1030 °C). The reason is that in gasification with air, there is no steam at the bed bottom to cause endothermic reaction of C with H_2O; however, the CO produced by heterogeneous oxidation in the bed bottom may still react with the moisture of the fuel downstream to produce CO_2 and H_2. The H_2 production with air only has been verified in the past by [25] when gasifying wet feedlot biomass (FB) with pure air as the oxygen source.

7.4.4. Peak temperature with air and steam for base fuel (DB)

Figure 49 shows the effect of change in S:F and ER on peak temperature (combustion zone). Figure 49 shows that the effect of the ER on peak temperature is strong compared to S:F. At S:F = 0.8, increasing ER from 1.59 to 6.36 decreases the peak temperature by about 311 °C whereas at ER = 1.59, increasing the S:F ratio from 0.35 to 0.80 decreased the peak temperature by about 185 °C. Also, at lower ER, the effect of the S:F ratio is higher. For instance, at ER = 1.59 the peak temperature difference between the curves of S:F = 0.35 and 0.80 is ~185 °C whereas at ER= 6.36 the difference between the same curves is only 91 °C. Figure 49 shows that at constant S:F, the peak temperature decreases almost linearly with increase in ER. Increased S:F

ratio causes the peak temperature to decrease, which can occur because of i) decreased amount of air, ii) change in c_p of the mixture, iii) change in regime of combustion-kinetics vs diffusion control, and iv) steam-char reaction.

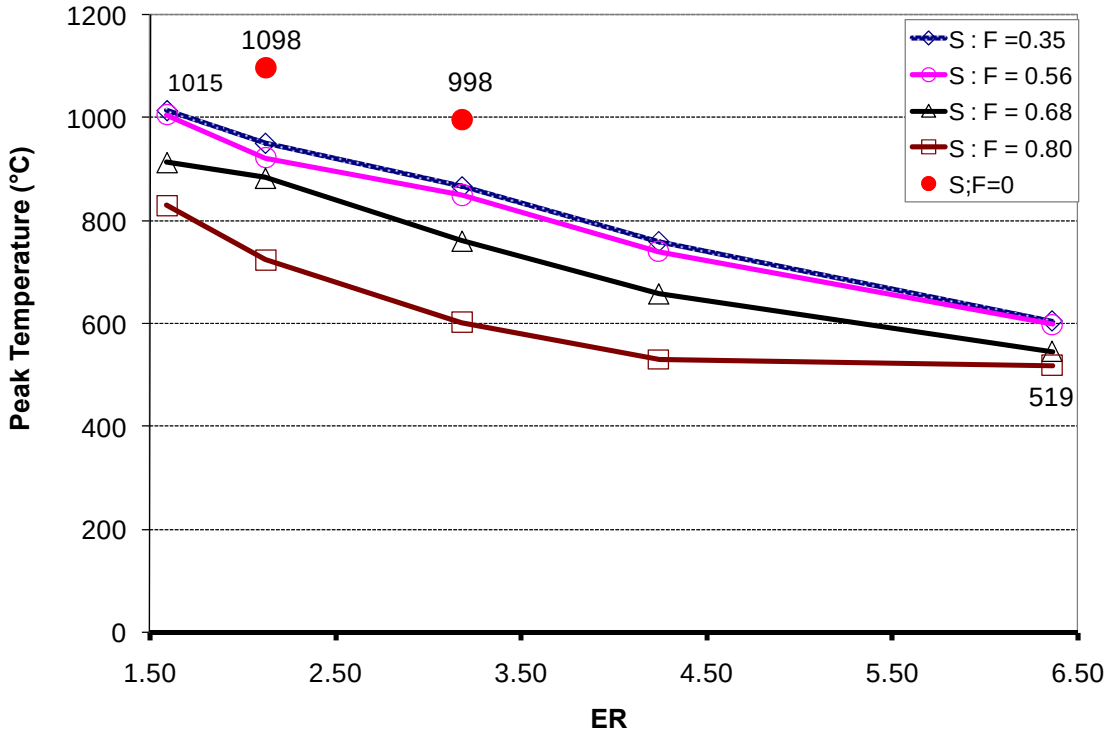

Figure 49. Peak temperature as a function of the ER and several S:F ratios. S:F = 0 indicates gasification only with air

As discussed before, the peak temperature for gasification with air only is higher than that for gasification with air-steam; it could be caused by decreasing c_p of the mixture, increasing diffusion rate, and negligible char-steam reaction. At ER = 2.12, the peak temperature for gasification with air only is about 147 °C (15.45%) higher as compared to that of gasification with air-steam at S:F = 0.35 while at ER = 3.18, the

difference in peak temperature between gasification with air and gasification with air-steam is ~ 132 °C (15.24%).

The percentage increase in peak temperature between gasification with air-steam at S:F = 0.35 and gasification with air only is almost constant; thus, it is appropriate to assume 15.35% as increase in temperature to estimate the peak temperature for gasification using air. Under that assumption, the peak temperature for gasification with air at ER = 1.59 and at ER = 6.36would be ~1190 °C and 704°C, respectively.

7.4.5. Fuel: ash blend (90% DB-10% ash) with air and steam

In this section, the results for temperature profiles obtained for co-gasification of DB-ash blend (90% DB-10% ash) are presented. The results presented in Figure 50 and Figure 51 show that the temperature curves for gasification of DB-ash blend are almost the same as those for gasification of DB presented earlier. The peak temperature lies between 4 and 7 cm above of the grate and increases with decreased S:F ratio (e.g., at S:F = 0.35 the peak temperature is about 1030 °C whereas at S:F = 0.8. it is about 860 °C).

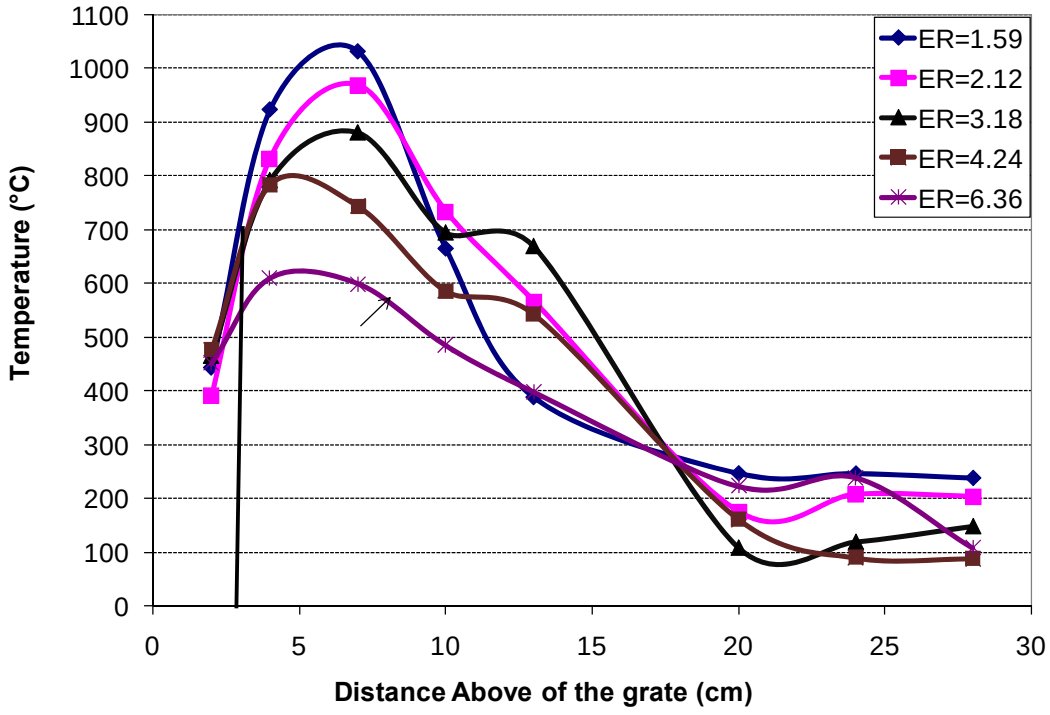

Figure 50. Temperature profile along the gasifier axis for gasification of DB-ash blend at S:F = 0.35

Although the temperature in the combustion region (peak temperature) depends mostly on the oxygen (ER) and steam concentration (S:F), the peak temperature for gasification of the DB-ash blend is a little higher (~15 °C) than the peak temperature of gasification DB under the same operating conditions (ER=1.59 and S:F=0.35); this can due to decreased porosity of the bed (void fraction). Adding ash to the DB decreases the bed porosity because the particle size of the ash is less than the particle size of the DB (~1/4”). From Equations 9 and 11, it can be seen that decreased porosity increase the burn rate per unit volume of the bed, causing a higher heat generation in the oxidation zone, which lead to a higher temperature. Lower bed porosities lead to higher oxidizer

velocity around of the char particles increasing the diffusion coefficient (equation 12), which also improve the char burn rate. As porosity decreases, the bulk density of char in the combustion region increases, increasing the bed heat capacity, which may require more sensible heat energy to heat it to a higher temperature. Nevertheless, from the above figures, it is apparent that the effect caused by a higher heat capacity in the oxidation zone is compensated by the temperature rise effect due to more heat generation.

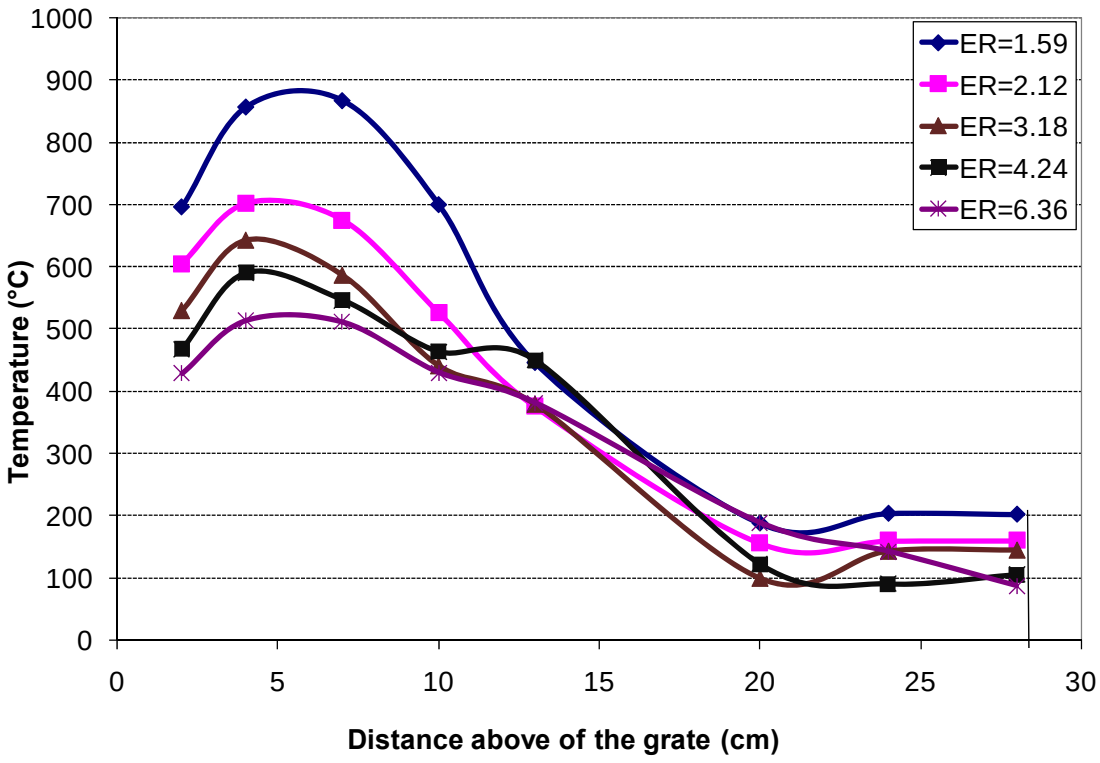

Figure 51. Temperature profile along the gasifier axis for gasification of DB-ash blend at S:F=0.80

Increased porosity leads to a higher convective heat transfer in the bed; thus, in case of larger bed porosity, the temperature may not only be lower because of the lower burn rate, but also may be lower because of the higher rate of heat loss from the oxidation zone.

The earlier figures show that adding ash does not affect much the temperature in the free-board region because the temperature measured in the gas stream region (100-250 °C) was almost the same for gasification of DB and DB-ash.

7.4.6. DB: WYC blend (90% WYC-10% ash) with air and steam

This section presents the temperature profile for co-gasification of DB and WYC. The temperature profile presented in Figures 52 and 53 for DB-WYC blend is almost the same as those of DB and DB-ash blend. The peak temperature, measured in the combustion region, lies about 5 cm above of the grate (Figure 52) and it is a slightly higher (1054 °C) compared to those of DB (1016 °C) and DB-ash blend (1030 °C), which were tested at ER =1 .59 and S:F = 0.35.

The small difference between the combustion temperatures indicates that the char in DB and WYC may have a similar composition. If the char of DB and WYC have the same composition, the increase in the peak temperature for gasification of DB-WYC may be attributed to decreased bed porosity because the particle size of WYC is lower than the particle size of ash and DB. As discussed above, decreased bed porosity increases combustion temperatures because of increased diffusion.

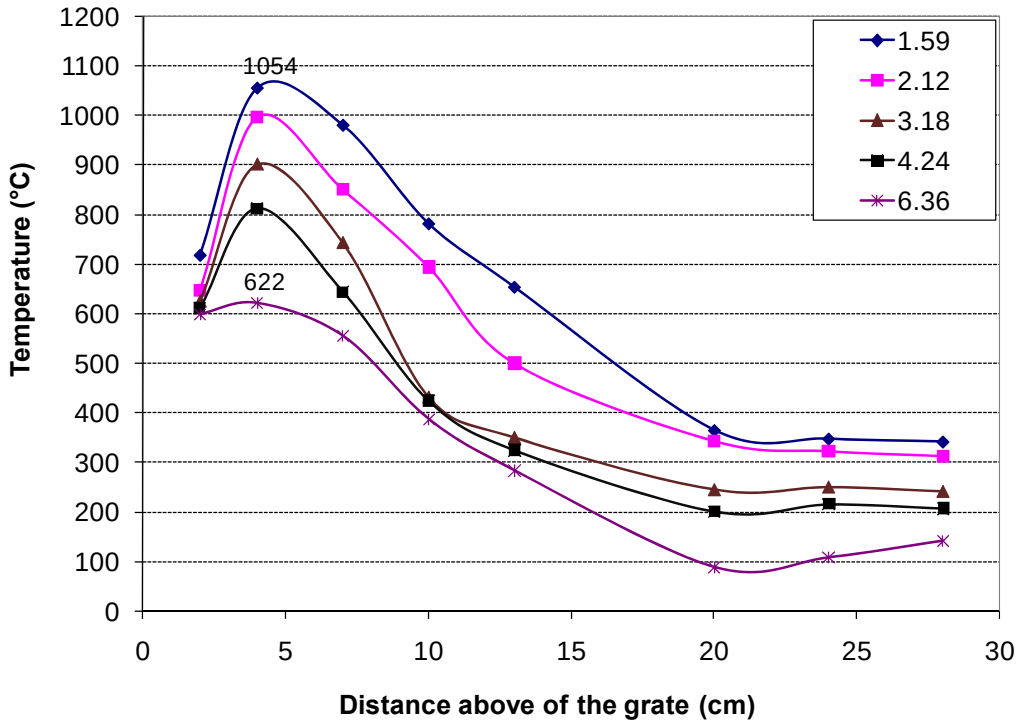

Figure 52. Temperature profile along the gasifier axis for gasification of DB-WYC blend at S:F = 0.35

The higher gas temperatures measured above of the bed for DB-WYC blend indicates that more heat is released per unit mass of fuel (higher HHV of fuel) and less sensible energy is absorbed in the pyrolysis and dry regions. In other words, because of lower moisture (22.81%) and VM (34.5%) content in WYC compared to those of DB (25.26% and 46.84%), gasification of DB-WYC blend produces less volatiles and steam. Therefore, the heat required in the devolatilization and drying regions is less and more sensible energy leaves the gasifier with the gases.

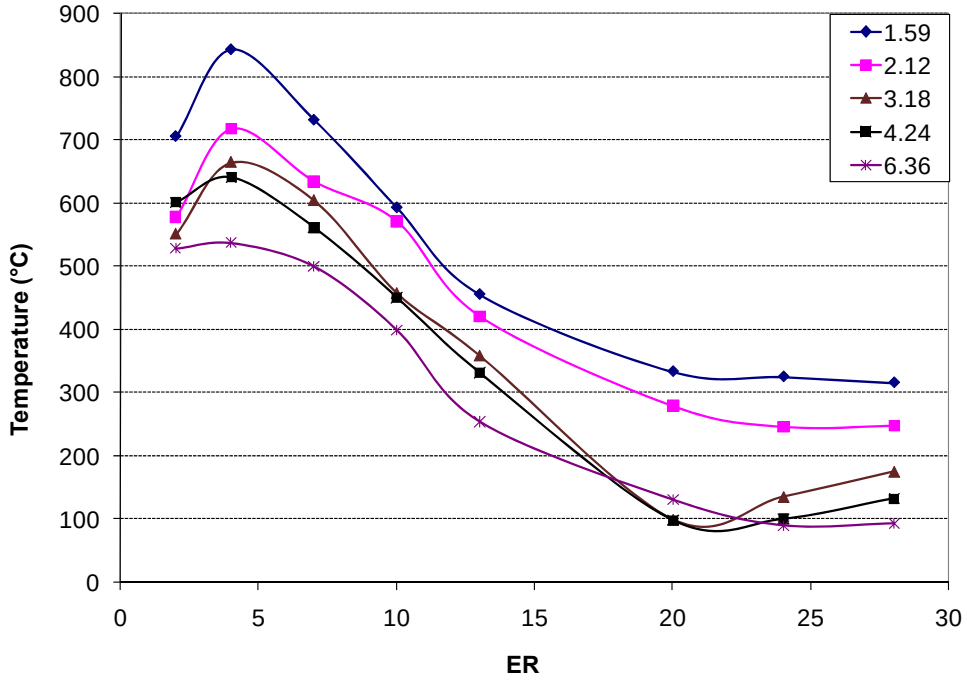

Figure 53. Temperature profile along the gasifier axis for gasification of DB-WYC blend at S:F = 0.80

Co-gasification of DB with WYC does affect the temperature very much in the regions closer to the grate because this temperature correspond to the ash temperature, which is more affected by the heat diffusion from the combustion region and by the convection of heat from the combustion zone.

7.4.7. Comparison of peak temperature of base fuel (DB), (90% DB-10% ash) and (90% DB-10% WYC)

Figure 54 presents the peak temperatures in the combustion region for gasification of DB, DB-ash and DB-WYC as function of ER and S:F ratio.

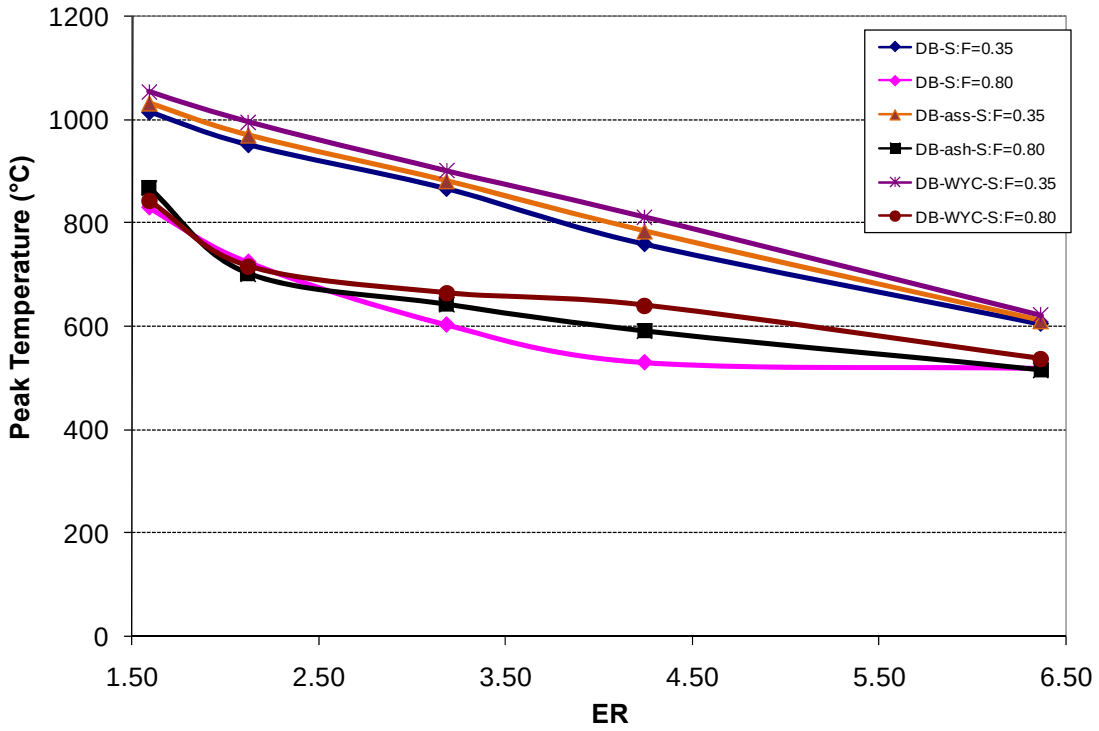

Figure 54. Comparison of peak temperature of gasification of DB and co-gasification of DB-ash and DB-WYC

At S:F = 0.35, the difference in peak temperatures between gasification of DB and co-gasification of DB-ash and DB-WYC is not much. The highest peak temperature was achieved for DB-WYC whereas DB had the lowest peak temperature. The peak temperature of DB-ash lies between the peak temperature of DB and DB-WYC. As discussed before, the dissimilarity in peak temperature may be caused by a variation between the bed porosity during DB gasification and co-gasification of DB-ash and DB-WYC blends. Also, higher char content for DB-WYC blend increases the amount of energy released in the bed, which increases the peak temperature. At S:F = 0.80 and 2.12

< ER < 6.36, the peak temperature of DB-WYC is higher than DB-ash and DB; however, at ER = 1.59 and ER = 6.36, the difference between the peak temperature for all cases is very small.

7.5. Gas composition

This section presents the gas composition results for gasification of base fuel and parametric fuels. The operational conditions were presented earlier in Table 11 and Table 12. The results obtained on gas composition are discussed in this section: i) base case, ii) base fuel, and iii) parametric fuels.

A mass spectrometer (ProLab Thermo ONIX) was used to analyze the gas composition. Appendix F discusses the principle of operation and the procedure used.

The gas samples were taken from the top of the gasifier and were passed through a sampling system to condense tar and water and to capture the particulate material to protect the mass spectrometer. Gases analyzed include nitrogen (N_2), carbon oxides (CO_2 and CO), hydrogen (H_2), hydrocarbons (CH_4 and C_2H_6), and oxygen (O_2). A typical gas analysis performed by the mass spectrometer is shown as a function of the time in Figure 55 for a typical experiment at ER = 4.24 and S:F = 0.35. As discussed before, gas analysis started as soon as the temperature in the combustion zone achieved almost steady state (T_{peak} at same location during the experiment) and gas composition was monitored continuously for 20 min in to decrease the uncertainty in the results. Figure 55 shows that the data on gas composition have a cyclic dynamic behavior in the

vicinity of an average value. However, at first glimpse, it appears that the average is almost constant during the experimental period. Figure 55 shows the mole fraction of N_2, H_2, CO_2, CO, CH_4, and C_2H_6 (on a dry basis) along with the average mole fraction and the standard deviation (STDEV) of the data. The gas analysis did not indicate presence of O_2 in the products obtained in the set of experiments; thus, O_2 is not discussed in this dissertation. The data on H_2 presents the major standard deviation(3.2) about of the average value of 18.62% whereas the data on CH_4, CO_2, and C_2H_6 show the lower standard deviation and the data on CO shows a standard deviation of 1.53. See section for the uncertainty in the analysis of gases.

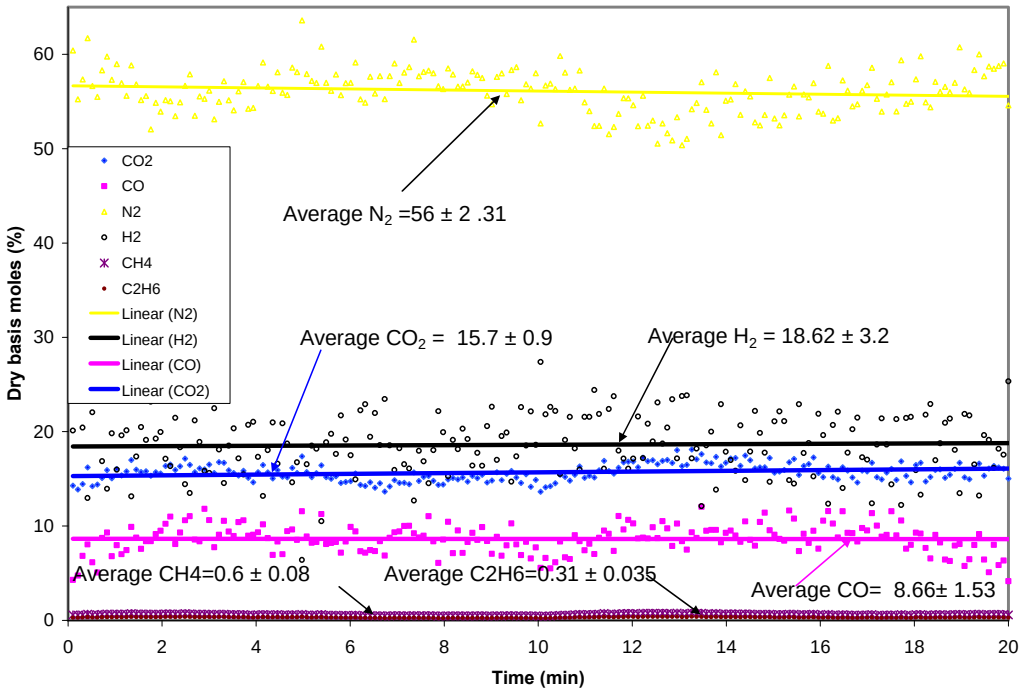

Figure 55. Typical gas analysis for a typical experiment at ER = 4.24 and S:F = 0.35 performed by mass spectrometer

Although temperature profiles along the gasifier axis show that the temperature reaches almost a steady state condition within 10 minutes after the start of gas analysis (Figure 42), the data on gas composition (Figure 55) show that the average gas composition is almost constant during the experiment period (20 min). The results on gas composition discussed in this dissertation (unless other-wise specified) correspond to the average value tested during the last 10 min of each experiment.

7.5.1. Gas composition for base case fuel DB with air and steam

Figure 56 shows a bar graphic of the average dry gas composition obtained during the last 10 min for the base-case fuel at ER = 3.18 and S:F = 0.68.

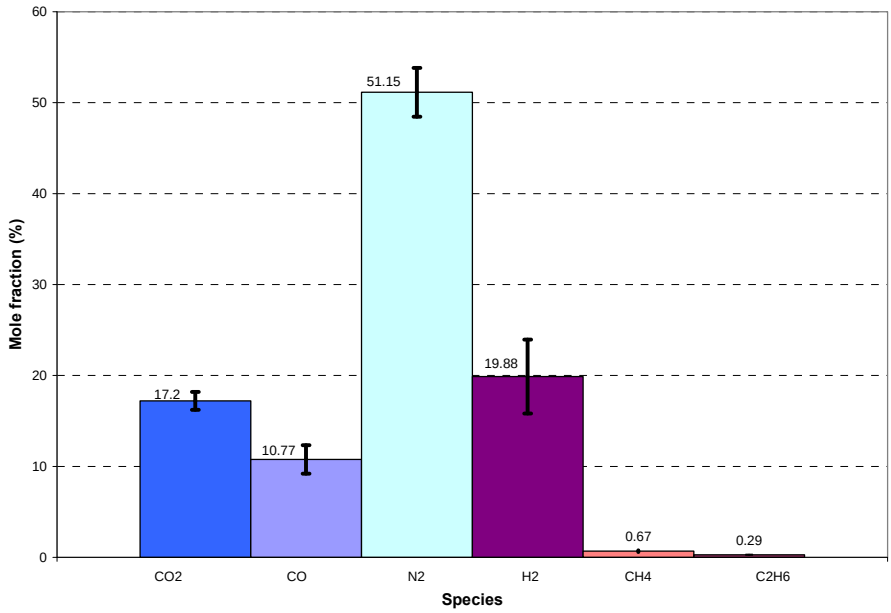

Figure 56. Gas composition for base case at ER=3.18 and S:F=0.68

The gas analysis shows the presence of both combustible and non-combustible gases. The primary products in the gases are non-combustibles, such as N_2 and CO_2 with a total of 68.39% whereas other combustibles species (H_2, CO, CH_4, and C_2H_6) achieve 31.61%. The dominant fuel component is H_2 (19.88 ±4%, which is almost 70% of the combustibles), which suggests that the steam supplied favors the steam reforming and shift reactions. In the earlier study developed by Priyadarsan et al., [25], steam was not supplied to the gasifier and the molar composition of H_2 was only of 7-10% with CO about 25%. Also, the current molar concentrations of CO (10.77±1.5%) and CO_2 (17.2±0.98%) indicates that the CO produced from char-O_2 reaction reacts with H_2O supplied in the oxidizer to produce H_2 and CO_2. Other hydrocarbons such as CH_4 and C_2H_6 show much lower concentrations in the products but they have high HHV. It may result because the lower temperatures generated by the endothermic reaction of char and steam in the combustion and reduction regions which are not enough for the heterogeneous reaction of char and H_2 to produce CH_4. In other words, the production of CH_4 and C_2H_6 is mainly due to pyrolysis of volatile matter and not to the heterogeneous reaction in the reduction region. In Figure 56, it may also be observed that the data on diatomic gases (H_2 and N_2) has the highest standard deviation whereas the hydrocarbons presented the lowest standard deviation.

7.5.2. Variation of gas composition base fuel (DB) with ER and S:F

This section describes the variation of gas composition of the products obtained for gasification of the base fuel (DB). Figures 57 through 60 show mole fraction on a dry basis of the H_2, CO_2, CO, CH_4, and C_2H_6 as a function of the ER and for different S:F ratios.

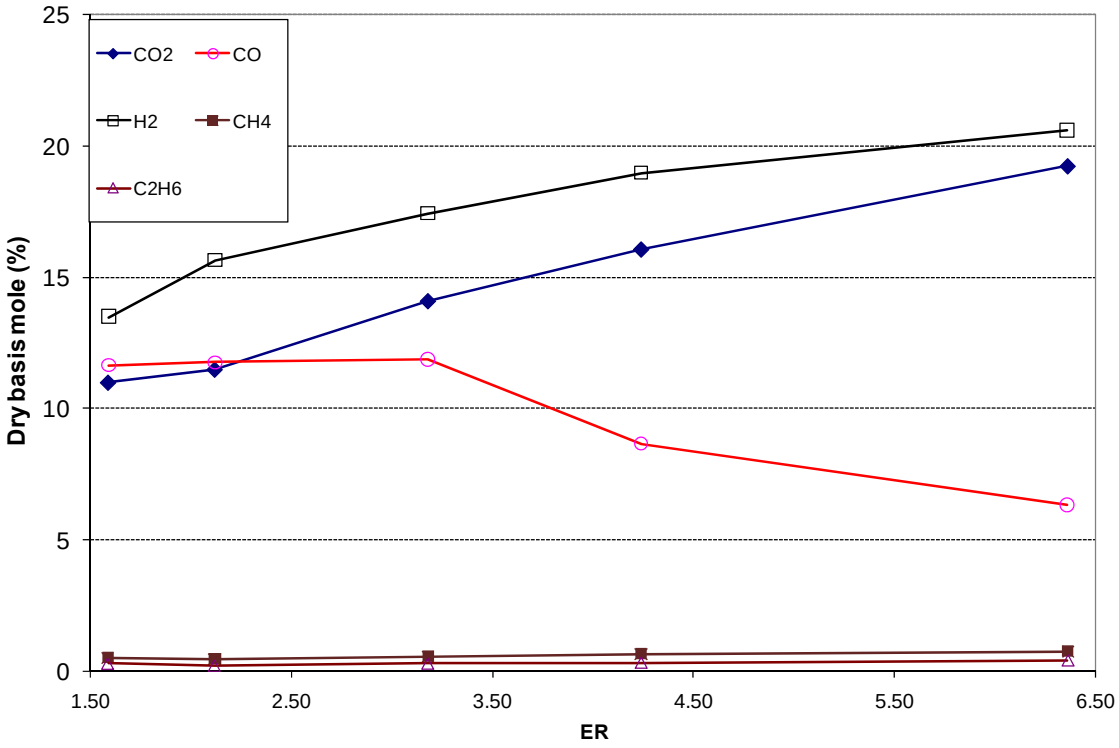

Figure 57. Gas composition for gasification of DB as a function of ER at S:F=0.35

At constant S:F, increasing the ER decreases the O_2 supplied with the air at the bottom, which decreases the peak temperature in the combustion zone; thus, as the

temperature is lowered, the thermodynamics favor the reaction $C+O_2 \rightarrow CO_2$. CO_2 increase at lower combustion temperatures. It is recalled that the CO/CO_2 ratio is function of temperature (Equation 16). When CO_2 is liberated, the heat delivered per unit mass of oxygen is 12,300 kJ/kg of O_2 whereas for CO, the heat delivered is 6910 kJ/kg of O_2 only. As CO decreases, CO_2 increases the heat input because the oxidation will increase, which tends to increase temperature. More CO_2 production implies consumption of more O_2 via CO_2 than via CO, and hence less CO is formed.

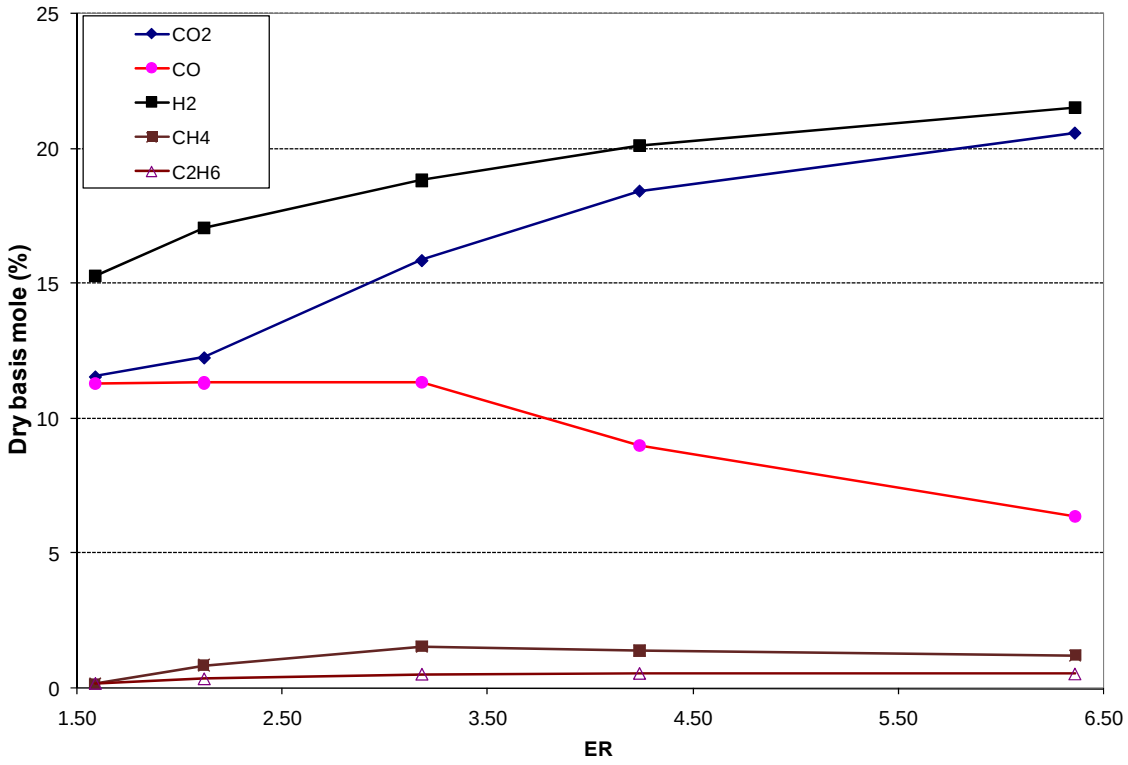

Figure 58. Gas composition for gasification of DB as a function of ER at S:F=0.56

Additionally, at constant S:F, increased ER implies decreased air supplied and hence increased steam: air ratio (S:A) and the char combustion occurs in a H_2O rich

mixture which favors the heterogeneous reaction of char with H_2O to produce CO and H_2. The rate of H_2 and CO produced by the heterogeneous reaction of the char with H_2O becomes important when the reaction occurs at low O_2. On the other hand, the concentrations of CH_4 and C_2H_6 were lower ($1 < CH_4 < 2$ and $0.5 < C2H6 < 1$) compared with those of other gases and were almost not affected by ER. However, for S:F = 0.56 and S:F = 0.68 the production of CH_4 shows a slight peak at ER = 3.18 and ER = 4.24 respectively (Figures 58 and 59**).** At other S:F ratios, the mole fraction of CH_4 and C_2H_6 tend to increase with increased ER.

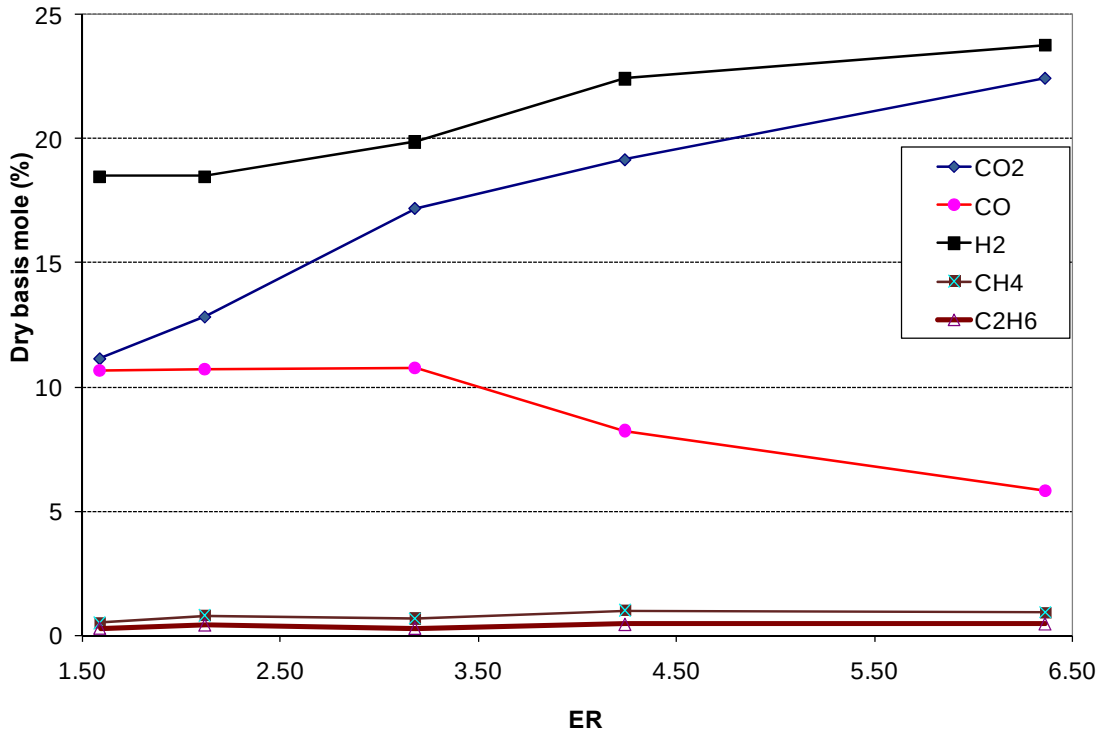

Figure 59. Gas composition for gasification of DB as a function of ER at S:F=0.68

From Figures 57 to 60, it may be observed that at constant S:F ratio, ER < 3.18 don affect much the production of CO. However, at ER > 3.18, the CO mole fraction decreases considerably with increased ER.

The H_2 trend curves show an increase in mole fraction with increased ER. At 3.18 < ER < 4.24, the H_2 production seems to increase faster with increased ER than at ER < 3.18. The tendency of the curves of H_2 and CO suggests that, at ER ranging from 3.18 and 4.2, the reaction $CO+H_2O \rightarrow H_2+CO_2$ is strongly favored by increased ER. At ER ranging from 1.59 to 3.18, the production of CO_2 seems to be more affected by changes in ER.

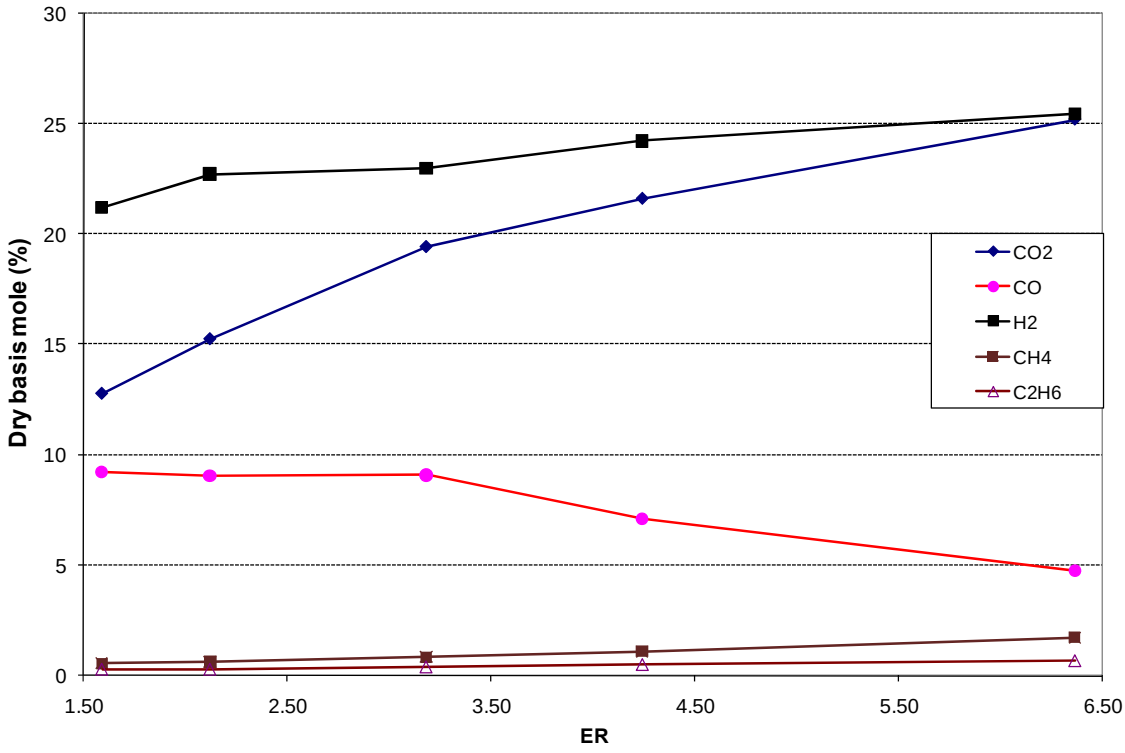

Figure 60. Gas composition for gasification of DB as a function of ER and S:F = 0.80

Figure 61shows the effect of the ER on the concentrations of H_2 at various S:F ratios. At constant ER, higher S:F ratios signify more steam available to react with char to produce CO and H_2 (steam char reaction) in the bottom of the bed (combustion zone). The CO produced by the steam reforming reaction posterior reacts with the surplus steam in the upper zones (reduction zone) to produce more H_2 and CO_2 (shift reaction.

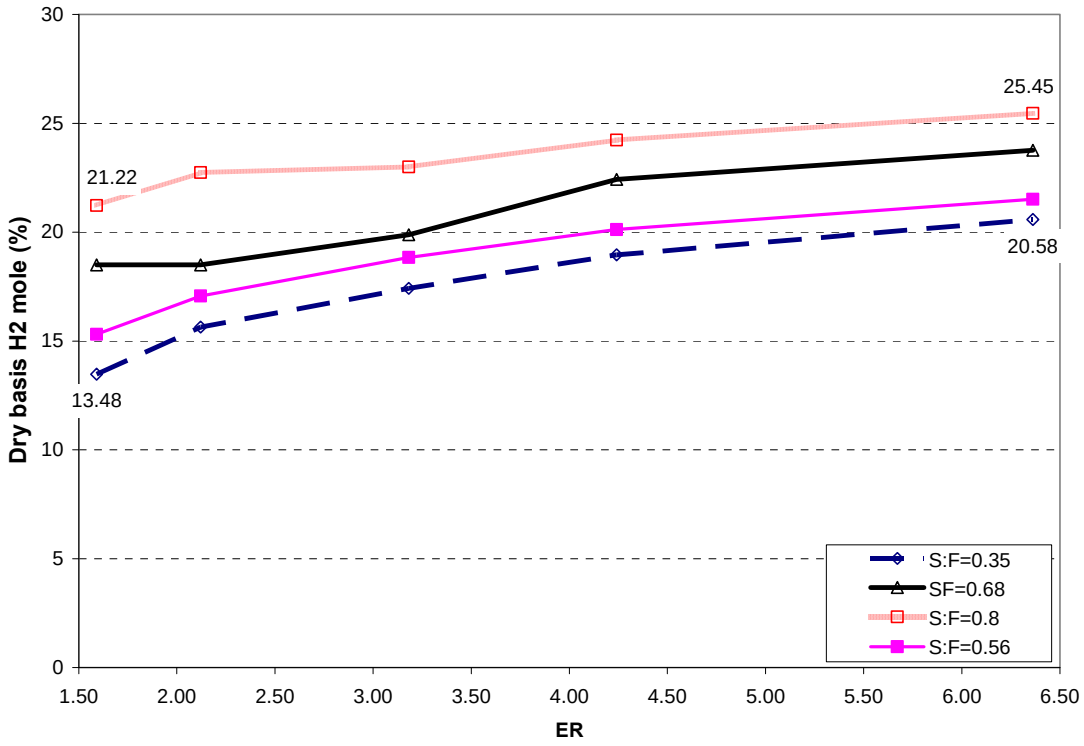

Figure 61. H_2 composition for gasification of DB as a function of ER at several S:F

It is evident from Figure 61 that at lower S:F ratios, ER affects the H_2production more than at higher S:F ratios. For instance, at S:F = 0.35 increasing the ER from 1.59 to 6.56 increases the H_2 mole fraction by about 53 % whereas at S:F=0.80, changing the ER

from 1.59 to 6.36 increases the H_2 by only 22%. Also, the effect of the S:F ratio on H_2 production is more significant at lower ER than at higher ER. At ER = 1.59, changing the S:F from 0.35 to 0.80 increases the production of H_2 by 57.5%, but at ER = 6.36, increasing the S:F from 0.35 to 0.68 increases the H_2 mole fraction by only 24%.

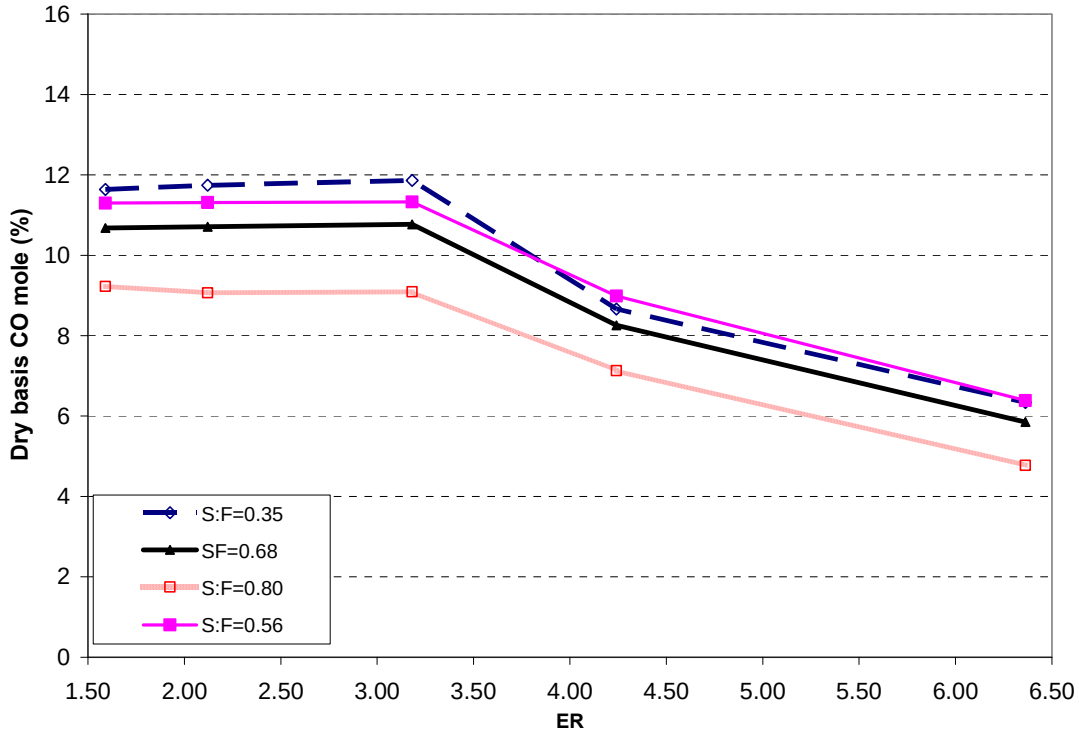

Figure 62. CO composition for gasification of DB as a function of ER at several S:F

From Figure 62, it appears that at constant S:F ratio, the effect of the ER on CO production at ER < 3.18 is practically insignificant, but at ER > 3.18, the increased ER strongly decreases the CO mole fraction. A comparison between the effect of ER and

S:F ratio shows that at ER > 3.18, the effect of ER is higher than that of the S:F; however, at ER < 3.18, S:F seems to affect CO production more than ER.

Also, the results show that at constant ER, changing S:F ratio affects H_2 production more than CO production. For instance, at ER = 1.59 changing the S: F from 0.35 to 0.8 increases H_2 production by ~57 % but decreases CO production of by only 20.7 %.

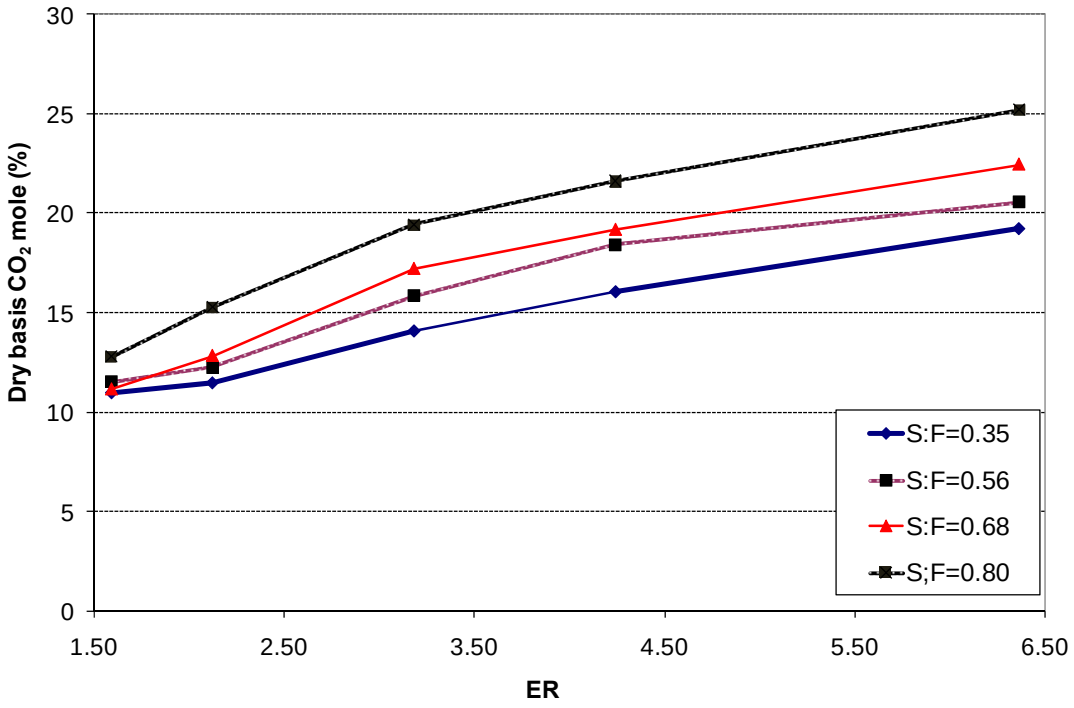

Figure 63. CO_2 composition for gasification of DB vs ER at several S:F

Figure 63 presents the CO_2 molar fraction is presented in as a function of the ER for several S:F ratios. As discussed earlier, at constant S:F ratio, increased ER signifies less oxygen entering with the air supplied to the gasifier; thus, the char reacts with the

oxidizer in an environment rich in H_2O, which favors the reaction $C+H_2O \rightarrow CO+H_2$. However, the remaining steam from the combustion region reacts in the downstream region with CO to produce CO_2 and H_2. Less C atoms leaving the gasifier as CO imply more C atoms leaving as CO_2. ER affects the CO_2production more than S:F.

7.5.3. Gas composition for DB in air

A set of experiments were performed on DB gasification using only air as oxidizing agent. This section presents the results of gas composition on a dry basis.

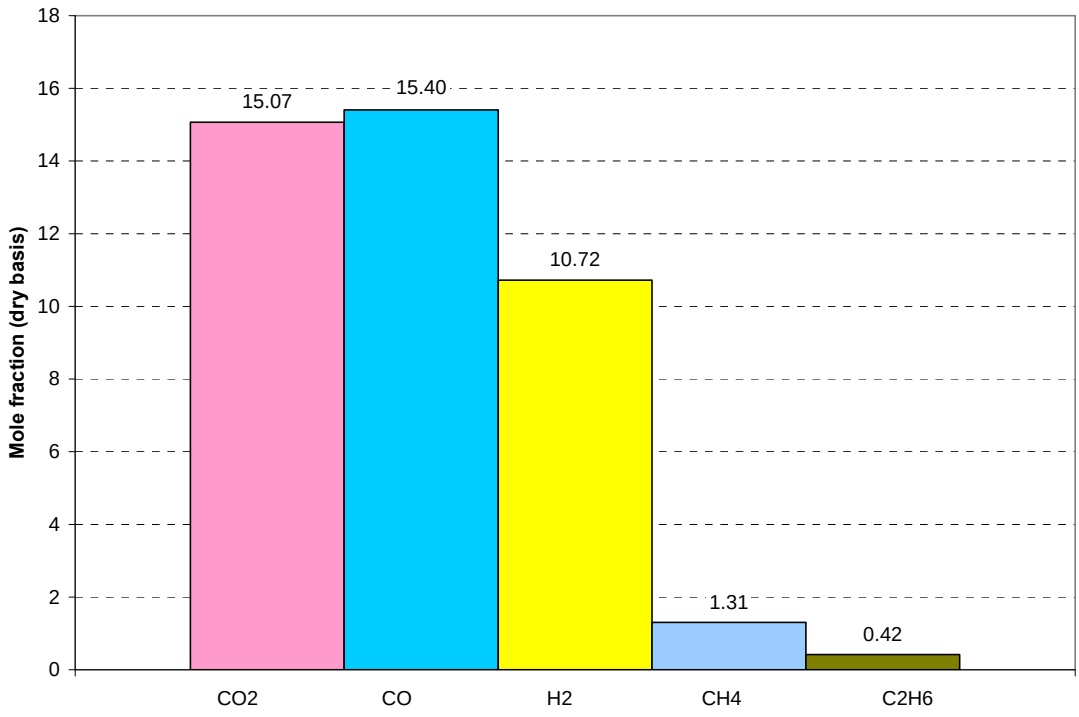

Figure 64. Gas composition for gasification of DB with air at ER = 2.12

Figures 64 and 65 report the gas composition obtained in gasification of DB with air only at ER = 2.12 and 3.18. Using air in fixed-bed gasification only the exothermic reactions $C+1/2\ O_2 \rightarrow CO$ and $C+O_2 \rightarrow CO_2$ occur in the combustion zone. Thus, H_2 is produced only by the homogeneous reaction $CO+H_2O \rightarrow H_2+CO_2$ (shift reaction) in the drying and stream-gas regions where there is available steam produced by the evaporation of the moisture contained in the biomass. Because the temperature in the evaporation region is low, H_2O must diffuse upstream to the high-temperature region for the $CO+H_2O$ reaction. Thus, H_2 production is not significant compared to the air and steam cases discussed earlier.

Less oxygen in the combustion zone caused by increased ER promotes the reaction of char with steam to produce CO. As showed in Figures 64 and 65, at ER = 2.12, the CO contained in the gases leaving the gasifier is about 15.40% whereas, at ER = 3.18, the CO production increased to about 23%.

More C atom consumed in the reaction of char to produce CO implies less C atoms available to produce CO_2. Also, CO_2 and H_2 decrease with increased ER. However, the effect of ER on the CO_2 production is as more significant compared with that on H_2 production. Increasing ER from 2.12 to 3.18 decreases the CO_2 contained in the gases by ~5% whereas the same increment in the ER (2.12 to 3.18) decrease the H_2 only by ~3%.

Comparing the results obtained for gasification with air to that obtained for gasification with air-steam suggests that the heterogeneous reaction of char with steam is very important if mixtures rich in H_2 must be produced. For gasification with air, at ER

=3 .18, the H_2molar fraction is ~7.2% whereas for gasification with air-steam under the same ER and S:F=0.68, the H_2molar fraction is ~20%. From this simple observation, one can estimate that the wet gas oxidation coupled with heterogeneous reactions produces an additional 13% of H_2.

The production of other hydrocarbons, such as CH_4 and C_2H_4, does not seem to be affected by ER. Decreasing H_2 and CO_2 means more C atoms and H atom are available for producing hydrocarbons; this may be the reason for slight increase in production of CH_4 and C_2H_6 with increase in the ER (Figures 64 and 65).

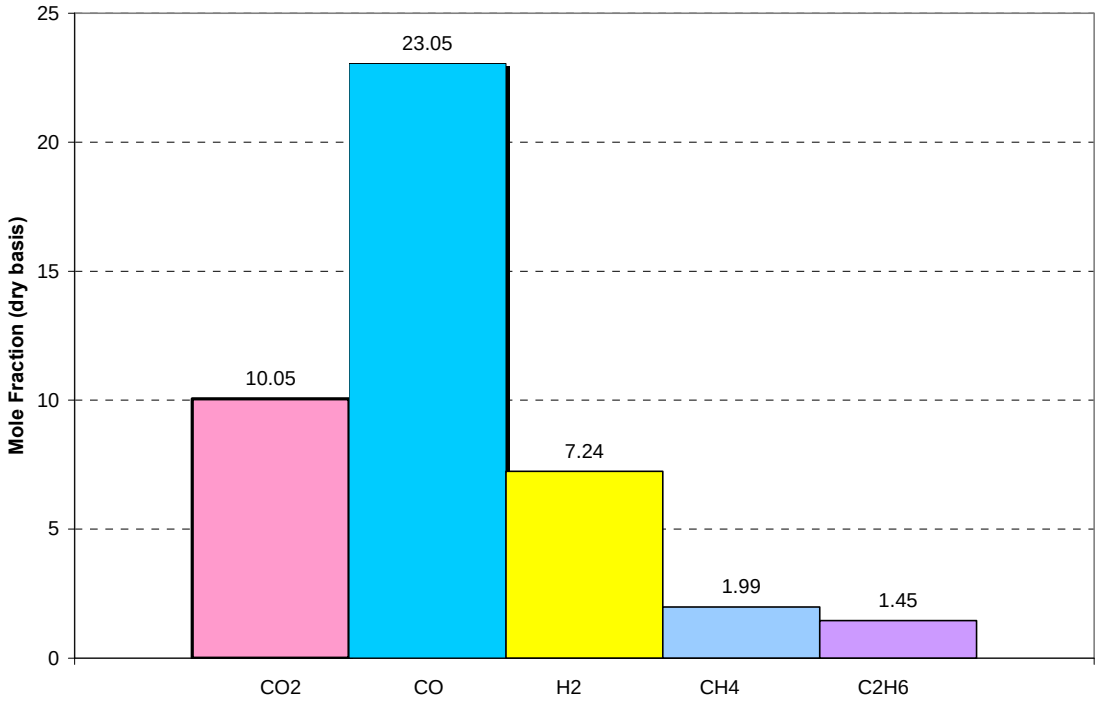

Figure 65. Gas composition for gasification of DB with air at ER=3.18

7.5.4.Gas composition for 90% DB: 10% ash blends in steam and air

A set of experiments of co-gasification of pure DB with ash from DB were performed to determine if ash has a catalytic effect on gas composition. Pure DB (1 kg) and DB ash (0.11 kg) were blended to maintain the same power supplied to the gasifier. The ash in DB is 14.95%; with the addition of ash, the total ash % in the blend is about 23%. The analysis of the ash used in the experiments was presented earlier.

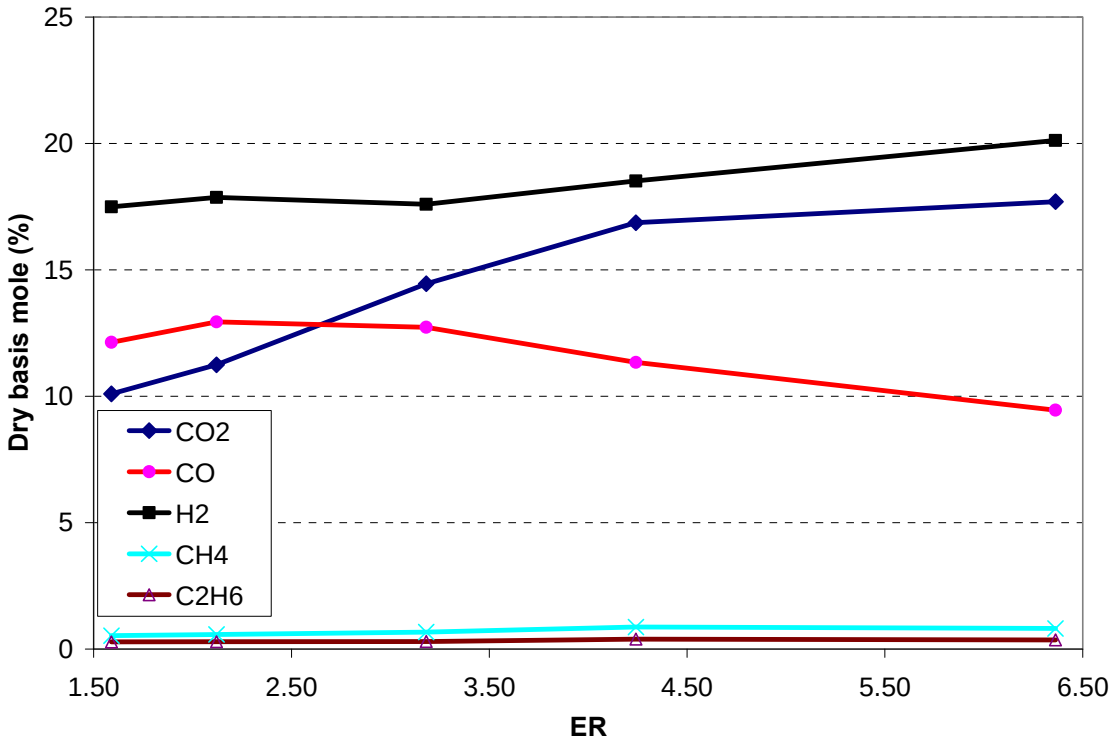

Figure 66. Gas composition for gasification of DB-ash blend with air-steam at S:F=3.15

The gasification experiments with DB:ash blends were made under the same operating conditions as for gasification of DB. Two S:F ratios were used and the results on gas composition are presented in this section as a function of the ER. At the end of the section, the CO and H_2 results obtained for gasification of DB-ash blends are compared with gasification of pure DB.

As expected, of gas composition for gasification of DB and gasification of DB-ash blends show the same tendency; thus, it can be stated that the effect of ER is the same for gasification of DB as for co-gasification of DB-ash.

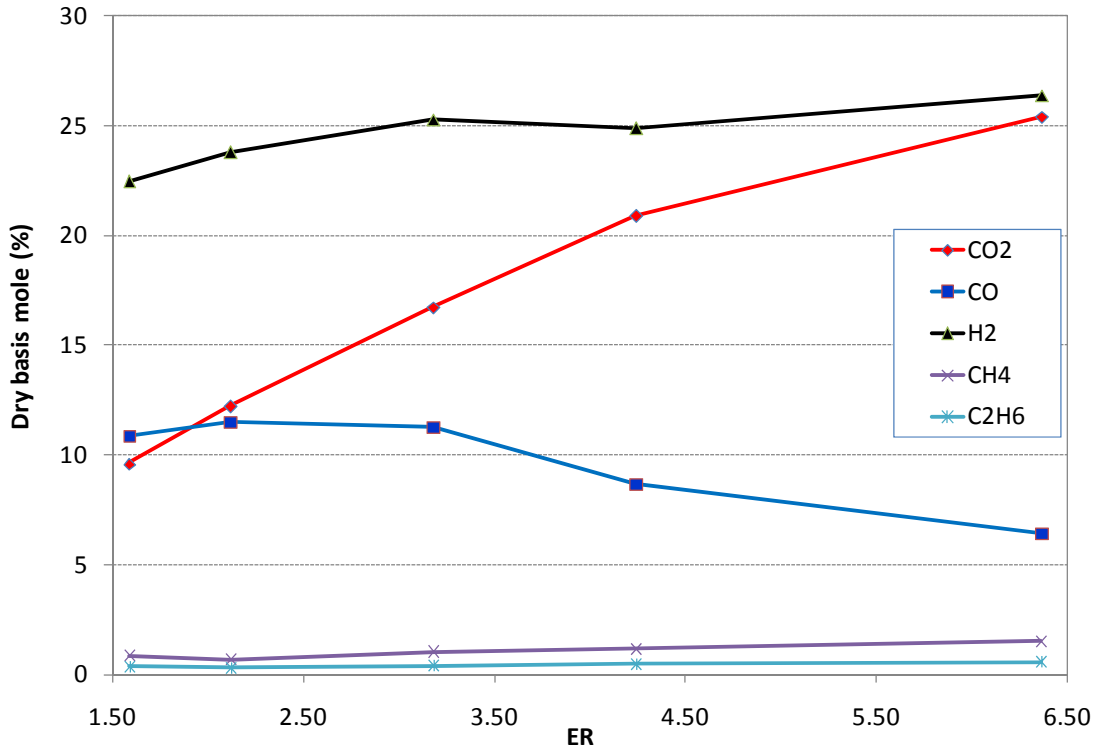

Figure 67. Gas composition for gasification of DB-ash blend with air-steam at S:F=0.8

Figures 66 and 67 show the effect of ER on gas composition at S:F = 0.35 and S:F = 0.80, respectively. Figures 68 and 69 compare CO produced by pure DB and 90:10 DB:ash blends.

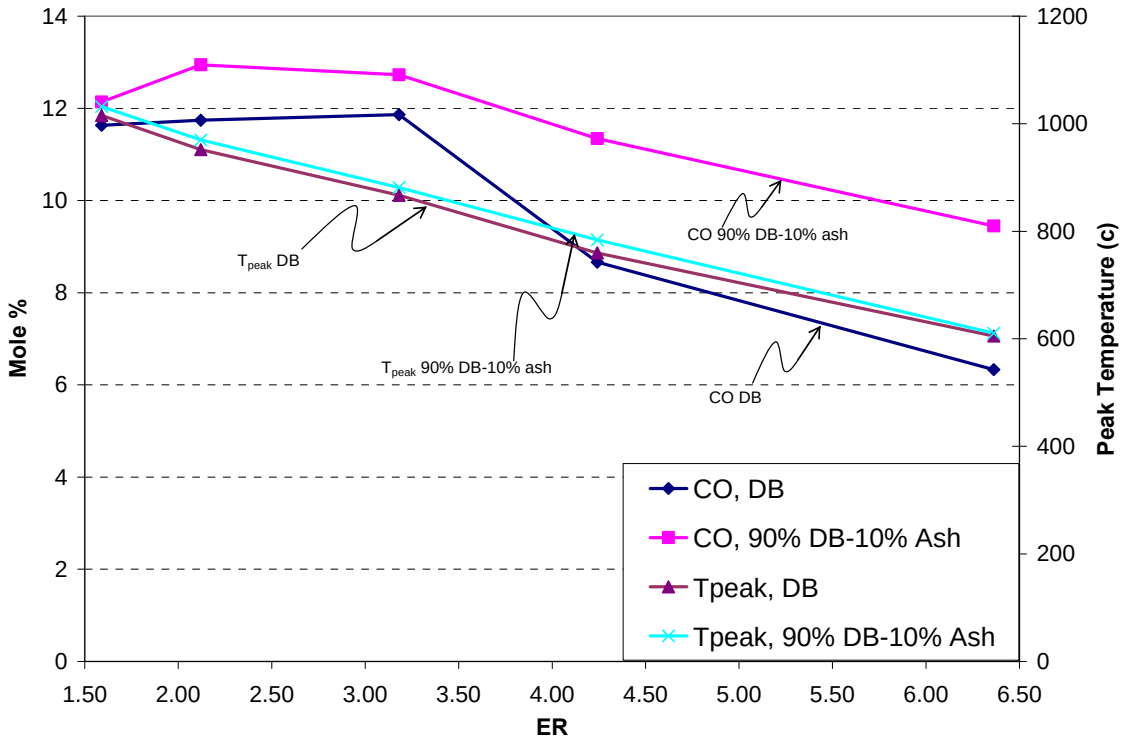

Figure 68. CO and T_{peak} for gasification of DB and DB-ash blend with air-steam at S:F=0.35

It is apparent from Figures 68 and 69 that the presence of ash produces some effect on the CO production. In other words, the addition of ash increases the rate of the reactions $C+1/2O_2 \rightarrow CO$ and $C+H_2O \rightarrow CO+H_2$. However, it appears, that the increase in the reaction rate of char with oxygen is higher than that of the reaction of char with steam, because in general almost for all the range of the operating condition (S:F and ER) studied, the peak temperature tested in the combustion region is higher for

gasification of DB-ash than that of gasification of pure DB. The temperature for gasification of DB-ash is only a little lower for S:F = 0.8 and ER < 3.18 (Figure 54).

Both heterogeneous reactions of char with O_2 and char with H_2O produce CO and occur in the combustion region, but the reactions $C+1/2O_2 \rightarrow CO$ is exothermic whereas the reaction $C+H_2O \rightarrow CO+H_2$ is endothermic. Thus, under the same operating conditions, a change in the peak temperature indicates a change in the reaction rate of any of those reactions. In other words, increasing the reaction rate of char with O_2, while the rate of reaction of char with steam is maintained constant, increases the peak temperature. On the contrary, at constant char-O_2 reaction rate, increasing the rate of reaction of char with steam decreases the peak temperature.

Figure 68 shows the effect of gasifying pure DB and DB-ash blend on the moles of CO are shown in for S:F=0.35 and various ER. The results show that the effect of ash on the moles of CO is more important at ER > 3.18 than that at ER < 3.18. This along with the fact that the difference between the peak temperature of DB-ash and pure DB is almost constant for 2.59 <ER <6.36 (Figure 54) suggests that at ER < .18 part of the CO produced in the heterogeneous reaction of char with steam and char with O_2 is consumed by the shift reaction ($CO+H_2O \rightarrow CO_2+H_2$). In others words, at constant S:F = 0.35 and ER < 3.18, the presence of ash effects the reaction rate of the shift reaction.

As shown in Figure 69, at S:F = 0.80, the catalytic effect of ash on the moles of CO production is almost constant for all ER investigated. Only at 2.12 < ER < 3.18, this effect appears to be more important.

The insignificant difference between the peak temperature of gasification of DB-ash and pure DB, at S:F = 0.80 and ER < 3.18, suggests that under this range of operating conditions, the presence of ash increases the reaction rate of char with O_2 and char with H_2O almost in the same proportion. On the other hand, the greatest difference of peak temperature tested at ER > 3.18 and S:F= 0.80 indicates that ash seems to increase the reaction rate of the char with O_2.

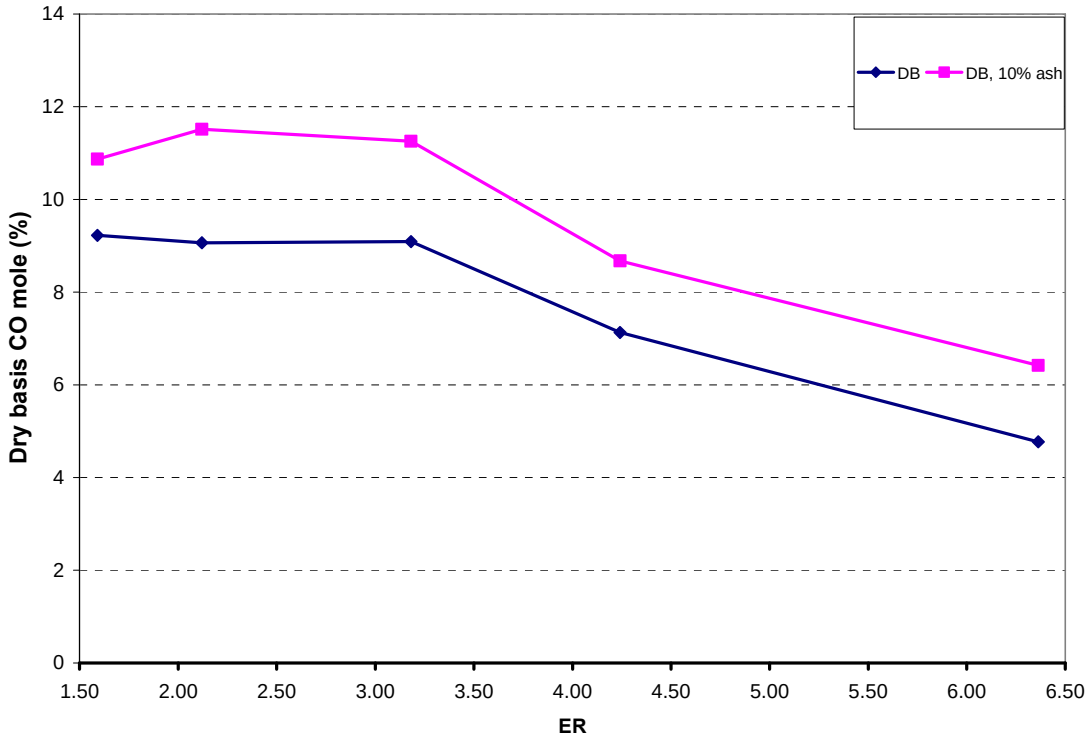

Figure 69. CO composition for gasification of DB and DB-ash blend with air-steam at S:F=0.8

Comparing the results presented in Figures 68 and 69, the catalytic effect of ash on CO production depends on the S:F ratio. At S:F = 0.35, the effect of the presence of

ash on CO is more important at ER > 3.18 than that at ER < 3.18 but at S:F = 0.80, that effect seems to be more important at ER < 3.18 than at ER > 3.18.

Figures 70 and 71 show the effect on H_2 production. The H_2 content increases with the addition of ash for all the experiments performed at ER < 3.18. However, at ER > 3.18, the effect of the presence of ash on H_2 content is insignificant. The increase in the production of H_2 at ER = 3.18 caused by the presence of ash is achieved at ER = 1.59 and S:F = 0.35.

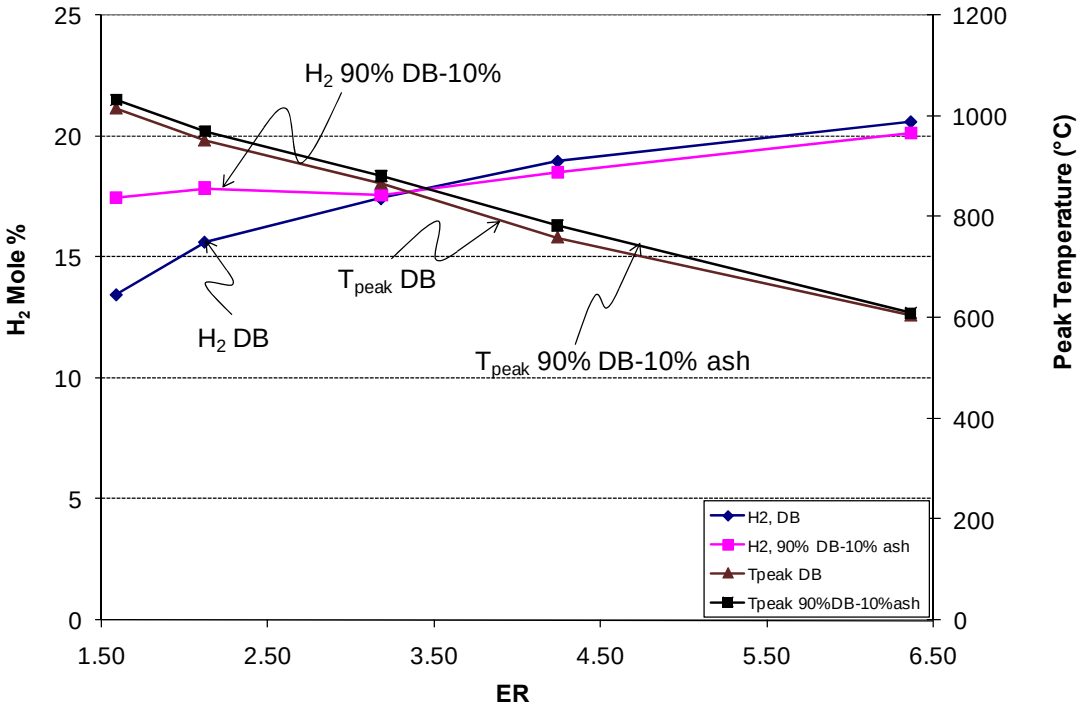

Figure 70. H_2 and T_{peak} for gasification of DB and DB-ash blend with air-steam at S:F=0.35

In general, the experiment performed with added ash, the highest increase in CO content is around 50%, obtained for S:F = 0.35 and ER = 6.36, whereas the highest increase in H_2 (~30%) was achieved at ER = 1.5 and S:F = 0.35.

The results obtained agree well with earlier results obtained by [15] for gasification of coal with agricultural biomasses, even when different biomass and different catalysts were used. In that study, the maximum increase in H_2 (28%) was obtained with the presence of Ni-Mg catalyst whereas the maximum increase in CO (70%) was obtained by using dolomite catalyst.

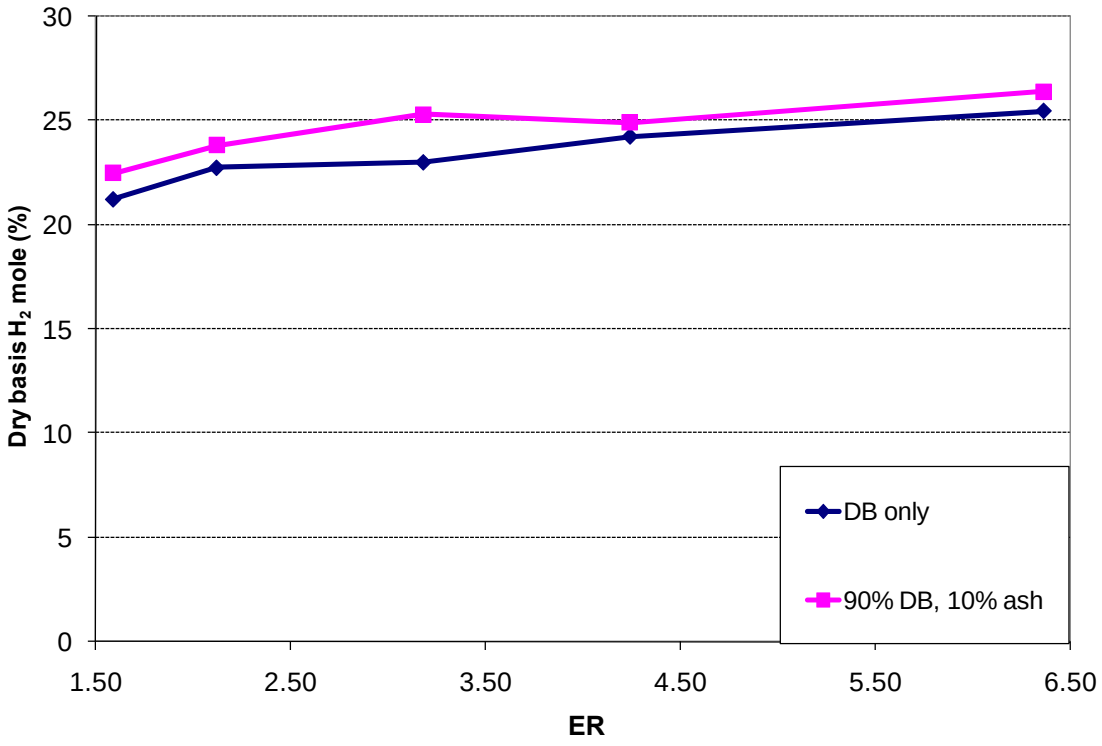

Figure 71. H_2 composition for gasification of DB and DB-ash blend with air-steam at S:F=0.80

7.5.5. Gas composition for 90% DB and 10% WYC in air and steam

This section presents the results on gas composition of co-gasification of DB with coal. A set of experiments using a blend of 90% DB and 10% WYC were performed under the same operating conditions used in gasification of DB-ash blends.

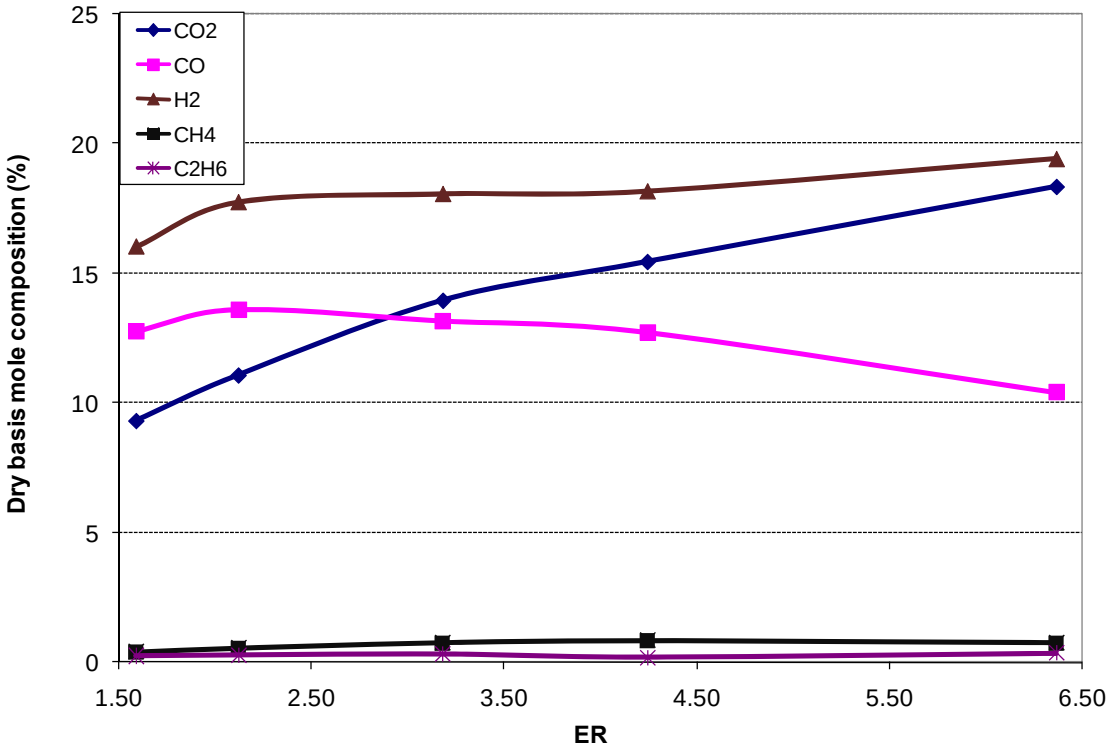

Figure 72. Gas composition of co-gasification of DB with coal at S:F=0.35 and various ERs

The trends are very similar for DB and DB:WYC (Figures 72 and 73). Increased ER increases H_2, CO_2, CH_4, and C_2H_6, but decreases the moles of CO. Even though the gasification curves of DB and DB-WYC are similar, the effects of the ER on the moles

of H_2 and CO are different. For instance, for gasification of DB at ER = 0.35, increasing the ER from 1.59 to 6.36 decreases the CO moles by 45% and increases the H_2 moles by 52.75% whereas for gasification of DB with WYC blend, the same change in the ER (1.59-6.36) increases H_2 by 21.1% and decreases CO by 18.43%.

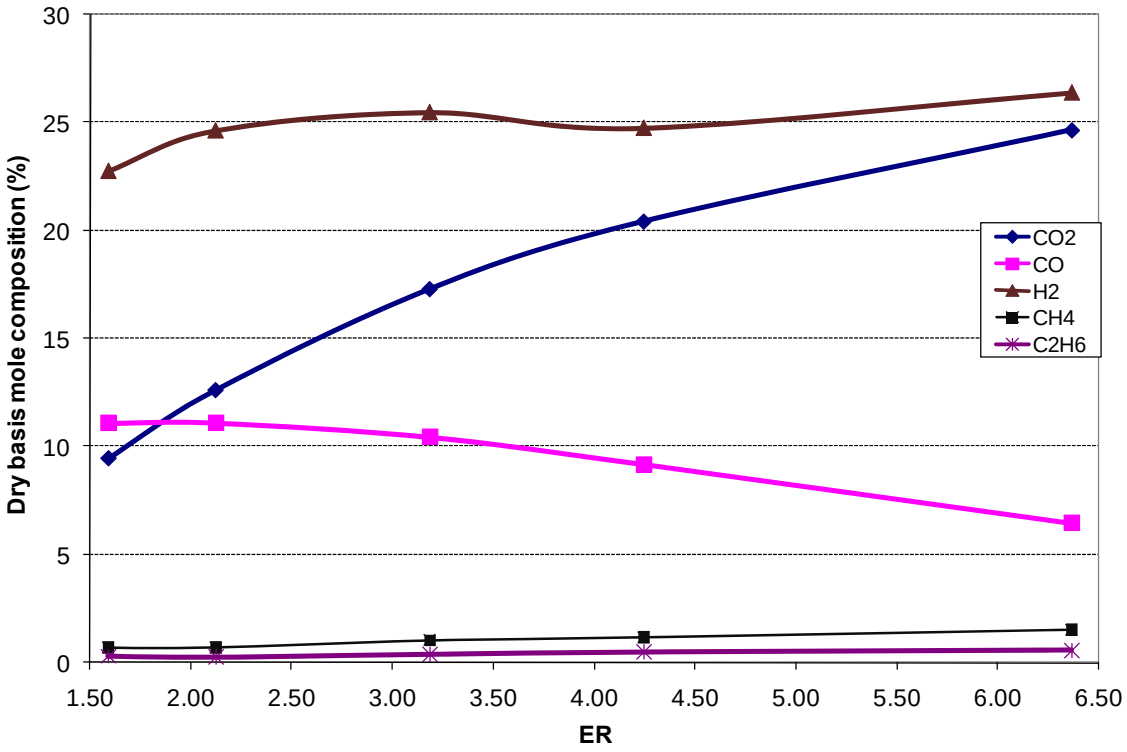

Figure 73. Gas composition of co-gasification of DB with coal at S:F=0.80 and various ERs

Figures 72 and 73 show that at constant ER, increased S:F tends to increase the moles of H_2, CO_2, CH_4, and C_2H_6, but decrease the moles of CO. The slight increase in CH_4 and C_2H_6 because of increased S:F ratios suggests that most hydrocarbons are produced by volatilizing VM in the pyrolysis region.

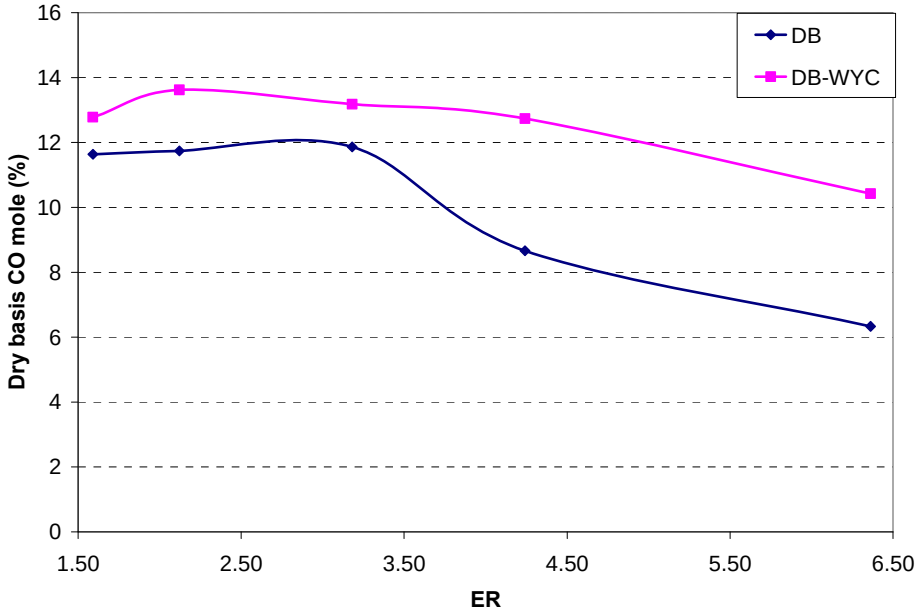

Figure 74. CO composition for gasification of DB and DB-WYC blend with air-steam at S:F=0.35

Figures 74 and 75 compare CO production from pure DB and DB-WYC blend for S:F = 0.35 and S:F = 0.80 and $1.59 < ER < 6.36$. In general, the presence of WYC shows an increase in CO. One expect more CO for pure DB than for DB:WYC blend because DB has more oxygen. However, coal has more fixed carbon than DB, resulting in more CO. The peak temperature in the combustion region of the bed is higher for gasification of DB-WYC (because of more fixed carbon in coal) than that of gasification of DB. Therefore, it is likely that the high CO content in the products obtained by gasification of DB-WYC is because of increased reaction of $C+1/2\ O_2 \rightarrow CO$. This reaction is exothermic, which signifies more heat released. The most increase in CO

(~64.5%) is achieved for ER = 6.36 and S:F = 0.35 whereas the lowest rise in CO (~11.1%) was at ER = 3.18 and S:F = 0.35.

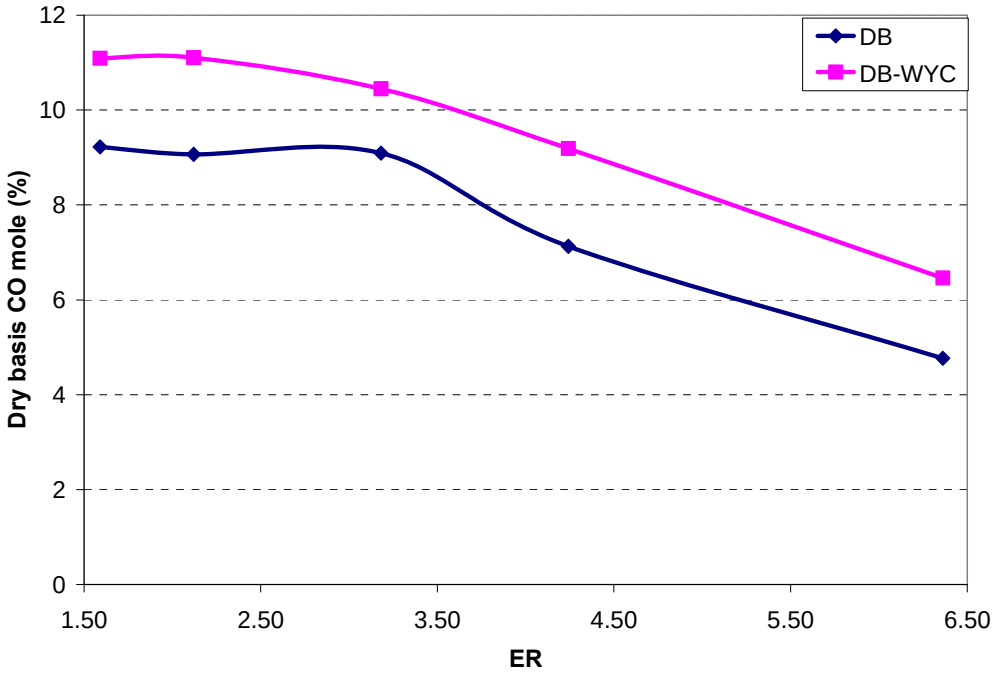

Figure 75.CO composition for gasification of DB and DB-WYC blend with air-steam at S:F=0.80

Figures 76 and 77 compare the effect of blend WYC with pure DB on H_2 production. At ER < 3.18, the presence of WYC produces more H_2 while at ER>3.18, this effect seems to be insignificant. Because the increase in CO caused by the presence of WYC is lower at ER < 3.18 than that at ER > 3.18 (Figures 74 and 75), it can be interpreted that at ER < 3.18, adding WYC increases the shift reaction, which consumes some CO produced in the combustion zone by the reactions of char with O_2 and char with H_2O to produce more H_2 and CO_2. In other words, at ER < 3.18, WYC seems to promote the shift reaction.

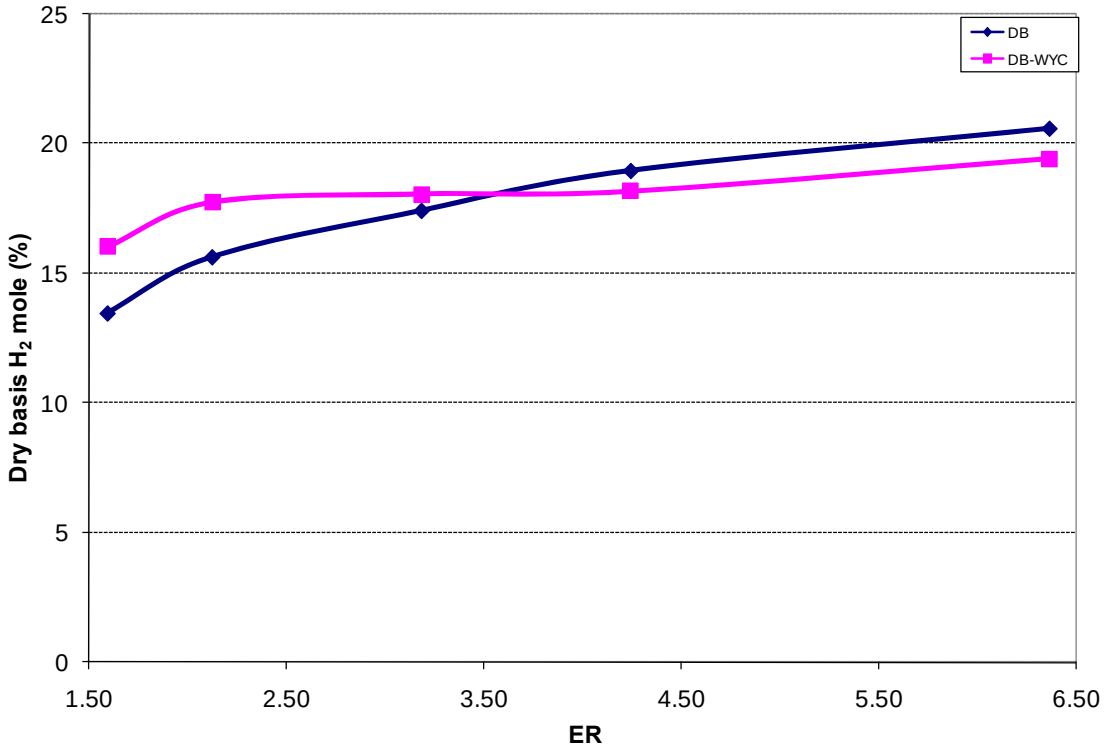

Figure 76. H_2 composition for gasification of DB and DB-WYC blend with air-steam at S:F=0.35

It is apparent, from the results that for this set of experiments, the adding WYC affects the reactions $C+1/2O_2 \rightarrow CO$ and $C+H_2O \rightarrow CO+H_2$. However, the effect of oxydation seems to be more important than char reforming, because as showed before, the presence of WYC increase the peak temperature (T_{peak}) in the combustion region. The H_2 curves (Figures 76 and 77) appear to indicate that the effect of WYC on the shift reaction is important at ER <3 .18 whereas at ER >3 .18, this effect is insignificant.

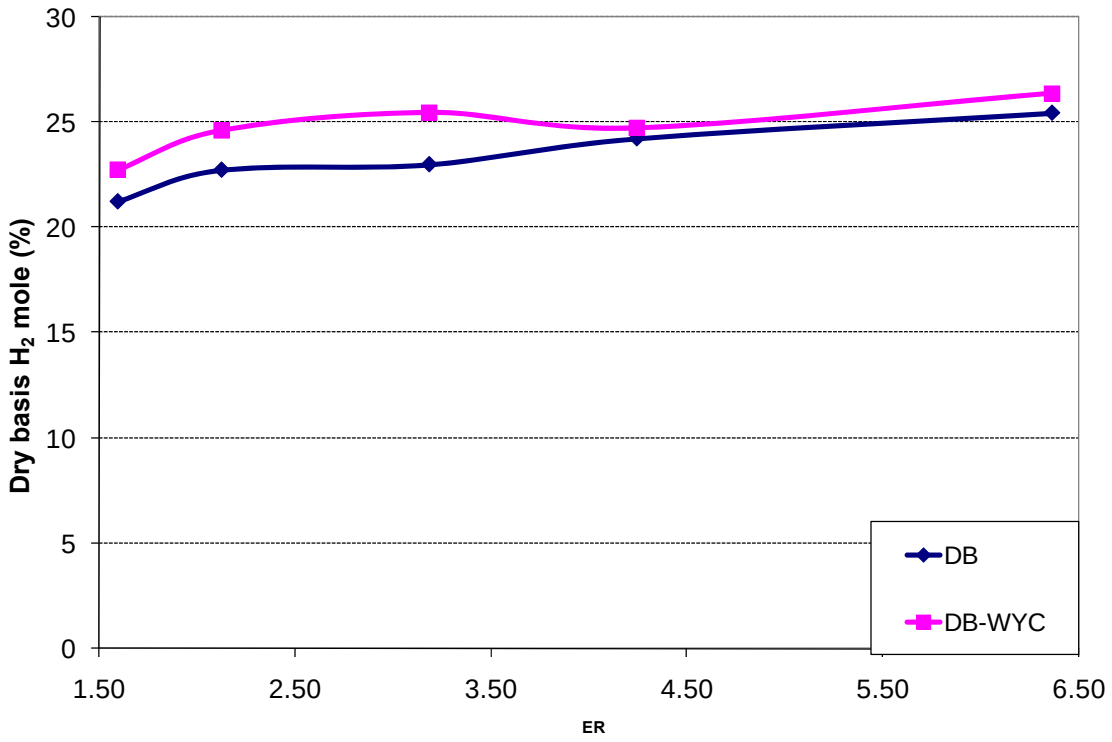

Figure 77. H_2 composition for gasification of DB and DB-WYC blend with air-steam at S:F=0.80

Figures 78 and 79 compare the effect of gasifying pure DB, DB-ash, and DB:WYC blends on CO. In general, the results show that gasification of blends produce more CO than pure DB. Because the T_{peak} is higher with blends, oxidation and reforming of char are favored. More CO is produced by gasifying the blends compared to gasification of DB indicating that both WYC and ash serve as catalysts to increase the reaction rate of char with steam and oxygen.

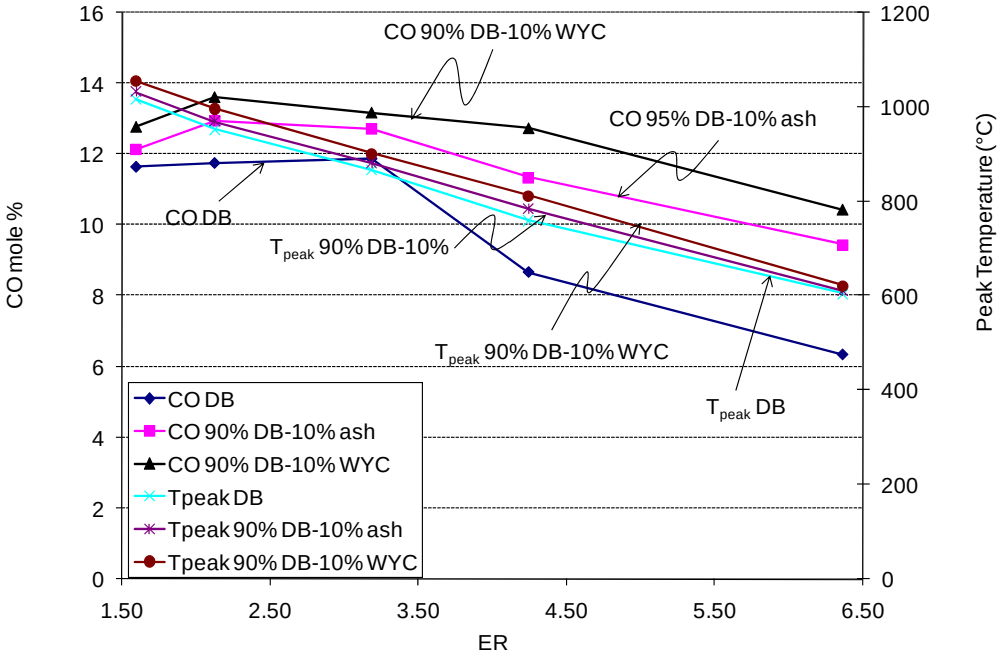

Figure 78. CO and T_{peak} from gasification of pure DB, DB-ash, and DB-WYC blends at S:F=0.35

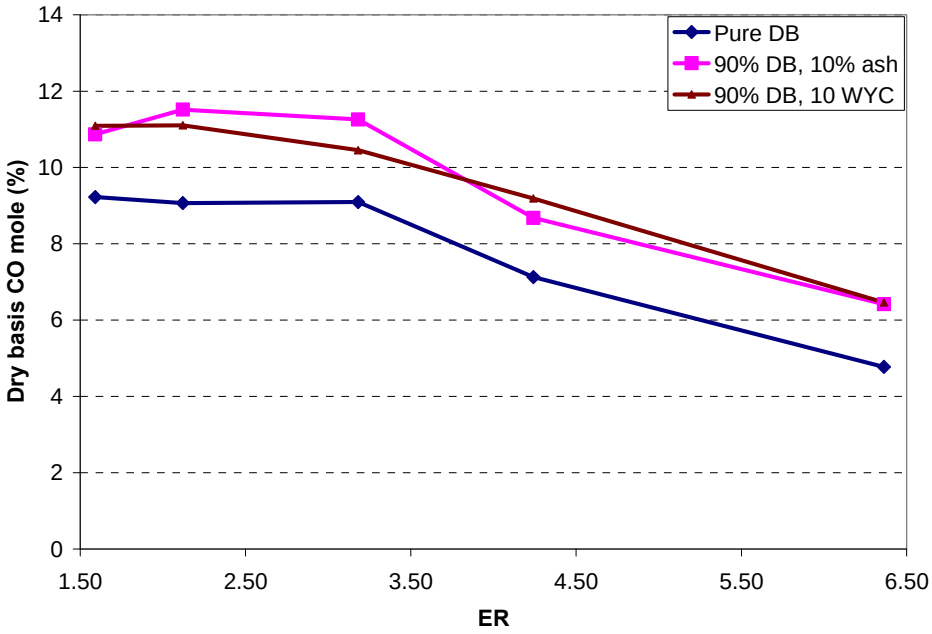

Figure 79. CO composition from gasification of pure DB, DB-ash, and DB-WYC blends at S:F=0.80

Comparing Figures 78 and 79, it is appears that the effect of WYC on CO is slightly higher than that caused by the ash. This could result because of the higher FC content in WYC, which increases the peak temperature compared to the DB:Ash blend.

Figures 80 and 81 present the H_2 leaving the gasifier for gasification of pure DB, and DB-ash and DB-WYC blends as a function of the ER and for S:F = 0.35 and S:F = 0.80. In general, the results show that at ER > 3.18 the effect of adding ash and WYC on H_2 is insignificant. However, at ER < 3.18, the presence of ash and WYC increase H_2, which indicate that both the ash and WYC have some catalytic effect of the shift reaction at low ER or high temperature.

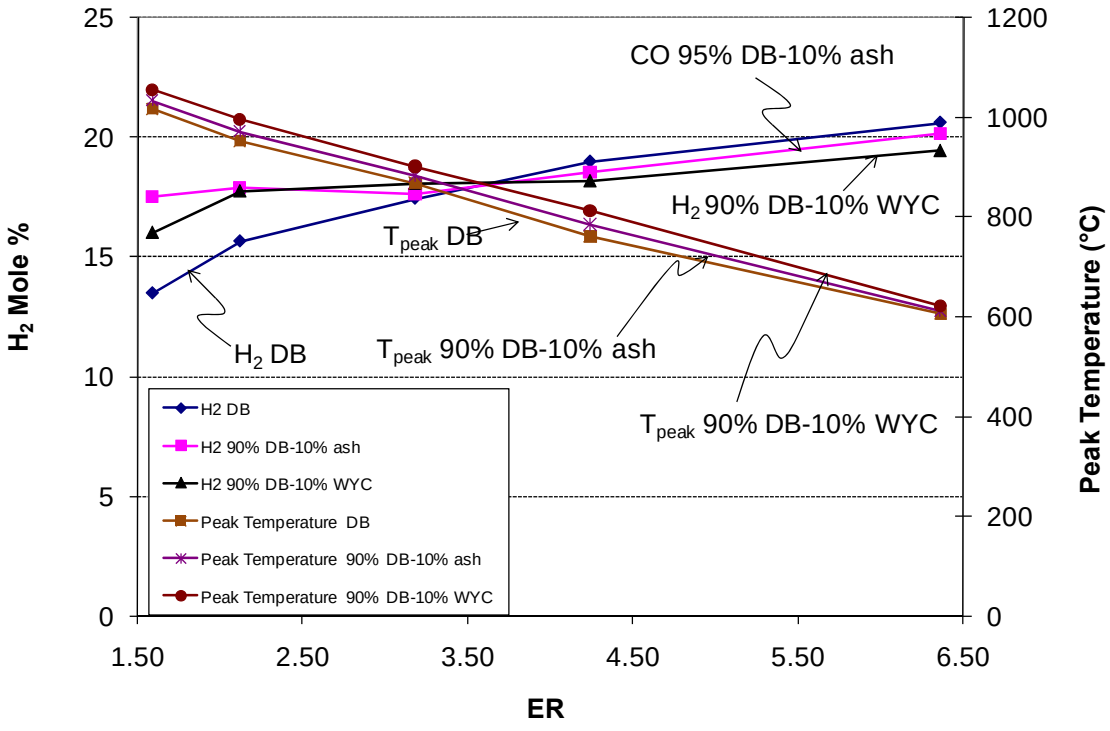

Figure 80. H_2 % and T_{peak} from gasification of pure DB, DB-ash, and DB-WYC blends at S:F=0.35

The difference between the H_2moles produced by gasification of DB-WYC and those produced by gasification of pure DB and DB-ash is insignificant, which appears to indicate the most difference in gas composition (CO) because of the higher FC content in WYC compared to DB-ash.

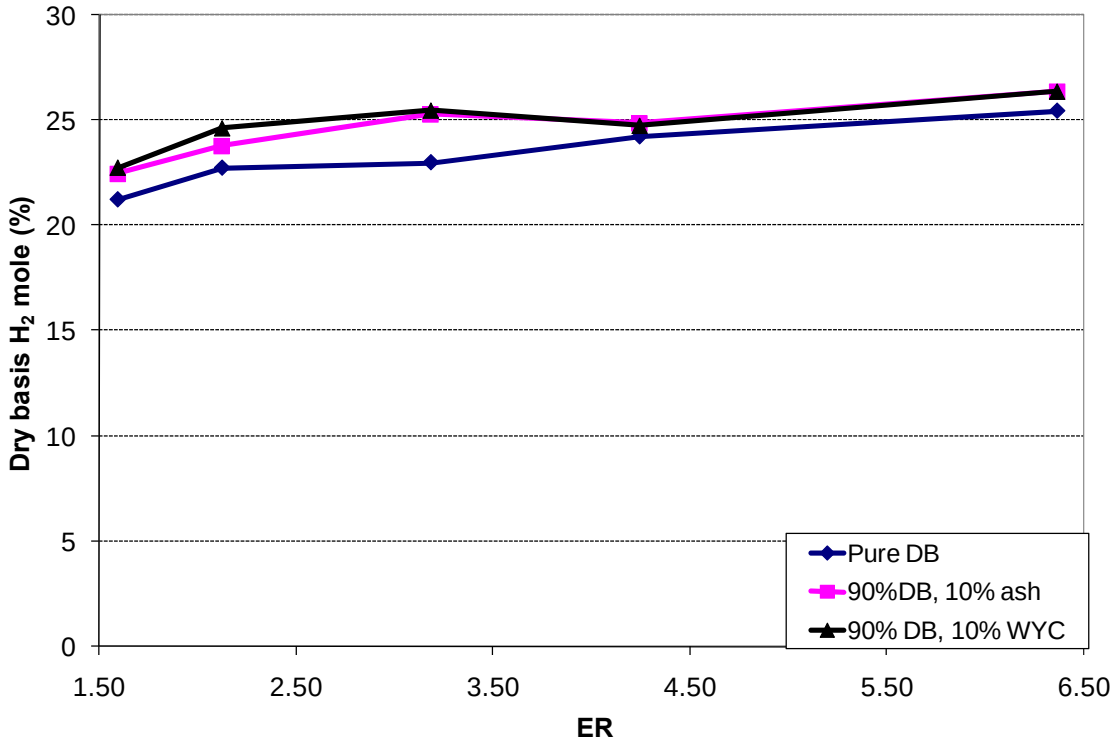

Figure 81. H_2 composition from gasification of pure DB, DB-ash, and DB-WYC blends at S:F=0.80

7.6. Gross heating value of gas mixtures (HHV) and energy conversion efficiency (ECE)

From biomass analysis: Since the heat value of volatile matter (HV_{VM}) is approximately equal to {HV_{Fuel}-HVC* FC}/{1-FC}; where HV_{fuel} is the heat value of

the fuel, HV_C is the heat value of the char carbon, and FC is the amount of fixed carbon in the fuel; then following [33] the heating value of the gas mixture (HV_{gas}) consisting of VM released by pyrolysis (Equation 22) and CO produced by char oxidation for non-adiabatic air blown gasification (Equation 23) can be estimated with Equation 26. Note that there is heat lost (non-adiabatic) to the surroundings during exothermic partial oxidation of C to CO.

The energy density or gross heating value of the products leaving the gasifier can be calculated as follows:

$$HHH_{Gases} = \sum_i X_i * HHV_i \quad (40)$$

where X_i and HHV_i are mole fraction and gross heating value (kJ/SATP m^3) on a dry basis of the fuel gases leaving the gasifier, i = CO, CH_4, H_2, etc. HHV_{Gases} is the energy density (kJ/ SATP m^3) of the fuel gases on a dry basis. Results for all three parametric fuels will be presented.

7.6.1. Pure DB

<u>HHV of DB</u>

Table 15 presents results on HHV of gasification of DB as a function of ER and various S:F ratios. The results indicate that increasing S:F increases the gross heating

value of the gases; this is caused principally by increased production of hydrocarbons and H_2 from increased S:F. At constant S:F, increasing ER tends to increase HHV until a critical ER beyond which HHV decreases. From Table 15, it is evident that the effect of S:F on HHV of gases is more significant than that of ER.

For the set of operating condition studied, the HHV of the gases ranged between 3268 and 4285 kJ/ SATP m^3, which is 9 and 12.6% of the energy density of the CH_4. The data on HHV indicate that gasification of DB under the operating conditions studied produces low "Btu" gases; however, gases without N_2 (N_2 free) have higher HHV. Appendix G presents the HHV of gases free of N_2 produced by DB gasification.

Table 15. Energy density of gases on a dry basis (kJ/ SATPm^3) for DB as a function of ER and various S:F ratios

S:F (mole ratio)	**ER**				
	1.56	2.12	3.18	4.24	6.36
0.35	3280	3473	3787	3648	3666
0.56	3268	3835	4402	4245	4032
0.68	3762	3955	3993	4217	4079
0.80	3934	4116	4291	4378	4585

Energy conversion efficiency of DB

Although the energy density or HHV of the products gives information on the amount of energy per unit of gas produced in the gasifier, it does not provide information on the fraction of energy recuperated as fuel gases per each fuel unit supplied to the gasifier. The fraction of energy recuperated in the gasifier can be calculated with Equation 41.

$$\eta_{Gas,E} = \frac{\mathrm{HHV_{Gases}}}{\mathrm{N_{Fuel}} * \mathrm{HHV_{Fuel}} + \mathrm{N_{steam}} * 18(\lambda + 4.18(373 - 298))} \quad (41)$$

where, NF_{uel} and N_{steam} correspond to the moles of fuel and steam supplied respectively to the gasifier by each normal m^3 of dry product gases and λ is the latent heat of steam. HHV_{Fuel} is the gross heat value (kJ/ kmol of DAF fuel) of the fuel and $\eta_{Gas,E}$ is the energy conversion efficiency (ECE).

Because it was impossible to measure the mass of tar produced during the experiments, the volumetric flow of gases, required to calculate the energy recovery, was estimated by mass balance using tar and gas compositions. Ultimate and proximate analyses were performed on tar to determine its composition. Table 16 presents the ultimate and proximate analysis of the heavy tar on a dry basis. Using the composition also the empirical formulae was derived.

Table 16. Heavy tar analysis

Dry loss (%)	0
Ash (%)	1.07
C (%)	52.38
H (%)	8.79
N (%)	3.92
O (%)	33.6
S (%)	0.24
Dry basis HHV (kJ/kg)	21556
DAF HHV(kJ/kg)	21789
Emprical Formula	$CH_{2.01}N_{0.064}O_{0.48}S_{0.0017}$

Table 17 shows ECE for various ER and S:F. The ECE was calculated using the yield of gases, energy density of the gases, and Equation 33. Appendix E presents a program developed in EES code to calculate the yields of gases, char, and tar. The program required input data such as, fuel composition, gas composition, ER, and S:F.

Table 17. Energy Conversion Efficiency (ECE) for DB as a function of the ER and various S:F ratios

S:F (mole ratio)	**ER**				
	1.56	2.12	3.18	4.24	6.36
0.35	0.65	0.56	0.45	0.33	0.24
0.56	0.60	0.59	0.53	0.41	0.27
0.68	0.69	0.60	0.47	0.41	0.29
0.80	0.69	0.64	0.53	0.44	0.35

As shown in Table 17, increased S:F ratio increases ECE. Even though the energy density of the gases increases with increased ER, ECE decreases with increased ER. When ER is large, gasification tends to be almost pure pyrolysis that produces lesser amounts of combustible gases with higher tar content and more combustible loss through char in ash because almost all fixed carbon is lost through ash.

For the range of the operating conditions studied, ECE ranged from 0.24 to 0.69; the remaining fraction corresponds to the energy returned in char, tar, and sensible heat of gases leaving the gasifier. ECE discussed in this dissertation is a little higher than that presented by [37] for non-adiabatic fluidized bed gasification of FB (0.20-0.60). This agrees with the fact that in fixed bed gasification, gases leave the gasifier at lower temperatures as compared to fluidized-bed gasification. Lower sensible heat of gases leaving the gasifier implies higher gasifier efficiency; thus, more energy is recovered in

the gases. However, the experimental EEC estimated is lower than that estimated by equilibrium model (~0.48-0.87).

Figure 82 shows ECE estimated by equilibrium model and obtained by experimentation. The trend of the curves obtained by modeling shows a peak at about ER=3.18 beyond which the ECE decrease. On the other hand, the trend of the experimental data do not shows peaks and the ECE decreases with increased ER.

As discussed before, the ECE decrease with increased ER because there is not enough oxygen to burn completely all char. Then, the process tends to be pure pyrolysis, which produces mixtures with higher concentrations of fuel gases, but lower ECE because of char production. The char production estimated by equilibrium model starts only at ER>3.18 (Appendix D) because equilibrium model supposes infinite time for the reactions. However, experimental results, where the time is finite, showed that char increases with ER and it is produced almost at all experimental conditions (Figure 88). Therefore, the experimental ECE curves shows a regular decrease with ER whereas the ECE from modeling show a peak at ER=3.18 where the char production starts (Figure 82).

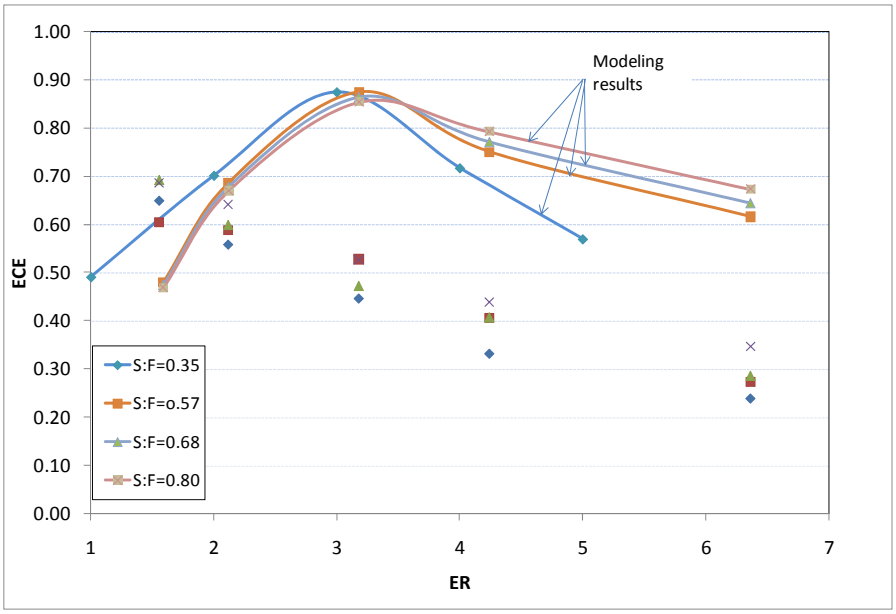

Figure 82. ECE estimated by equilibrium model and obtained experimentally

7.6.2. DB-ash blends

HHV of DB-ash blends

Table 18 shows that the effect of both ER and S:F ratio on the HHV of the gases for gasification of DB-ash blend is practically the same as pure DB. Also, increased ER tends to increase HHV of gases until a critical value beyond which HHV starts to decrease. The maximum and minimum HHVs were 4544 and 3815 kJ/SATP m^3, respectively, which corresponds to 10.5 and 13.5% of HHV of CH_4 calculated on a mole basis. It is apparent from Table 15 and Table 18 that gasification of DB-ash produces gases with slightly more HHV than gasification of pure DB.

Table 18. Energy density of gases on a dry basis (kJ/ $SATPm^3$) for DB-ash as a function of ER and various S:F ratios

S:F	ER				
	1.56	2.12	3.18	4.24	6.36
0.35	3815	3972	3960	4039	3968
0.80	4423	4544	4882	4633	4740

Energy conversion efficiency of DB-ash blend

Table 19 presents ECE for gasification of DB-ash blend for different ER and S:F. Increased ER decreases ECE whereas increased S:F increases ECE. For the set of operating condition discussed in this dissertation, the ECE of gasification of DB-ash blends estimated by atom balance was between 0.26 and 0.80. This range is a slightly higher than the range estimated by pure DB, but lower than that estimated by equilibrium modeling.

Table 19. Energy Conversion Efficiency (ECE) for DB-ash blends as a function of the ER and various S:F ratios

S:F	ER				
	1.56	2.12	3.18	4.24	6.36
0.35	0.78	0.66	0.48	0.39	0.26
0.80	0.80	0.71	0.62	0.48	0.38

7.6.3. DB-WYC blends

HHV of DB-WYC blends

It is apparent from Table 20 that the HHV of the gases produced by gasification of DB-WYC is higher than that of DB; however, the the results seems to indicate that

increased S:F produces gases with higher HHV. The HHV increases with increased ER until a critical value beyond which it starts to decrease.

Table 20. Energy density of gases on a dry basis (kJ/ SATPm^3) for DB-WYC as a function of ER and various S:F ratios

S:F	ER				
	1.56	2.12	3.18	4.24	6.36
0.35	3649	4023	4115	4007	3972
0.80	4377	4573	4793	4679	4738

The HHV for the selected operating conditions varied from 3649 to 4793 kJ/ SATP m^3. The highest HHV (4679 kJ/SATP m^3) was measured for a ER =3 .18 and S:F = 0.80 whereas the lowest HHV was measured at ER = 1.56 and S:F = 0.35.

Energy conversion efficiency of DB-WYC blends

Table 21 presents ECE estimated by atom balance for gasification of DB-WYC for various ER and S:F. As discussed before, high ER decreases ECE because of more char and tar production. On the other hand, increased S:F increases ECE because more hydrocarbons and hydrogen are produced with higher S:F.

Table 21. Energy Conversion Efficiency (ECE) for DB-WYC blends as a function of the ER and various S:F ratios

S:F	ER				
	1.56	2.12	3.18	4.24	6.36
0.35	0.70	0.64	0.48	0.37	0.26
0.80	0.77	0.70	0.58	0.46	0.35

Figure 83 compares the HHV of all fuels studied for S:F = 0.35 and S:F = 0.80 and various ER.

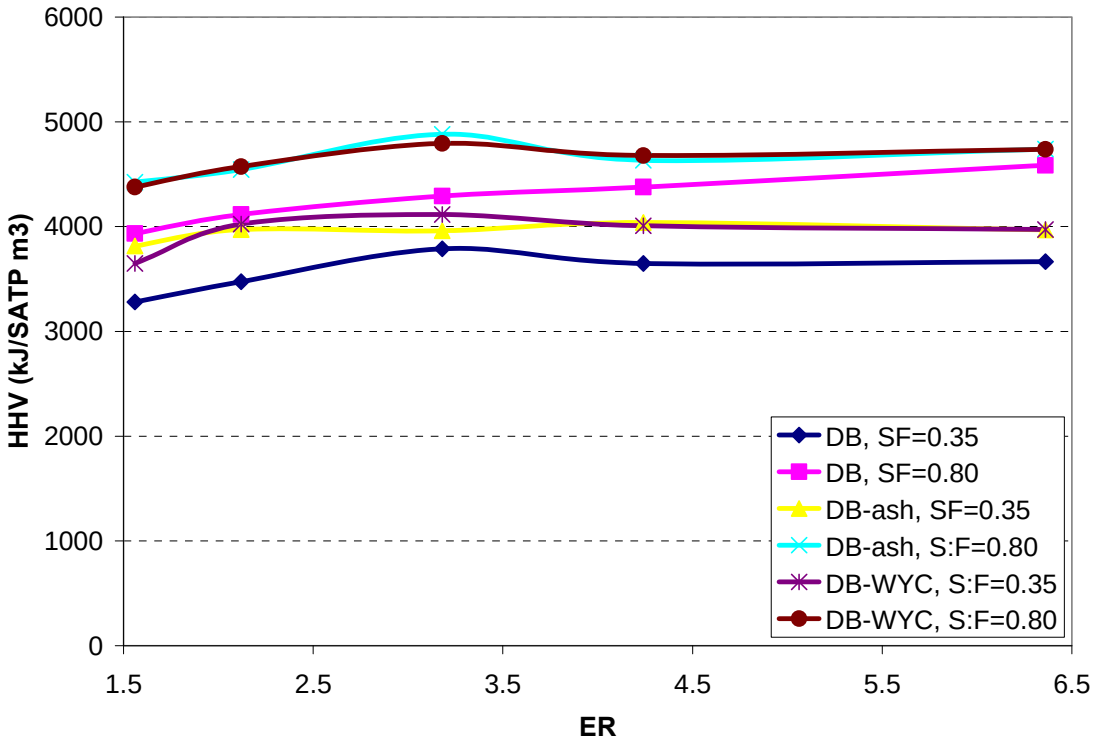

Figure 83. HHV of the gases produced by gasification of DB, DB-ash blend, DB-WYC blend as a function of ER and various S:F ratios

From the results, it is evident that the presence of ash, and blend with WYC increases HHV of gases. As discussed before, the blends of DB with ash and WYC produce gases with higher CO and H_2 content, which increases the HHV. As shown in Figure 83, the difference in the HHV of gases produced by gasification of DB-ash and DB-WYC is negligible. A maximum difference of 591 kJ/ SATP m^3 was observed between the HHV of gases using DB-WYC and gases from pure DB on HHV was at ER

= 3.18 and S:F = 0.80 whereas the minimum difference (153 kJ/ SATP m^3) was observed at ER = 6.36 and S:F = 0.80.

Figure 84 shows that the presence of both WYC and ash improves ECE. The maximum ECE was achieved for gasification of DB-ash blend at S:F = 0.80 where the minimum for pure DB was at S:F = 0.35.

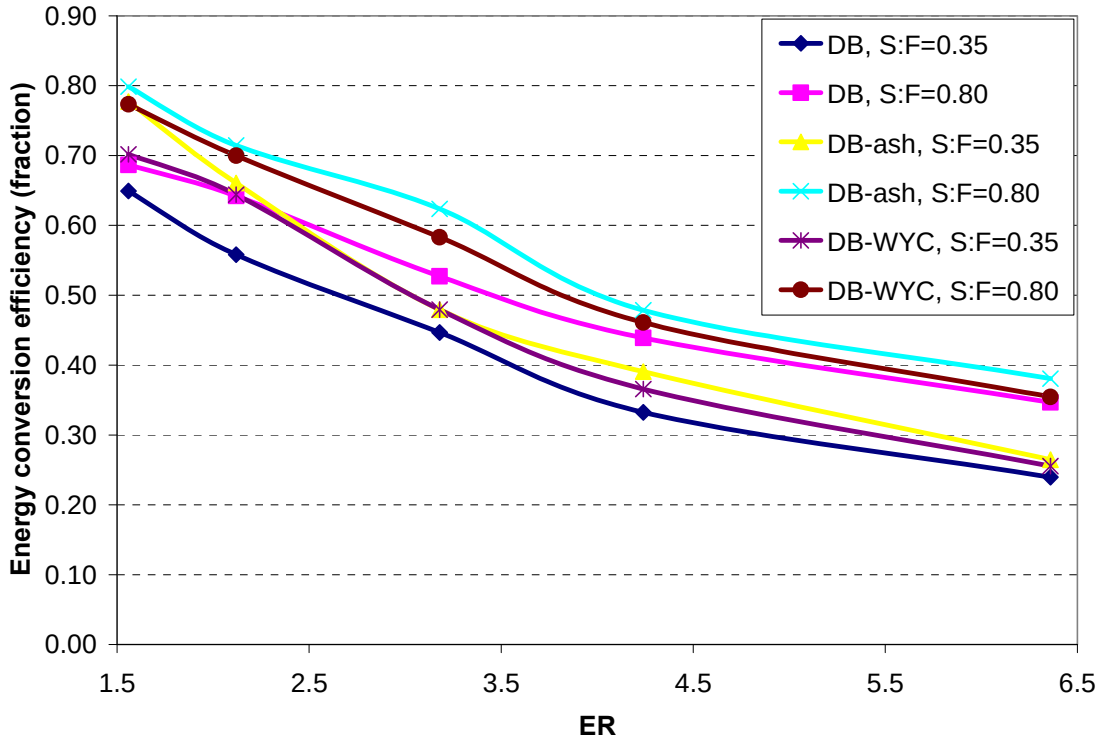

Figure 84. Energy conversion efficiency (ECE) of the gases produced by gasification of DB, DB-ash blend, DB-WYC blend as a function of ER and various S:F ratios

Even though the difference between the HHV of DB-ash and DB-WYC is insignificant, the ECE reached for gasification of DB-ash is a little higher than that of DD-WYC gasification. This is because DB-WYC gasification produces gases with high

tar content than gasification of DB-ash. Following section presents results on char and tar production. The maximum difference in ECE (20%) was achieved between DB-ash and pure DB gasification at ER = 1.59 and S:F = 0.35.

In general for all fuels studied, the results show that the effect of S:F ratio on HHV of the gases is more important than ER. However, the effect of S:F on the ECE is weaker compared to that of the ER. For instance, for pure DB gasification at ER = 0.35, increasing the ER from 1.56 to 6.36 decreases ECE by about 171% whereas at ER = 6.36, increasing S:F from 0.35 to 0.80 increases the ECE by about 44.6%.

7.7. Yield of gases, char, and tar

This section presents yield on gases, char, and tar. Because it is impossible to measure the tar and the steam produced, the yields was estimated using reverse atom balance. The program presented in Appendix E required as input data the dry gas, ER, and S:F.

7.7.1. Yield of gases

Figures 85, 86, and 87 present the yield of gases for gasification of pure DB on a dry tar free basis as function of the ER and various S:F ratios. At constant S:F, increased ER implies less air entering the gasifier per each kg of DB gasified; thus, the gas yield

decrease with increased ER. On the other hand, at constant ER, increase in S:F tends to produce more mass of gases per each kg of DB gasified.

For the set of experiments performed using DB, the gas yield was1.54 to 5.30 dry tar-free kg of gases per each kg of DAF DB gasified. The missing mass to complete the total mass entering to the gasifier in the reactants (fuel, air, and steam) corresponds to the mass of the steam in the gases, char in the ash, and tar in the gases. The stochiometric A:F ratio of DB is 5.077 kmol of air per kmol of DB, thus, burning 1 kg of DB at stochiometric conditions requires about 7 kg of air because the molar mass of DB is 20.35 kg /kmol. However, gasification which required ER > 1 the mass of air required per each mass unit of fuel gasified is lower than that required for complete combustion, and hence, the gas mass produced per kg of fuel gasified is less than that produced in complete combustion.

The difference between the yield of gases produced by gasification of pure DB (Figure 85), DB-ash (Figure 86), and DB-WYC (Figure 87) under the same ER and S:F ratio is negligible, because the total mass of gases leaving the gasifier depends upon principally on the mass of the reactants entering to the gasifier. In other words, the total yield of gases is affected by the fuel type, ER, S:F, and unburned solid (char). Because the yield of gases discussed in this dissertation is presented on a dry, tar-free basis, the most difference between the yield produced by each fuel correspond to the tar, char, and steam, which are different for each fuel gasified.

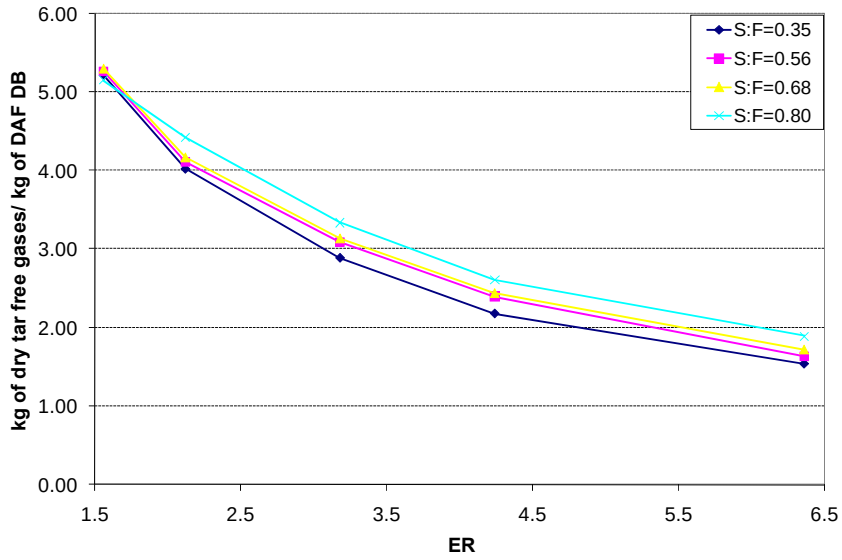

Figure 85. Mass of gases produced per kg of DAF DB on a dry tar free basis for gasification of pure DB

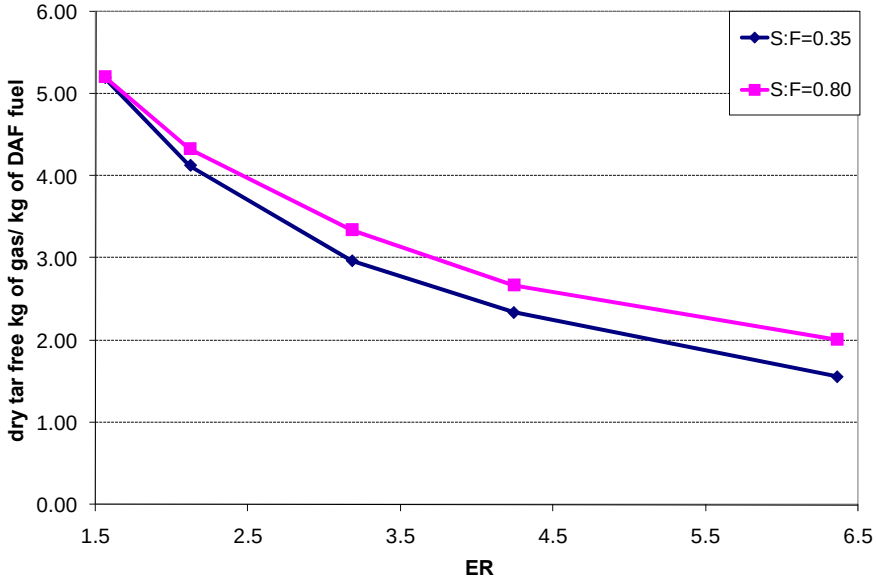

Figure 86. Mass of gases produced per kg of fuel on a dry tar free basis for gasification of DB-ash

If the masses of char, tar, and steam produced in each process are added to the yield of gases (dry and tar-free) the resulting total mass corresponds to the total mass entering to the gasifier in the reactants including fuel.

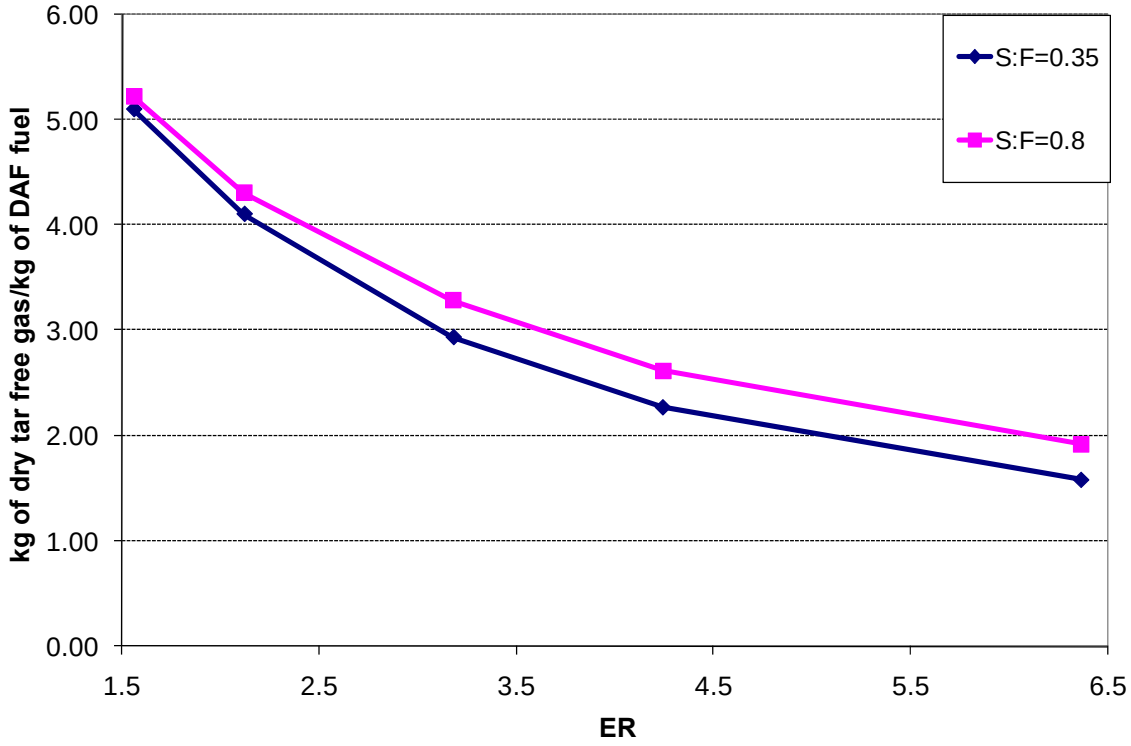

Figure 87. Mass of gases produced per kg of DAF fuel on a dry tar free basis for gasification of DB-WYC

7.7.2. Yield of tar and char

This section presents the char and tar produced in gasification of pure DB, DB-ash, and DB-WYC and estimated by atom balance (mass balance) as a function of ER S:F.

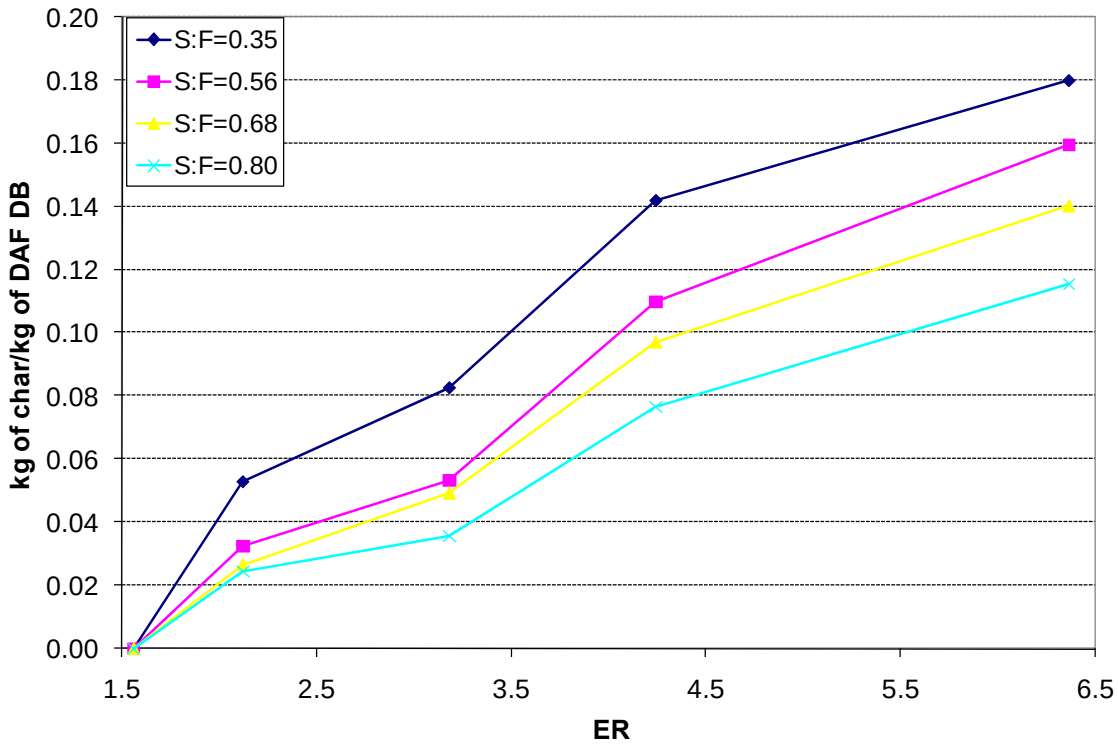

Figure 88. Mass of char produced per kg of DAF DB

The mass of char produced by gasification of pure DB, DB-ash, DB-WYC blends are presented in Figures 88, 89, and 90 as a function of ER and various S:F. The trend of all the figures is the same for all fuels studied. At constant S:F, increasing ER increase char production, Because of the less oxygen entering the gasifier for each kg of fuel gasified. Also, the results show, that at constant ER, increased S:F ratios produce lower char indicating that the more H_2O in the reactant react with char. For all cases, at ER = 1.59, the char produced was almost zero.

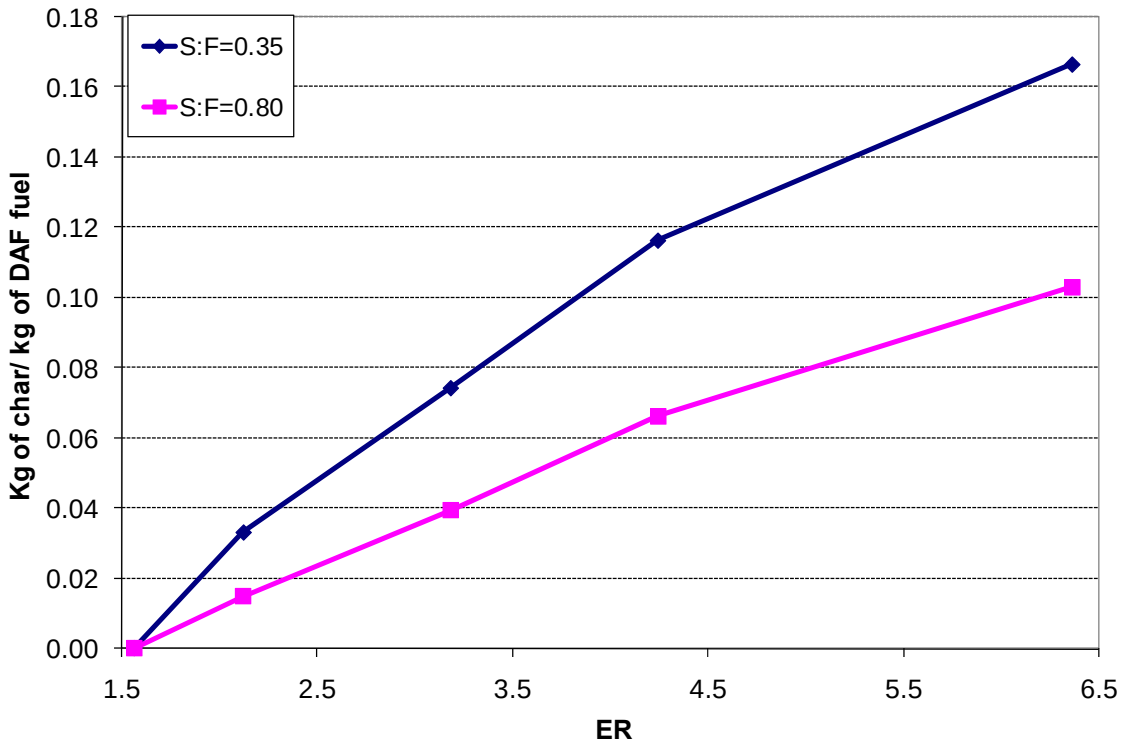

Figure 89. Mass of char produced per kg of DAF DB-ash

From the results, it is evident that under the same operating conditions, gasification of DB-ash blends produces the least amount of char whereas the largest amount of char is produced by gasifying pure DB. The char produced by gasification of DB-WYC lies between pure DB and DB-ash.

The highest yield of char (~0.18 kg per kg of DAF DB gasified) was reached for gasification of DB at ER = 6.36 and S: = 0.35. This indicates that under those operating conditions, only about 18% of the FC content in a kg of DAF DB is gasified; the remaining 82% correspond to char yield. This indicates that gasification of DB at ER = 6.36 and S:F=0.35 tend to be close to pyrolysis in which the gases produced are

principally due to devolatilization of the VM content in the DB. As discussed before, under those operating conditions, the ECE is very low (24%); hence, more of the energy entering the gasifier is removed as char and tar. However, at ER = 6.36, increasing S:F from 0.35 to 0.80 increases the char gasified by about 27.5%, which suggests that increasing S:F ratio increases the reaction rate of char with steam to produce CO and H_2 by about 27.5%.

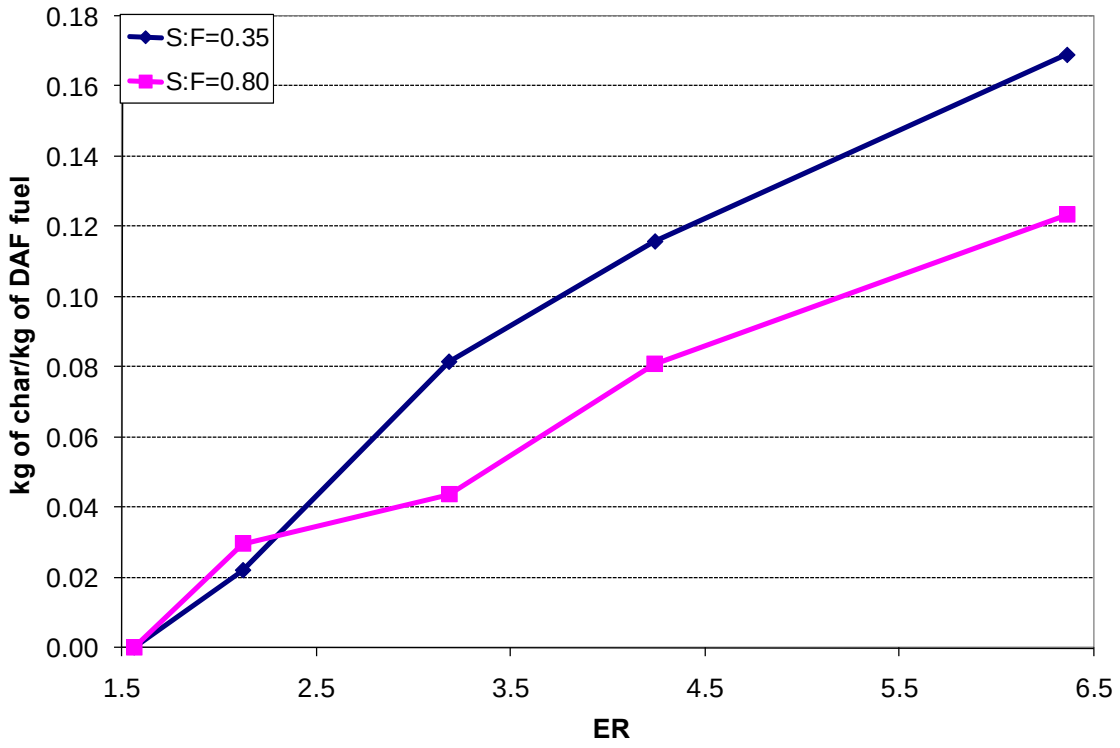

Figure 90. Mass of char produced per kg of DAF DB-WYC

As discussed before, tar was estimated by atom balance using the gas composition measured in the MS and the tar composition. Figures 91, 92, and 93 present

the yields of tar (kg of tar/ kg of SATP m^3 of gas) in the product gases leaving the gasifier as a function of the ER and S:F for pure DB, DB-ash, and DB-WYC, respectively.

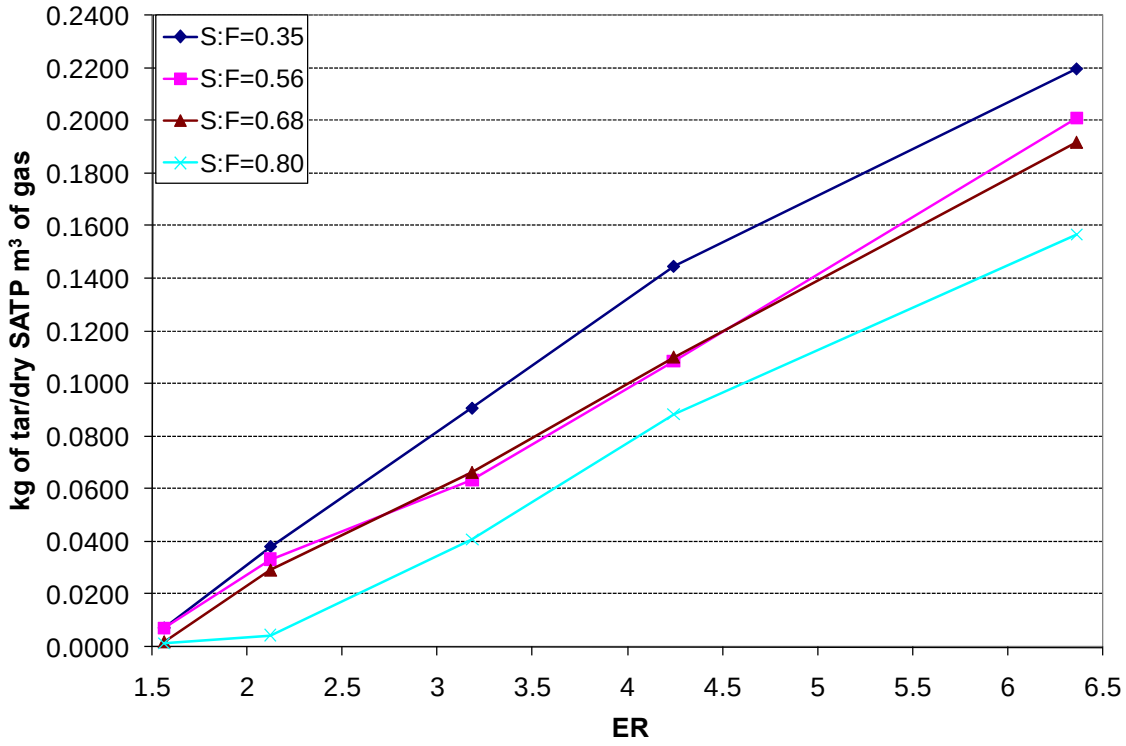

Figure 91. Tar concentration in the gases leaving the gasifier for gasification of pure DB

For all fuels tested, increased ER produce gases with more tar whereas increasing S:F reduces tar production. This could result because increasing ER tends to decrease the temperature profile in the gasifier, which leads to less tar molecules breaking to produce lighter gases. Increasing steam or oxygen in the gasifier accelerates the destruction of primary products and inhibits the formation of aromatics, which are the principal

components of tar [46]. In addition, to enhanced H_2 production with steam, it also has been reported that reduces refractory tar, enhances phenol formation, reduces the formation of other oxygenates, breaks few of the aromatics tar, and produces tar easier to reform catalytically [47].

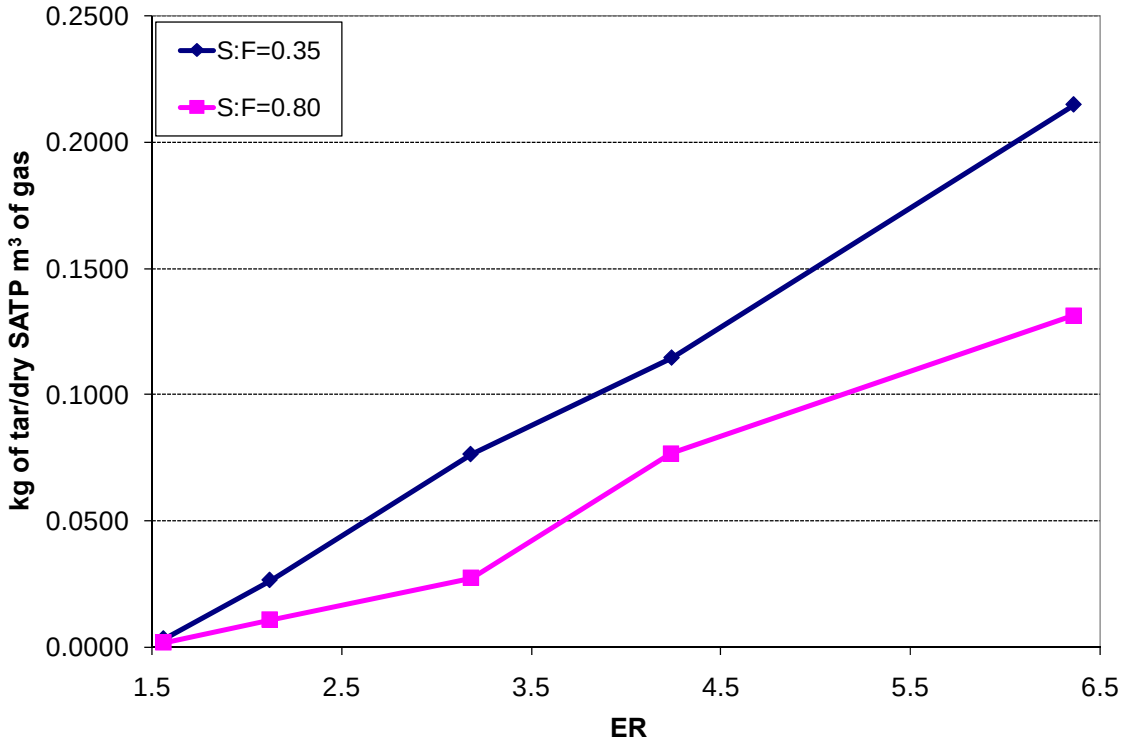

Figure 92. Tar concentration in the gases leaving the gasifier for gasification of DB-ash

Figure 91 shows that the differences in the amount of tar formation for pure DB at S:F = 0.56 and S:F = 0.68 is practically negligible.

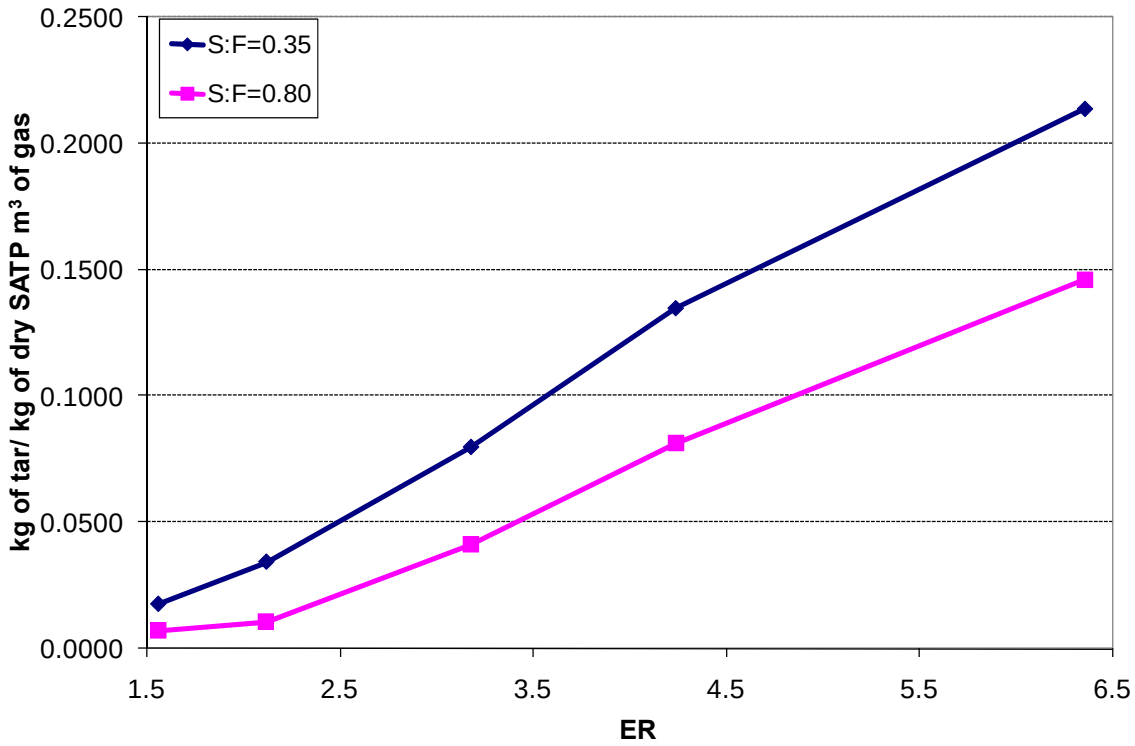

Figure 93. Tar concentration in the gases leaving the gasifier for gasification of DB-WYC

For all the experiments performed with pure DB, the average of tar was estimated to be of about 80 g/ SATP m^3 of gas. The average of tar concentration is higher than that presented by [16] and [47] for average fixed-bed gasification of biomass with air (50 g/SATP m^3 of gas). Pinto et al. [15] has reported concentration of tar ranging between 20 and 40 g/SATP m^3 for fluidized co-gasification of coal with wastes biomass using a mixture of steam-oxygen as oxidizer. Milne et al. [47] has reported an average of tar concentration of ~10 g/SATP m^3 for air-blown fluidized bed gasification of biomass. Zhang et al. [46] reported tar concentration of 10.4 g/SATP m^3 in an air-blown fluidized bed gasifier using seed corn wastes as feedstock.

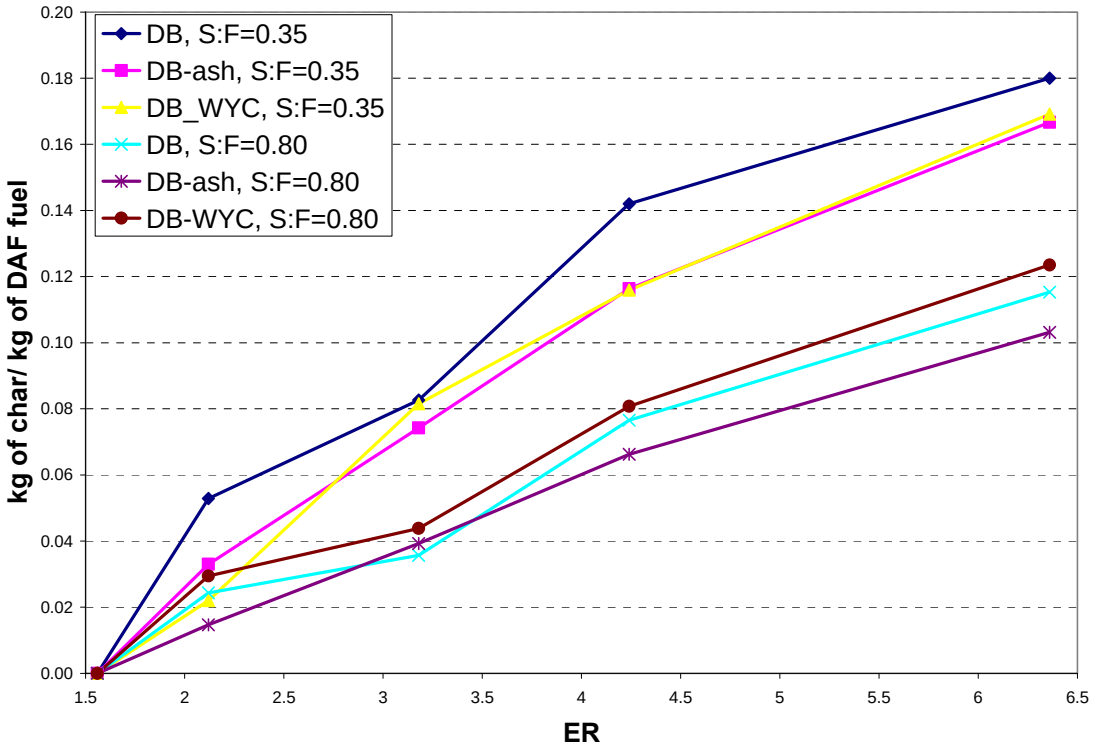

Figure 94. Mass of char non-burned by kg of DAF fuel for gasification of pure DB, DB-ash, and DB-WYC at S:F=0.35, A:F=0.80 and various ERs

At S:F = 0.35, DB is the fuel that produces the most char while at S:F = 0.80, DB-WYC produces more char than the other fuel (Figure 94). In general, for all experiments, the fuel that produces the least char is DB-ash blend, because ash increases the bed temperature profile without increasing the amount the FC content in the fuel. Increased peak temperatures lead to increase the heterogeneous reaction rate of char with oxygen and steam, which decreases the amount the char removed in the ash.

The more char obtained at S:F = 0.80 by DB-WYC compared to other fuels could result from more FC content of coal. As discussed before, the addition of WYC leads to higher bed temperatures, but also increases the char concentration in the bed. Char

burned by effect of higher bed temperature is less than that of char added in the WYC; then, more char would be removed in the ash. The results presented for S:F = 0.35 in Figure 94 suggests that the char gasified by the effect of the increased temperatures generated by the presence of WYC is higher than that added in the WYC. On the other hand, at S:F = 0.8, it seems that char gasified is lesser than the char added in the WYC.

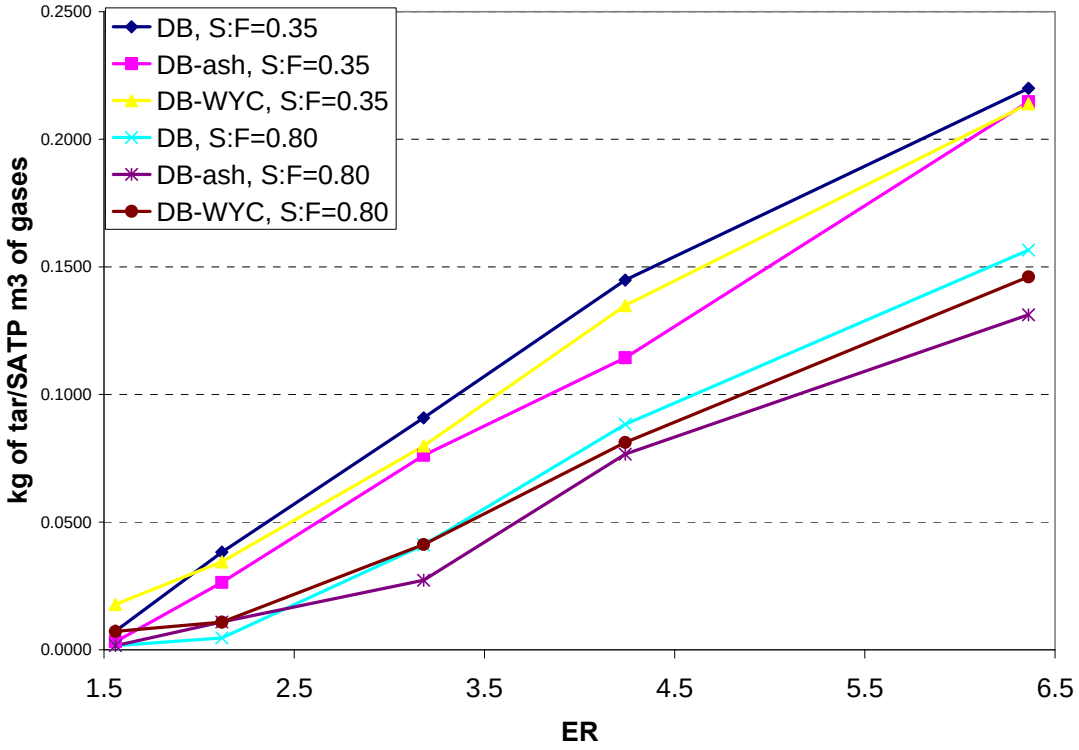

Figure 95. Concentration of tar for gasification of pure DB, DB-ash, and DB-WYC at S:F=0.35, A:F=0.80 and various ERs

Figure 95 presents the concentration of tar in the gases produced by gasification of all fuel studied, at S:F = 0.35 and S:F = 0.80, as a function of ER. In general, the results show that under the same operating conditions, gasification of pure DB produces

gases with the highest tar content whereas gasification of DB-ash produces gases with the smallest amount of tar. The tar curves obtained by gasifying DB-WYC lie between the curves of pure DB and DB-ash.

As stated before, an average of 80 g of tar/SATP m^3 was achieved for all the experiments performed with pure DB whereas for gasification of DB-WYC, the average was 77 g of tar/SATP m^3. The average for DB-ash blend was of 68 g of tar /SATP m^3. In general, the presence of ash in DB decreases the tar concentration in the gases leaving the gasifier by about 15% whereas the addition of WYC decreases the tar concentration only by about 4%. For all experiments, the tar concentration ranged between 2 and 220 g/SATP m^3.

The current results cannot be compared with results from previous studies because, as discussed before, there are no previous studies published on experimental gasification of DB. Also,the previous studies on cattle biomass, tar production has been not reported. According to Milne et al. [47] air-blown fixed-bed counter-flow gasifiers produce about 400% more tar than an air-blown fluidized bed gasifiers.

If the results obtained by Pinto et al. [15] in a steam-oxygen fluidized bed gasifier were extrapolated to a fixed gasifier, the maximum concentration of tar would be of about 200 g/SATP m^3, which agrees well with the maximum tar concentration (220 g/SATP m^3) achieved in the current experiments.

7.8. Pyrolysis

In this section results are present for pure pyrolysis of DB. Pure DB biomass was subjected to a pyrolysis process to produce chlorinate char to be used in the absorption of mercury produced in coal plants.

7.8.1. Results on profile temperature

This section presents the temperature profile along the gasifier, the temperature of the carrier gas, and the temperature of the gases leaving the gasifier as a function of the time during the heating and cooling period of the experiment.

Figure 96 presents the bed temperature profile of the gasifier during an experiment using N_2 as carrier gas. In general, the temperatures measured along the gasifier axis keeps increasing above the initial value until it reaches a peak where the propane torch is turned off (Region I). Then biomass is added (Region II). After DB is added, the bed temperatures stars to increase again (Region III) until a second peak is achieved beyond which the temperature starts to decrease again until achieving the final temperature (Region IV). As shown in Figure 96, the temperatures at the thermocouples closer to the grate achieve the second temperature peak (T_{peak}) faster than that placed farther of the grate.

The peak of the gases (gases leaving the gasifier) also indicates the moment in which the propane torch is turned off. In contrast to the bed temperatures (or particle

temperature) which presents two peaks, the temperatures of the carrier gas and gases leaving the gasifier shows only one peak.

The results show a heating time of about 2 ¼ hours and the cooling time of about 8 hours. The initial temperature along the gasifier axis (at zero time) ranged between ~650 and 450 °C, because this profile of temperature corresponds to the temperature of the gases produced by the combustion of the propane. After ~2 ¼ hours of heating, the bed temperatures achieved the heating peak temperature (~ 800 °C -620 °C), whereas the temperatures (peak temperature) of the gases leaving the gasifier and the carrier gas were ~240 and 160 °C, respectively.

The bed temperature 2 cm above the grate achieved the second peak (500 °C) almost immediately after DB was added. On the other hand, the bed temperatures between 4 and 20 cm above the grate achieved the second peak temperature (~400°C) ~2 hours after the biomass was added. The fact that the bed temperature between 4 and 20 cm above the grate takes a longer time (~2 hours) to reach the second peak seems to indicate that the global pyrolysis reaction of DB may be slightly exothermic or some gases volatilized during pyrolysis such as CO and H_2O react to produce secondary compounds resulting in CO_2 and H_2, which is exothermic. The temperatures show a gradient along the gasifier axis.

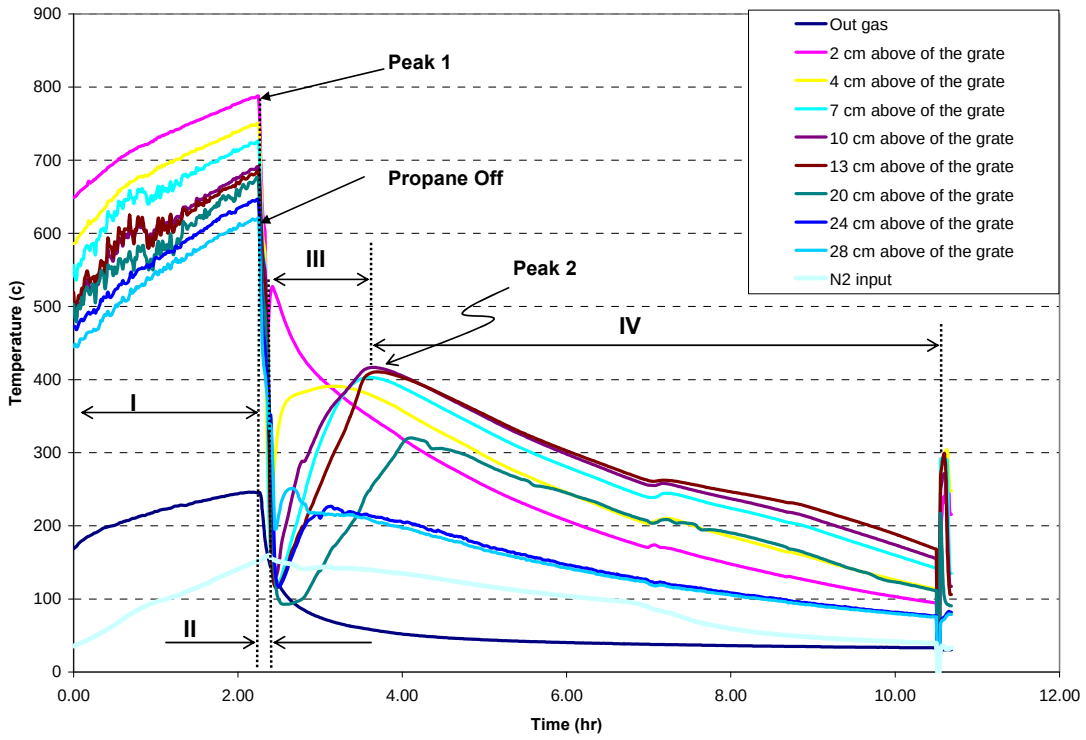

Figure 96. Temperature profile, temperature of the carrier gas, and temperature of gases leaving the gasifier for pyrolysis of DB using N_2 as carrier gas. Region I = heating period with propane torch, Region II = biomass addition, Region III = heat up period with radial heat from the walls, Region IV = cooling

During the heating period and before the second temperature peak is achieved, the temperatures measured closer to the grate were higher than those measured farther the grate. However, after the second peak, the temperatures closer to the grate ere lower as compared to those farther to the grate, which also suggest that some gases produced in the lower zones (closer to the grate) react in the upper zones and release heat.

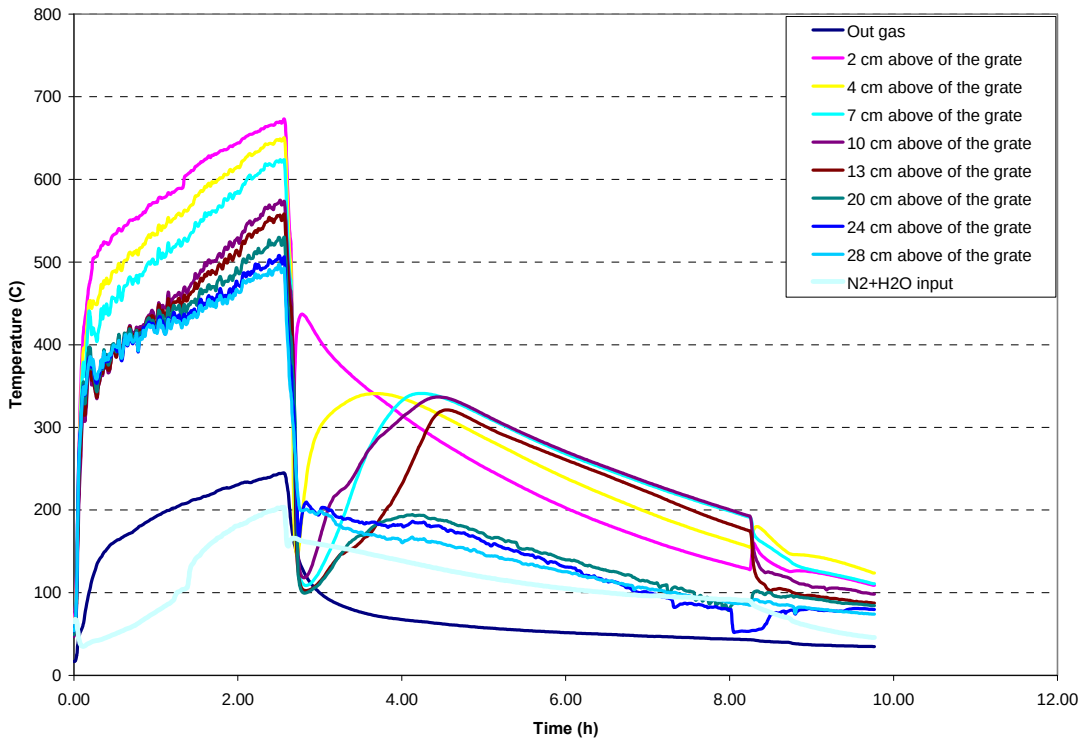

Figure 97. Temperature profile, temperature of the carrier gas, and temperature of gases leaving the gasifier for pyrolysis of DB using N_2 and steam as carrier gas

According to [27], DB pyrolyzes at temperatures ranging between 500 and 600 K; thus, the higher peak temperature (670 K) measured between 2 and 20 cm above of the bed (Figure 96) also appears to validate the fact that there may be exothermic reactions. After ~ 8 hours of cooling, the temperatures measured in the bed ranged between 100 and 170 °C. At this time, the carrier gas was turned off and the gasifier was closed completely to be cooled to ambient temperature.

Figure 97 presents the temperatures measured along the gasifier, the carrier gas, and the gases produced by pyrolysis of DB using N_2 and steam as carrier gas as a function of the time. Although, the temperatures are lower compared to those of

pyrolysis using only N_2 as carrier gas, the trend is the same. It is apparent that although the heating time was a little longer (2 ½ hours), the peak temperatures are slightly lower as compared to those of N_2 pyrolysis.

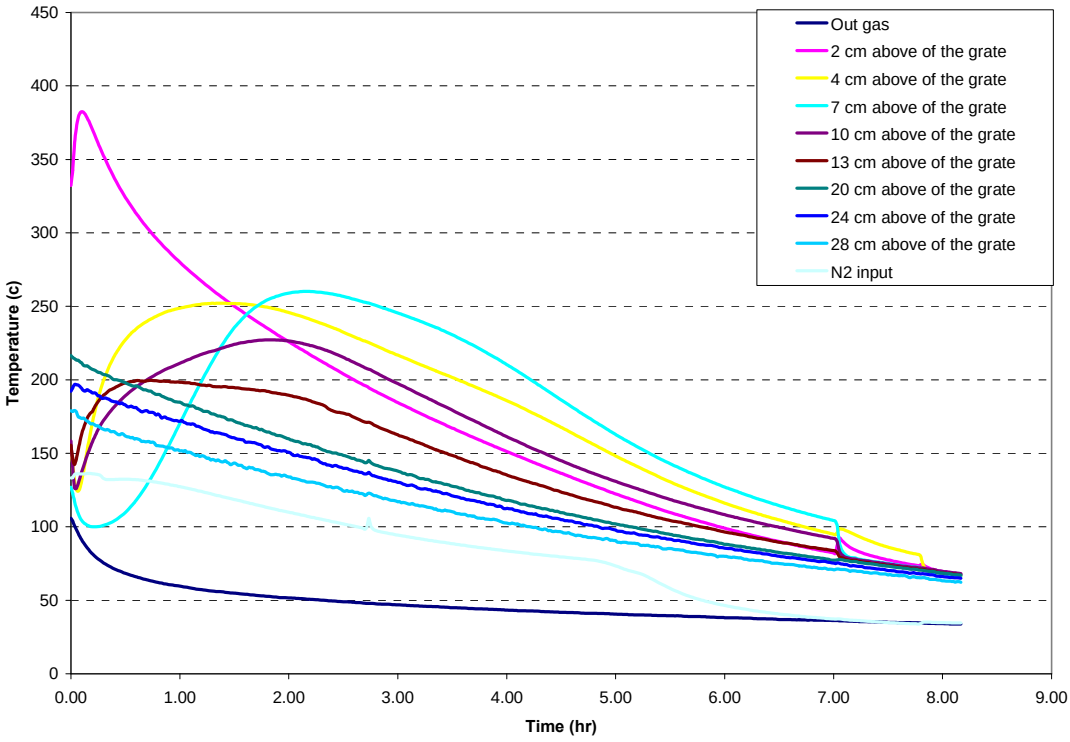

Figure 98. Temperature profile of cooling, temperature of the carrier gas, and temperature of gases leaving the gasifier for pyrolysis of char produced in pyrolysis using N_2 as carrier gas

At about 8 ¼ hours, the temperatures show a sudden decrease because at that time, the grate was rotated to cool down quickly the gasifier. Although, the peak temperature with N_2 and steam are slightly lower, the reduction in weight was the same as with N_2 only.

To produce chlorinate char with a lower content of VM, some of the char produced by pyrolysis of DB with N_2 as carrier gas was used in a second pyrolysis process with N_2 as carrier gas. The char pyrolysis temperatures are presented in Figure 98. The bed cooling trends are the same as that of pure DB pyrolysis. The temperatures above 13 cm correspond to gas temperature, which decreases continuously and there is no peak. In contrast, the bed temperatures which corresponds to the temperature of the particles of char, present a peak, which suggests the presence of homogeneous exothermic reactions. Because the weight of char was reduced by ~16%, the lower of the peak temperatures (~200 °C), measured at 13 cm above of the grate, also indicates that char pyrolysis starts a lower temperatures than 500 K.

7.8.2. Results on activated carbon

Table 22 presents the results of ultimate and proximate analysis of pure DB and the char produced by pyrolysis of pure DB using pure N_2 and N_2-H_2O blend as carrier gases. The analyses of DB and chlorinated char show that DB has more volatile matter (VM) and moisture contents than those of chlorinated char (31.85% and 6.07%, respectively). The content of other components-such as fixed carbon (FC), ash, and carbon-are higher in the activated carbons. The moisture contents in the chlorinated char obtained by pyrolysis with N_2 and pyrolysis with N_2-steam are 76 and 79%, respectively lower than those of DB. The VM content was reduced by 32% by N_2 pyrolysis whereas by 24.5% for N_2-H_2O. Pyrolysis with N_2 increased the FC content by 130.6% and the

ash content by 115.5% whereas pyrolysis with N_2-steam increased the FC and ash by 121 and 104% respectively. The carbon atom content increased with pyrolysis, but the changes in the content of other components, such as O, N, S, H, and Cl were negligible.

Because of the higher FC content in the chlorinated chars as compared to the FC content in DB, the HHVs (on a DAF basis) of the activated carbons with N_2 and N_2-steam are about 20.4 and 17.4% higher than that of pure DB respectively.

Table 22. Analysis of DB and activated carbon obtained by pyrolysis of DB using N_2 and N_2+steam as gas carrier on an as received basis

Components	DB	Chlorinated char using N_2 as carrier gas	Chlorinated char using N_2 + H_2O as carrier gas
Dry loss (%)	25.26	6.07	5.41
Ash (%)	14.95	32.22	30.6
VM (%)	46.84	31.85	35.33
FC (%)	12.95	29.86	28.66
C (%)	35.27	43.26	43.52
H (%)	3.1	2.89	3.16
N (%)	1.9	2.62	2.62
O (%)	19.1	18.53	19.63
S (%)	0.42	0.48	0.47
Cl (%)	0.1345	0.14	0.12
As receibed HHV (kJ/kg)	12844	15963	16128
Dry basis HHV (kJ/kg)	17185	16995	17050
DAF HHV (kJ/kg)	21474	25868	25204

Table 23 presents a mass balance (on a 100-kg basis) of all components in DB and in the chlorinated chars. As shown in Table 23 , for each 100 kilograms of DB that was pyrolyzed with N_2, about 47 kg of chlorinate char (CC) were produced. In other words, the yield of CC obtained by pyrolysis of DB with N_2 was 0.47 kg/kg of pure DB pyrolyzed. The yield of CC produced by pyrolysis of DB with N_2 and steam was of 0.49 kg/kg of DB pyrolyzed.

In general, with the exception of ash, the mass of all components content in DB were reduced during pyrolysis. The mass of ash obtained after pyrolysis is practically the same as that in DB because ash is inert. The 68% of VM mass contained in DB was volatilized during pyrolysis using N_2 whereas only 63% of VM was pyrolyzed using N_2-steam.

Table 23. Mass balance of the components, on a 100 basis

Components	DB	After pyrolysis with N_2		After pyrolysis with N_2+H_2O	
	mass (kg)	Mass (kg)	%		%
Moisture	25.26	2.85	11.29	2.65	10.49
Ash	14.95	15.14	101.29	14.99	100.29
VM	46.84	14.97	31.96	17.31	36.96
FC	12.95	14.03	108.37	14.04	108.44
C	35.27	20.33	57.65	21.32	60.46
H	3.10	1.36	43.82	1.55	49.95
N	1.90	1.23	64.81	1.28	67.57
O	19.10	8.71	45.60	9.62	50.36
S	0.42	0.23	53.71	0.23	54.83
Cl	0.13	0.07	48.92	0.06	43.72
Total mass (kg)	100.00	47.00	47.00	49.00	49.00

The mass balance shows that during pyrolysis, a fraction of H_2O, C, H, and O was volatilized, which suggests that some of the fuel gases produced during the volatilization could react with the steam and the oxygen to produce secondary products and release heat in a process known as auto-gasification.

As shown in Table 23, more chlorine is volatilized (less Cl in char) by pyrolysis of DB with N_2 than by pyrolysis with N_2-steam. The results show that about 51% and 56% of the Cl content in DB were volatilized during pyrolysis with N_2 and N_2-H_2O, respectively, whereas 68% and 64% of the VM in DB were volatilized by pyrolysis with N_2 and N2-H_2O, which indicates that the rates of volatilization of chlorine during

pyrolysis are lower than those of VM. VM% to Cl% pyrolyzed ratios were1.34 and 1.12 during pyrolysis with N_2 and N_2-staam respectively.

8. SUMMARY, CONCLUSIONS, AND FUTURE WORK

This section presents the summary and conclusions of this study on gasification of DB, DB-ash, and DB-WYC and the future work.

8.1. Gasification facility

A small-scale (10-kW) gasification facility was rebuilt with the following modifications:

a) An ash disposal system so that experiments could be run continuously with periodic ash disposal
b) A steam generator to produce the steam for the gasifier
c) A MS and the gas mixtures necessary to calibrate the MS were acquired
d) A sampling system to prepare the gas samples before they were analyzed continuously and in real time by a mass spectrometer
e) A data acquisition system to measure the temperature in different places of the gasification facility
f) A control panel to control the flow of steam, air, and heat to the heater elements of the steam generator and combustion chamber of the gasifier.

8.2. Modeling studies

Global modeling studies (atom balance and equilibrium) on gasification were performed to determine the operating conditions (ER and S:F). The effect of modified equivalence ratio ER_M and AOF on gasification of feedlot biomass (FB), dairy biomass (DB), Wyoming coal (WYC), and Texas Lignite coal (TXL) were also estimated by modeling:

a) Modeling results showed that biomass gasification under increased ER_M (decreased oxygen supplied through the oxidizer) yield poor hydrogen and CO_2 mixtures and rich CO and CH_4 mixtures whereas mixtures rich with steam (decreased AOF) produce rich hydrogen and CH_4 mixtures but poor CO and CO_2 mixtures.
b) From the modeling results, it is apparent that for the same ER_M and AOF, FB and DB produce more H_2 than WYC and TXL, but the coals are better if more production of CO is desired.
c) Decreased AOFs produce mixtures richer in CH_4 and H_2, which have higher HHV. On the other hand, increased ER_M tends to produce mixtures with a higher HHV. Generally, mixtures rich in methane and hydrogen have greater HHV and provide better energy conversion efficiency because methane has higher energy density (36,250 kJ m^{-3}) as compared to CO (11,543 kJ/ m^3).
d) The increase in AOF decreases ECE, but at higher ER_M the decrease is not much. At constant AOF, higher ER_M implies lesser oxygen supplied in the oxidizers and

the process is nearly pyrolysis (production of char), which produces less mass of gases per kg of fuel resulting in lower energy recovery.

e) At constant ER, increasing the S:F implies increased steam supplied with the oxidizing source; thus, the reactions occur in a steam-rich ambient which favors the steam reforming reaction (Equation 6) and the shift reaction (Equation 7) producing mixtures rich in H_2, CO_2, and CH_4 but poor in CO.

f) The increase in ER at constant S:F implies decreased oxygen entering through the air and, hence, the reactions occurs in an enviroment poor in O_2 but rich in H_2O, which favors the reactions of char and CO with steam to produce more CO_2 and H_2. More C atoms leaving the gasifier as CO_2 means less C atoms leaving as CO. The curves of CO and H_2 show a peak that is best illustrated in Figures 32 and 33. At ER < 3.18, increasing ER improves the CO concentration but at ER >3.18, the CO concentration decrease as ER increase. Modeling results shows that the increase in ER produces mixtures rich in CH_4.

g) Gasification at high ER produces CH_4-and H_2-rich mixtures that have high HHV because of the higher HHV of CH_4 and H_2. At ER < 3.18, the gross heating value of the gases is not affected by changes in S:F. This result because at ER < 3.18, the changes in the S:F do not affect the CH_4concentration.

h) Increasing ER at constant S:F tends to increase the ECE until a critical value beyond which it starts to decrease. At ER < 3.18, increased ER increases the ECE until 0.87, where it starts to decrease (Figure 38). Gasification under ER > 3.18 tends to produce char because of the lack of oxygen for the reaction of char.

8.3. Experimental studies

Experiments on gasification with air-steam were performed and data on bed temperature profile and gas composition under various operating conditions were obtained. Additionally, chlorinated char was produced through the pyrolysis of DB using N_2 and N_2-steam blends:

a) The adiabaticity of the reactor was checked by determining the overall heat transfer coefficient (*U*) and then estimating the heat loss; the *U* was measured by allowing the reactor to cool down after the experiment and storing the changes of temperature. The results showed that the global heat transfer coefficient is very low (U=6.37016x10^{-6} kW/ m^2.K) and is almost constant along the gasifier axis.

b) The bed temperature profile measured along the gasifier axis showed a peak in the combustion region where the char reacts with the oxidizer. The peak temperature lies somewhere between 3 and 5 cm above the grate and depends upon the concentration of O_2, H_2O, and CO_2 in the combustion zone. Above the combustion zone in the reduction, pyrolysis, and dry zones, the temperature decreased because most of the reactions occurring there are endothermic.

c) Increased ER and S:F ratios decrease the peak temperature. Operating at ER > 6.36 can lower peak temperatures below that required for char combustion. Thus, under those operating conditions, the process becomes near pyrolysis which requires heat input. In general, for the set operating conditions, the peak

temperature for gasification of DB ranged between 519 and 1015°C. Gasification of DB-ash and DB-WYC blends showed the maximum peak temperatures (1032 and 1054 °C respectively).

d) From the results, it is apparent that H_2-rich mixtures could be produced by adiabatic gasification of DB using mixtures of air-steam as an oxidizing source. Increased ER and S:F tends to produce H_2-and CO_2-rich mixtures, but mixtures poor in CO. In general, the effect of the ER and S:F on the production of CH_4 and C_2H_6 is negligible. For gasification of DB under the set of operating conditions, the CO ranged from ~4.77 to ~11.73%, H_2 from 13.48 to 25.45%, CO_2 from 11 to 25.2%, CH_4 from 0.43 to 1.73 %, and C_2H_6 from 0.2 to 0.69%.

e) The addition of ash and WYC seems to affect the production of CO and H_2. The highest increase in CO (caused by the addition of ash) at S:F = 0.35 and ER = 6.36 was around 50%, whereas the highest increase in H_2 (~30%) was achieved at ER = 1.5 and S:F = 0.35. At ER > 3.18, the effect of adding ash and WYC on the production of H_2 was insignificant. Gasification of DB-ash blends produced mixtures with CO ranging between 6.7 and 13% and H_2 ranging between 17.5 and 25.3% whereas gasification of DB-WYC blends produced mixtures with CO from 6.5 to 13.6% and H_2 raging from 16 to 26.3%.

f) The effect of the S:F ratio on the HHV of gases is more important than that of the ER. Although increased ER produces gases with higher gross heating value, the energy recovery decreases with increased ER because of higher tar and char production.

g) At constant S:F, increasing ER increases char production whereas at constant ER, increased S:F produces lower char. At ER = 1.59, the char produced was almost zero. The highest yield of char (~0.18 kg per kg of DAF DB gasified) was reached for gasification of DB at ER = 6.36 and S:F = 0.35. This indicates that under those operating conditions, only about 18% of the FC content in a kg of DAF DB is gasified; the remaining 82% corresponds to char. Thus, gasification of DB at ER = 6.36 and S:F = 0.35 tends to be near pyrolysis.

h) For all the cases, increased ER tends to produce gases with high concentrations of tar whereas increased S:F reduces the production of tar. For pure DB, the tar average was estimated to be about 80 g/SATP m^3 of gas. The tar average concentration is higher than that presented by [16] and [47] for fixed bed gasification of biomass with air (50 g/SATP m3 of gas). However, if the results obtained by Pinto et al. [15] (40 g/ SATP m^3 of gas) in a steam-oxygen fluidized -bed gasifier were extrapolated to a fixed gasifier, the maximum concentration of tar would be about 200 g/SATP m^3 because a fixed bed gasifier produces about 400% more tar that a fluidized-bed gasifier [47]. This agrees well with the maximum tar concentration (220 g/SATP m^3) achieved in the current study.

i) About 51% and 56% of the Cl content in DB was volatilized during pyrolysis with N_2 and N_2-H_2O respectively whereas 68 % and 64% of the VM in DB were volatilized by pyrolysis with N_2 and N_2-H_2O. This indicates that the rates of volatilization of chlorine during pyrolysis are lower than those of VM. VM% to

Cl% pyrolyzed ratios were1.34 and 1.12 during pyrolysis with N_2 and N_2-staam respectively.

8.4. Future work

The following are suggested for future work:

a) Perform experiments on gasification of pure FB and pure coal using air-steam mixtures as oxidizer in order to compare the results to the results obtained in this study.
b) Do experiments on gasification of DB using pure oxygen and steam as oxidizer to compare the results to the results obtained in this study.
c) Perform experiments on pyrolysis using pureN_2 and N_2-steam mixtures as carrier gases to study ash and gas quality
d) Studies on pyrolysis of biomass supplemented with chlorine in order to increase the Cl content in char since char is a porous medium which diffuses Cl.

REFERENCES

[1] Energy Information Administration (EIA). International Energy Outlook 2008, World Energy Demand and Economic, Web site http://www.eia.doe.gov/oiaf/ieo/world.html, accessed June 2008.

[2] Energy Information Administration (EIA)-International Energy Outlook 2008, Energy Related Carbon Dioxide, Web site, http://www.eia.doe.gov/oiaf/ieo/emissions.html, accessed June 2008.

[3] Energy Information Administration (EIA), International Energy Outlook 2008, Highlights Sections, Web site http://www.eia.doe.gov/oiaf/ieo/highlights.html, accessed June 2008.

[4] Demirbas A. Potential applications of renewable energy sources, biomass combustion problems in boiler power systems and combustion related environmental issues. Prog. Energy Combust. Sci. 2005; 31:171-192.

[5] Klass DL. Biomass for Renewable Energy, Fuels, and Chemicals. San Diego: Academic Press; 1998.

[6] DI Blasi C, Signorelli G, Portoricco G. Countercurrent fixed-bed gasification of biomass at laboratory scale. J. Ind. Eng. Chem. Res. 1999; 38: 2571-2581

[7] Annamalai K, Sweeten JM, Freeman M, Mathur M, O'Dowd W, Walbert G, Jones S. Co-firing of coal and cattle biomass (FB) fuels. Part III: Fouling result from a 500,000 Btu/h pilot plant scale burner. Fuel 2003; 82:1195-1200.

[8] Sami M, Annamalai K, Wooldridge M. Co-firing of coal and biomass fuel blends. J. Prog. Energy Combust. Sci. 2001; 27:171-214.

[9] Carlin N, Annamalai K, Sweeten JM, Mukhtar S. Thermo-chemical conversion analysis on dairy manure-based biomass through direct combustion. Int. J. Green Energy 2007; 4:1-27.

[10] Galloway T, Waidl J, Annamalai K, Sweeten JM, Tomlinson T, Weigle D. Energy resources recovery applications using gasification and steam reforming. Unpublished In: Proceedings of the Bi-annual Incineration and Thermal Alternatives Conference, New Orleans; 2002.

[11] Kalisz S, Lucas C, Jansson A, Blasiak W, Szewczyk D. Continuous high temperature air/steam gasification (HTAG) of biomass. Draft In: Proceedings of the 6th

Int. Conference on Science in Thermal and Chemical Biomass Conversion, Victoria, Canada; 2004.

[12] Jangsawang W, Klimanek, Gupta AK. Enhanced yield of hydrogen from wastes using high temperature steam gasification. J. Energy Res. Technol. 2006; 128:179-185.

[13] Ferdous D, Dalai AK, Bej SK, Thring RW. Production of H_2 and medium heating value gas via steam gasification of lignins in fixed-bed reactors. J. Can. Chem. Eng. 2001;.79:913-922

[14] Gil J, Corella J, Azner MP, Caballero MA. Biomass gasification in atmospheric and bubbling fluidized bed: Effect of the type of gasifying agent on the product distribution. J. Biomass and Bioenergy 1999; 17:389-403.

[15] Pinto F, Lopez H, Neto RA, Gulyurtlu I, and Cabrita I. Effect of catalysts in the quality of syngas and by-products obtained by co-gasification of coal and wastes. Tars and nitrogen compounds abatement. J. Fuel 2007; 86:2052-2063.

[16] Brown RC, Center for Sustainable Environmental Technologies Iowa State University. Chemicals and power via biomass gasification and fast pyrolysis, presentation In: Proceedings of the Forty-Third Rural Energy Conference, St. Paul, MN; 2005.

[17] NASA: Earth Observatory, the carbon cycle, Web site http://earthobservatory.nasa.gov/Library/CarbonCycle/carbon_cycle4.html, accessed June 2008.

[18] Berndes G, Hoogwijk M, and van den Brek R. The contributions of biomass in the future global supply: A review of 17 studies. J. Biomass & Bioenergy 2003: 25:1-28

[19] Anamalai K, Carlin NT, OH H, Gordillo AG, Lawrence B, Arcot U, Sweeten JM, Heflin K, Harman WL. Thermo-chemical energy conversion using supplementary wastes with coal. In: Proceedings of the ASME International Mechanical Engineering Congress and Exposition, Seattle, WA; 2007: 93-106

[20] Texas Cattle Feeders Association, TCFA. TCFA industry statistics. Web http://www.tcfa.org, accessed June 2008.

[21] Eghball B. Nitrogen mineralization from field-applied beef cattle feedlot manure or compost. J. Soil Sci. Soc. America 2000; 64:2024-2030.

[22] Harman WL. Pen cleaning costs for dust control, southern great plains feedlots, Texas Agricultural Experiment Station, Texas A&M University, BRC Report No. 04-01, 2004.

[23] Department of Primary Industries and Fisheries (DPI&F). Feedlot waste management series: Manure production data. Government of Queensland, Australia, 2003, http//www.dpi.qld.gov.au//environment/5166.html.

[24] United States Department of Agriculture (USDA), Economics, statistics, and market information system, 2007, http://usda.mannlib.cornell.edu/

[25] Priyadarsan S, Annamalai K, Sweeten JM, Holtzapple M. Co-gasification of blended coal with feedlot and chicken litter biomass. Proc. Combust. Inst. 2005; 30:2973-2980.

[26] Priyadarsan S, Annamalai K, Sweeten JM, Mukhtar S, Holtzapple MT. Fixed bed gasification of feedlot and poultry litter biomass. Trans. ASAE 2005; 47**:**1689-1696.

[27] Lawrence B, Cofiring coal and dairy biomass in a 100,000 Btu/hr furnace. M.S. Thesis. Texas A&M University 2007.

[28] Hobbs ML, Radulovic PT, Smoot LD. Combustion and gasification of coals in fixed-beds. J. Prog. Energy Combust. Sci. 1993; 19:505-586

[29] Bridgwater AV. The technical and economic feasibility of biomass gasification for power generation. Fuel 1995; 74(5):631-653.

[30] Hobbs ML, Radulovic PT, Smoot LD. Modeling fixed-bed coal gasifier. J. AIChe. 1992; 38:681-702.

[31] Di Blasi C. Modeling wood gasification in a countercurrent fixed-bed reactor. J. AIChe. 2004; 50 (9):2306-2318.

[32] Walker Jr PL, Ruskino Jr F, Austin LG. Gas reaction of carbon. Adv. in Catal. 1959;11:167-179.

[33] Annamalai K, Puri I. Combustion Science and Engineering.1st ed. Boca Raton, FL: CRC Press, 2006.

[34] Annamalai K, Willian R. Interactive processes in gasification and combustion-II. Isolated carbon, coal and porous char particles. J. Prog. Energy Combust. Sci. 1993; 19: 383-446.

[35] Turns SR. An Introduction to Combustion: Concepts and Applications. New York: McGraw-Hill, 1996.

[36] Parent JD, Katz S. Equilibrium Compositions and Enthalpy Changes for the Reactions of Carbon, Oxygen and Steam. Chicago Institute of Gas and Technology, 1948.

[37] Raman KP, Walawender WP, Fan LT. Gasification of feedlot manure in a fluidized bed reactor: The effect of temperature. J. Ind. Eng. Chem. Process Des. Dev. 1980; 19: 623-629.

[38] Rhinehart RR, Felder R, Ferrell J. Coal gasification in pilot-scale fluidized bed reactor. Gasification of Texas lignite. J. Ind. Eng. Chem. Res. 1987; 26:2048-2057.

[39] Young L, Pian C. High temperature, air-blown gasification of dairy-farm wastes for energy production. J. Energy 2003; 28:655-672.

[40] McLendon TR, Lui AP, Pineat RL, Beer SK, Richardson SW. Hugh pressure co-gasification of coal ad biomass in a fluidized bed. J. Biomass and Bioenergy 2004; 26:377-388.

[41] Jiang H, Shu X, Guo Q, Zhu Q. Gasification of rice husk in a fluidized-bed gasifier without inert additives. Ind. Eng. Chem. Res. 2003; 42:5745-5750.

[42] Priyadarsan, S. Fixed bed gasification studies on coal-feedlot biomass and coal-chicken litter biomass under batch mode operation. M.S. Thesis, Texas A&M University, 2002.

[43] Incropera FP, DeWitt DP. Fundamentals of Heat and Mass Transfer. 5th edition. Hoboken, NJ: John Wiley & Sons, 2002.

[44] Changdong Sheng, Azevedo J.L.T. Estimating the higher heating value of biomass fuels from basic analysis data. J. Biomass and Bioenergy 2005; 28:499-507.

[45] Annamalai K, Priyadarsan S, Arumugam S, Sweeten JM. Energy conversion: Principles of coal, animal waste, and biomass fuels. Encyclopedia Energy Eng. Technol. 2007;1(1):476-497.

[46] Zhang R, Brown RC, Suby A, and Cummer K. Catalytic destruction of tar in biomass derived producer gas. J. Energy Conversion & Management. 2004; 45:995-10014.

[47] Milne TA, Abatzoglou N, Evans RJ. Biomass gasifier “tars”: Their nature, formation, and conversion. NREL/TP-570-25357. 1998, DOE Information Bridge, http://www.doe.gov/bridge/home.html.

APPENDIX A

MODIFICATIONS PERFORMED IN THE GASIFICATION FACILITY

Figure A-1. Combustion chamber built in castable alumina with inner and outer diameter of 6 in and 10 in respectively

Figure A-2. Combustion chamber and outer steel tube with a inner diameter of 13.5 in

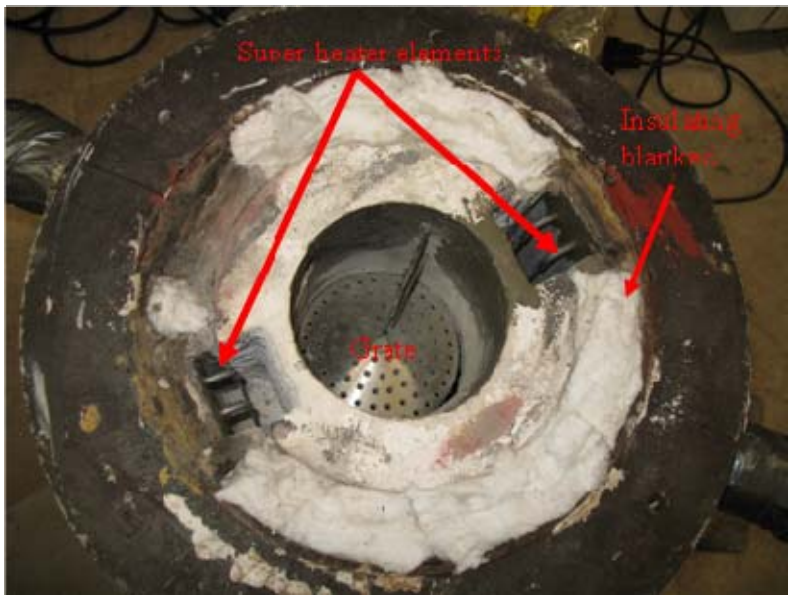

Figure A-3. Combustion chamber with two super heater elements and cash iron conical grate

Figure A-4 cast iron conical grate with 144 of o.25 in drilled holes

Figure A-5 pneumatic vibrator of variable frequency coupled to the grate and placed under the plenum

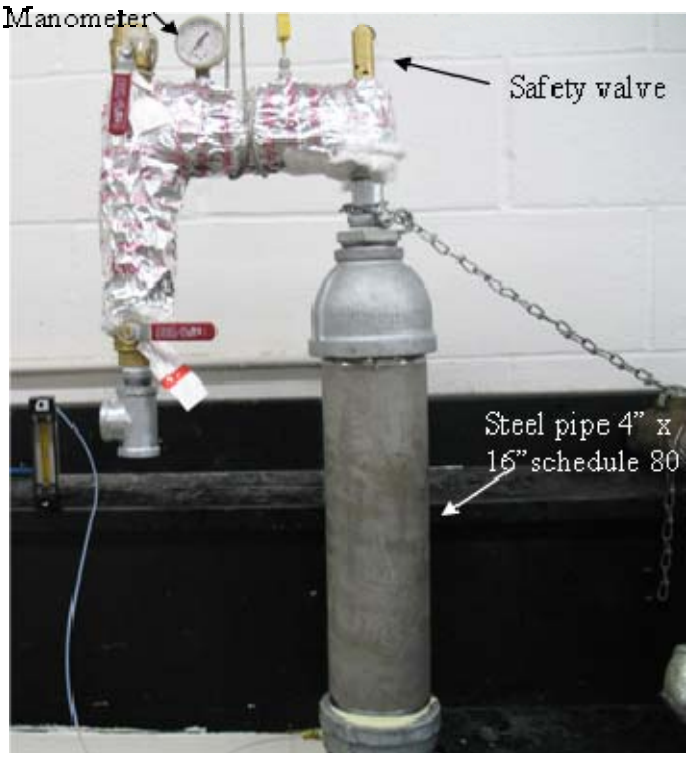

Figure A-6 Steam generator

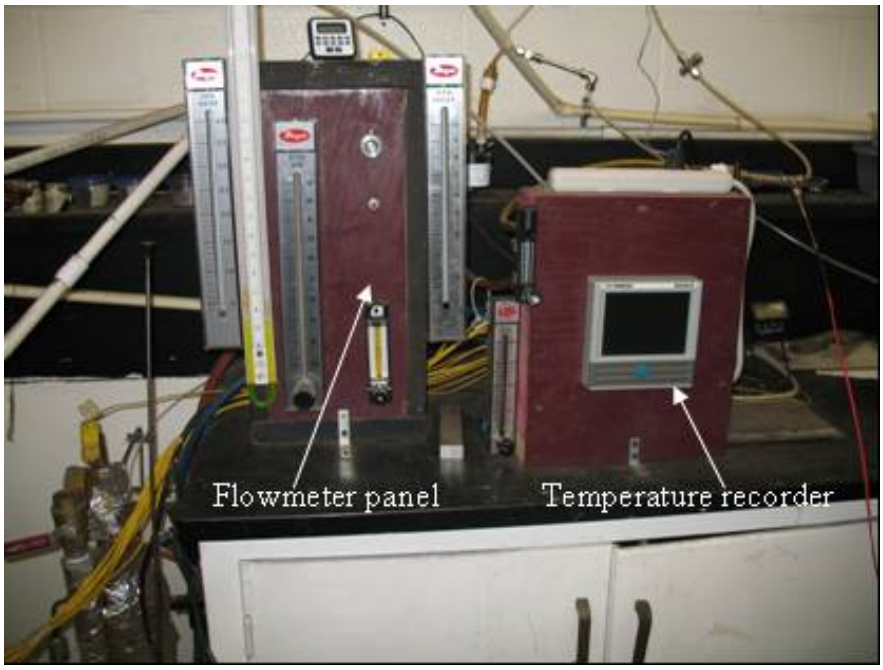

Figure A-7 Control panel

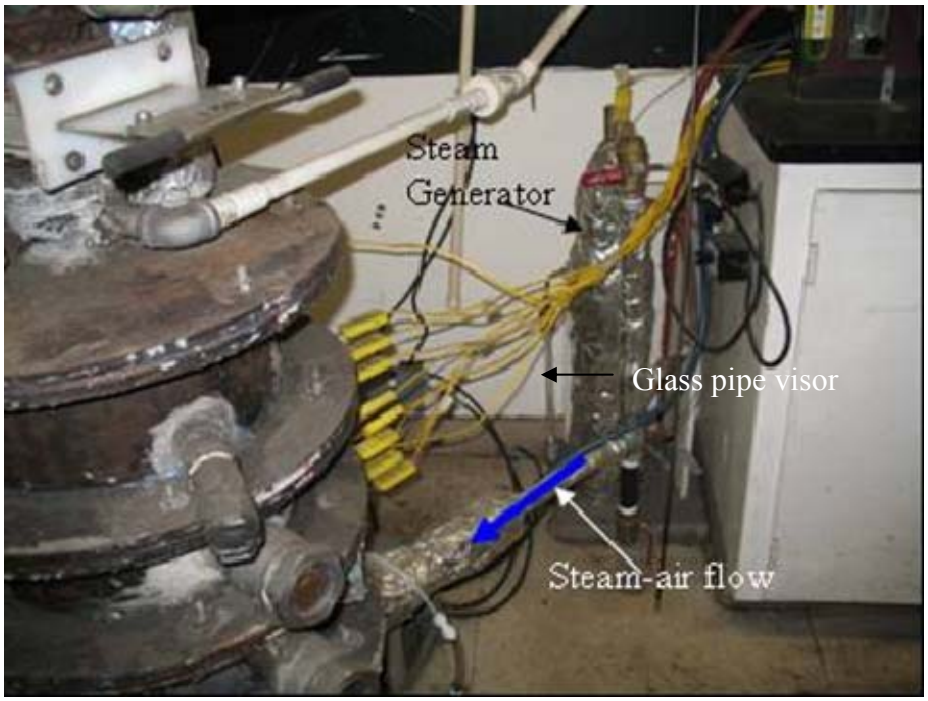

Figure A-8 Oxidizing resource feeding view

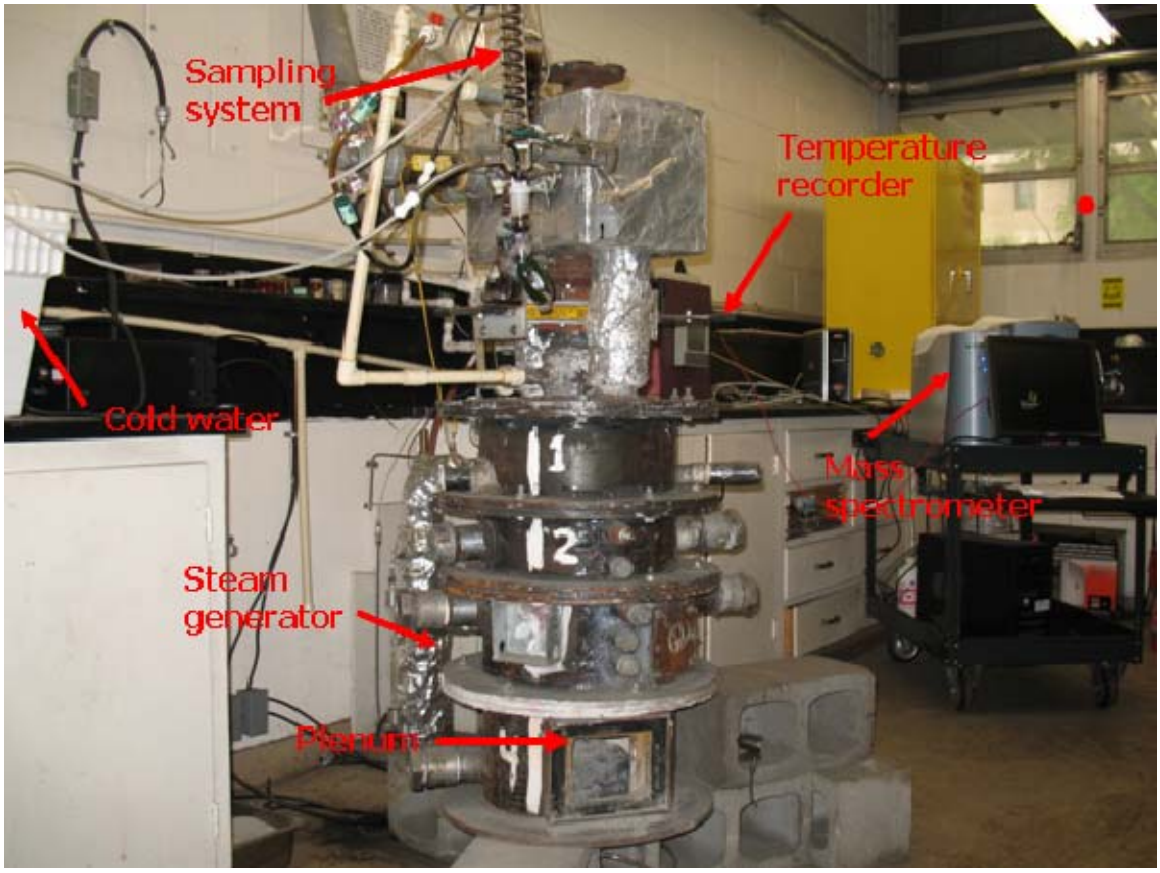

Figure A-9 Gasification facility

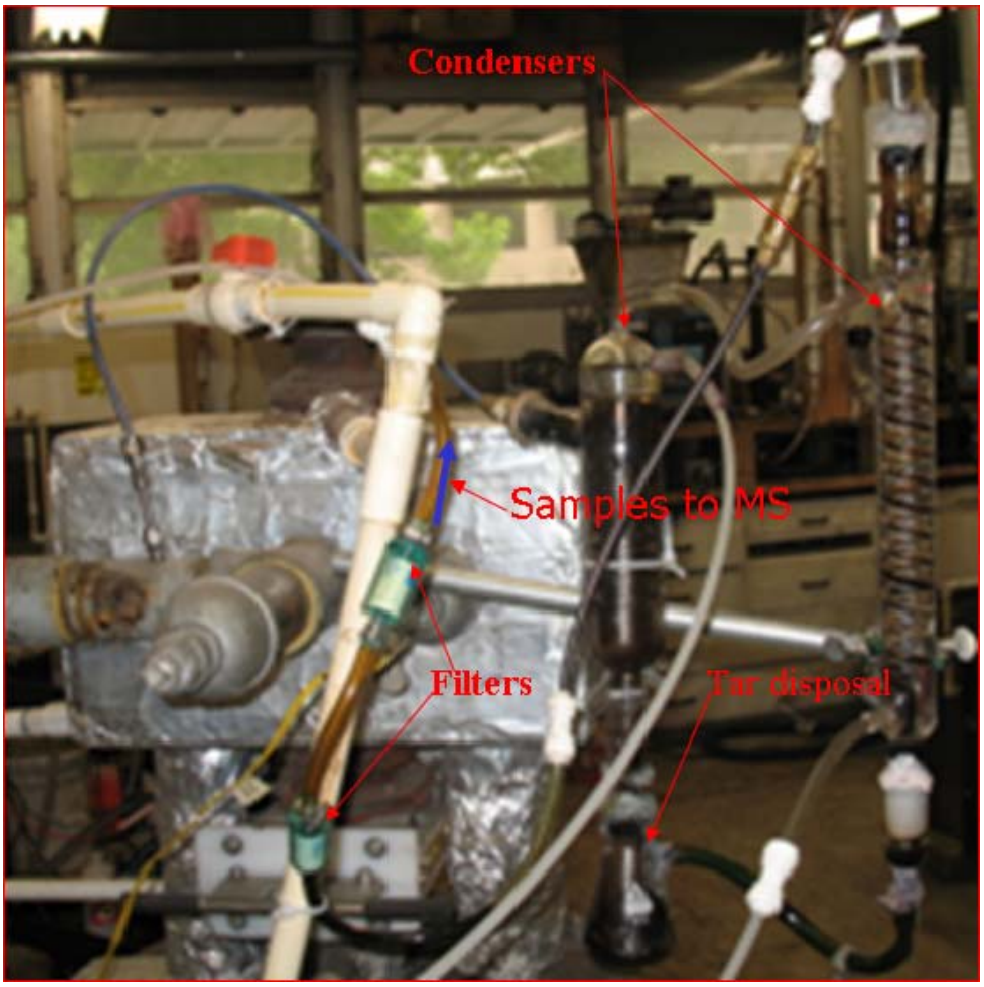

Figure A-10 Sampling system

APPENDIX B

EES CODE TO ESTIMATE GAS COMPOSITION BY ATOM BALANCE

The Engineering Equation Solvers (EES) code which was performed to estimate the gas composition by atom balance is presented in this appendix. Running the program requires entering the properties of the fuel and the parameters investigated (ER, ERM, AOF, and S:F, etc.)

"EES PROGRAM TO ESTIMATE GAS COMOPSITION, HHV, AND ENERGY RECOVERY BY ATOM BALANCE MODEL"

```
HHVmanure=21481*M_manure                "Enter DAF HHV of fuel"
HHVco=10100*28/24.5
hhvh2=141800*2/24.5
HHVCh4=55530*16/24.5
ER=1.45                                 "ER= ERM=Stochiometric oxygen/total oxygen"
Temperature_k=1000                      “Temperature_K=Tp=adiabatic temperature"
"ratioair_steam=0.54"                   "Ratioair_steam=AOF=Oxygen from air/total
oxygen"
```

T_1=Temperature_K "Adiabatic temperature=Tp"

Moisture=25.26

ash=14.95

"NER=2.7" "NER=ER=equivalence ratio (stochiometric air/actual air)"

"SAR=1.24" "Steam/air ratio"

Nair_act=0.64 "Nair_actual=Moles of air actual"

"N_steam=0.43" "N_steam= S:F (moles of steam/mole of DAF fuel)"

"STOCHIOMETRIC CALCULATIONS"

" C H0.68 O0.19N 0.016 S0.006 +a (O2+3.76N2)======bCO2+c H2O+d N2+e SO2"

ac=1 "Enter this data"

aH=1.06 "Enter this data"

aO=0.406 "Enter this data"

aN=0.046 "Enter this data"

aS=0.0045 "Enter this data"

b=aC

c=aH/2

aO+2*a=2*b+c+2*e

e=aS

d=3.76*a+aN/2

Nair_stch=4.76*a

Oxigen_stch=2*a

M_manure=12*aC+aH*1+aO*16+aN*14+aS*32

" Manure formation enthalpy calculations"

hf_manure=b*Enthalpy(CO2,T=298)+c*Enthalpy(H2O,T=298)+d*Enthalpy(N2,T=298)
+e*Enthalpy(SO2,T=298)+HHVmanure

"ACTUAL ATOM BALANCE CALCULATIONS"

"C H1.29 O0.53 N 0.05 S0.001 +Nair
(O2+3.76N2)+Nsteam*H2O======Nco2*CO2+Nco*CO+eNch4*CH4+Nh2*H2+Nh2
s*H2S+Nn2*N2"

aC=Nco+Nco2+Nch4	"C : balance equation "
aH+2*N_steam=2*Nh2+4*Nch4+2*Nh2s	"H: balance equation "
aO+2*Nair+N_steam=Nco+2*Nco2	"O: balance equation "
3.76*2*Nair+aN=2*Nn2	"N: balance equation"
aS=Nh2s	"S: balance equation"

Oxigen_act=2*Nair+N_steam

ER=Oxigen_stch/Oxigen_act

2*Nair/(2*Nair+N_steam)=ratioair_steam

Nair_act=4.76*Nair

NER=Nair_stch/Nair_act

SAR=N_steam/Nair_act

"Energy equation"

hf_manure+N_steam*Enthalpy(H2O,T=373)+0.79*Nair_act*enthalpy(N2,T=298)+0.21*Nair_act*enthalpy(O2,T=298)=Nch4*enthalpy(ch4,T=T_1)+Nco*Enthalpy(CO,T=T_1)+Nco2*Enthalpy(CO2,T=T_1)+NH2*enthalpy(H2,T=T_1)+Nn2*enthalpy(N2,T=T_1)+Nh2s*Enthalpy(HydrogenSulfide,T=760,P=100)

"Mole fracción calculations"

Nmoles=Nco+Nch4+Nco2+Nh2+Nn2+Nh2s

yco=Nco/Nmoles

YCO2=Nco2/Nmoles

Yh2=Nh2/Nmoles

Ych4=Nch4/Nmoles

yN2=Nn2/Nmoles

"HHV and energy recovery calculations"

HHVgases=HHVco*yco+HHVh2*Yh2+HHVCh4*ych4 "HHV= gross heating value of gases (kj/m3)"

Efficiency=(Nco*HHVco+NCH4*HHVCH4+Nh2*HHVH2)*24.5/(HHVmanure+N_steam*2260*18)

N_mixture=1+Nair_act+N_steam

hf_mixture=1*hf_manure/N_mixture+0.79*Nair_act*enthalpy(N2,T=298)/N_mixture+0.21*Nair_act*enthalpy(O2,T=298)/N_mixture+N_steam*Enthalpy(H2O,T=373)/N_mixture

M_mixture=M_manure/N_mixture+28.84*Nair_act/N_mixture+N_steam*18/N_mixture

hf_R=hf_mixture/(M_mixture*8.3142) "h_R=enthalpy required to run NASA program"

APPENDIX C

TABLES OF GAS COMPOSITION ESTIMATED BY ATOM BALANCE

In this appendix are presented tables on results of gas composition of DB, FB, TXL, and WYC as function of AOF and ER_M. Additionally, tables of gas composition as function of ER and A:F are presented for DB gasification.

Table C.1. Gas composition as function of T_P, AOF, and ER_M estimated using atom balance model for gasification of DB

			Mole fraction				
Temperature (T_P), K	**ER_M**	**ASTR**	**Y_{ch4}**	**Y_{co}**	**y_{co2}**	**Y_{H2}**	**Y_{N2}**
600	2	0.25	0.09936	0.0233	0.2978	0.3587	0.22084
700	2	0.25	0.1174	-0.00617	0.3219	0.3394	0.22747
800	2	0.25	0.1372	-0.03836	0.3482	0.3183	0.23466
900	2	0.25	0.1589	-0.07369	0.3771	0.2951	0.24259
1000	2	0.25	0.1828	-0.1126	0.4089	0.2695	0.2514
1100	2	0.25	0.2092	-0.1558	0.4441	0.2412	0.2613
1200	2	0.25	0.2387	-0.2037	0.4833	0.2097	0.272
1300	2	0.25	0.2716	-0.2573	0.5271	0.1745	0.2841
1400	2	0.25	0.3085	-0.3176	0.5763	0.1349	0.2979
1500	2	0.25	0.3503	-0.3857	0.6319	0.09023	0.31327
800	1	0.25	-0.00313	-0.1227	0.3652	0.515	0.24563
800	2	0.25	0.1372	-0.03836	0.3482	0.3183	0.23466
800	3	0.25	0.2602	0.03556	0.3333	0.1458	0.22514
800	4	0.25	0.3688	0.1009	0.3202	-0.00647	0.21657
800	5	0.25	0.4654	0.159	0.3085	-0.142	0.2091
800	6	0.25	0.552	0.211	0.2981	-0.2634	0.2023
800	7	0.25	0.63	0.2579	0.2886	-0.3727	0.1962
800	8	0.25	0.7006	0.3003	0.2801	-0.4717	0.1907
800	9	0.25	0.7648	0.3389	0.2723	-0.5618	0.1858
800	10	0.25	0.8235	0.3742	0.2652	-0.6441	0.1812
800	2	0	0.3502	-0.3572	0.657	0.3347	0.0153
800	2	0.1	0.2454	-0.2003	0.505	0.3266	0.1233
800	2	0.2	0.1684	-0.08514	0.3935	0.3207	0.20254
800	2	0.3	0.1096	0.00291	0.3082	0.3161	0.26319
800	2	0.4	0.06318	0.07244	0.2409	0.3125	0.31098
800	2	0.5	0.02557	0.1287	0.1864	0.3096	0.34973
800	2	0.6	-0.0055	0.1752	0.1413	0.3072	0.3818
800	2	0.7	-0.0316	0.2143	0.1035	0.3052	0.4086
800	2	0.8	-0.05384	0.2476	0.07125	0.3035	0.43149
800	2	0.9	-0.07301	0.2763	0.04345	0.302	0.45126
800	2	1	-0.08971	0.3013	0.01924	0.3007	0.46847

Table C.2. Gas composition as function of T_P, AOF, and ER_M estimated using atom balance model for gasification of FB

Temperature (T_P), K	ER_M	ASTR	Mole fraction				
			Y_{ch4}	Y_{co}	y_{co2}	Y_{H2}	Y_{N2}
600	2	0.25	0.03336	0.08199	0.2451	0.4513	0.18825
700	2	0.25	0.04829	0.05628	0.266	0.436	0.19343
800	2	0.25	0.06438	0.02858	0.2885	0.4194	0.19914
900	2	0.25	0.08182	-0.00142	0.3128	0.4015	0.2053
1000	2	0.25	0.1008	-0.0341	0.3394	0.382	0.2119
1100	2	0.25	0.1216	-0.06983	0.3684	0.3606	0.21923
1200	2	0.25	0.1444	-0.1091	0.4002	0.3371	0.2274
1300	2	0.25	0.1695	-0.1524	0.4354	0.3113	0.2362
1400	2	0.25	0.1974	-0.2004	0.4744	0.2826	0.246
1500	2	0.25	0.2285	-0.2539	0.5178	0.2506	0.257
800	1	0.25	-0.03264	-0.07661	0.3292	0.5559	0.22415
800	2	0.25	0.06438	0.02858	0.2885	0.4194	0.19914
800	3	0.25	0.1386	0.1091	0.2573	0.315	0.18
800	4	0.25	0.1973	0.1727	0.2327	0.2325	0.1648
800	5	0.25	0.2448	0.2242	0.2127	0.1657	0.1526
800	6	0.25	0.284	0.2667	0.1963	0.1105	0.1425
800	7	0.25	0.317	0.3025	0.1824	0.06413	0.13397
800	8	0.25	0.3451	0.333	0.1706	0.02461	0.12669
800	9	0.25	0.3694	0.3593	0.1604	-0.00948	0.12038
800	10	0.25	0.3905	0.3821	0.1516	-0.03917	0.11497
800	2	0	0.139	-0.09102	0.4053	0.4453	0.10142
800	2	0.1	0.08648	-0.00684	0.3231	0.4271	0.17016
800	2	0.2	0.0445	0.06045	0.2574	0.4125	0.22515
800	2	0.3	0.01018	0.1155	0.2036	0.4006	0.27012
800	2	0.4	-0.01841	0.1613	0.1589	0.3907	0.30751
800	2	0.5	-0.04259	0.2001	0.121	0.3823	0.33919
800	2	0.6	-0.0633	0.2333	0.0886	0.3751	0.3663
800	2	0.7	-0.08125	0.262	0.06051	0.3689	0.38984
800	2	0.8	-0.09695	0.2872	0.03593	0.3635	0.41032
800	2	0.9	-0.1108	0.3094	0.01425	0.3587	0.42845
800	2	1					

Table C.3. Gas composition as function of T_P, AOF, and ER_M estimated using atom balance model for gasification of TXL

Temperature (T_P), K	ER_M	ASTR	Mole fraction				
			Y_{ch4}	Y_{co}	y_{co2}	Y_{H2}	Y_{N2}
600	2	0.25	0.0853	0.1501	0.2045	0.333	0.2271
700	2	0.25	0.102	0.1258	0.2247	0.3139	0.2336
800	2	0.25	0.1202	0.09944	0.2465	0.2932	0.24066
900	2	0.25	0.14	0.07066	0.2704	0.2707	0.24824
1000	2	0.25	0.1617	0.03912	0.2965	0.2459	0.25678
1100	2	0.25	0.1856	0.0044	0.3253	0.2187	0.266
1200	2	0.25	0.2121	-0.03396	0.3571	0.1886	0.27616
1300	2	0.25	0.2414	-0.07656	0.3924	0.1551	0.28766
1400	2	0.25	0.2741	-0.1241	0.4318	0.1178	0.3004
1500	2	0.25	0.3108	-0.1773	0.476	0.07603	0.31447
800	1	0.25	-0.01613	-0.05333	0.3126	0.5078	0.24906
800	2	0.25	0.1202	0.09944	0.2465	0.2932	0.24066
800	3	0.25	0.2457	0.24	0.1857	0.09579	0.23281
800	4	0.25	0.3615	0.3699	0.1295	-0.08654	0.22564
800	5	0.25	0.4689	0.4901	0.07749	-0.2554	0.21891
800	6	0.25	0.5686	0.6018	0.02916	-0.4123	0.21274
800	7	0.25	0.6614	0.7059	-0.01585	-0.5584	0.20695
800	8	0.25	0.7481	0.803	-0.05787	-0.6948	0.20157
800	9	0.25	0.8292	0.8938	-0.09719	-0.8224	0.19659
800	10	0.25	0.9052	0.9791	-0.1341	-0.9421	0.1919
800	2	0	0.3409	-0.1759	0.5289	0.3002	0.0059
800	2	0.1	0.2304	-0.03802	0.3876	0.2972	0.12282
800	2	0.2	0.1511	0.06096	0.2861	0.295	0.20684
800	2	0.3	0.09142	0.1355	0.2098	0.2934	0.26988
800	2	0.4	0.04485	0.1936	0.1502	0.2922	0.31915
800	2	0.5	0.00751	0.2402	0.1024	0.2911	0.35879
800	2	0.6	-0.02309	0.2784	0.06323	0.2903	0.39116
800	2	0.7	-0.04864	0.3103	0.03055	0.2896	0.41819
800	2	0.8	-0.07028	0.3373	0.00286	0.289	0.44112
800	2	0.9	-0.08885	0.3605	-0.0209	0.2885	0.46075
800	2	1	-0.105	0.3806	-0.04151	0.2881	0.47781

Table C.4. Gas composition as function of T_P, AOF, and ER_M estimated using atom balance model for gasification of WYC

Temperature (T_P), K	ER_M	ASTR	Mole fraction				
			Y_{ch4}	Y_{co}	y_{co2}	Y_{H2}	Y_{N2}
600	2	0.25	0.07282	0.1553	0.1916	0.3599	0.22038
700	2	0.25	0.08894	0.1316	0.2111	0.3419	0.22646
800	2	0.25	0.1064	0.1059	0.2321	0.3224	0.2332
900	2	0.25	0.1254	0.07788	0.255	0.3012	0.24052
1000	2	0.25	0.1461	0.04729	0.2801	0.278	0.24851
1100	2	0.25	0.1689	0.01372	0.3076	0.2525	0.25728
1200	2	0.25	0.194	-0.0233	0.3379	0.2245	0.2669
1300	2	0.25	0.2218	-0.06429	0.3715	0.1934	0.27759
1400	2	0.25	0.2527	-0.1099	0.4088	0.1589	0.2895
1500	2	0.25	0.2873	-0.1609	0.4505	0.1202	0.3029
800	1	0.25	-0.02147	-0.04772	0.3041	0.5201	0.24499
800	2	0.25	0.1064	0.1059	0.2321	0.3224	0.2332
800	3	0.25	0.2211	0.2437	0.1676	0.1449	0.2227
800	4	0.25	0.3247	0.3681	0.1093	-0.01519	0.21309
800	5	0.25	0.4186	0.4809	0.05646	-0.1604	0.20444
800	6	0.25	0.5042	0.5837	0.00831	-0.2928	0.19659
800	7	0.25	0.5825	0.6778	-0.03574	-0.4139	0.18934
800	8	0.25	0.6544	0.7642	-0.07621	-0.5251	0.18271
800	9	0.25	0.7206	0.8438	-0.1135	-0.6275	0.1766
800	10	0.25	0.7819	0.9174	-0.148	-0.7223	0.171
800	2	0	0.2109	-0.02717	0.3666	0.332	0.11767
800	2	0.1	0.1364	0.0676	0.2708	0.3251	0.2001
800	2	0.2	0.07995	0.1395	0.1981	0.3199	0.26255
800	2	0.3	0.03562	0.1959	0.1411	0.3159	0.31148
800	2	0.4	-9.5E-05	0.2414	0.09511	0.3126	0.35099
800	2	0.5	-0.02948	0.2788	0.0573	0.3099	0.38348
800	2	0.6	-0.05409	0.3102	0.02563	0.3076	0.41066
800	2	0.7	-0.07499	0.3368	-0.00127	0.3057	0.43376
800	2	0.8	-0.09297	0.3597	-0.02441	0.304	0.45368
800	2	0.9	-0.1086	0.3796	-0.04452	0.3026	0.47092
800	2	1					

Table C.5. Gas composition as function of S:F, and ER estimated using atom balance model for gasification of DB

Temperature (T_P), K	ER	S:F	Mole fraction				
			Y_{ch4}	Y_{co}	y_{co2}	Y_{H2}	Y_{N2}
1000	1.59	0.35	-0.0999	0.1822	0.0986	0.3581	0.4602
1000	1.59	0.45	-0.0986	0.1605	0.1151	0.3717	0.4505
1000	1.59	0.56	-0.0975	0.1417	0.1295	0.3836	0.4420
1000	1.59	0.68	-0.0963	0.1199	0.1461	0.3972	0.4322
1000	1.59	0.8	-0.0951	0.0991	0.1620	0.4103	0.4228
1000	2.12	0.35	-0.0593	0.1738	0.1178	0.3219	0.4447
1000	2.12	0.45	-0.0588	0.1464	0.1383	0.3403	0.4327
1000	2.12	0.56	-0.0583	0.1228	0.1561	0.3561	0.4223
1000	2.12	0.68	-0.0578	0.0959	0.1764	0.3741	0.4105
1000	2.12	0.8	-0.0573	0.0704	0.1955	0.3911	0.3993
1000	3.18	0.35	0.0137	0.1588	0.1522	0.2570	0.4169
1000	3.18	0.45	0.0116	0.1215	0.1794	0.2847	0.4013
1000	3.18	0.56	0.0099	0.0899	0.2024	0.3083	0.3881
1000	3.18	0.68	0.0080	0.0547	0.2281	0.3345	0.3734
1000	3.18	0.8	0.0063	0.0220	0.2519	0.3588	0.3597
1000	4.24	0.35	0.0773	0.1457	0.1823	0.2003	0.3926
1000	4.24	0.45	0.0718	0.1002	0.2145	0.2373	0.3745
1000	4.24	0.56	0.0673	0.0623	0.2413	0.2680	0.3594
1000	4.24	0.68	0.0624	0.0207	0.2708	0.3018	0.3428
1000	4.24	0.8	0.0578	-0.0173	0.2976	0.3326	0.3276
1000	6.36	0.35	0.1829	0.1240	0.2322	0.1062	0.3523
1000	6.36	0.45	0.1694	0.0657	0.2714	0.1603	0.3310
1000	6.36	0.56	0.1584	0.0185	0.3031	0.2042	0.3137
1000	6.36	0.68	0.1467	-0.0321	0.3371	0.2511	0.2952
1000	6.36	0.8	0.1363	-0.0770	0.3673	0.2928	0.2788

APPENDIX D

TABLES OF GAS COMPOSITION ESTIMATED BY ATOM BALANCE

Results on equilibrium modeling are presented in this appendix. Tables on adiabatic temperature, gas composition, HHV of species, and energy recovery are presented as function of ER_M, and AOF for TXL, FB, and DB and as function of AR and S:F for DB. Although in the calculations were included ~150 species only the more significant are presented here. Others are in trace amount. The ER_M and AOF were studied without the presence of water in the products; therefore the gas composition as function of AOF and ER_M is presented only in a dry basis.

Table D.1. Adiabatic temperature, gas composition (mole fraction), HHV of gases, and energy recovery calculated with equilibrium model for TXL at ER_M=2

ER_M	**2**	**2**	**2**	**2**
ASTR	**0.2**	**0.4**	**0.6**	**0.8**
adiabatic Temperature(K)	799.18	888.2	1007.55	1416.24
*Ar	0.00234	0.00367	0.00483	0.00604
CH4	0.136	0.03538	0.00172	0
*CO	0.05248	0.14723	0.23941	0.22787
COS	0	0.00001	0.00001	0.00001
*CO2	0.28309	0.16905	0.09321	0.08552
*H2	0.31304	0.30609	0.25509	0.17464
H2S	0.00029	0.00022	0.00019	0.00018
NH3	0.00024	0.00013	0.00005	0
*N2	0.19868	0.30891	0.40549	0.50574
C(gr)	0.01384	0.02931	0	0
HHHV (kJ kg^{-1})	10057.59	7455.263	6209.937	4593.7
HHHV (kJ normal m^{-3})	9190.231	6553.954	5802.274	4668.003
HHVgas $(HHVch4)^{-1}$ (%)	18.08847	13.40289	11.1655	8.261412
Energy Recovery	0.830099	0.733342	0.735276	0.636985

Table D.2. Adiabatic temperature, gas composition (mole fraction), HHV of gases, and energy recovery calculated with equilibrium model for TXL at ER_M=4

ER_M	**4**	**4**	**4**	**4**
ASTR	**0.2**	**0.4**	**0.6**	**0.8**
adiabatic Temperature(K)	823.82	890.83	953.35	1031.35
*Ar	0.00144	0.00248	0.0034	0.00427
CH4	0.09403	0.0343	0.01141	0.00301
*CO	0.05529	0.11846	0.19694	0.27244
COS		0.00001	0.00001	0.00002
*CO2	0.19208	0.12916	0.07404	0.0263
*H2	0.27475	0.27282	0.2392	0.19305
H2S	0.00036	0.0003	0.00027	0.00025
NH3	0.00016	0.00011	0.00006	0.00003
*N2	0.12482	0.21041	0.28691	0.35933
C(gr)	0.25706	0.23196	0.18776	0.14131
HHHV (kJ kg^{-1})	11385.88	8824.494	7623.621	6934.868
HHHV (kJ normal m^{-3})	7253.899	5794.503	5478.036	5506.437
HHVgas $(HHVch4)^{-1}$ (%)	20.47472	15.86423	13.70745	12.4731
Energy Recovery	0.593067	0.548976	0.5678	0.608196

Table D.3. Adiabatic temperature, gas composition (mole fraction), HHV of gases, and energy recovery calculated with equilibrium model for TXL at ER_M=6

ER_M	**6**	**6**	**6**	**6**
ASTR	**0.2**	**0.4**	**0.6**	**0.8**
adiabatic Temperature(K)	838.77	893.28	945.37	1005.57
*Ar	0.00104	0.00187	0.00261	0.0033
CH4	0.07637	0.0338	0.01392	0.005
*CO	0.05682	0.10448	0.16157	0.21928
COS		0.00001	0.00001	0.00001
*CO2	0.15172	0.10877	0.06902	0.03278
*H2	0.25638	0.25632	0.23463	0.20257
H2S	0.00039	0.00034	0.00031	0.00029
NH3	0.00013	0.0001	0.00007	0.00004
*N2	0.09205	0.16014	0.22149	0.27947
C(gr)	0.36511	0.33417	0.29637	0.25725
HHHV (kJ kg^{-1})	12454.54	9969.323	8593.602	7759.945
HHHV (kJ normal m^{-3})	6416.797	5422.478	5107.46	5076.056
HHVgas $(HHVch4)^{-1}$ (%)	22.39488	17.92221	15.45021	13.95466
Energy Recovery	0.498236	0.470377	0.476774	0.499789

Table D.4. Adiabatic temperature, gas composition (mole fraction), HHV of gases, and energy recovery calculated with equilibrium model for TXL at ER_M=8

ER_M	**8**	**8**	**8**	**8**
ASTR	**0.2**	**0.4**	**0.6**	**0.8**
adiabatic Temperature(K)	848.96	894.93	939.59	989.34
*Ar	0.00082	0.0015	0.00212	0.0027
CH4	0.06667	0.0336	0.016	0.00692
*CO	0.05772	0.09574	0.14022	0.18639
COS		0.00001	0.00001	0.00001
*CO2	0.12888	0.09653	0.06571	0.0367
*H2	0.24548	0.246	0.23106	0.20754
H2S	0.0004	0.00037	0.00034	0.00032
NH3	0.00011	0.00009	0.00007	0.00004
*N2	0.0735	0.12981	0.18093	0.22935
C(gr)	0.42642	0.39637	0.36355	0.33002
HHHV (kJ kg^{-1})	13323.73	10918.44	9451.218	8508.124
HHHV (kJ normal m^{-3})	5948.243	5193.925	4894.792	4824.023
HHVgas $(HHVch4)^{-1}$ (%)	23.95676	19.62838	16.99129	15.29838
Energy Recovery	0.448043	0.427384	0.428662	0.442665

Table D.5. Adiabatic temperature, gas composition (mole fraction), HHV of gases, and energy recovery calculated with equilibrium model for DB at ER_M=2

ER_M	**2**	**2**	**2**	**2**
ASTR	**0.2**	**0.4**	**0.6**	**0.8**
adiabatic Temperature(K)	587	824	916	1239
*Ar	0.00213	0.00361	0.00458	0.00564
CH4	0.12571	0.06794	0.01056	0
*CO	0.00004	0.06432	0.14837	0.15687
COS	0	0.00002	0.00004	0.00004
*CO2	0.32152	0.24694	0.16182	0.13974
*H2	0.34291	0.30571	0.2841	0.21907
H2S	0.00201	0.00169	0.00141	0.00129
NH3	0.0046	0.00022	0.0001	0.00001
*N2	0.18557	0.30955	0.38903	0.47734
C(gr)	0	0	0	0
HHHV (kJ kg^{-1})	947718.6	715912.1	574079.1	435404.8
HHHV (kJ normal m^{-3})	8560.283	6773.246	5410.462	4366.859
HHVgas $(HHVch4)^{-1}$ (%)	17.04077	12.87088	10.31864	7.826793
Energy Recovery	0.865795	0.796192	0.741318	0.651603

Table D.6. Adiabatic temperature, gas composition (mole fraction), HHV of gases, and energy recovery calculated with equilibrium model for DB at ER_M=4

ER_M	**4**	**4**	**4**	**4**
ASTR	**0.2**	**0.4**	**0.6**	**0.8**
adiabatic Temperature(K)	713	791	855	909
*Ar	0.00149	0.00254	0.00328	0.004
CH4	0.2342	0.10614	0.04374	0.01718
*CO	0.0108	0.0381	0.08782	0.15309
COS	0.00001	0.00002	0.00004	0.00006
*CO2	0.3104	0.23127	0.17167	0.12062
*H2	0.17732	0.23817	0.25163	0.23111
H2S	0.00304	0.00238	0.00203	0.00183
NH3	0.00025	0.00022	0.00014	0.00008
*N2	0.13939	0.22356	0.28363	0.34283
C(gr)	0.1231	0.15762	0.15603	0.1292
HHHV (kJ kg^{-1})	1188698	875402.2	703083	620262.8
HHHV (kJ normal m^{-3})	10686.66	7067.817	5535.912	5086.725
HHVgas $(HHVch4)^{-1}$ (%)	21.39132	15.74437	12.64029	11.1516
Energy Recovery	0.818548	0.680901	0.616504	0.620487

Table D.7. Adiabatic temperature, gas composition (mole fraction), HHV of gases, and energy recovery calculated with equilibrium model for DB at ER_M=6

ER_M	**6**	**6**	**6**	**6**
ASTR	**0.2**	**0.4**	**0.6**	**0.8**
adiabatic Temperature(K)	694	768	824	871
*Ar	0.00118	0.00195	0.00256	0.00312
CH4	0.23282	0.12556	0.06436	0.03161
*CO	0.00644	0.02424	0.0542	0.09554
COS	0.00001	0.00002	0.00003	0.00004
*CO2	0.27991	0.22209	0.17785	0.13963
*H2	0.13634	0.20314	0.23059	0.23044
H2S	0.00334	0.00275	0.00239	0.00217
NH3	0.00022	0.00021	0.00016	0.00011
*N2	0.11529	0.17669	0.22582	0.27164
C(gr)	0.22445	0.24334	0.24203	0.22568
HHHV (kJ kg^{-1})	1252603	986309.2	801945.2	690581.5
HHHV (kJ normal m^{-3})	10108.14	7203.348	5650.106	4937.897
HHVgas $(HHVch4)^{-1}$ (%)	22.54375	17.74234	14.41983	12.41512
Energy Recovery	0.727272	0.623472	0.557943	0.53364

Table D.8. Adiabatic temperature, gas composition (mole fraction), HHV of gases, and energy recovery calculated with equilibrium model for DB at ER_M=8

ER_M	**8**	**8**	**8**	**8**
ASTR	**0.2**	**0.4**	**0.6**	**0.8**
adiabatic Temperature(K)	688	753	803	845
*Ar	0.00093	0.00159	0.00212	0.00259
CH4	0.22747	0.1393	0.0819	0.04641
*CO	0.00518	0.01737	0.03746	0.06557
COS	0.00001	0.00002	0.00002	0.00004
*CO2	0.25958	0.21603	0.18087	0.15022
*H2	0.12073	0.17922	0.21125	0.2221
H2S	0.0035	0.00299	0.00265	0.00241
NH3	0.0002	0.00021	0.00018	0.00014
*N2	0.09513	0.14774	0.19012	0.22833
C(gr)	0.28728	0.29553	0.29344	0.28219
HHHV (kJ kg^{-1})	1311754	1072101	890071.4	764153.1
HHHV (kJ normal m^{-3})	9717.442	7343.216	5867.287	5031.35
HHVgas $(HHVch4)^{-1}$ (%)	23.60917	19.28808	16.00699	13.73882
Energy Recovery	0.675777	0.594422	0.534256	0.500048

Table D.9. Adiabatic temperature, gas composition (mole fraction), HHV of gases, and energy recovery calculated with equilibrium model for FB at ER_M=2

ER_M	**2**	**2**	**2**	**2**
ASTR	**0.2**	**0.4**	**0.6**	**0.8**
adiabatic Temperature(K)	796	905	1213	1558
*Ar	0.00186	0.00314	0.00432	0.00545
CH4	0.07063	0.01364	0	0
*CO	0.02644	0.11471	0.13054	0.1239
COS	0.00001	0.00003	0.00003	0.00003
*CO2	0.3003	0.20769	0.17795	0.16797
*H2	0.43343	0.38848	0.31714	0.23898
H2S	0.00238	0.00199	0.00182	0.00157
NH3	0.00036	0.00015	0.00002	0
*N2	0.16459	0.27018	0.36817	0.46194
C(gr)	0	0	0	0
HHHV (kJ kg^{-1})	9406.739	7396.09	5644.059	4219.927
HHHV (kJ normal m^{-3})	7923.784	6351.523	5207.213	4218.596
HHVgas $(HHVch4)^{-1}$ (%)	16.90546	13.28956	10.14172	7.583911
Energy Recovery	0.830072	0.774561	0.693865	0.600971

Table D.10. Adiabatic temperature, gas composition (mole fraction), HHV of gases, and energy recovery calculated with equilibrium model for FB at ER_M=4

ER_M	**4**	**4**	**4**	**4**
ASTR	**0.2**	**0.4**	**0.6**	**0.8**
adiabatic Temperature(K)	811	864	910	954
*Ar	0.00131	0.00224	0.00304	0.0038
CH4	0.1274	0.05935	0.02701	0.01183
*CO	0.05838	0.10959	0.17268	0.23958
COS	0.00003	0.00005	0.00007	0.0001
*CO2	0.26446	0.19661	0.14145	0.09293
*H2	0.31753	0.32116	0.29915	0.26336
H2S	0.0033	0.0028	0.00251	0.00232
NH3	0.00019	0.00015	0.0001	0.00007
*N2	0.12282	0.19853	0.26456	0.3271
C(gr)	0.10459	0.10953	0.08943	0.05892
HHHV (kJ kg^{-1})	11341.84	9256.626	8070.203	7372.867
HHHV (kJ normal m^{-3})	8998.854	7164.561	6463.218	6267.36
HHVgas $(HHVch4)^{-1}$ (%)	20.39711	16.64204	14.5087	13.25731
Energy Recovery	0.773661	0.715495	0.712296	0.740327

Table D.11. Adiabatic temperature, gas composition (mole fraction), HHV of gases, and energy recovery calculated with equilibrium model for FB at ER_M=6

ER_M	**6**	**6**	**6**	**6**
ASTR	**0.2**	**0.4**	**0.6**	**0.8**
adiabatic Temperature(K)	820	861	897	932
*Ar	0.00094	0.00167	0.00231	0.00291
CH4	0.11304	0.06325	0.03484	0.01876
*CO	0.06006	0.09755	0.14206	0.19114
COS	0.00004	0.00005	0.00007	0.00009
*CO2	0.23326	0.186	0.14551	0.1086
*H2	0.30548	0.31004	0.29845	0.27704
H2S	0.00354	0.00314	0.00288	0.00269
NH3	0.00016	0.00014	0.00011	0.00008
*N2	0.09304	0.15271	0.20521	0.25419
C(gr)	0.19044	0.18545	0.16857	0.1445
HHHV (kJ kg^{-1})	12036.36	10206.07	9003.771	8227.859
HHHV (kJ normal m^{-3})	8356.896	7037.264	6385.551	6119.144
HHVgas $(HHVch4)^{-1}$ (%)	21.64516	18.34938	16.18665	14.79282
Energy Recovery	0.689274	0.650023	0.64006	0.65217

Table D.12. Adiabatic temperature, gas composition (mole fraction), HHV of gases, and energy recovery calculated with equilibrium model for FB at ER_M=8

ER_M	**8**	**8**	**8**	**8**
ASTR	**0.2**	**0.4**	**0.6**	**0.8**
adiabatic Temperature(K)	827	859	889	918
*Ar	0.00073	0.00134	0.00187	0.00237
CH4	0.10438	0.06587	0.04071	0.02482
*CO	0.06232	0.09056	0.1249	0.1626
COS	0.00004	0.00005	0.00006	0.00008
*CO2	0.21555	0.1797	0.14761	0.11801
*H2	0.30075	0.30306	0.29665	0.28261
H2S	0.00367	0.00335	0.00311	0.00293
NH3	0.00014	0.00013	0.00011	0.00009
*N2	0.07615	0.12546	0.16912	0.20986
C(gr)	0.23627	0.23049	0.21585	0.19664
HHHV (kJ kg^{-1})	12533.38	10896.44	9738.096	8921.691
HHHV (kJ normal m^{-3})	8013.747	6970.148	6379.34	6074.458
HHVgas $(HHVch4)^{-1}$ (%)	22.53817	19.5909	17.50681	16.0394
Energy Recovery	0.646715	0.614436	0.602975	0.606321

Here are presented tables of gas composition, HHV, and energy recovery for DB as a function of S:F and ER.

Table D.13. Adiabatic temperature, gas composition (mole fraction, wet basis), HHVcalculated with equilibrium model for DB at ER=1.59

S:F	0.35	0.45	0.56	0.68	0.8
ER	1.59	1.59	1.59	1.59	1.59
Adiabatic Temperature, K	1714.82	1683.75	1656.46	1626.18	1596.92
Yar	0.00675	0.00659	0.00645	0.00629	0.00613
Y_{CH4}	0	0	0	0	0
Y_{CO}	0.12527	0.11774	0.11136	0.10428	0.0977
Y_{CO2}	0.10084	0.10289	0.10451	0.10615	0.10754
Y_{H2}	0.05232	0.05555	0.05819	0.061	0.06351
Y_{H2O}	0.14643	0.16263	0.17685	0.19334	0.20918
Y_{NH3}	0	0	0	0	0
Y_{N2}	0.56835	0.55457	0.54262	0.52893	0.51592
C(gr)	0	0	0	0	0

Table D.14. Adiabatic temperature, gas composition (mole fraction, wet basis) calculated with equilibrium model for DB at ER=2.12

S:F	0.35	0.45	0.56	0.68	0.8
ER	2.12	2.12	2.12	2.12	2.12
Adiabatic Temperature, K	1367	1343.87	1324.27	1301.16	1279.89
Yar	0.00591	0.00574	0.0056	0.00544	0.00528
Y_{CH4}	0	0	0	0	0
Y_{CO}	0.17803	0.16481	0.15383	0.14171	0.13072
Y_{CO2}	0.08559	0.09138	0.09597	0.10082	0.10496
Y_{H2}	0.11715	0.12206	0.12588	0.12986	0.13318
Y_{H2O}	0.11465	0.13137	0.14619	0.16338	0.18003
Y_{NH3}	0	0	0	0	0
Y_{N2}	0.49867	0.48463	0.47253	0.45879	0.44583
C(gr)	0	0	0	0	0

Table D.15. Adiabatic temperature, gas composition (mole fraction, wet basis) calculated with equilibrium model for DB at ER=3.18

S:F	0.35	0.45	0.56	0.68	0.8
ER	3.18	3.18	3.18	3.18	3.18
Adiabatic Temperature, K	937.03	925.01	919.9	913.68	907.25
Yar	0.00481	0.00466	0.00452	0.00436	0.00421
Y_{CH4}	0.00892	0.01073	0.01022	0.00978	0.00949
Y_{CO}	0.20841	0.18902	0.16983	0.14963	0.13201
Y_{CO2}	0.09867	0.11236	0.1225	0.13251	0.14057
Y_{H2}	0.21233	0.22196	0.22927	0.23577	0.24021
Y_{H2O}	0.05279	0.06531	0.0798	0.0976	0.11565
Y_{NH3}	0.00006	0.00007	0.00007	0.00008	0.00008
Y_{N2}	0.40821	0.3959	0.38378	0.37028	0.35778
C(gr)	0.0058	0	0	0	0

Table D.16. Adiabatic temperature, gas composition (Mole fraction, wet basis) calculated with equilibrium model for DB at ER=4.24

S:F	0.35	0.45	0.56	0.68	0.8
ER	4.24	4.24	4.24	4.24	4.24
Adiabatic Temperature, K	908.37	894.59	883.25	870.89	859.45
Yar	0.00405	0.00392	0.00382	0.00371	0.00361
Y_{CH4}	0.01422	0.0179	0.02146	0.02595	0.03067
Y_{CO}	0.15241	0.13602	0.1228	0.10892	0.09671
Y_{CO2}	0.11417	0.12741	0.13814	0.14957	0.15972
Y_{H2}	0.21564	0.22251	0.22706	0.23084	0.23295
Y_{H2O}	0.07346	0.08812	0.1015	0.11749	0.13344
Y_{NH3}	0.00007	0.00008	0.00009	0.0001	0.00011
Y_{N2}	0.34566	0.33519	0.32646	0.31684	0.30805
C(gr)	0.08032	0.06886	0.05867	0.04658	0.03475

Table D.17. Adiabatic temperature, gas composition (mole fraction, wet basis) calculated with equilibrium model for DB at ER=6.36

S:F	0.35	0.45	0.56	0.68	0.8
ER	6.36	6.36	6.36	6.36	6.36
Adiabatic Temperature, K	868.07	853.61	841.53	828.19	815.87
Yar	0.0031	0.003	0.00292	0.00284	0.00276
YCH4	0.0251	0.03088	0.03637	0.04316	0.0501
YCO	0.09019	0.0779	0.06829	0.0585	0.05027
YCO2	0.1275	0.13932	0.14879	0.15882	0.16763
YH2	0.20745	0.20991	0.21049	0.20962	0.20737
YH2O	0.10696	0.12577	0.14276	0.16289	0.18267
YNH3	0.00009	0.0001	0.00011	0.00012	0.00013
YN2	0.26782	0.2595	0.25262	0.2451	0.23824
C(gr)	0.17179	0.15362	0.13763	0.11897	0.10084

Table D.18. Adiabatic temperature, gas composition (mole fraction, dry basis without C), HHV of gases, and energy recovery calculated with equilibrium model for DB at ER=1.59

S:F	0.35	0.45	0.56	0.68	0.8
ER	1.59	1.59	1.59	1.59	1.59
Yar	0.007908	0.00787	0.007836	0.007798	0.007751
YCH4	0	0	0	0	0
YCO	0.14676	0.140607	0.135285	0.129274	0.123543
YCO2	0.118139	0.122873	0.126963	0.131592	0.135985
YH2	0.061296	0.066339	0.070692	0.07562	0.080309
YNH3	0	0	0	0	0
YN2	0.66585	0.662276	0.659199	0.655704	0.652386
HHHV (kJ kg^{-1})	2077.172	2070.552	2064.704	2058.203	2051.94
HHHV (kJ normal m^{-3})	2409.247	2397.065	2386.429	2374.547	2363.099
HHVgas $(HHVch4)^{-1}$ (%)	3.74063	3.728708	3.718178	3.706471	3.695191
Energy Recovery	0.491207	0.48574	0.480858	0.475136	0.469558

Table D.19. Adiabatic temperature, gas composition (mole fraction, dry basis without C), HHV of gases, and energy recovery calculated with equilibrium model for DB at ER=2.12

S:F	0.35	0.45	0.56	0.68	0.8
ER	2.12	2.12	2.12	2.12	2.12
Yar	0.006675	0.006608	0.006559	0.006502	0.006439
YCH4	0	0	0	0	0
YCO	0.201084	0.189736	0.180169	0.169384	0.15942
YCO2	0.096674	0.1052	0.112402	0.120509	0.128005
YH2	0.132321	0.14052	0.147433	0.15522	0.162421
YNH3	0	0	0	0	0
YN2	0.563246	0.557925	0.553437	0.548385	0.543715
HHHV (kJ kg^{-1})	3611.523	3588.862	3569.546	3547.631	3527.385
HHHV (kJ normal m^{-3})	3865.032	3829.706	3799.941	3766.304	3735.314
HHVgas $(HHVch4)^{-1}$ (%)	6.503733	6.462924	6.428139	6.388675	6.352216
Energy Recovery	0.701058	0.693281	0.686321	0.678161	0.670185

Table D.20. Adiabatic temperature, gas composition (mole fraction, dry basis without C), HHV of gases, and energy recovery calculated with equilibrium model for DB at ER=3.18

S:F	0.35	0.45	0.56	0.68	0.8
ER	3.18	3.18	3.18	3.18	3.18
Yar	0.005109	0.004986	0.004912	0.004832	0.004761
YCH4	0.009475	0.01148	0.011106	0.010838	0.010731
YCO	0.221381	0.202227	0.184558	0.165813	0.149273
YCO2	0.104811	0.120211	0.133123	0.146842	0.158953
YH2	0.225545	0.237469	0.249152	0.26127	0.271623
YNH3	6.37E-05	7.49E-05	7.61E-05	8.87E-05	9.05E-05
YN2	0.433616	0.423563	0.417062	0.410328	0.404568
HHHV (kJ kg^{-1})	5694.429	5705.812	5643.774	5577.262	5517.353
HHHV (kJ normal m^{-3})	5530.659	5521.403	5440.217	5355.502	5281.514
HHVgas (HHVch4)$^{-1}$ (%)	10.25469	10.27519	10.16347	10.04369	9.935805
Energy Recovery	0.873844	0.882837	0.874345	0.864152	0.853921

Table D.21. Adiabatic temperature, gas composition (mole fraction, dry basis without C), HHV of gases, and energy recovery calculated with equilibrium model for DB at ER=4.24

S:F	0.35	0.45	0.56	0.68	0.8
ER	4.24	4.24	4.24	4.24	4.24
Yar	0.004786	0.00465	0.004549	0.004438	0.00434
YCH4	0.016804	0.021233	0.025553	0.031043	0.036871
YCO	0.180107	0.161348	0.14622	0.130298	0.116265
YCO2	0.134918	0.151135	0.164486	0.178926	0.192015
YH2	0.254827	0.263944	0.270364	0.276148	0.280052
YNH3	8.27E-05	9.49E-05	0.000107	0.00012	0.000132
YN2	0.408475	0.397606	0.388722	0.379027	0.370337
HHHV (kJ kg^{-1})	5921.034	5981.766	6043.022	6126.189	6215.756
HHHV (kJ normal m^{-3})	5661.684	5712.143	5769.075	5851.872	5946.792
HHVgas (HHVch4)$^{-1}$ (%)	10.66277	10.77213	10.88245	11.03222	11.19351
Energy Recovery	0.716542	0.734183	0.750647	0.771374	0.792584

Table D.22. Adiabatic temperature, gas composition (mole fraction, dry basis without C), HHV of gases, and energy recovery calculated with equilibrium model for DB at ER=6.36

S:F	0.35	0.45	0.56	0.68	0.8
ER	6.36	6.36	6.36	6.36	6.36
Yar	0.004298	0.004163	0.004058	0.003955	0.003852
YCH4	0.034801	0.042853	0.050541	0.0601	0.069924
YCO	0.125047	0.108103	0.094899	0.08146	0.070161
YCO2	0.176776	0.193336	0.206765	0.221155	0.23396
YH2	0.287626	0.291295	0.292506	0.291893	0.289425
YNH3	0.000125	0.000139	0.000153	0.000167	0.000181
YN2	0.371328	0.360112	0.351051	0.341298	0.33251
HHHV (kJ kg^{-1})	6450.34	6578.252	6701.728	6857.938	7020.431
HHHV (kJ normal m^{-3})	6061.444	6200.666	6341.199	6525.56	6722.615
HHVgas $(HHVch4)^{-1}$ (%)	11.61595	11.8463	12.06866	12.34997	12.64259
Energy Recovery	0.569531	0.593863	0.616573	0.644654	0.673445

APPENDIX E

EES CODE TO ESTIMATE TAR AND GAS YIELD

The Engineering Equation Solvers (EES) code performed to estimate the tar composition by atom balance is presented in this appendix. Running the program require entering fuel composition, gas moles, char moles, fuel rate (kg/h), and flows of steam (cm^3/min) and air (SFCH). The atom balance is presented in the following reaction

$$CH_hO_0N_n + \text{air} + H_2O \rightarrow \text{Char} + \text{dry tar} + H_2O + \text{dry gases}$$

Input data

Fuel composition (input data)

ash = 14.95

Moisture = 25

MassMolecular = 20.34

aC = 1

Ah = 1.06

aO = 0.406

an = 0.046

Flows of reactants (input data)

Manurerate = 1

Waterflow = 7.12

airflow = 40

Gas mole on a dry basis (input data)

Ychar = 0

$$YCO2 = \frac{16.75}{100}$$

$$yco = \frac{11.26}{100}$$

$$YN2 = \frac{44.99}{100}$$

$$YH2 = \frac{25.28}{100}$$

$$YCH4 = \frac{1.035}{100}$$

$$YC2H6 = \frac{0.4047}{100}$$

Tar Composition

yo2 = 0

CT = 1

HT = 2.01

NT = 0.064

OT = 0.48

Stochiometric Calculations

b = aC

aO + 2 · a = 2 · b + c

$$d = 3.76 \cdot a + \frac{an}{2}$$

$$Ah = 2 \cdot c$$

$$Oxigen_{stch} = 2 \cdot a$$

$$Nair_{stch} = 4.76 \cdot a$$

$$AF_{stochiometric} = \frac{Nair_{stch}}{1}$$

$$M_{manure} = 12 \cdot aC + Ah \cdot 1 + aO \cdot 16 + an \cdot 14$$

$$DAFManurerate = Manurerate \cdot \left[1 - \frac{ash}{100} - \frac{Moisture}{100}\right]$$

$$DAFManureMoles = \frac{DAFManurerate}{MassMolecular}$$

$$ExperimentalAirfuelratio = \frac{airflow \cdot \frac{1.2}{35.31 \cdot 28.84}}{DAFManureMoles}$$

$$ExperimentalSteamfuelratio = \frac{Waterflow \cdot 1000 \cdot \frac{60}{1000000 \cdot 18}}{DAFManureMoles}$$

$$ER = \frac{AF_{stochiometric}}{ExperimentalAirfuelratio}$$

$$TotalSF_{ratio} = \frac{Waterflow \cdot 1000 \cdot \frac{60}{1000000 \cdot 18} + Manurerate \cdot \frac{Moisture}{18 \cdot 100}}{DAFManureMoles}$$

$$SF_{ratio} = ExperimentalSteamfuelratio$$

Actual calculations

$$ManureMoles = yco + YCH4 + YCO2 + 2 \cdot YC2H6 + Ychar + Ytar$$

$$an \cdot ManureMoles + 3.76 \cdot 2 \cdot aircoefficient = 2 \cdot YN2 + NT \cdot Ytar$$

$$Ah \cdot ManureMoles + 2 \cdot N_{steam} = 2 \cdot YH2 + 4 \cdot YCH4 + 2 \cdot YH2O + 6 \cdot YC2H6 + HT \cdot Ytar$$

$$aO \cdot ManureMoles + 2 \cdot aircoefficient + N_{steam} = yco + 2 \cdot YCO2 + 2 \cdot yo2 + YH2O + OT \cdot Ytar$$

$$Actair = 4.76 \cdot aircoefficient$$

$$AirFuelRatio = \frac{Actair}{ManureMoles}$$

$$ER = \frac{Nair_{stch}}{AirFuelRatio}$$

$$TotalSF_{ratio} = \frac{N_{steam}}{ManureMoles}$$

$$masamanure = ManureMoles \cdot MassMolecular$$

$$watermanure = masamanure \cdot \frac{0.25}{0.6 \cdot 18 \cdot 1 \quad [moles]}$$

$$externalwater = N_{steam} - watermanure$$

$$steamfuelratio = \frac{externalwater}{ManureMoles}$$

APPENDIX F

CALIBRATION AND ANALYSIS OF MASS SPECTROMETER

The procedure used for operating, calibrating, and analyzing of the mass spectrometer are presented in this appendix. The basic operating instructions of the MS can be seem in the operation manual, which is available in the coal and biomass laboratory. The operation manual is also available in the Gas Works software. Before any attempt is made to operate the system, it is important to read the basic operating conditions to avoid damages in the filament. The filament of the MS can be connected only after that the pressure of the system has fallen into the safe operating region of below $2x10^{-5}$ mbar. This pressure is achieved approximately 10 min after the MS is powered. For the MS to function correctly, the probability of collisions between ions and molecules must be low, hence, the necessity for operation at low pressure (vacuum < 10^{-6} Torr). Ionization is a process in which exited electrons emitted by a hot filament collide with the atoms and molecules of gas samples to remove electrons from their outer orbits leaving the atoms and molecules of the samples with a positive charge. As discussed before, the ions can have a charge of 1e, 2e, or 3e depending on whether they have one, two, or three electrons removed during the ionization process. The ion is said to be singly charged, doubly charged, or triply charged. The MS operates by measuring the molecular mass-to-charge ratio of the atoms and molecules of the gas samples entering the MS. Thus, it is evident that the mass spectrum of a gas is not just its molecular mass,

but is in practice identified by a family of peaks, called cracking pattern. As with a mixture of gases, the spectrum can be very complex because of the superposed cracking pattern; calibration using gas mixtures with non-overlapping masses is required to analyze the samples. Using the information gained during the calibration, an analysis of one matrix of known component gases but unknown concentrations can be performed. The calibration frequency of the MS depends on the amount of gases present in the samples to be analyzed. Increased amount of gases in the samples requires more frequent calibrations. The calibration of the MS must be performed in the same conditions used in the analysis. The mixture samples used in the calibrations must be taken almost at atmospheric pressure to ensure a sample flow of 12 mL/min which is required by the MS for a successfull calibration and analysis. If the downstream pressure where the samples are taken by the capillary is far from atmospheric pressure, the flow of samples into the MS could increase or decrease and the calibration and analysis are not reliable. To avoid possible condensate into the MS (tar and steam), calibration and analysis must be performed with the heater elements of the MS turned on to heat the samples in the capillary (capillary tube which takes the samples from the downstream to the MS) at 180 °C and into the MS jacket at 80 °C. It is necessary to have mixtures with known gas compositions to perform the calibration. For each gas analyzed, it is necessary to purchase a cylinder with a known composition closer to that of the gas to be analyzed. For example, to analyze CO in a gasifier, a mixture of 30% CO and 70% gas balance (argon) must be acquired. However, because in gasification the concentration of the

gases varies with the operating conditions, it is important to have a mixture with all gases to obtain linearities for each of the gases to be analyzed.

Table F1 shows the mixtures used to calibrate the MS and calibration configuration set-up. Where F = Fragmentation, S = Sensitivity and L = Linearity. Mixture 1 contains all the gases which are later analyzed and is used to obtain the linearities. Mixtures 2 to 8 are used to measure the sensitivities (system response to a determined gas) and fragmentation patterns (overlapping) of the gases analyzed (CO, H_2, C_2H_6, CH_4, CO_2, NO_2, N_2, and O_2). Mixture 9 is used to measure the background in the vacuum. The mass 4 peak, which is the only peak in He, is not used during the analysis; thus, this gas can be used to quantify the system background.

Table F1. calibration mixtures and calibration configuration set up

	Calibration Mixtures								
Gas	1	2	3	4	5	6	7	8	9
CO	15% L			30% FS					
H_2	15% L	20% S							
C_2H_6	5% L						1% FS		
CH_4	5% L				1% FS				
CO_2	15% L		0.04%					20% FS	
NO_2	5% L					5% FS			
N_2	40% L		78.08% FS						
O_2			20.95% FS						
He									100%
Ar		Balance	0.93%	Balance	Balance	Balance	Balance	Balance	

The characteristic masses (peaks) measured in the gasification analysis are represented in Table AF2. As discussed before, the peaks are determined by the molecular weight of each gas and the ion charge. The peaks are defined as: M/charge, e.g., for N_2, 28/1, 28/2, 28/3 etc. A gas can present many peaks if there is a peak that does not overlap with the peaks of other gases; this peak can be analyzed alone to

decrease the number of peaks measured. All the overlapping peaks present in the gas matrix must be selected to be analyzed.

Table F2 analysis configuration set up

	Analyzed Gases							
	H_2	CO	N_2	CH_4	C_2H_6	O_2	CO_2	NO_2
Characterisc Peaks	2	12	14	15	27	32	44	46
2	100			0.4	3			
12		100	100	4	2		2.5	
14		8	100	23	13			26
15				100	18			
27					100			
32						100		
44							100	
6								100

As discussed before, the MS was calibrated every 72 hours under the configuration set-up presented in Table F1. The analysis was performed according to the analysis set-up presented in Table F2. The samples were suctioned by the MS from a downstream of samples which were previously taken at the top of the gasifier at the rate of 0.14 SATP m^3 h^{-1} and conditioned by the sampling unit to remove tar and particulate material (Figure 14). The pressure in the sample line where the capillary of the MS took the samples was maintained constant almost at atmospheric conditions to ensure a flow of 12 mL/min into the MS. After the calibration, mixtures of well-known composition were analyzed using the MS in order to verify the accuracy of the calibration.

The MS is shown in Figure F3. As discussed before, during the calibration and analysis, the capillary was heated at 180 °C to ensure no condensation into the MS during the analysis. Additionally to the capillary heater, the MS has another internal heater which allows the heating of samples within the internal jacket of the MS at 80 °C.

Although the gas samples analyzed were conditioned to remove the tar, water, and particulate material before they were suctioned by the capillary, the calibrations and analyses of gases were performed with the two heaters turned on (capillary and jacket) to remove the possibility of particulate material disrupting measurements. As the samples analyzed were heated in the capillary and jacket, the samples of calibration mixtures were also heated to ensure that the calibration and analyses were performed at the same conditions. If the temperature of the calibration mixtures is different to the temperature of the gas samples to be analyzed, the analysis in the MS would be no reliable. As the temperature or pressure is changed, the distance traveled by the molecules between collisions (mean-free-path) also changes, and hence the information obtained in the calibration is not useful in the analysis.

Figure F-1 Mass Spectrometer

APPENDIX G

ANALYSIS ON HHV OF N_2-FREE GASES USING BOIE EQUATION

This appendix presents results on HHV, determined using the Boie equation, of gas mixtures (N_2-free) obtained for gasification of DB and compares the results with HHV values given by the gas mixtures. Considering a mixture of gases composed of CO, CO_2, CH_m, and H_2 and knowing its composition an empirical formula (CH_hO_o) can be derived. Table G1 shows the composition with N_2 content and N_2-free of a gas mixture obtained from DB gasification at ER = 3.18 and S:F = 0.68. Using the gas composition the empirical formulas were also derived. The results show that the HHV of the N_2-free mixture is higher than that of the mixture with N_2 content.

Table G1. N_2 and N_2-free composition (mol basis) of a mixture obtained for DB gasification at ER = 3.18 and S:F = 0.68

Especies (%)	With N_2	N_2-free
CO_2	17.22	35.25
CO	10.77	22.04
N_2	51.15	0.00
H_2	19.88	40.70
CH_4	0.67	1.38
C_2H_6	0.29	0.60
Empirical formula	$CH_{1.51}O_{1.54}N_{3.5}$	$CH_{1.51}O_{1.54}$
HHV (kJ/kg of gas)	3836	8748

For N_2-free gas mixtures obtained from DB gasification, table G2 compares HHV determined using the Boie Equation to the HHV given by the gas mixtures as a function of ER and S:F. The results show that the HHV determined using the Boie Equation is very close to the HHV of the mixtures. The error between the value given by the gas mixtures and the HHV determined using the Boie equation lies between 0.03% and 6.50%. In general, the error teds to decrease with increased ER.

Table G2. HHV (kJ/kg of gas) of gases (free of N2) determined using Boie Equation and gas composition for DB gasification

	ER														
	1.56			2.12			3.18			4.24			6.36		
S:F	Gas Composition	Boie Equation	Error %	Gas Composition	Boie Equation	Error %	Gas Composition	Boie Equation	Error %	Gas Composition	Boie Equation	Error %	Gas Composition	Boie Equation	Error %
0.35	9422	8964	4.85	9683	9147	5.53	9236	8846	4.22	8876	8662	2.42	8250	8252	0.03
0.56	9266	8765	5.41	10266	9747	5.06	9858	9564	2.99	9102	8992	1.21	8489	8528	0.47
0.68	10919	10209	6.50	10446	9921	5.02	8748	8511	2.70	8991	8845	1.62	8138	8200	0.76
0.8	10930	10280	5.94	10183	9701	4.73	8899	8720	2.00	8702	8659	0.49	8371	8533	1.93

Although for N_2-free gas mixtures the HHV value determined using the Boie Equation is very close to the HHV value given by the gas mixtures, for mixtures with N_2 content, the HHV determined using the Boie equation is very different from that given by the gas mixture. For example, the HHV shown in table G1 for the mixture with N_2 content is 3836 kJ/kg whereas the HHV for the same mixture determined using the Boie Equation is 7261 kJ/kg, which leads to an error of ~47.2%. From results, it is apparent that for N_2-free mixtures, the Boie equation gives HHV values very close to the values given by the gas mixtures but gives values very far for gas mixtures with N_2 content.

VITA

Gerardo Gordillo Ariza is an assistant professor in the Mechanical Engineering Department at the Universidad de Los Andes at Bogotá, Colombia. In 1983 he earned his B.S. degree in mechanical engineering from the Universidad Nacional de Colombia, Bogotá. He then obtained his M.S. in mechanical engineering from the Universidad de Los Andes in 1994. He worked as graduate research assistant from January 2006 to December 2008 in Texas A&M University and received his Ph.D. in 2009 in mechanical engineering from Texas A&M University. He has a strong background in thermodynamics, heat transfer, fluid mechanics, computer modeling, combustion and gasification with a vast experience in combustion and gasification of biomass (sugar-cane bagasse, coal and cattle manure). His research interests include thermodynamics, thermal energy combustion processes of biomass to produce heat, gaseous or liquid combustible fuels. His email is: gordillo53@hotmail.com, and can be contacted at:

Texas A&M University
Department of Mechanical Engineering
3123 TAMU
College Station, TX 77843-3123